

Confidential
Limited distribution

Zn-Mg Automotive Steel Coatings

Final Report

Nicolas Larché & Tomas Prosek & Andrej Nazarov & Dominique Thierry

Executive summary

Recently, it was shown by several research groups that alloying of zinc coatings with magnesium and eventually aluminum significantly improves their corrosion resistance under atmospheric conditions. Red rust appearance and onset of paint delamination from defects were delayed in comparison to traditional zinc coated steel with comparable coating thickness. Two methods for line production of zinc-magnesium coatings are under development by several steel makers: hot dipping and physical vapor deposition technology. In the latter case, magnesium is applied in a thin layer on the surface of electro galvanized or hot dip galvanized steel sheets by PVD in vacuum. Zinc-magnesium alloys are thereafter manufactured by heat treatment.

Already available data indicate that ZnMg and ZnAlMg coatings can be particularly interesting for the application in the automotive industry. These coatings can be either thinner than traditional zinc coatings or provide higher level of corrosion protection at comparable thickness. In the latter case, additional corrosion protection such as waxes, pre-painting etc. might not be necessary.

Corrosion properties of ZnAl, ZnMg, and ZnAlMg model alloys, Rhesca-coated steel panels, and line products were studied in a number of laboratory and accelerated tests. The effects of relative humidity, temperature, chloride contamination, cyclic exposure conditions, presence of carbon dioxide, confined areas, and forming were addressed.

Addition of aluminum and magnesium decreased the weight loss of zinc-based materials substantially. The effect was usually low up to 1 wt. % of alloying elements. The weight loss dropped strongly with increasing content of Al and Mg from 2 to 5 wt. % and it was low and relatively constant at a higher content of alloying elements. The boundary of 5 wt. % was shifted to 9 wt. % at elevated temperature of 35 or 40°C. In most exposure conditions, the effect of aluminum and magnesium was comparably strong and additional. However, lower alloyed ZnAlMg materials outperformed more alloyed ZnAl under certain exposure conditions. It is supposed that it was due to a synergistic effect of Al and Mg. This behavior was observed mainly in cyclic tests.

Corrosion properties of metallic coatings under static exposure conditions were studied at the relative humidity from 65 to 95 %, temperature from 10 to 40°C, and surface chloride contamination from 500 to 5000 mg/m² in climatic chambers. The weight loss of ZnAlMg coating with 1.5 % of magnesium and the same amount of aluminum was 53–82% lower than that of traditional hot-dip galvanized steel. Galfan (Zn-5Al), ZAM (Zn-6Al-3Mg), Super Dyma (Zn-11Al-3Mg-0.2Si), and Galvalume (Zn-55Al) provided 59–82, 81–93, 76–89, and 77–94% better performance than GI depending on exposure conditions. The alloyed materials were usually less sensitive to the chloride contamination and thus the most efficient at the highest chloride contamination of 5000 mg/m².

Corrosion stability of less alloyed materials with the Al and Mg content from 2 to 5 wt. % was more affected by exposure conditions. They provided somewhat worse protection at low relative humidity of 65 % RH, elevated temperature of 40°C, and reduced content of carbon dioxide in air. They were also less protective when exposed to cyclic exposure conditions with a short dry phase. More alloyed materials with the content of Al and Mg from 9 wt. % provided stable protection little affected by the exposure conditions.

The main aim of this work was to study perforation corrosion of ZnMg(Al) coated steel sheets. Corrosion protection in crevices such as hem flanges is often crucial for lifetime of cars and the application of coatings with magnesium addition could lead to significant cost reduction. In an accelerated automotive test, ZnAlMg coating with 1.5 wt. % of Mg and the same amount of Al with the thickness of 10 µm provided similar protection as Galfan coating at 20 µm in both confined and open configurations. In comparison to hot-dip galvanized steel (GI) with the same thickness of 10 µm, the ZnAlMg coating delayed red rust appearance by a factor of 2 and the maximal depth of corrosion in steel substrate was 42% lower.

Even higher efficiency provided ZnAlMg in the open configuration. In comparison to GI, red rust appeared 4 to 10 weeks later, the maximal depth of corrosion in steel was 66% lower, and the red rusted area after the end of the test was 13 instead of 73 %. The best corrosion resistance was clearly obtained for the same coating with higher thickness of 14 μm .

Red rust appearance on formed panels of Galfan 20 μm and ZnAlMg 7, 10, and 14 μm was delayed in comparison to GI 10 μm by a factor of 2.8, 3.5, 3.8, and >4.5 , respectively. It shows that ZnAl(Mg) panels are well formable as well.

It is supposed that formation of bulk corrosion products with better protective ability was not the reason of the positive effect of alloying elements on corrosion stability of zinc alloys. So far acquired data suggest that the mechanism of aluminum and magnesium protection might be similar. The superior corrosion stability of ZnAl, ZnMg, and ZnAlMg alloys is probably connected to presence of oxide layers with better protective properties than those of zinc-based oxide layers. They may either limit the rate of oxygen reduction or anodic dissolution.

Several research activities should be further undertaken to fully understand the mechanism and application limits of ZnMg and ZnAlMg coated materials. Detail analysis of corrosion products by several complementary techniques, particularly surface sensitive ones and a study of the initial phases of the corrosion process should be done. This is necessary in order to reveal the nature of the protective surface layers providing superior corrosion stability of the alloyed materials. The electrochemistry of these materials in air and water environments should be also studied. Climatic conditions limiting the efficiency of low alloyed ZnAlMg alloys should be addressed, e.g. elevated temperature, low relative humidity, full immersion conditions, and exposure in air with reduced content of carbon dioxide. Corrosion performance in real environments need to be studied as well. On-vehicle exposures and static outdoor exposures in industrial, marine, tropical, and urban conditions are needed for acceptance of these materials by end-users.

Table of contents

1	Introduction	7
2	Aims of the project	8
3	Experimental	9
3.1	Material selection and preparation	9
3.1.1	Model alloys	9
3.1.2	Panels with metallic coatings	11
3.1.3	Painted panels	13
3.2	Laboratory exposure of samples with deposited salts in humid air	14
3.3	Accelerated testing	15
3.4	Characterization of corrosion products	17
3.5	SKP investigation of painted materials	17
3.5.1	Introduction	17
3.5.2	Experimental procedure	18
4	Results and discussion	18
4.1	Metallographic characterization of model alloys	18
4.2	Corrosion testing of model alloys in humid atmosphere	18
4.2.1	Corrosion properties at 20°C and 80 % of RH	18
4.2.2	Soluble species	23
4.2.3	Phase analysis of corrosion products	27
4.2.4	Comparison of ZnAl and ZnAlMg alloys to ZnMg alloys	32
4.3	Corrosion testing of metallic coated panels in humid atmosphere	34
4.3.1	Corrosion properties at 20°C and 80 % of RH	34
4.3.2	Soluble species	38
4.3.3	Phase composition of corrosion products	45
4.3.4	Effect of temperature	47
4.3.5	Effect of relative humidity	51
4.4	Effect of dry time in a cyclic test at 35°C	56
4.5	Effect of CO ₂ on metallic coated panels at 20°C and in air saturated with water	69
4.6	Corrosion in confined areas	75
4.6.1	Renault crevice configuration	75
4.6.2	Volvo crevice panels	79
4.7	Accelerated corrosion testing of formed and flat panels	84
4.8	Evaluation of painted panels with Scanning Kelvin Probe	91
4.8.1	Delamination from scratches	91

4.8.2	Delamination from cut edges.....	93
4.8.3	Delamination from large defects in the polymeric coating	95
5	Summary	98
6	Conclusions	101
7	Agreement with aims of proposal.....	103
8	Acknowledgements	103
9	References	103

1 Introduction

The application of steel construction materials is often linked to the use of protective metallic coatings containing zinc. The coatings provide a barrier and a galvanic protection to steel applied in the automotive, building, and other industries, improving thus durability and aesthetic properties of the final products. In order to increase the performance of zinc coated steel products and to reduce costs, great efforts are invested into the optimization of the zinc coating composition by alloying. Successful examples of the coating development are coatings alloyed with aluminum, e.g. Galfan and Galvalume.

First trials to improve the corrosion performance of zinc coatings with magnesium can be dated back to 1960s [1]. Zhang refers to superior corrosion protection of vapor-deposited zinc alloy coatings containing 10 weight % of magnesium in the salt spray test [2]. This was assumed to relate to the presence of a high relative amount of basic zinc chloride, simonkolleite in corrosion products on the zinc alloy surface. Bruno and Memmi studied ZnMg coatings containing 0.4–1.7 % of Mg [3]. ZnMg galvanized samples were subjected to corrosion testing by intermittent immersion in a solution of artificial seawater. A marked beneficial effect of magnesium was observed. The addition of magnesium was supposed to be efficient because of its ability to restrain attack by chloride ions in a slightly alkaline environment and because of the galvanic protection that it afforded.

Commercial products such as Dymazinc, Superzinc (Zn-5Al-0.1Mg), Super Dyma (Zn-11Al-3Mg-0.2Si), or ZAM (Zn-6Al-3Mg) for heavy corrosive building applications have been available since late 1990s. At the same time, several European steelmakers are developing zinc-magnesium coated products for automotive and building applications using either more traditional hot dipping [1] or physical vapor deposition (PVD) technology [4,5]. In the latter case, magnesium is applied in a thin layer on the surface of electro-galvanized or hot dip galvanized sheets by PVD in vacuum. Zinc-magnesium alloys are thereafter produced by heat treatment.

It was shown that zinc-magnesium coatings have excellent corrosion properties in atmospheric conditions in both non-painted and painted state. MagiZinc™ of Corus, a hot-dip galvanized zinc coating with 1–2 % Mg and 1–2 % Al, provides an improvement in the corrosion stability in salt spray test by a factor 4–20 in comparison to traditional hot dip galvanized materials [1]. A combination of a standard coating process like hot-dip galvanizing or electro galvanizing with a physical vapor deposition (PVD) process to produce zinc-magnesium coatings has been developed by several research teams. Koll *et al.* stated that a considerable improvement of corrosion performance of ZnMg coated steel products was observed while other properties like weldability, formability, and paint adhesion were comparable or better than that of an untreated galvanized material [4]. Formation of red rust on unpainted samples tested in accelerated corrosion tests was delayed with a factor 8–13 compared to an HDG reference. The onset of both red rust formation and undercreep of samples painted with different types of automotive paints was significantly delayed at scratches down to zinc and at places of stone chipping damage for ZnMg coated samples, i.e. 20 weeks instead of 3–4 weeks.

Schwerdt *et al.* described corrosion, forming, and joining performance of ZnMg materials produced in a continuous pilot line at DOC Dortmunder Oberflächencentrum GmbH in a combined electro galvanizing and PVD process [5]. In salt spray testing, ZE-Mg 35/35 (3.0–3.5 μm of Zn and 0.4–0.6 μm of MgZn₂ intermetallic phase) displayed corrosion resistance twice than that of conventional electro galvanized sheet ZE 75/75. By retaining the layer of around 7.5 μm for ZE-Mg 75/75 (7.0–7.5 μm of Zn and 0.8–1.6 μm of MgZn₂ intermetallic phase), the corrosion resistance compared to that of ZE 75/75 was higher by a factor of 10. The delamination at scribe marks on ZE-Mg 75/75 was reduced by a factor from two to five.

Hosking et al.[6,7] tested similar coatings consisting of about 2- μm MgZn_2 layer on an EG-deposited Zn layer of 6 μm in a standard automotive laboratory corrosion test comprising cycles of humidity, drying and intermittent spraying with 1 wt. % NaCl solution at pH 4.2. The time to appearance of significant red rust was 3 times longer for ZnMg compared to the EG and HDG references.

In recent investigations carried out at Institut de la Corrosion / French Corrosion Institute, it was found that the presence of Mg^{2+} ions decreased corrosion of zinc considerably. Magnesium ions inhibited the atmospheric corrosion of zinc with deposited chloride at temperatures ranging from 10 to 40°C, relative humidity ranging from 64–98 %, and surface chloride concentrations ranging from 700 to 2800 mg/m^2 [8–10]. The inhibition was observed even when magnesium formed only a minor part in a mixture of deposited cations. This strong positive effect of magnesium ions was also found in lapped areas of galvanized steel. The corrosion of coil-coated steel at cut-edges and scribes was significantly reduced under mud containing magnesium salts compared to that containing NaCl at the same chloride concentrations.

The following study showed that the alloying of zinc with magnesium substantially decreased weight loss of ZnMg alloys in atmospheric conditions in the presence of chloride [11]. The effect of magnesium was the most profound at 4–8 wt. % magnesium in the structure. Weight loss of these alloys was up to 10-fold lower than that of zinc. The superior corrosion properties of ZnMg alloys were connected to the presence of magnesium-containing phases $\text{Mg}_2\text{Zn}_{11}$ and MgZn_2 . The results indicated that the former phase provided the best corrosion stability. The phases were covered with a magnesium-based oxide film. Contrary to zinc oxide, it was stable even in chloride environments, forming an interlayer adjacent to the metal surface. It was proposed that the film ensured stable passivity of ZnMg alloys due to a lower potential gradient across the metal/metal oxide/electrolyte interface. Moreover, the film is supposed to be more insulating, reducing the rate of electron transfer and hindering oxygen reduction. The positive effect of magnesium disappeared when the increasing content of magnesium in the metal structure caused such a shift in the free corrosion potential that enabled water reduction reaction. Therefore, the optimal corrosion protection of ZnMg alloys in atmospheric conditions is probably related to a combination of more noble free corrosion potentials close to that of zinc and the presence of magnesium-based oxide films providing good barrier properties to ion and electron transfer.

Based on the results of mentioned research and commercial activities, it is clear that magnesium addition to zinc coatings leads to improvement of their corrosion performance. This is particularly interesting for applications in the automotive industry. Corrosion resistance is an important property requirement for materials used in car production. Car manufacturers are pushed to look for alternative ways of corrosion protection due to regulations limiting the use of hexavalent chromium compounds. Moreover, the rising price of raw zinc pushes carmakers to seek ways for reduction of the zinc coating thickness. ZnMg coatings can be either thinner or provide higher level of corrosion protection at a thickness comparable to traditional zinc coatings. In addition, a positive effect of magnesium is also expected in lapped areas. In this latter case, additional corrosion protection such as waxes, pre-painting etc. might not be necessary. However, there is only limited understanding to the mechanism of corrosion protection of the coatings and several aspects of their eventual application were only touched or even fully omitted.

2 Aims of the project

The main objectives of this project were:

- *To evaluate the corrosion stability of non-painted ZnMg coated panels during several laboratory and accelerated tests.* The effect of temperature, relative humidity, and detrimental ions

contamination on corrosion of cosmetic panels were addressed. The objective was to gain a greater understanding of the influence of climatic parameters on the degradation of ZnMg coated steel.

- *To study perforation corrosion (corrosion protection in crevices, hem flanges) of ZnMg coated steel sheets.* This constituted a new approach in research of corrosion properties of ZnMg coatings. Important gaps of knowledge were identified in available literature on behavior of ZnMg in shield areas, which is often crucial for the capability of car bodies to resist corrosion deterioration.
- *To understand the mechanisms of the protective action of magnesium in the coatings.*

3 Experimental

3.1 Material selection and preparation

3.1.1 Model alloys

Zinc, aluminum, and magnesium with purity of 99.99 % were used for alloys preparation. Melting was performed in an electrical resistance furnace without use of inert atmosphere. Maximum melt temperature before pouring into a mould was 150 K higher than the temperature of liquidus of each alloy. A mould with quatrefoil section was used in order to eliminate microshrinks. Binary ZnAl and ternary ZnAlMg phase diagrams are given in Figure 1 and Figure 2.

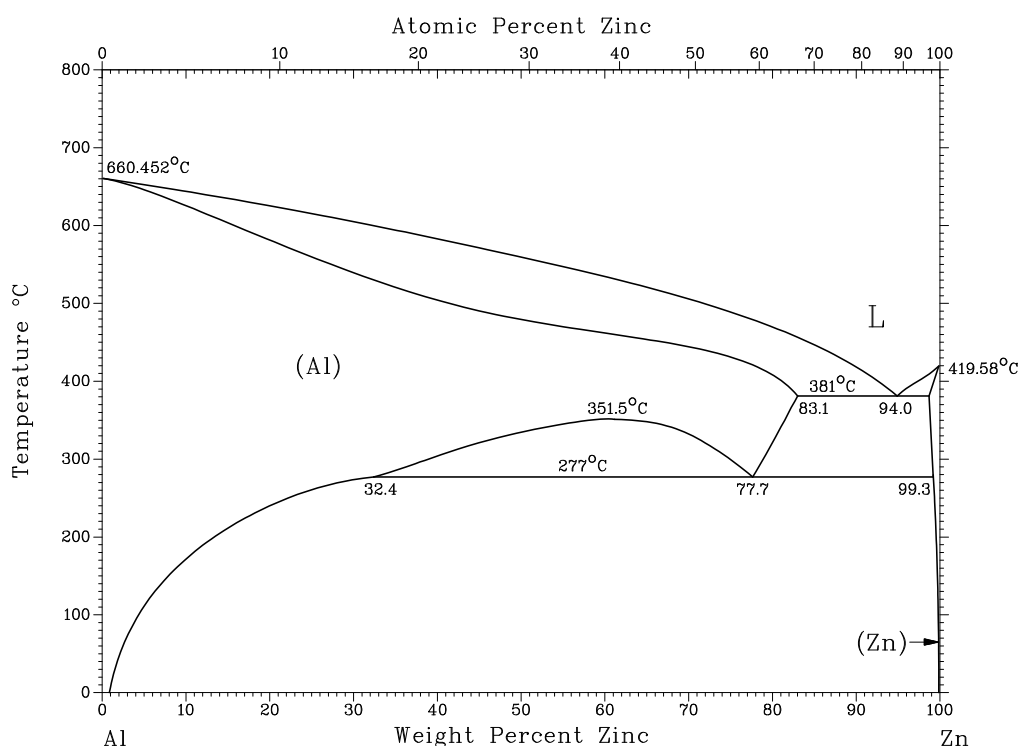


Figure 1 ZnAl phase diagram

The chemical composition of the alloys was determined using energy dispersive x-ray diffraction (EDX) technique. Each alloy was analyzed three times. The results are summarized in Table 1.

The behavior of ZnAl and ZnAlMg model alloys will be compared to that of ZnMg alloys studied in a previous project [12]. The phase diagram of ZnMg is shown in Figure 3 and the chemical and phase composition of these last alloys are given in Table 2.

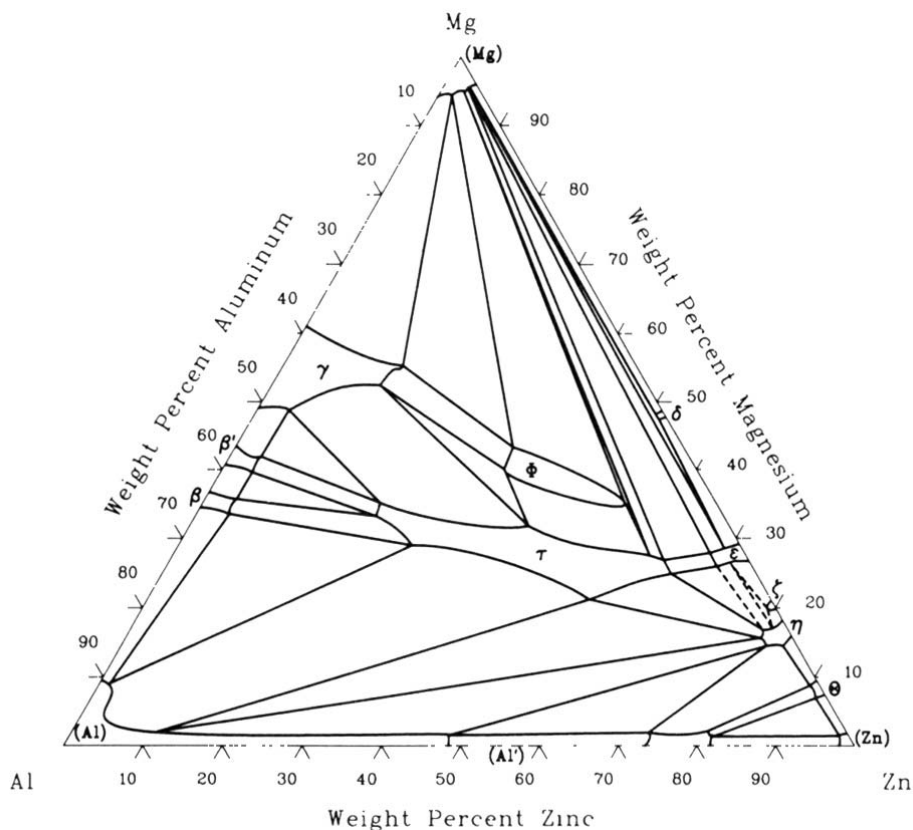


Figure 2 ZnAlMg isothermal section at 20°C

Table 1 Chemical composition of ZnAl and ZnAlMg model alloys; in weight % (impurities max. 0.01 %)

Alloy	Zn	Mg	Al
Zn	99.99	–	–
Mg	–	99.99	–
Al	–	–	99.99
ZnAl0.2	99.81	–	0.18
ZnAl0.5	99.55	–	0.45
ZnAl1	98.86	–	1.13
ZnAl2	97.68	–	2.31
ZnAl5	95.07	–	4.92
ZnAl11	89.40	–	10.59
ZnAl55	43.87	–	56.12
ZnAl1Mg1	97.65	1.11	1.23
ZnAl2Mg2	95.85	2.22	1.92
ZnAl5Mg5	90.09	5.12	4.78

Microstructures of the alloys were studied by light microscope Olympus PME 3 equipped with an image analyzer after etching in aqueous solution containing 5 % CrO₃ and 0.4 % Na₂SO₄. The phase composition was measured by x-ray diffraction analysis using a Philips X'PERT PRO equipment.

Rods of 20 mm in diameter were prepared by mechanical machining and cut to 5–7 mm high samples. In all experiments, the bottom and side faces of the samples were masked with a tape. The exposed surface area was 3.14 cm².

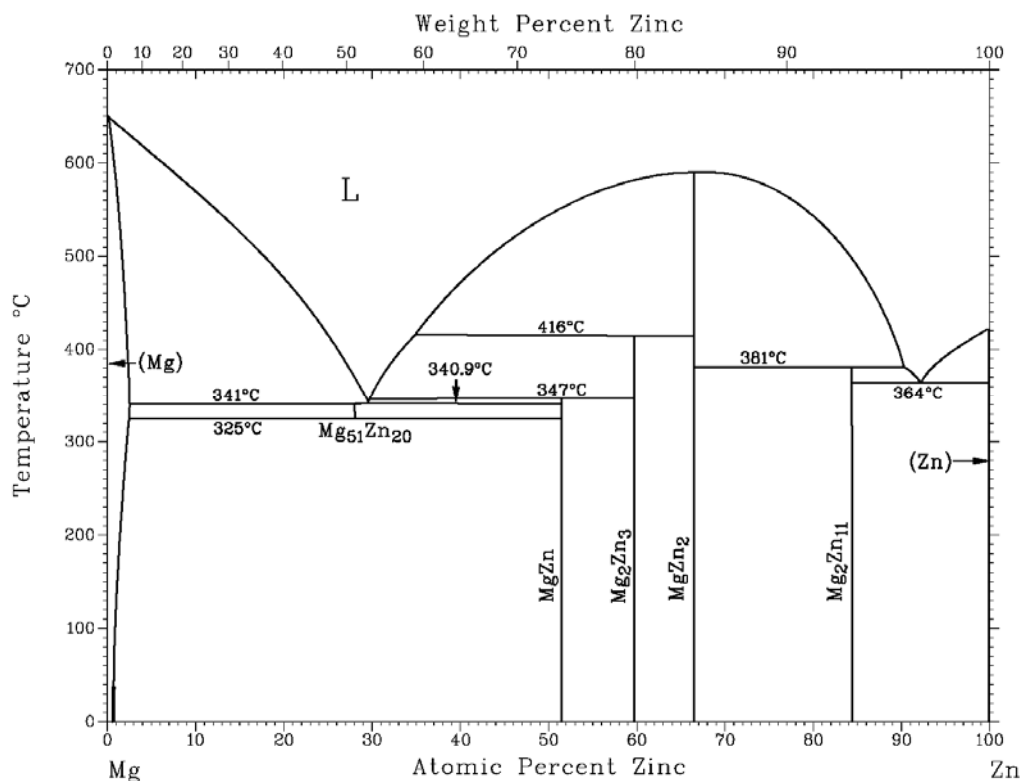


Figure 3 Mg-Zn phase diagram [11]

Table 2 Chemical and phase composition of model ZnMg alloys

Alloy	Zn [wt. %]	Mg [wt. %]	Phase composition*
ZnMg1	98.92	1.07	67 % η -Zn, 33 % Zn+ Mg_2Zn_{11} eutectic
ZnMg2	97.90	2.09	65 % Zn+ Mg_2Zn_{11} eutectic, 35 % η -Zn
ZnMg4	95.77	4.22	71 % Zn+ Mg_2Zn_{11} eutectic, 29 % MgZn ₂
ZnMg6	93.77	6.22	83 % Mg_2Zn_{11} , 17 % MgZn ₂
ZnMg8	92.06	7.93	53 % Zn+ Mg_2Zn_{11} eutectic, 47 % MgZn ₂
ZnMg16	84.89	15.10	100 % MgZn ₂
ZnMg32	68.64	31.35	51 % Mg+MgZn eutectoid, 49 % MgZn

* Approximate volume fraction of each phase was obtained by image analysis

3.1.2 Panels with metallic coatings

Steel panels coated with ZnAlMg alloy were used in the study. The materials were line-produced by hot dipping and contained about 1.5 wt. % of magnesium and 1.5 wt. % of aluminum. Panels with three different coating thicknesses were studied. For selected experiments, samples differing in the coating composition prepared in a Rhesca simulator were used as well. As reference materials, carbon steel (CRS), hot dip galvanized steel (GI), electro-galvanized steel (GE), Galfan, Super Dyma (SD), ZAM, and Galvalume (AZ) were selected. A list of materials is given in Table 3.

Before each experiment, samples were cut to desired size, cleaned in ethanol in an ultrasonic bath and degreased with acetone.

Formed cup-shaped samples were tested in an accelerated corrosion test. Specimens were prepared by punching with the process parameters given in Table 4. A photograph of a formed panel is given in Figure 4.

Table 3 Coated steel and reference materials used in the study

Material	Composition [wt. %]		Coating thickness		Ref. in this document
	Al	Mg	[μm] ²	[g/m^2] ³	
ZnAl1.5Mg1.5 50	1.5	1.5	7	100	HD ZnAlMg 7 μm
ZnAl1.5Mg1.5 70	1.5	1.5	10	140	HD ZnAlMg 10 μm
ZnAl1.5Mg1.5 100	1.5	1.5	14	200	HD ZnAlMg 14 μm
ZnAl0.3Mg1.2 (Rhesca Simulator)	0.3	1.2	12	170	Rhesca Mg 1.2
ZnAl1.2Mg1.2 (Rhesca)	1.2 ¹	1.2 ¹	13	190	Rhesca AlMg 1.2
ZnAl1.4Mg1.3 (Rhesca)	1.4 ¹	1.3 ¹	26	370	Rhesca AlMg 1.4
ZnAl1.6Mg1.6 (Rhesca)	1.6 ¹	1.6 ¹	22	310	Rhesca AlMg 1.6
ZnAl1.8Mg1.8 (Rhesca)	1.8 ¹	1.8 ¹	8	120	Rhesca AlMg 1.8
ZnAl2.0Mg2.0 (Rhesca)	2.0 ¹	2.0 ¹	5	65	Rhesca AlMg 2.0
Carbon steel reference	–	–	–	–	CRS
Hot dip galvanized reference	low	0	10	140	GI 10 μm
Hot dip galvanized reference	low	0	20	280	GI 20 μm
Electro galvanized reference	low	0	9	130	GE
Galfan reference	5	0	20	265	Galfan
Super Dyma reference	11	3	18	200	SD
ZAM reference	6	3	20	200	ZAM
Galvalume reference	55	0	20	150	AZ

¹ Composition of bath; the composition of the coating is usually 0.1–0.2 % higher in Al; ² Each side;

³ Approximate total coating weight, i.e. both sides

Table 4 Process parameters used for the punching of the formed panels

Tester	Bruine
Speed	60.000 mm/min
Max. amount of sheet drawing force	44.098 kN
Max. amount of punch stroke	33.200 mm
Initial value of sheet holder force	40.000 kN
Type of lubrication	n6130
Sample thickness	0.8 mm
Blank size	95 mm
Punch diameter	50 mm
Die	54.78



Figure 4: Photograph of a formed panel (after one week in the Volvo test cycle)

3.1.3 Painted panels

Selected materials with metallic coatings were painted by cathoresis in an industrial production line. The materials are listed in Table 5. Two different designs of crevice panels, denoted as ‘Renault’ and ‘Volvo’ were prepared using the painted panels.

Table 5 Painted materials used for the crevice testing

Material	Ref. in this document	Metallic coating thickness [μm]	Organic coating thickness [μm]
ZnAl1.5Mg1.5 50	HD ZnAlMg 7 μm	7	~20
ZnAl1.5Mg1.5 70	HD ZnAlMg 10 μm	10	~20
ZnAl1.5Mg1.5 100	HD ZnAlMg 14 μm	14	~20
Carbon steel reference	CRS	–	~20
Hot dip galvanized reference	GI	10	~20
Galfan reference	Galfan	20	~20

Renault crevice panels. A scheme and photograph of the Renault crevice panel are shown in Figure 5. Two panels of 100×50 and 20×50 mm were laser-cut in order to assure a flat geometry. The panels were assembled to gap 0 and painted using a standard procedure applied in the automotive industry. The sample was phosphated and painted by cathoresis. After the paint application, it was disassembled and a gap ranging from 0 to 250 μm was formed by fixing a 250- μm PTFE spacer on one side of the uncoated surface. The panels were joined with plastic screws and nuts using a torque of 0.2 N·m.

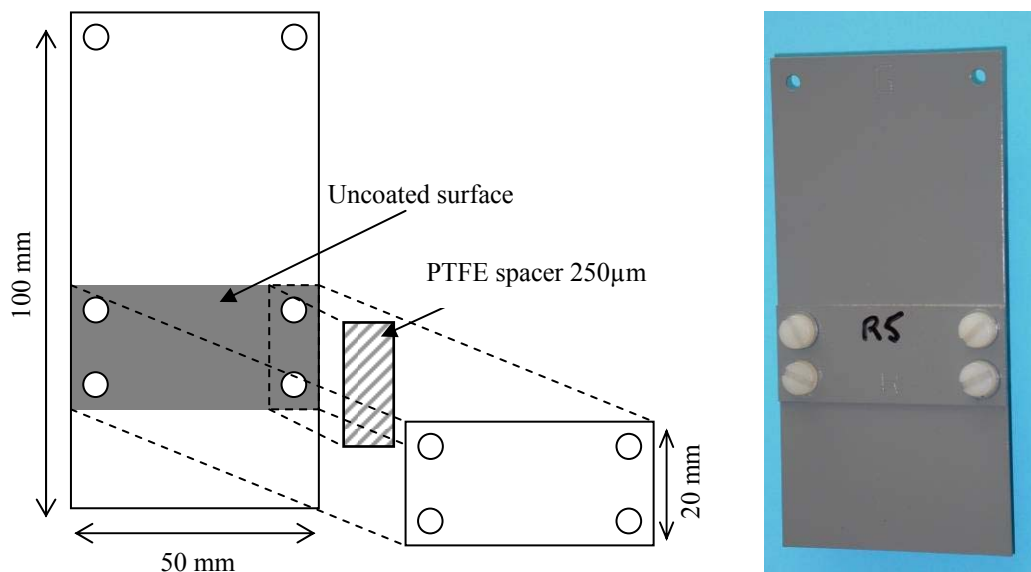


Figure 5: Scheme and photograph of the Renault crevice panel

Volvo crevice panels. A photograph of the Volvo crevice panel is shown in Figure 6. Temperature resistant polyester tape Shercon PC21 was used to mask a rectangular area of 66×20 mm centered on the surface of a laser-cut sheet. The sample was phosphated and painted in an industrial production line. The tape was removed after cathoresis. Crevice test samples were obtained by fixing a standard microscope glass slide of 75×25 mm with plastic clips over the unpainted metallic surface. A 250- μm Teflon spacer was applied on one side of the glass in order to obtain a gap in between 0 and 250 μm .

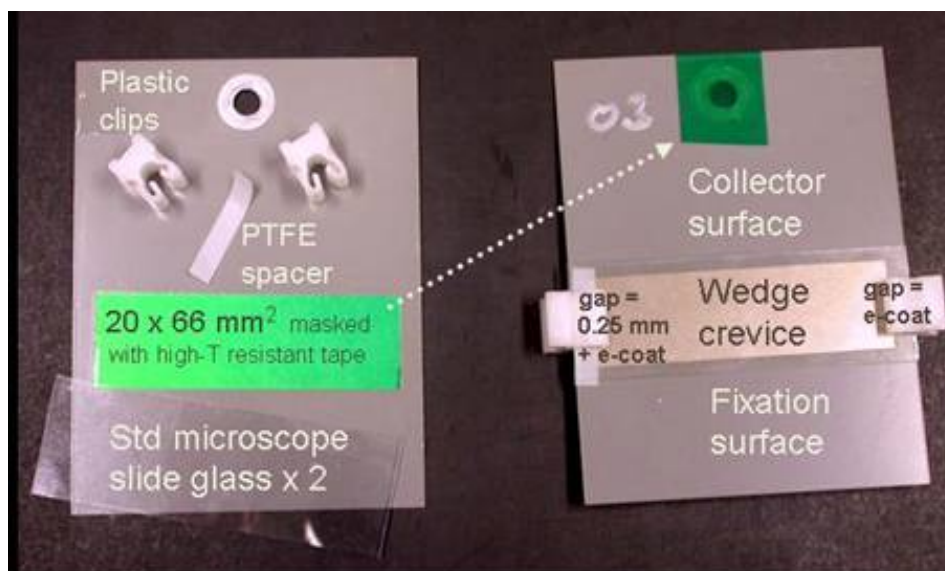


Figure 6 Photograph of the Volvo crevice panel from Ref. 13

3.2 Laboratory exposure of samples with deposited salts in humid air

In order to accelerate the corrosion process, sodium chloride was deposited on the surface of model alloys and coated steel panels with diameter of 20 mm and size of 40×40 mm (or 50×32 mm), respectively. The exposed area was 314 and 1600 mm². Samples of model alloys were polished to 400-grit paper in ethanol, dried in air and stored in a desiccator over silica gel. Coated panels were used as-received. They were only cleaned in ethanol and degreased in acetone. All samples were weighted after a minimum of 24 hours of drying in a desiccator and a salt solution was applied to the surface.

Solutions of sodium chloride in a mixture of ethanol and water or methanol and water were prepared and applied with a micropipette in two or four doses. The deposit on the sample surface was dried out before application of the next dose. This procedure ensured rather even distribution of salt deposits over the surface. Solutions, application conditions, and composition of obtained deposits are reviewed in Table 6.

Table 6 Application of NaCl deposits to metal samples

Sample type	Solution*	NaCl concentration in solution [g/l]	Applied volume [μl]	Surface chloride deposits [mg/m ²]
Alloy	Ethanol 76%**	4.04	2 × 32	500
Alloy	Ethanol 76%**	11.32	2 × 32	1400
Coating	Methanol 88%	6.59	2 × 100	500
Coating	Methanol 88%	11.32	2 × 100	1400
Coating	Methanol 76%	32.96	2 × 100	2500
Coating	Methanol 76%	32.96	2 × 100	5000

* Volume concentration of ethanol or methanol in water solution; ** Sodium chloride is more soluble in methanol/water mixture, but ethanol/water was used for this test condition to allow comparison to results previously obtained for ZnMg model alloys

The chloride surface concentration from 500 to 5000 mg/m² was selected to model conditions in natural coastal atmospheres, where deposition rates 10–4000 mg/m²·day of Cl⁻ have been reported [14]. In

Australian marine environments, 120, 45, and 15 mg/m²-day of salt are typical of conditions at a distance of approximately 100 meters from surf beaches, protected surf beaches, and bay beaches, respectively [15].

Samples with salt deposits were stored for 48 hours in a desiccator to dry out completely and thereafter weighted and exposed for 28 days in a climatic chamber at different conditions. The samples were weighted during exposure to monitor the kinetics of the corrosion process. The wet mass gain was measured rather than the dry mass gain in order to minimize the disturbance of the corrosion process. Additionally, photos of the samples were taken at the same time. At the end of exposure, panels were allowed to dry in a desiccator over silica gel for 48 hours and the dry weight gain was recorded. Weight loss was measured after removal of masking tape from the back side and pickling in saturated solution of glycine for 10 minutes.

Some specimens were tested in ambient air and CO₂-free air at 100 % of relative humidity. For this test, two hermetic boxes were used. Ambient air and CO₂-free air passing through flasks with water were fed into the boxes. Carbon dioxide was removed from air using an absorber VCD3-21 from Twin Tower Engineering. The relative humidity and CO₂ content were not monitored during the experiment. The CO₂ content was measured by FTIR before the test and it was below 1 ppm. The relative humidity was between 95 to 100 % prior to the test. It is expected to be close to 100 % during exposure. A photograph of the experimental set-up is given in Figure 7.

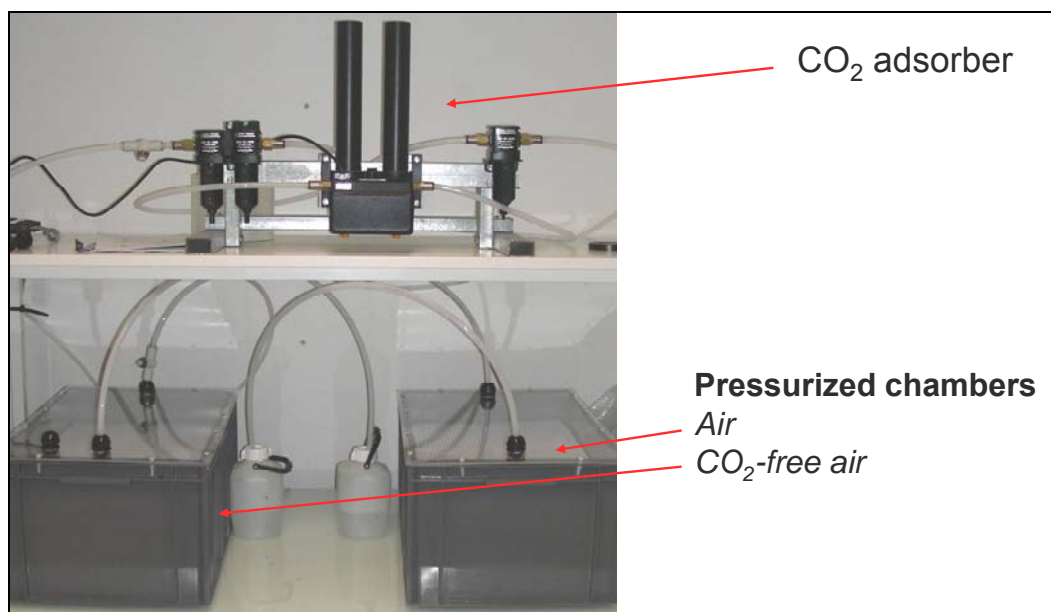


Figure 7: Photograph of the experimental set-up for the ambient air / CO₂-free air test

3.3 Accelerated testing

Painted, non-painted, and formed panels with different metallic coatings were tested in an automated test chamber in accordance with the standard procedure Volvo VCS1027, 149-ACT (ACT). This cyclic accelerated corrosion test provides significantly better correlation to a mode and extent of degradation observed in real exposure conditions than the traditional neutral salt spray test. The test runs at cyclic temperature ranging from 35 to 45°C. The relative humidity varies between 50 and 95 %. Twice a week, samples are sprayed with sodium chloride solution containing 1 wt. % NaCl at pH 4. A weekly cycle of the test is described in Figure 8 and characteristics of the test are given in Table 7. The total test duration was 6 weeks for specimens in Renault crevice configuration, and 18 weeks for specimens in Volvo crevice configuration.

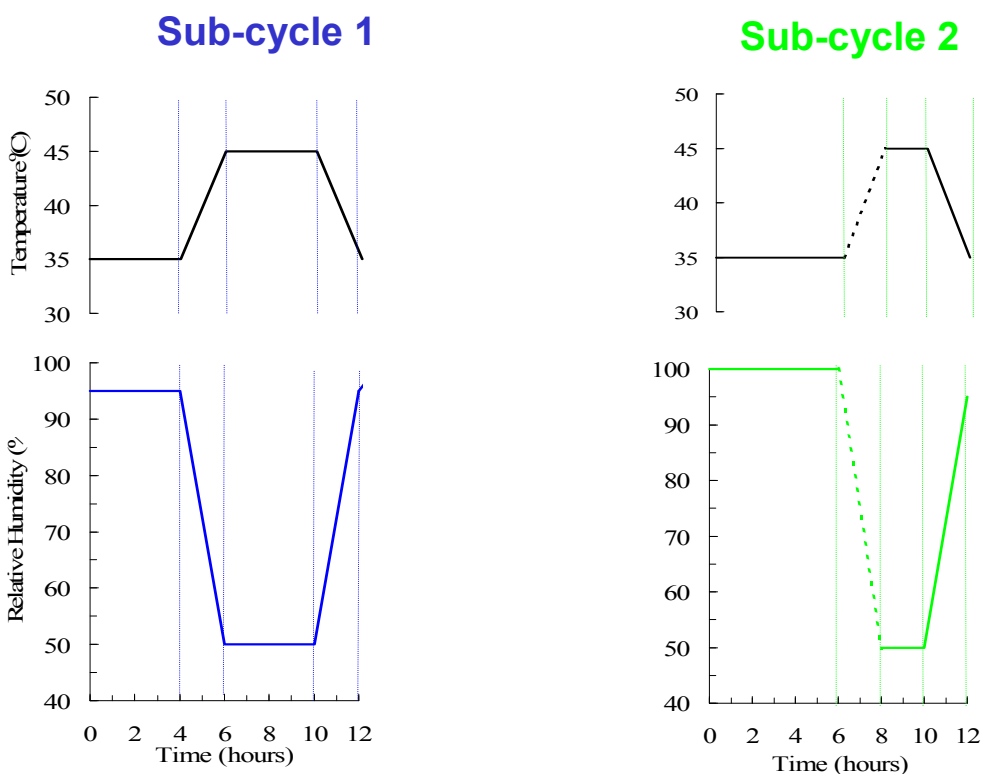
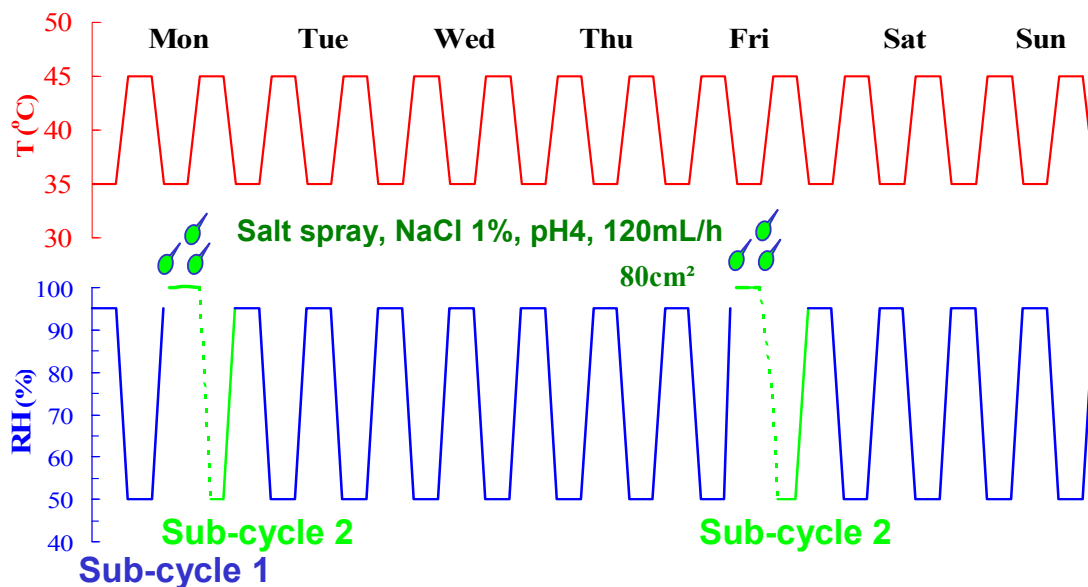


Figure 8 Weekly cycle of the Volvo ACT test

Table 7 Characteristics of the Volvo ACT test

Pollution			T	RH	ToW*	Typical duration
Salt solution	Frequency	Cl ⁻ deposition [mg/cm ² , test]	[°C]	[%]	[%]	[days]
NaCl 1% wt, pH 4, 120 ml/h	3x15 min twice a week 1.5h/week	27	45 35	50, 4 h 95, 4 h	~44	42

* Time of wetness: Percentage of time when RH > 80 %

3.4 Characterization of corrosion products

Leaching experiments have been conducted to enable the determination of the amount of soluble ions on the metal surface after exposure. Before pickling, corrosion products on the surface of selected samples were dissolved in 60 ml of deionized water in an ultrasonic bath for 10 minutes at laboratory temperature. The solutions obtained in the above-described procedure were analyzed for the concentration of zinc, magnesium, sodium, and chloride ions with *ion chromatography (IC)*. pH of the solutions was measured as well.

Corrosion products formed on the metal surface were analyzed by *Fourier transformed infrared spectroscopy (FTIR)*. Samples were analyzed using the KBr pellet method. A small mass of 0.70 mg of corrosion products or a reference mineral was mixed with a spectroscopic grade potassium bromide (KBr) powder to obtain 140 mg of a mixture. The mixture was then grinded in a mortar and pressed to pellets in a die. Spectra were obtained by adding 16 scans at 8 cm^{-1} resolution in the range from 220 to 4000 cm^{-1} . The background spectrum was obtained from a pure KBr pellet of the same weight and size.

X-ray powder diffraction (XRD) data of corrosion products were collected at a room temperature with an X'Pert PRO θ - θ powder diffractometer with parafocusing Bragg-Brentano geometry using CuK_α radiation ($\lambda = 1.5418\text{ \AA}$, $U = 40\text{ kV}$, $I = 30\text{ mA}$). The data were scanned over the angular range 5 – 80° (2θ) with a step size of 0.02° (2θ) and a counting time of 0.3 s/step . The data were evaluated using the HighScore Plus software package. These measurements were performed at Institute of Chemical Technology, Prague.

3.5 SKP investigation of painted materials

3.5.1 Introduction

SKP is *in situ* electrochemical method that provides information about corrosion processes taking place at the metal surface below polymeric coating [16-24]. SKP is able to determine the mechanism of the degradation, stability of adhesion, activation of the metal surface, location of rust clusters, and distribution of anodic and cathodic zones. The mechanism of cut edge corrosion and coating delamination from defects was investigated for steel and galvanized steel. It was shown that corroding metal in the defect and surrounding metal beneath the polymer coating form a galvanic couple that leads to cathodic delamination of the coating starting from the defect. Cathodic delamination is caused by the electrode potential difference between a defect in the paint and the surrounding intact area. Cathodic delamination is the main mechanism of failure for carbon steel/polymer and galvanized steel/polymer joints.

Corrosion of steel beneath a thin intact model coating was studied by SKP, EIS and scanning acoustic microscopy [20]. It was found that the metal was anodic in the defect with respect to the surrounding area at the beginning. However, a gradual increase in the potential of the metal in the defect due to formation of rust took place in time. Iron corrosion products blocked the defect area and started to be cathodic relatively to the surrounding intact metal/polymer interface. This study showed that steel in a defect can be anode or cathode depending on the time of exposure.

MgZn_2 phase and ZnAlMg alloys are not prone to cathodic delamination from defects in a polymer coating [17]. The rate of de-adhesion decreases by orders of magnitude and the potential profile is reversed comparing to zinc coatings. The effect was explained by the presence of a magnesium oxide layer decreasing the rate of oxygen reduction.

Coating delamination from edges of galvanized steel panels is governed by the anodic undermining mechanism [24]. In this case, the cathodic reaction of oxygen reduction is taking place on steel surface at the edge and the anodic front spreads from the edge to the intact metal/polymer interface.

Above-mentioned SKP studies were carried out using model metal/polymer systems with low corrosion stability. The goal of the present prescreening study was to apply SKP for evaluation of the delamination mechanism of industrially coated zinc, zinc-aluminum, and zinc-magnesium alloys.

3.5.2 Experimental procedure

A SKP vibrating condenser from UBM Messtechnik was used allowing measurement of the geometrical profile and Volta potential distribution over a metal surface in atmospheres of different gases and humidity. The air gap between substrate and probe was kept at 50 μm , vibration frequency around 2 kHz and the vibration amplitude 20 μm . The Volta potential of the probe, CrNi alloy needle with diameter of the tip of 80 μm , was calibrated above a Cu/CuSO₄ electrode in humid air. The Volta potential is given relatively to the Standard Hydrogen Electrode (SHE). Previous calibration results indicate that the change in the Volta potential of the probe material in different atmospheric environments is small, 10–15 mV.

The Volta potential difference $\Delta V_{p/s}$ depends on the probe-to-polymer distance. A surface contour measurement was made prior to each potential measurement to keep the gap constant at 50 μm . The accuracy of the geometrical profile measurement is about 1–3 μm .

4 Results and discussion

4.1 Metallographic characterization of model alloys

Metallographic samples were prepared by conventional metallographic technique and studied by a light microscope. Structures of the alloys and their phase composition analyzed by XRD are described below. Images of the microstructures of ZnAl and ZnAlMg alloys are shown in Figure 9 and Figure 10, respectively.

ZnAl0.2 and ZnAl0.5 were formed of grains of Zn solid solution clearly separated by grain boundaries with the average grain size of about 150 μm . Traces of aluminum phase were detected in ZnAl0.5 by XRD. ZnAl1 and ZnAl2 were composed of grains of Zn solid solution with average size of 90 μm surrounded by Zn+Al eutectic. The amount of the eutectics was higher for ZnAl2. ZnAl5 alloy contained Zn+Al eutectic grains with the average grain size of 490 μm . In alloys ZnAl11 and ZnAl55, primary α -Al dendrites were surrounded by Zn+Al eutectic. Al dendrites appear dark in the structure of ZnAl11 and light in ZnAl55.

ZnAl1Mg1 and ZnAl2Mg2 alloys were composed of dendrites of Zn solid solution (light phase) and Zn+Mg₂Zn₁₁ eutectic. Al phase was identified in XRD spectra. ZnAl5Mg5 contained particles of Zn solid solution (light phase), ZnMg₂, and Zn+Mg₂Zn₁₁ eutectic. Al phase was also identified in XRD spectra.

4.2 Corrosion testing of model alloys in humid atmosphere

4.2.1 Corrosion properties at 20°C and 80 % of RH

The wet mass gain versus time was measured for all model alloys to follow the corrosion kinetics of the specimens. It must be mentioned that wet mass gain is both due to water absorption in the layer of NaCl deposits on the metal surface and to the formation of corrosion products. Examples of these measurements are given in Figure 11 and in Figure 12 for chloride contaminations of 500 and 1400 mg/m², respectively. Model alloys can be separated into 3 groups at both chloride concentrations. The first group contains Zn, ZnAl0.2, ZnAl0.5 and ZnAl1. Their weight gain increased rapidly with time and stabilized after about two weeks of exposure. The second group consists of ZnAl2 (which would actually be between group 1 and 2),

ZnAl1Mg, ZnAl2Mg2, ZnAl5Mg5, and Al. The weight gain of these alloys increased slowly and did not completely stabilize before the end of the exposure. The third group is composed of ZnAl5, ZnAl11, and ZnAl55. Their weight gain remained rather low during the exposure and did not change after Week 2 of exposure. In general, the wet weight gain decreased with the content of alloying elements. The weight gain after drying for 48 hours in a desiccator over silica gel is given in Figure 13. It shows similar trends.

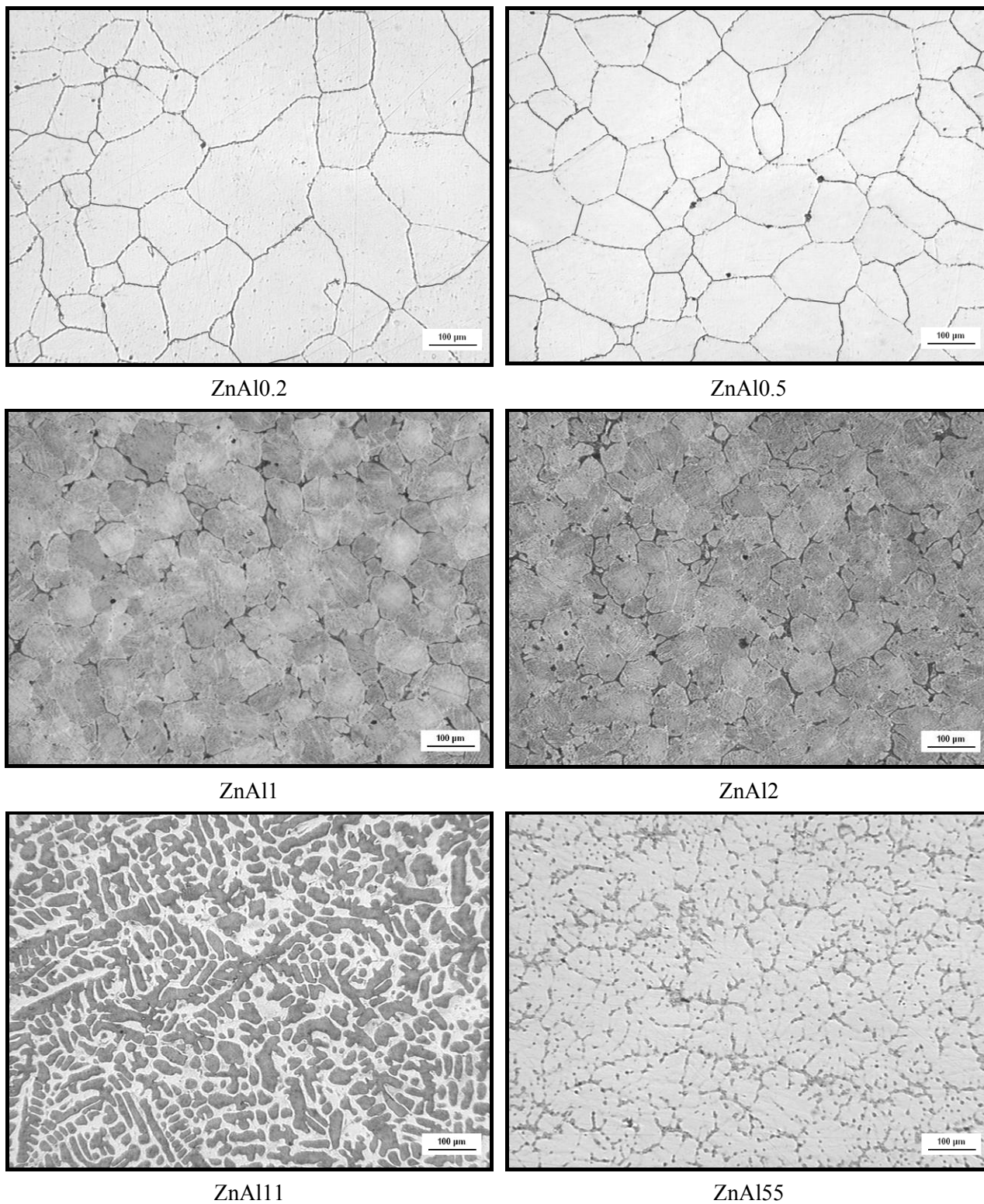


Figure 9 *Microstructure of ZnAl alloys*

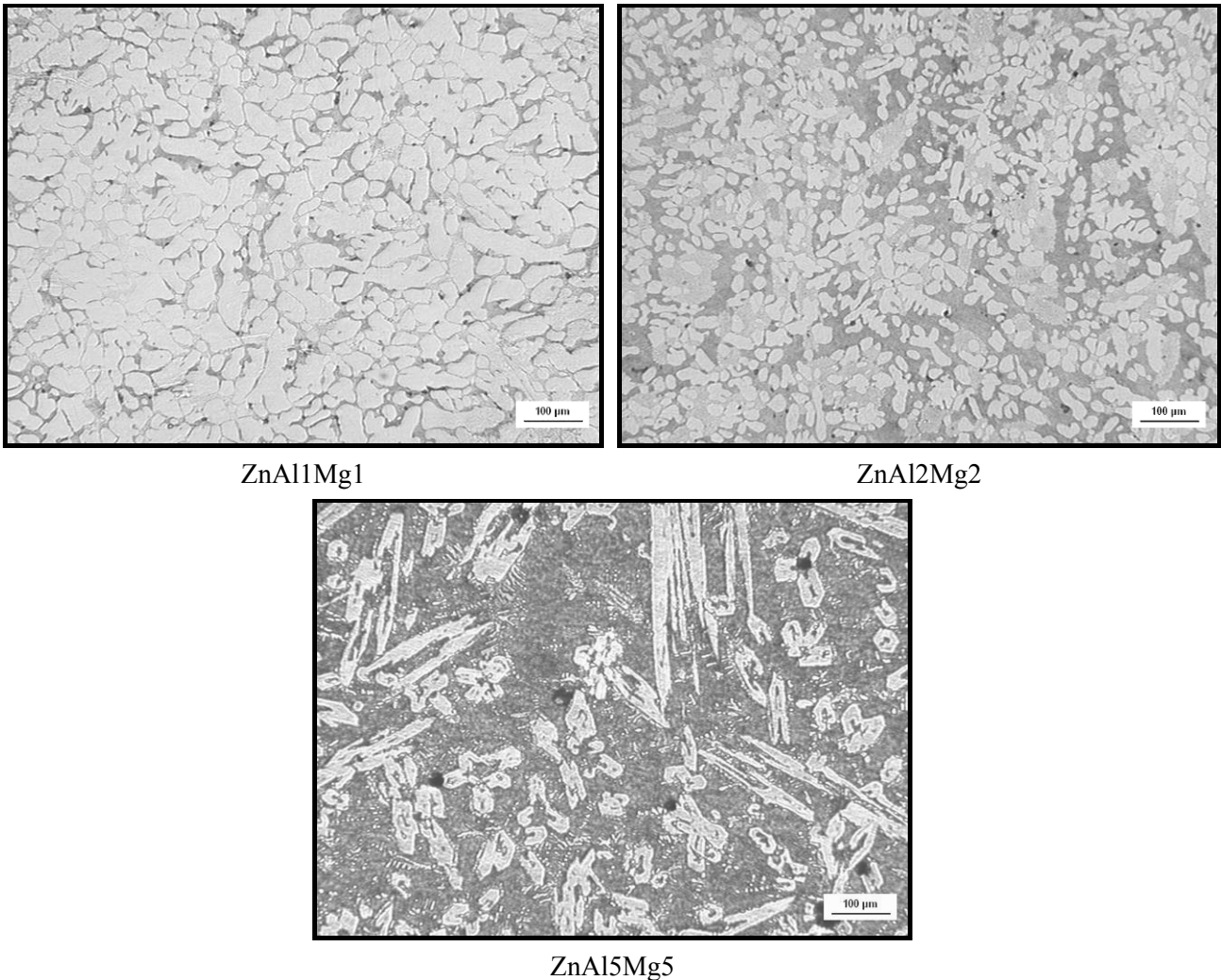


Figure 10 *Microstructure of ZnAlMg alloys*

The weight loss of model alloys after 4 weeks of exposure at 20°C and 80 % of relative humidity (RH) is given in Figure 14 and is in agreement to the previous measurements. Weight loss is logically higher for specimens contaminated with 1400 mg/m² of chloride than for specimens contaminated with 500 mg/m² (from 1.1 to 2.6 times). For ZnAl model alloys, the weight loss decreased with the increasing amount of aluminum. For specimens contaminated with 1400 mg/m² of chloride, a strong decrease in the weight loss was observed from 1 to 5 % of Al in the structure, see Figure 15. The effect of aluminum addition up to 1 wt. % seems to be negligible. A slower decrease in the weight loss as a function of the aluminum content in the alloy was seen over 5 wt. % of Al. For specimens contaminated with 500 mg/m² of chloride, the weight loss was lower than that of zinc even for alloy with only 0.2 % of Al in the structure. From 0.2 % to 5 % Al, strong and approximately linear dependence of the weight loss on the aluminum content was observed as for specimens contaminated with 1400 mg/m² of chloride. The weight loss was about 6 times lower for model alloys with 55 % of Al than for specimens with 11 % of Al at both levels of the chloride contamination. The weight loss of ZnAl55 was even lower than that of aluminum.

The weight loss of model alloys containing both Al and Mg decreased with the Al+Mg content, see Figure 14 and Figure 15. It seems that the effect of Al and of Mg was additive under these experimental conditions. Indeed, similar corrosion rates are observed for ZnAl2 and ZnAl1Mg1 with the total alloying of 2 %, for ZnAl5 and ZnAl2Mg2 with the total alloying of 5 and 4 %, and for ZnAl11 and ZnAl5Mg5 with the total alloying of 11 and 10 %. This is well visible in Figure 15, where the effect of the total alloying is plotted against the weight loss for both groups of model alloys.

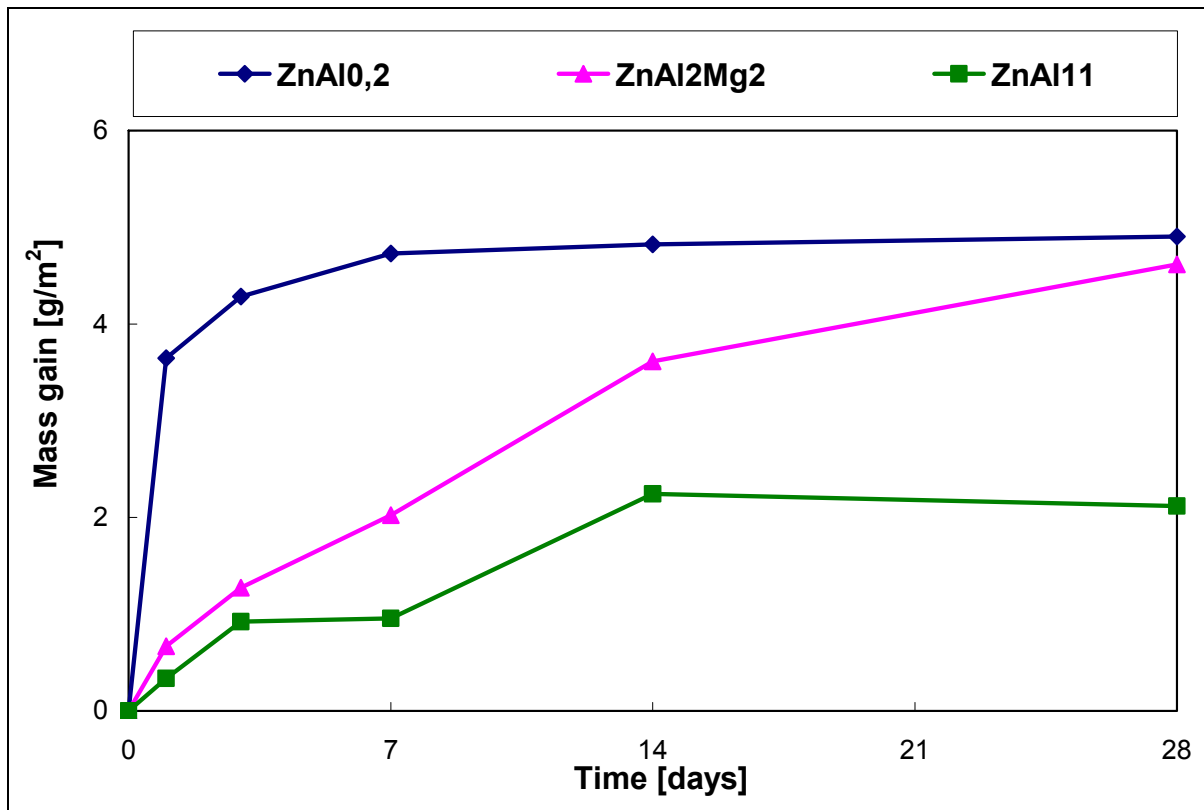


Figure 11 Wet mass gain of some model alloys with chloride contamination of 500 mg/m² during exposure at 20°C and 80 % RH

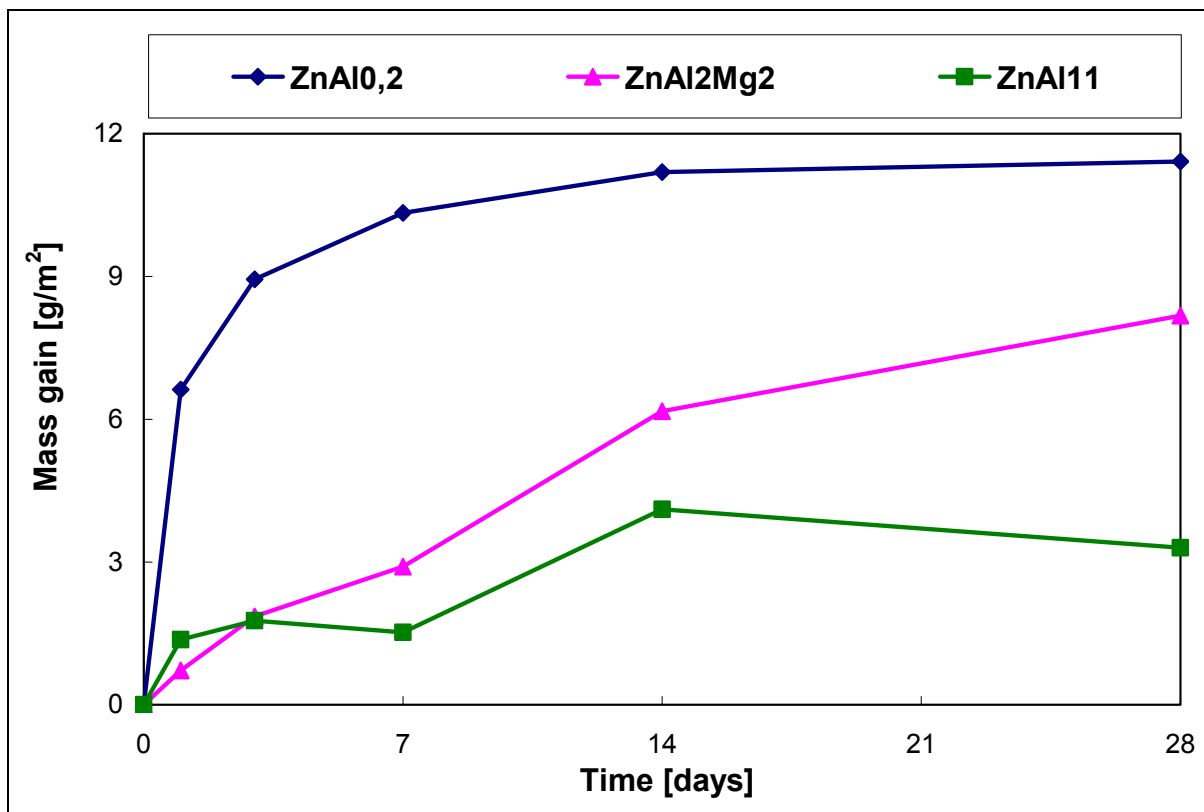


Figure 12 Wet mass gain of some model alloys with chloride contamination of 1400 mg/m² during exposure at 20°C and 80 % RH

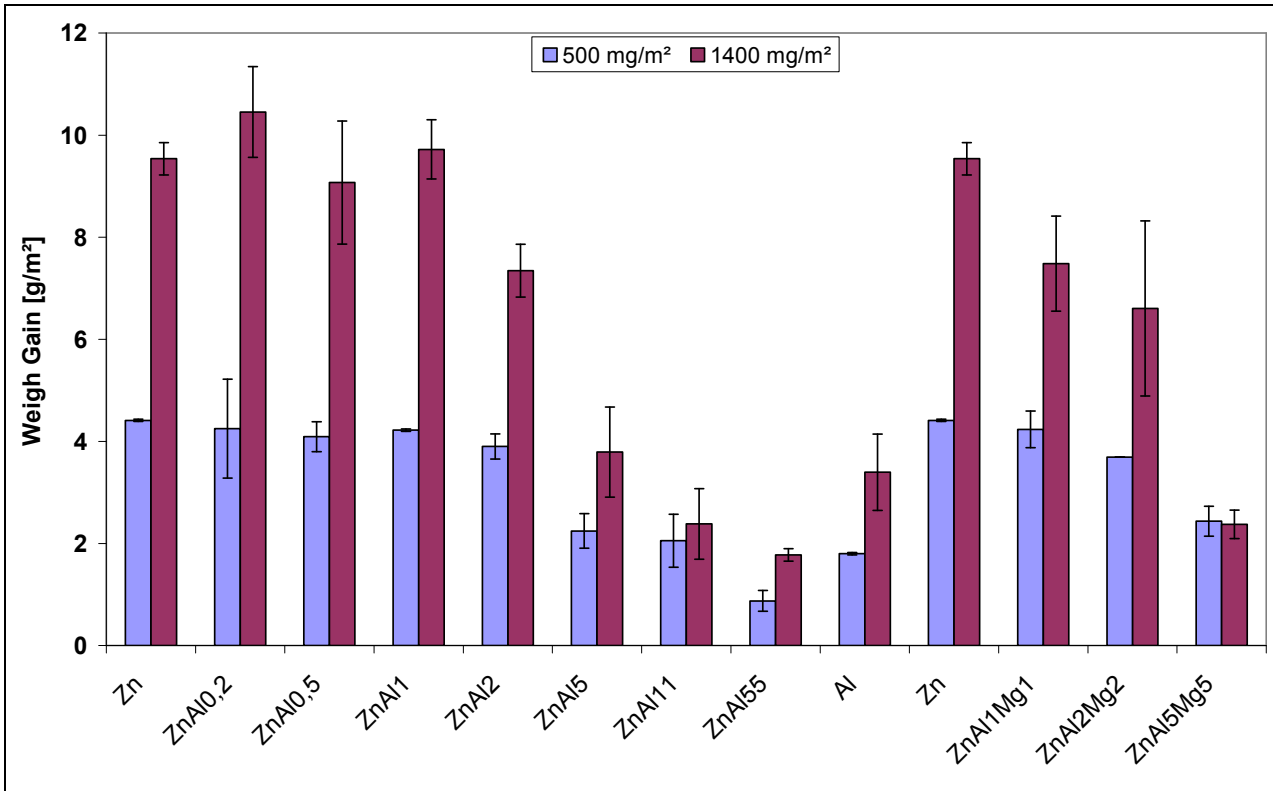


Figure 13 Dry weight gain of model alloys after 4 weeks of exposure at 20°C and 80 % RH; model alloys were contaminated with 500 and 1400 mg/m² of chloride (drying for 48 hours in desiccator)

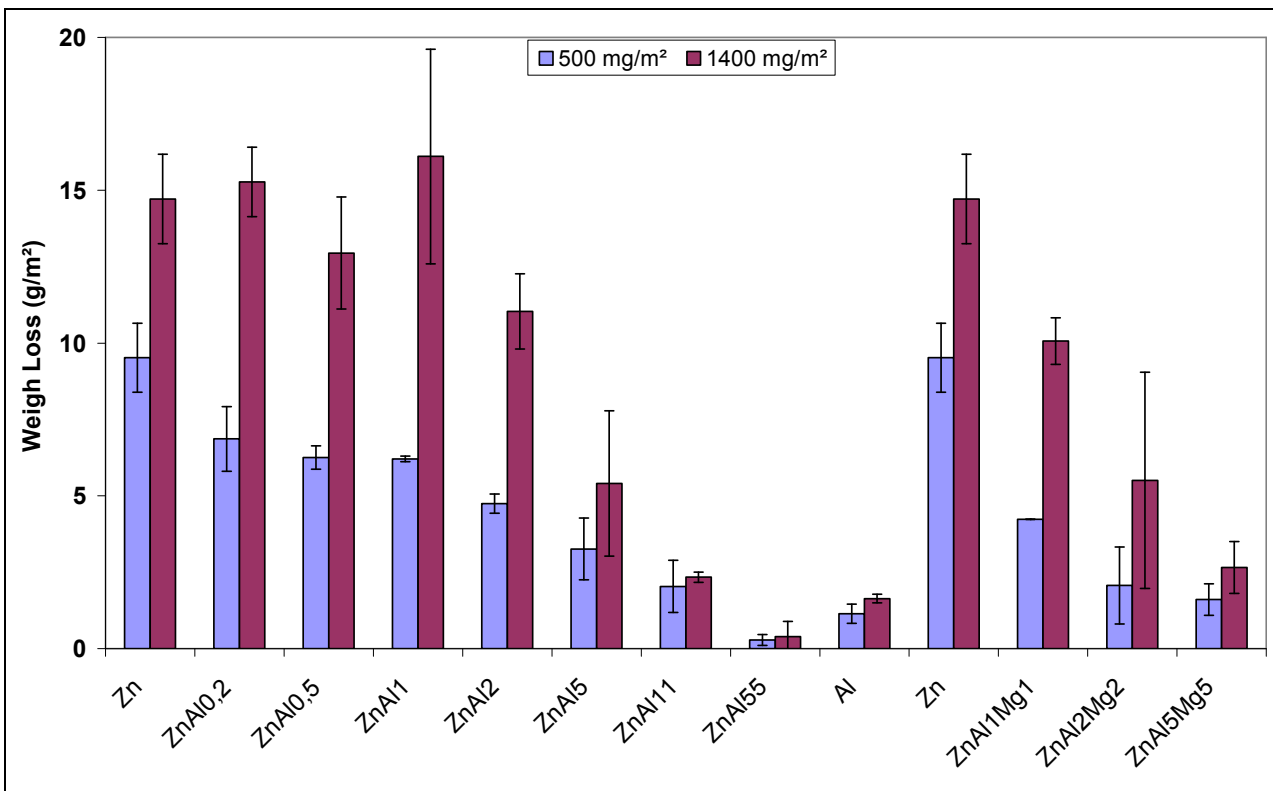


Figure 14 Weight loss of model alloys after 4 weeks of exposure at 20°C and 80 % RH; model alloys were contaminated with 500 and 1400 mg/m² of chloride

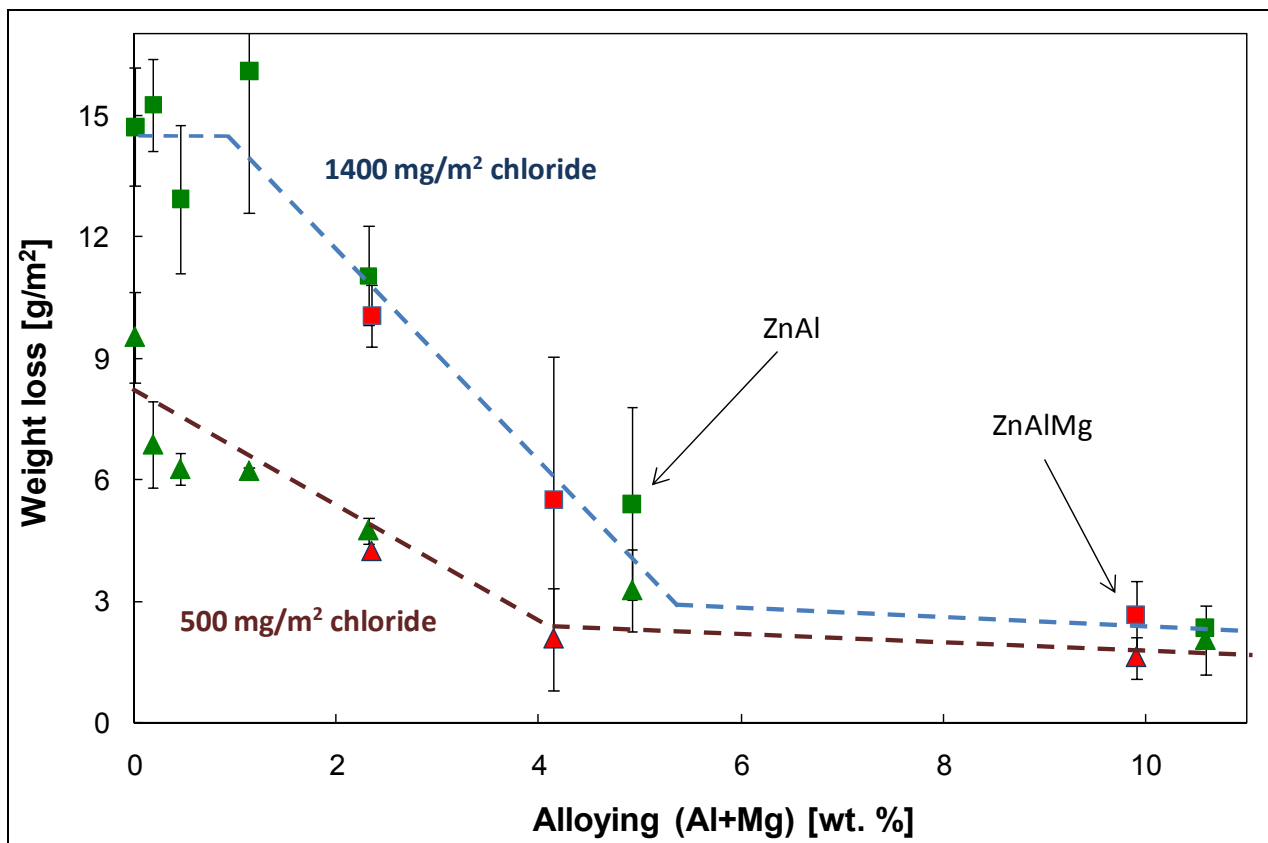


Figure 15 Weight loss vs. alloying for model alloys after 4 weeks of exposure at 20°C and 80 % RH; ■ ... 1400 mg/m² chloride, ▲ ... 500 mg/m² chloride; green marks ... ZnAl alloys, red marks: ZnAlMg alloys

It is clear that some materials were more sensitive to the surface chloride concentration than the others. A ratio between the weight loss at the chloride contamination of 1400 mg/m² and 500 mg/m² increased from 0 to 1 % of alloying elements. It decreased again from 2 to 10 % showing decreasing sensitivity to chloride contamination.

4.2.2 Soluble species

Ion chromatography analysis of soluble ions was performed after leaching of corrosion products in deionized water. The amount of soluble chloride and sodium analyzed in the extract was deduced from the initially applied amount to obtain the amount of insoluble species bonded in corrosion products. It was related to the total quantity of given species on the surface and plotted in Figure 16 as a percentage of chloride and sodium bonded after the test in corrosion products. It correlates well to the weight loss data given in chapter 4.2.1, see Figure 17.

Thus, more chloride was present in a soluble form on less corroded materials. Practically no chloride was bonded in corrosion products on the surface of Al and ZnAl55, whereas more than 90 % of chloride species were bonded on the surface of Zn and ZnAl0.2. This clearly shows that the superior corrosion stability of materials alloyed with magnesium and aluminum cannot be caused by inactivation of chloride ions in stable products. The same observation was made for model ZnMg alloys in the previous study [12].

The amount of soluble sodium was relatively lower than that of soluble chloride. Thus, some sodium must be present in stable corrosion products.

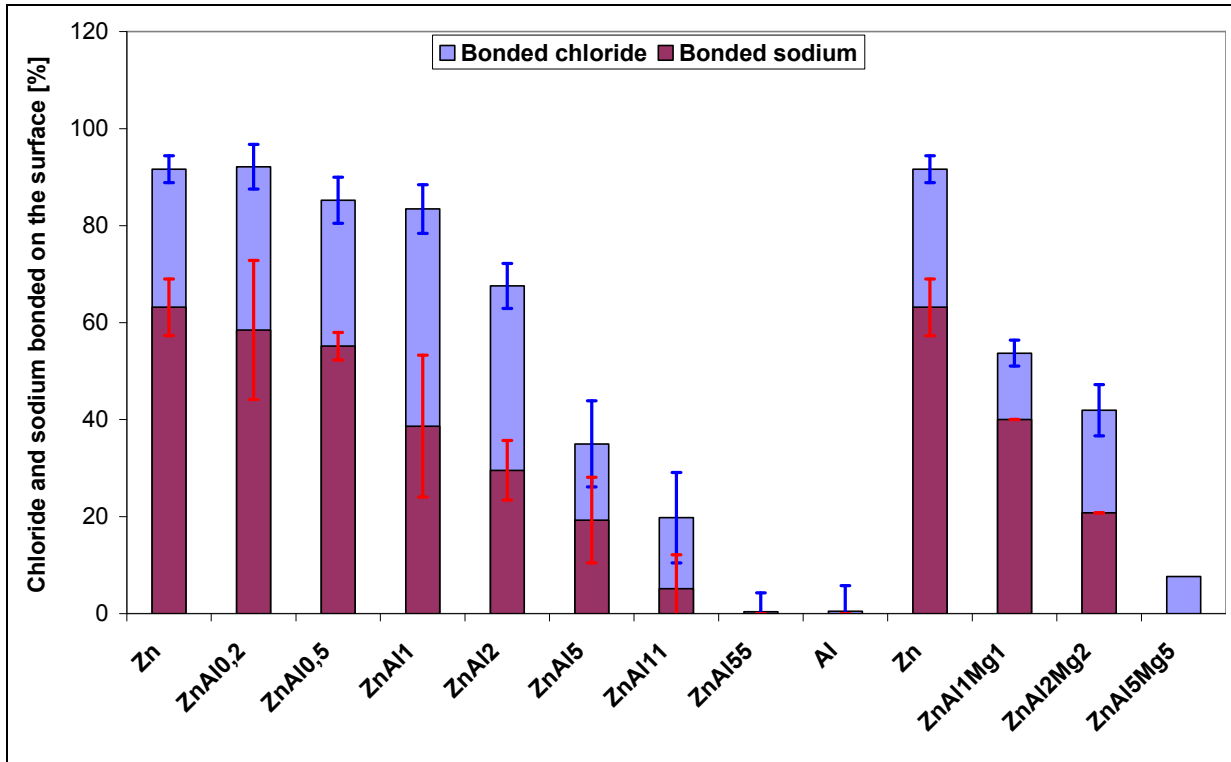


Figure 16 Bonded chloride and bonded sodium on the surface from ion chromatography of water extract of corrosion products; results for model alloys exposed 4 weeks at 20°C and 80 % RH contaminated with NaCl at 1400 mg/m² of chloride and 907 mg/m² of sodium

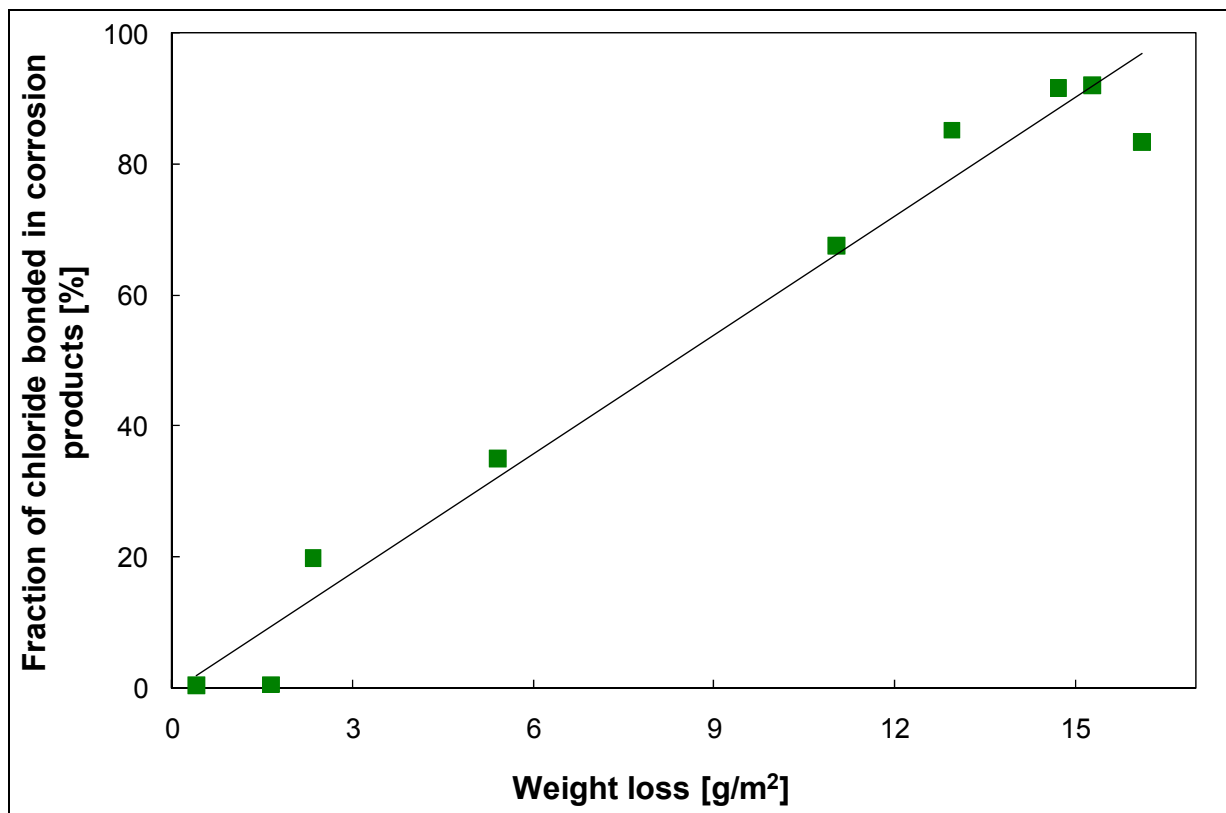


Figure 17 Fraction of chloride bonded in corrosion products versus weight loss for model ZnAl and ZnAlMg alloys

The amount of zinc leached out of the corrosion products is given in Figure 18. Because of high experimental error of the zinc analysis, differences between tested model alloys is mostly overlapped by the scatter of results. Although the interpretation of the results must be done cautiously, it is possible to suppose that the amount of soluble zinc somewhat increased with the aluminum content in alloys. The relative amount of soluble zinc to total corroded metal from weight loss is given in Figure 19. It is clearly seen that the amount of soluble zinc increased with the Al content in the alloy. It should be noted that the relative amount of soluble zinc to corroded metal is correlating to weight loss measurements. Zinc was the most corroded of all tested materials and had the lowest amount of soluble Zn of only 0.5 %, i.e. practically all Zn was bonded in corrosion products. ZnAl5 and ZnAl11 exhibited much better corrosion resistance than less alloyed model alloys and soluble zinc accounted for 9 and 11 % of oxidized metal. ZnAl55 was the most corrosion resistant model alloy and was also the one exhibiting the highest relative amount of soluble Zn of 47 %.

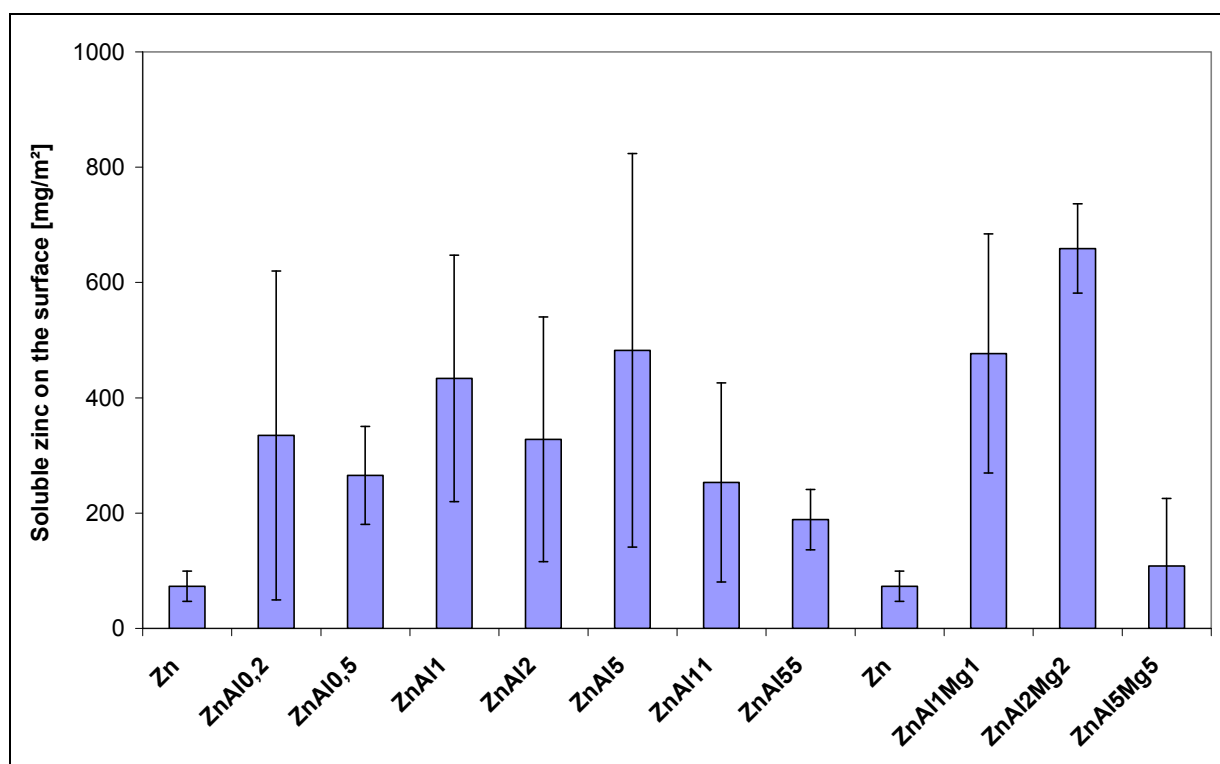


Figure 18 Soluble zinc from ion chromatography of water extract of corrosion products; results for model alloys exposed 4 weeks at 20°C and 80 % RH and contaminated with 1400 mg/m² of chloride

The effect of alloying on the amount of bonded zinc in stable corrosion products is less obvious for ZnAlMg model alloys. No trend is observable from data plotted in Figure 18 and Figure 19.

The total amount of soluble magnesium is given in Figure 20. A decrease in soluble Mg is observed with increasing Mg and Al content in alloys. This can be due to either higher tendency of magnesium to form more stable corrosion products on the surface of model alloys with a higher Mg content or the fact that less metal was corroded in case of more alloyed materials, see Figure 14.

pH of water extracts obtained by dissolving corrosion products in demineralized water is given in Figure 21. For ZnAl model alloys, a general trend is a decrease of pH with increasing Al content. This may be connected to the observed increasing relative amount of soluble zinc shown in Figure 19. It can be expected that soluble zinc species were present on the surface mainly as ZnCl₂, which is acidic. For ZnAlMg model alloys, water extract pH for alloys ZnAl1Mg1 and ZnAl5Mg5 was about 7.9 while water extract pH for alloy ZnAl2Mg was 8.3.

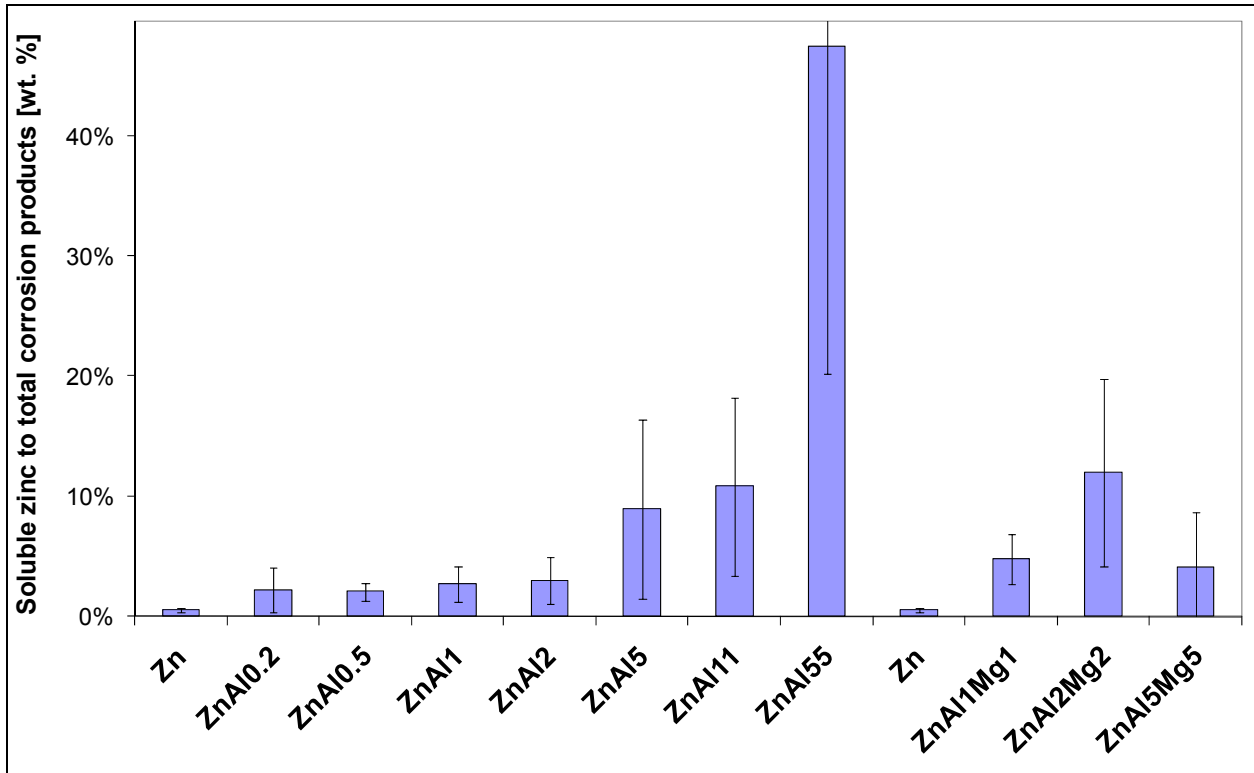


Figure 19 Ratio of soluble zinc to weight loss (total corroded metal); results for model alloys exposed for 4 weeks at 20°C and 80 % RH and contaminated with 1400 mg/m² of chloride.

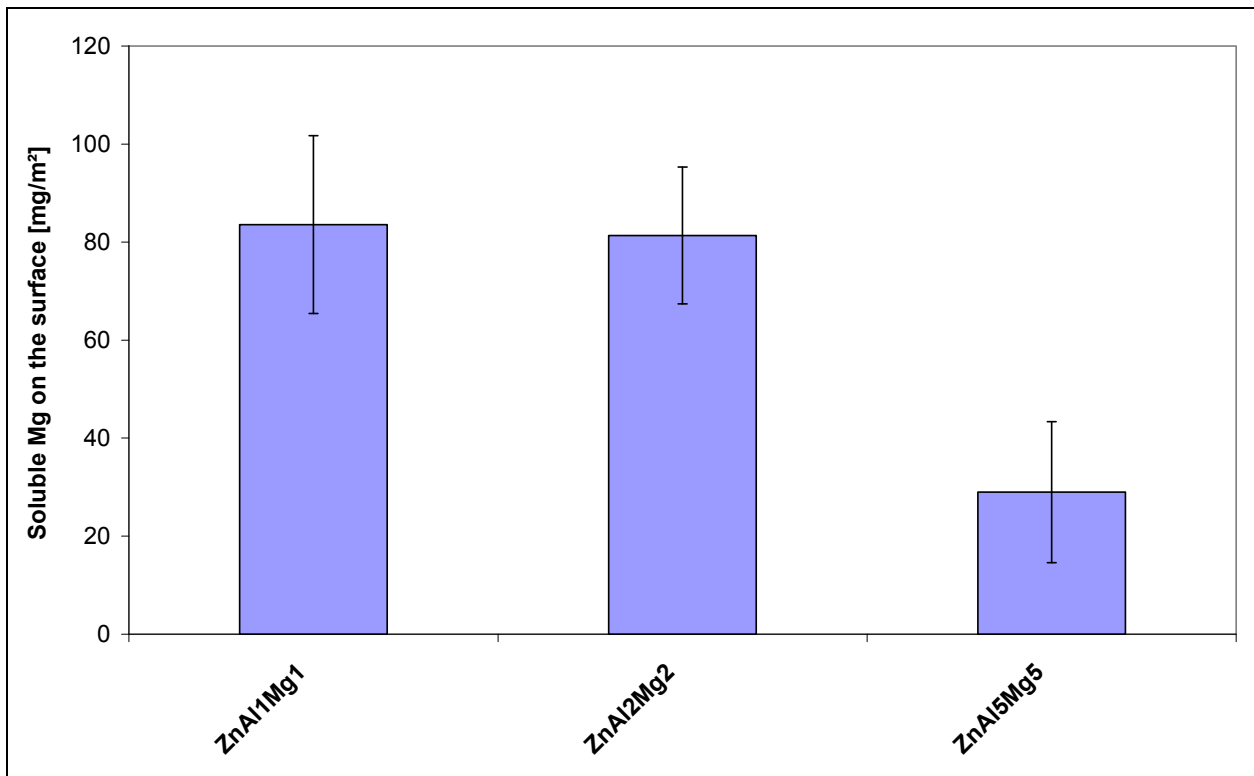


Figure 20 Soluble magnesium on the surface from ion chromatography of water extract of corrosion products; results for ZnAlMg model alloys exposed 4 weeks at 20°C and 80 % RH and contaminated with 1400 mg/m² of chloride

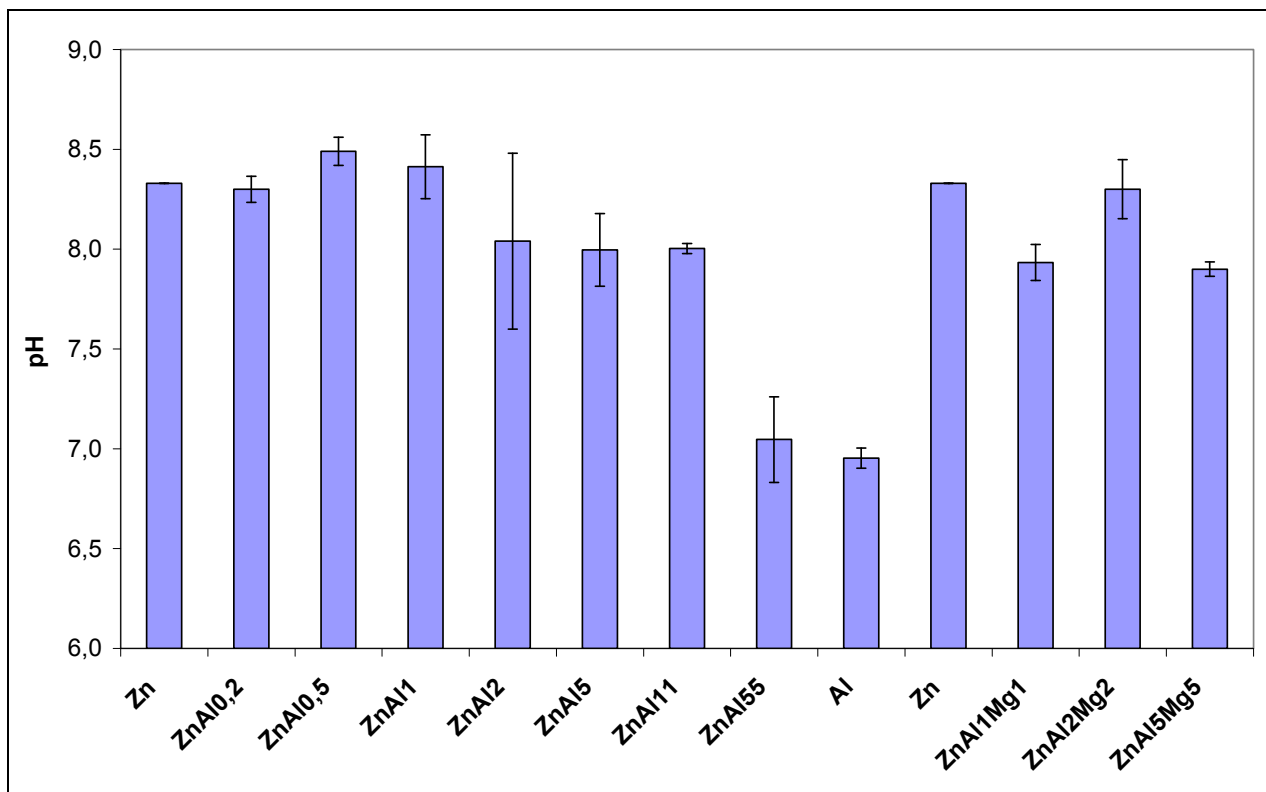


Figure 21 pH of water extracts obtained by dissolving corrosion products from model alloys exposed for 4 weeks at 20°C and 80 % RH and contaminated with 1400 mg/m² of chloride

4.2.3 Phase analysis of corrosion products

Corrosion products formed on the surface of selected samples were analyzed by FTIR spectroscopy using the KBr pellet method. Reference spectra of simonkolleite, zinc hydroxychloride [Zn₅(OH)₈Cl₂·H₂O], hydrozincite, zinc hydroxycarbonate [Zn₅(OH)₆(CO₃)₂], sodium carbonate [Na₂CO₃·10H₂O], and magnesite [MgCO₃] are shown in Figure 22. Reference spectra of aluminum-based reference minerals gibbsite [Al(OH)₃], boehmite [AlOOH], and aluminum oxide [γ-Al₂O₃] are plotted in Figure 23.

Selected infrared spectra of corrosion products collected on samples of ZnAl and ZnAlMg model alloys after exposure with deposited sodium chloride at the chloride concentration of 1400 mg/m² for 28 days at 20°C and at 80 % RH are shown in Figure 24.

Broad peaks with maxima at 3500–3400 cm⁻¹ correspond to vibrations and rotations of water molecules and OH group. As seen in Figure 24, this peak broadens with the increasing amount of aluminum in ZnAl model alloys. The principal difference of the spectra can be seen in the region below 1700 cm⁻¹. The peak at 1635 cm⁻¹ is due to the presence of water. It is stronger in spectra from samples with higher content of aluminum.

The spectrum of corrosion products from pure zinc has a broad peak at 1600–1300 cm⁻¹, which is due to the bending of CO₃²⁻. The peak at 840 cm⁻¹ is due to CO₃²⁻ bending vibration band. This peak and peaks at 1505 and 1395 cm⁻¹ reveal the presence of hydrozincite. The peaks at 905, 725, and 280 cm⁻¹ indicate the presence of simonkolleite in corrosion products. Peaks at 1040 and 460 cm⁻¹ can be seen both in the spectrum of simonkolleite and hydrozincite. The small peak at 1455 cm⁻¹ is most likely the asymmetric CO₃²⁻ peak of sodium carbonate (Na₂CO₃ or Na₂CO₃·10H₂O) [25]. The origin of another small peak at 1425 cm⁻¹ is not clear. Thus, the dominant compounds in corrosion products on zinc were hydrozincite and simonkolleite. Presence of a lower quantity of other carbonates such as sodium carbonate is very probable.

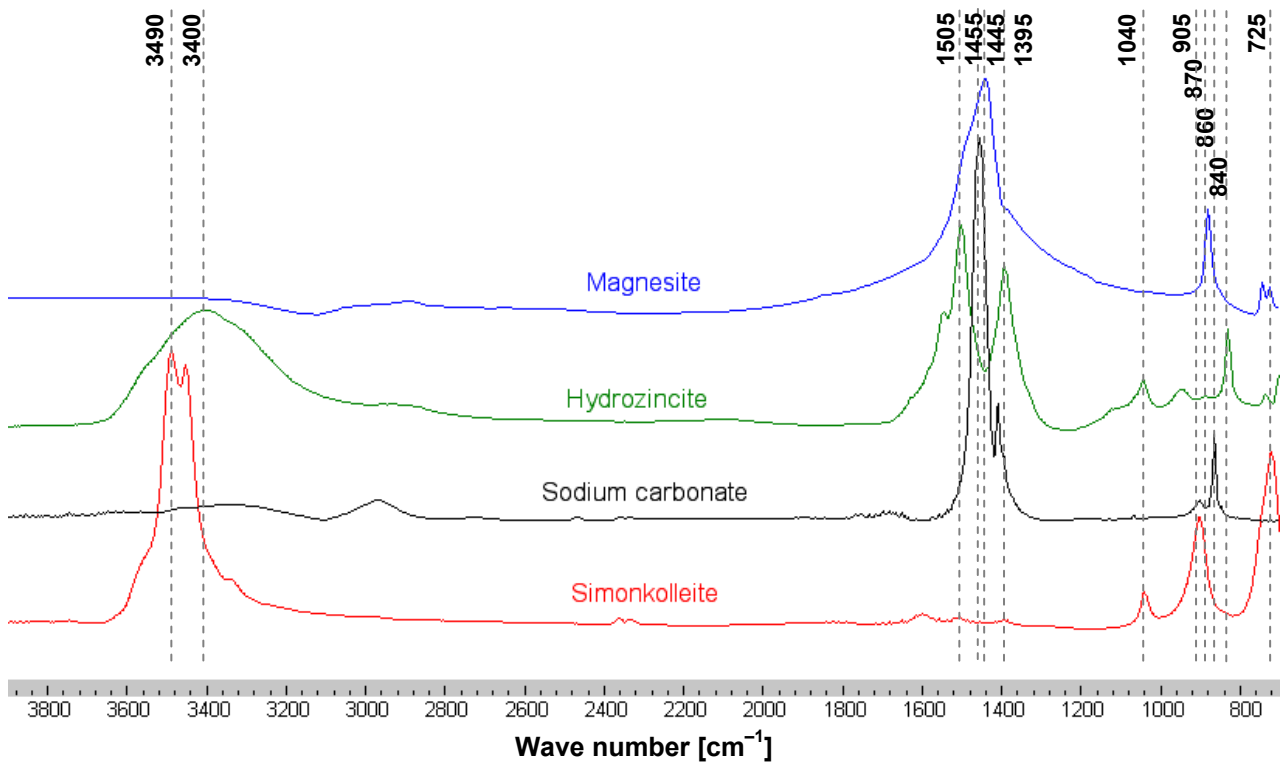


Figure 22 Infrared transmission spectra of reference minerals

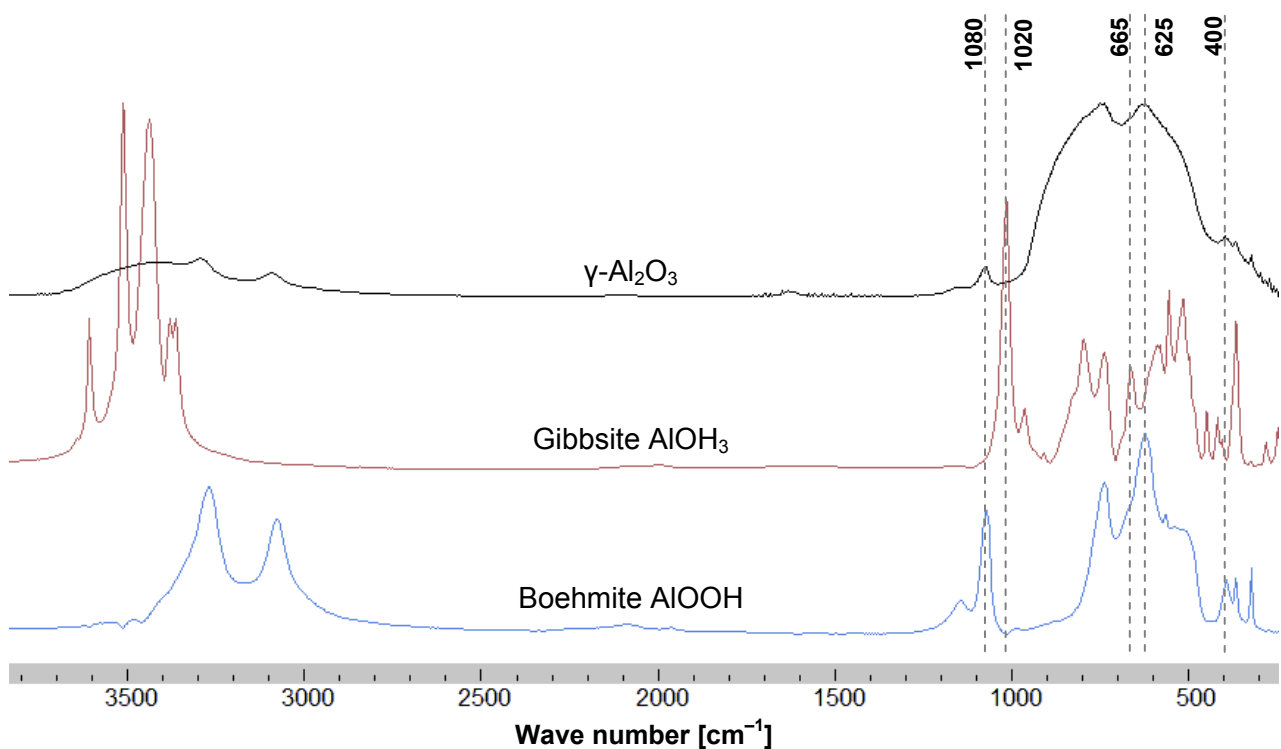


Figure 23 Infrared transmission spectra of aluminum-based reference minerals

The spectra of ZnAl_{0.2} was very similar but the carbonate peak at 1600–1300 cm⁻¹ was relatively stronger. The spectra of ZnAl_{0.5} showed even stronger carbonate peak and presence of water (peak at 1635 cm⁻¹). Moreover, two small peaks at 1095 and 620 cm⁻¹ were found. Because there are no peaks at these frequencies in any zinc-based corrosion product known to the authors, it is supposed that they belong to aluminum compound(s). Peaks at about 1080 cm⁻¹ can be found in spectra of several aluminum

compounds, e.g. boehmite and diasporite, AlOOH , and aluminum oxide, $\gamma\text{-Al}_2\text{O}_3$, see Figure 23. The peak at 625 cm^{-1} is also found in spectra of boehmite and aluminum oxide. Because the peak positions agree fairly well, it is supposed that one or both compounds were formed on the surface of ZnAl0.5 . However, aluminum oxide is usually found only on long-term exposed samples, being considered as a mature corrosion products. Thus, it is more probable that AlOOH was formed under present exposure conditions. The height of both peaks increased with the aluminum content. The spectra of corrosion products from ZnAl1 and ZnAl2 were similar. A small peak at 405 cm^{-1} could be also attributed to the presence of boehmite, compare Figure 23 and Figure 24.

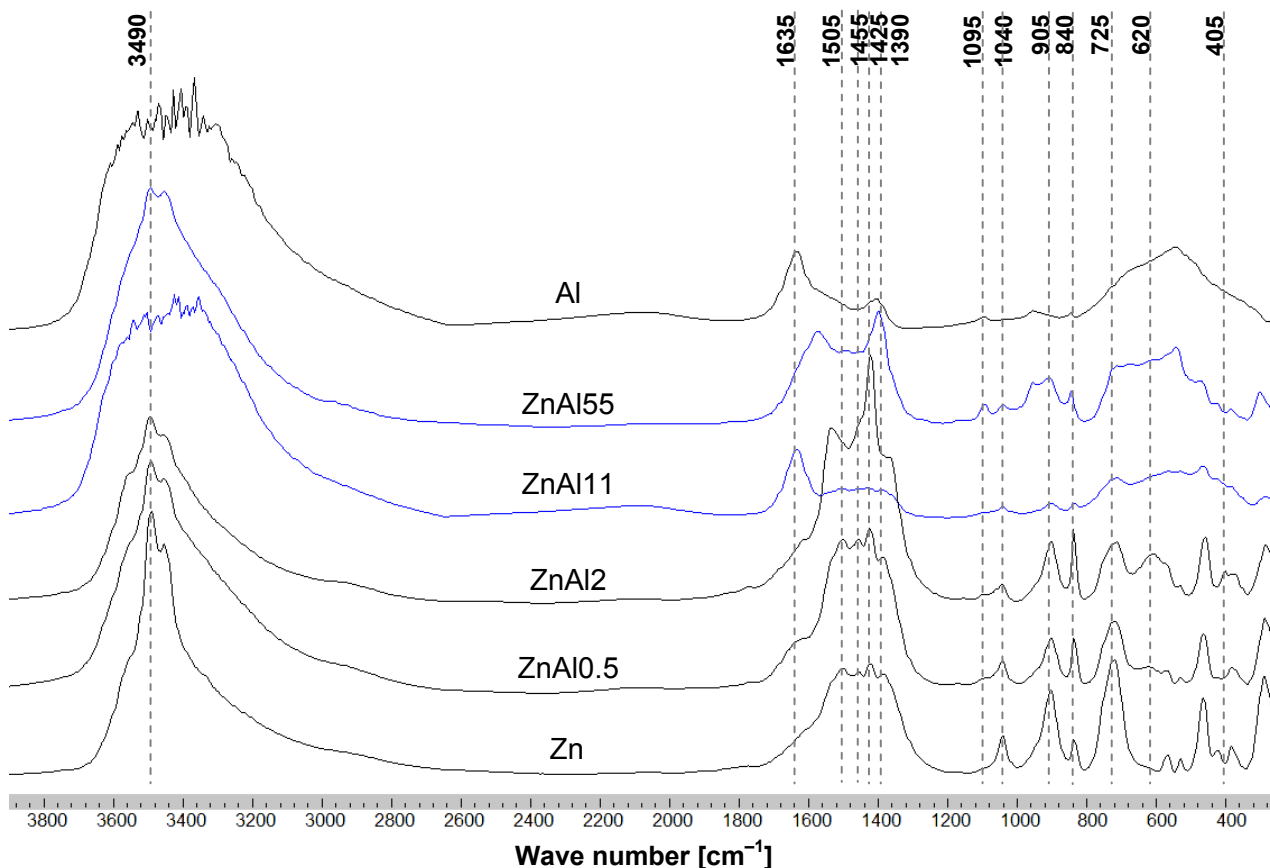


Figure 24 Infrared transmission spectra of corrosion products collected on model alloys of Zn, ZnAl0.5 , ZnAl2 , ZnAl11 , ZnAl15 , and Al with deposited sodium chloride at the chloride concentration of 1400 mg/m^2 exposed for 28 days at 20°C and at 80 % RH

The corrosion products from ZnAl5 and ZnAl11 were similar to each other. There was a lot of water in the products as shown by the strong peak at 1635 cm^{-1} . No peak at 405 cm^{-1} was identified. The spectra obtained from analysis of corrosion products from ZnAl11 , ZnAl15 , and Al were more difficult to read. Peaks are broad and less distinct. However, a small peak at about 665 cm^{-1} in the spectra of ZnAl15 and Al indicate presence of gibbsite, $\text{Al}(\text{OH})_3$. Obviously, no hydrozincite and simonkolleite was found on the surface of aluminum. There was some limited amount of hydrozincite and simonkolleite on the surface of ZnAl15 ; however, another unidentified carbonate dominated in the corrosion products. It is suggested by presence of the peak at 1580 cm^{-1} .

Because the amount of simonkolleite and carbonate-based corrosion products visibly varied with coating composition, a ratio of the peak height of carbonates taken in the region of $1600\text{--}1300\text{ cm}^{-1}$ and simonkolleite taken at 905 cm^{-1} , C/S ratio, was calculated. It is given together with other data on the phase composition of the corrosion products in Table 8.

Table 8 Phase composition of corrosion products collected from model ZnAl alloys contaminated with 1400 mg/m² chloride after 28 days of exposure in humid air at 80 % RH and at 20°C

Alloy	Hydrozincite (1505 cm ⁻¹)	Simonkolleite (905 cm ⁻¹)	C/S ratio [×]	Sodium carbonate (1455 cm ⁻¹)	Unidentified carbonate (1425 cm ⁻¹)	Water (1630 cm ⁻¹)	AlOOH (1095, 620 cm ⁻¹)	Others
Zn	Yes	Yes	1.4	Yes	Yes	No	No	
ZnAl0.2	Yes	Yes	2.4	Yes	Yes	No	No	
ZnAl0.5	Yes	Yes	3.5	Yes	Yes +	Yes	Yes –	
ZnAl1	Yes	Yes	3.4	Yes	Yes +	Yes	Yes	
ZnAl2	Yes –	Yes	4.2	Yes	Yes +	Yes	Yes	
ZnAl5	Yes	Yes	5.3	Yes	Yes –	Yes +	Yes	
ZnAl11	Yes –	Yes	2.4–3.7	Yes	Yes –	Yes +	Yes	
ZnAl55	Yes –	Yes	4.1–7.4	Yes –	No	No	Yes	Al(OH) ₃
Al	No	No	–	No	No	Yes +	Yes	Al(OH) ₃

[×] Carbonate to simonkolleite peak height ratio; – Weak peak, lower quantity; + Strong peak, higher quantity

The amount of carbonates on the surface increased relatively to the amount of simonkolleite with the aluminum content, see Figure 25. This is in agreement with the data on soluble chloride given in Figure 16. The amount of bonded chloride clearly decreased with the aluminum content. In particular, it increased rapidly from pure zinc to ZnAl0.5. With the aluminum content, the OH peak broaden, the amount of water in the corrosion product increased, the amount of aluminum-based corrosion products (most probably boehmite or diasporite) increased, and the total amount of hydrozincite and simonkolleite decreased. The peak at 1425 cm⁻¹ increased from zinc to alloy with 2 wt. % aluminum.

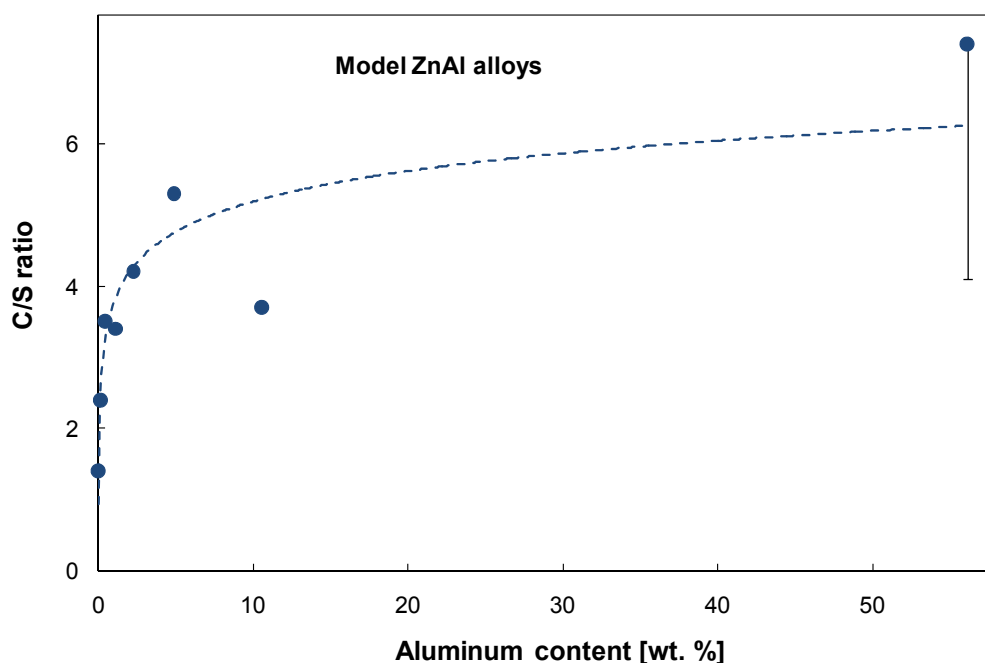


Figure 25 Effect of the aluminum content in model alloys on C/S ratio (carbonate to simonkolleite peak height) in corrosion products after exposure with deposited sodium chloride at the chloride concentration of 1400 mg/m² for 28 days at 20°C and at 80 % RH

Results for ZnAlMg model alloys are shown in Figure 26 and Table 9. The width of the OH peak at 3600–3200 cm⁻¹ and height of the water peak at 1635 cm⁻¹ and the peak of aluminum-associated corrosion products at 620 cm⁻¹ increased with the content of alloying elements. A C/S ratio increased as well. This is

in agreement with results discussed above. The height of peaks associated with aluminum corrosion products, i.e. the peaks at 1095 and 620 cm^{-1} was generally higher on alloys containing only aluminum than on alloys with the same aluminum content and presence of magnesium, compare e.g. spectra for ZnAl2 and ZnAl2Mg2 in Figure 24 and Figure 26. It may indicate that less aluminum was oxidized in alloys containing magnesium. In other respects, spectra of corrosion products from alloys with the same aluminum content were similar, e.g. those of ZnAl1 and ZnAl1Mg1, ZnAl2 and ZnAl2Mg2, and ZnAl5 and ZnAl5Mg5. The very weak peak at 1440 cm^{-1} identified in spectra of ZnAl1Mg1 and ZnAl2Mg2 might be due to presence of magnesium carbonate MgCO_3 , magnesite (see the reference spectrum in Figure 22) or magnesium hydroxycarbonate. However, it was not found in the spectra of ZnAl5Mg5.

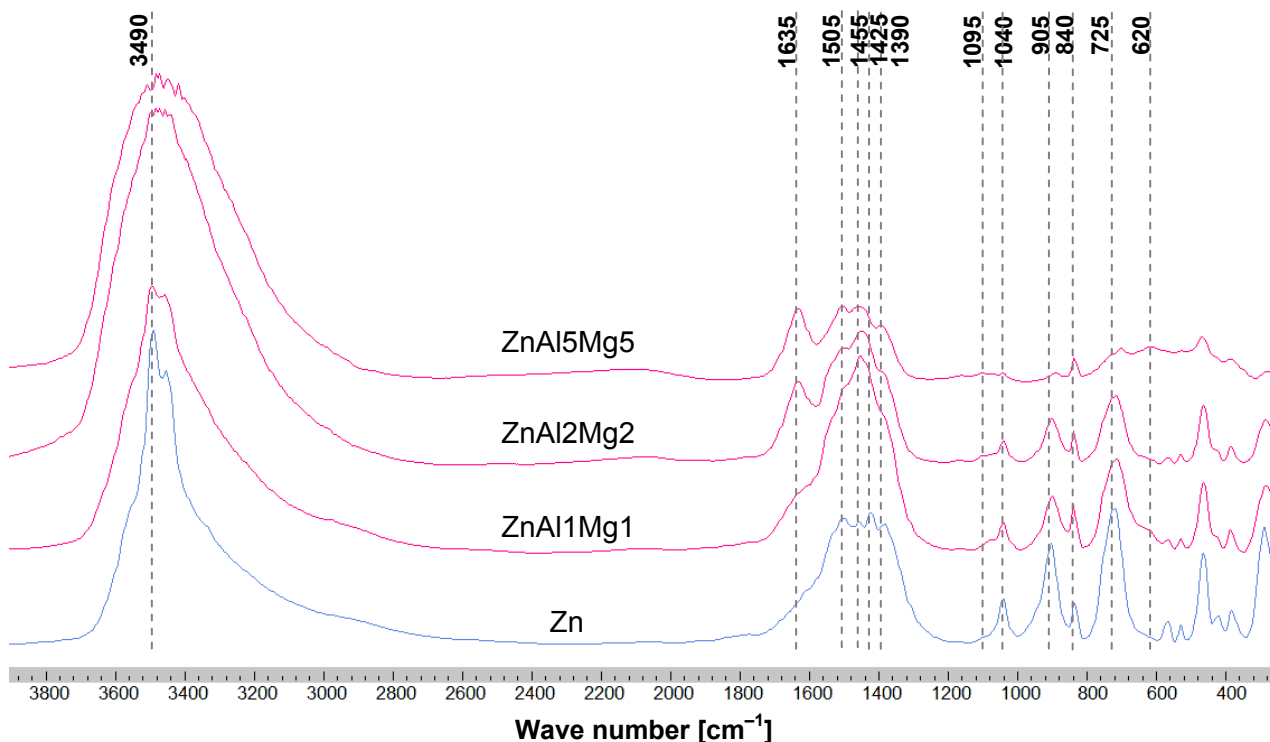


Figure 26 Infrared transmission spectra of corrosion products collected on model alloys of Zn, ZnAl1Mg1, ZnAl2Mg2, and ZnAl5Mg5 with deposited sodium chloride at the chloride concentration of 1400 mg/m^2 exposed for 28 days at 20°C and at 80 % RH

Table 9 Phase composition of corrosion products collected from model ZnAlMg alloys contaminated with 1400 mg/m^2 chloride after 28 days of exposure in humid air at 80 % RH and at 20°C

Alloy	Hydrozincite (1505 cm^{-1})	Simonkollite (905 cm^{-1})	C/S ratio [×]	Sodium carbonate (1455 cm^{-1})	Unidentified carbonate (1425 cm^{-1})	Water (1630 cm^{-1})	AlOOH (1095, 620 cm^{-1})	Others
Zn	Yes	Yes	1.4	Yes	Yes	No	No	
ZnAl1Mg1	Yes	Yes	3.6	Yes	Yes	Yes –	Yes –	MgCO_3
ZnAl2Mg2	Yes	Yes	3.6	Yes	Yes	Yes +	Yes –	MgCO_3
ZnAl5Mg5	Yes	Yes	14.9	Yes	No	Yes +	Yes –	
Al	No	No	–	No	No	Yes +	Yes	$\text{Al}(\text{OH})_3$

[×] Carbonate to simonkollite peak height ratio; – Weak peak, lower quantity; + Strong peak, higher quantity

The corrosion products on ZnAlMg alloys were composed of hydrozincite, simonkollite, sodium carbonate, other unidentified carbonate, and an aluminum compound, probably AlOOH (boehmite or diasporite). The presence of magnesium carbonate or magnesium hydroxycarbonate is not clear. It can be

concluded that the presence of magnesium did not affect the spectra significantly. It is in agreement to the study on model ZnMg alloys [12, 26]. It is not clear if it was mainly because of a real low effect of magnesium on the composition of the corrosion products or due to a lower detection limits of Mg-based compounds by FTIR. It was shown in previous work [27] that magnesium-based corrosion products in mixtures with zinc corrosion products are difficult to detect by FTIR. More than 10 wt. % of magnesium oxide, hydroxide, or carbonate must be present in the products to be visible in a spectrum. Moreover, it was shown in the previous study on ZnMg model alloys that magnesium was mainly present on the metal/corrosion product layer interface making its analysis in the bulk corrosion products more difficult.

4.2.4 Comparison of ZnAl and ZnAlMg alloys to ZnMg alloys

One of the objectives of this study was to compare results obtained for ZnAl and ZnAlMg model alloys to the ones obtained in a previous study for ZnMg alloys [12]. In this previous work it was clearly shown that alloying with Mg from 1 to 16 wt. % significantly increased the corrosion resistance of ZnMg materials tested at 20°C and 80 % RH. As shown in Figure 27, the weight loss was reduced from 50 to 90 % compared to zinc. The improved corrosion resistance of alloys with 1 to 16 wt. % Mg was attributed to presence of Mg-containing phases Mg_2Zn_{11} and $MgZn_2$. They were covered with Mg-based oxide layer that is supposed to be more stable than Zn-based oxide layer in presence of chloride and limiting the rate of oxygen reduction on the surface. The significant increase of corrosion of model alloys with Mg content above 16 wt. % was attributed to hydrogen depolarization, as illustrated in Figure 28.

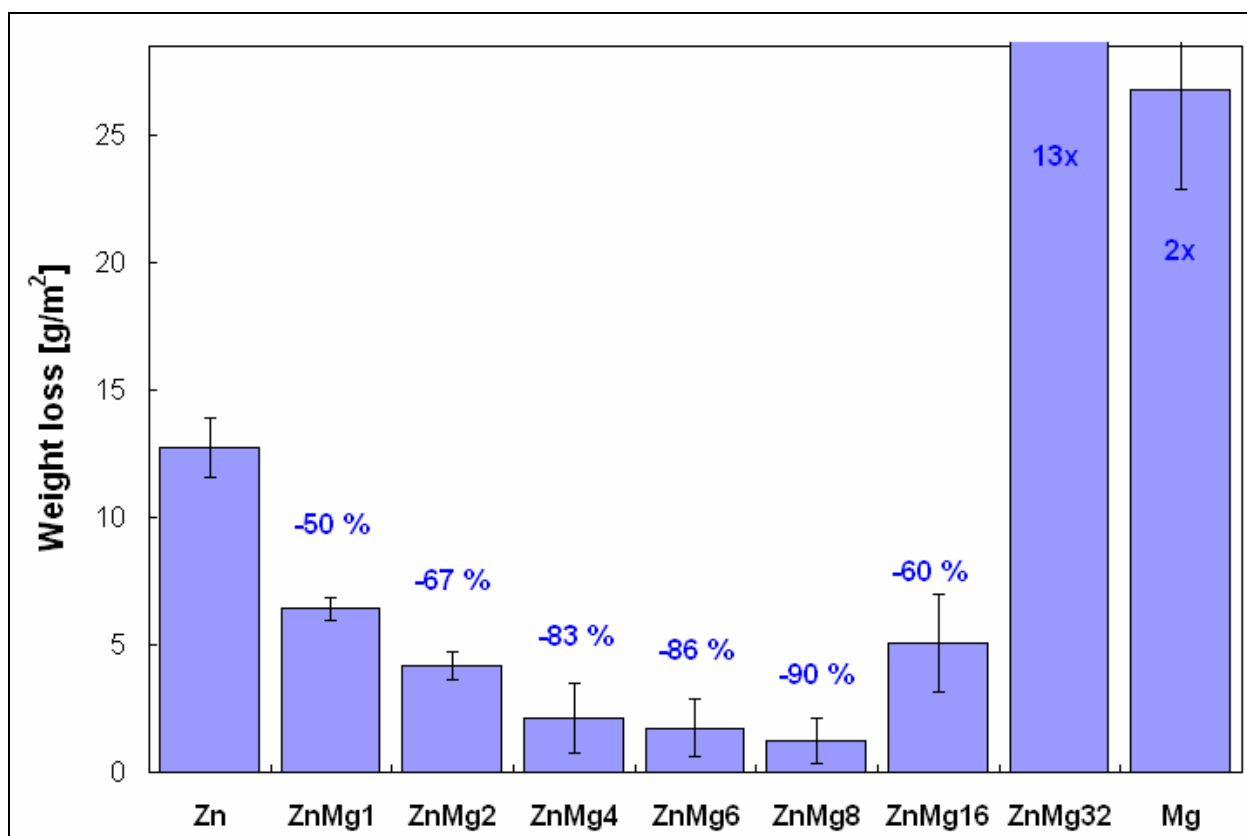


Figure 27 Weight loss of ZnMg model alloys after 4 weeks of exposure at 20°C and 80 % RH; model alloys were contaminated with 1400 mg/m² of chloride; results from [12]

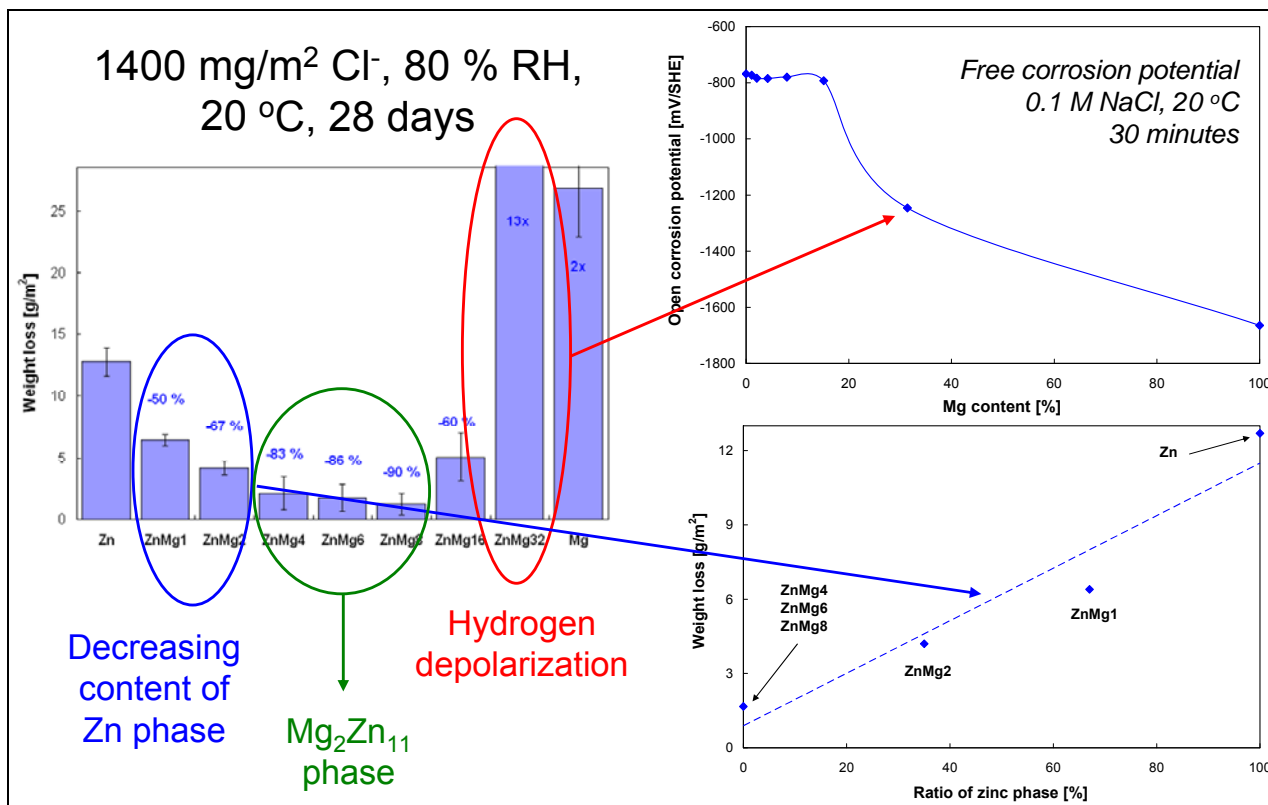


Figure 28 Relation between corrosion resistance and amount of pure Zn phase; free corrosion potential of ZnMg32 showing possible hydrogen depolarization; results from [12]

Although the experimental conditions were kept as much as possible the same, raw data for ZnAl and ZnAlMg model alloys and raw data for ZnMg model alloys cannot be directly compared as the two experimental campaigns were not led in the same time. However, the corrosion resistance improvement related to zinc might be compared as the same Zn models were tested as reference in both tests. The weight loss of Zn in the current study was about 15 g/m² while it was about 12.5 g/m² in the previous study [12] after 4 weeks of exposure at 20°C and 80 % RH. For model alloys with up to 11 % of alloying elements tested in both studies, the corrosion resistance improvement as a function of the content of alloying elements is given in Figure 29. Mg, Al, and Al+Mg content improved the corrosion resistance. The curves of the corrosion stability improvement versus total alloying for ZnAl and ZnAlMg are practically superimposed. The curve for ZnMg alloys has very similar shape, but it is shifted by 20 to 40 %. This indicates that ZnMg alloys were more corrosion resistant than ZnAl and ZnAlMg alloys in these exposure conditions. However, if ZnMg model alloys would have been more corrosion resistant than ZnAl model alloys at identical alloying content, a better corrosion resistance of ZnAlMg alloys compared to ZnAl would be expected. Results of this study show almost the same effect of magnesium and aluminum to corrosion of zinc alloys. The positive effect of magnesium seems to be only very slightly more profound than that of aluminum, see Figure 29. Thus, it is supposed that the shift observed for ZnMg model alloys is mainly due to variations of experimental conditions, particularly in terms of pickling of specimens after exposure. This process can introduce rather high error especially in case of highly corrosion resistant materials. To prove clearly whether the effect of magnesium is similar to that of aluminum or not, a test involving all model alloys at once is planned.

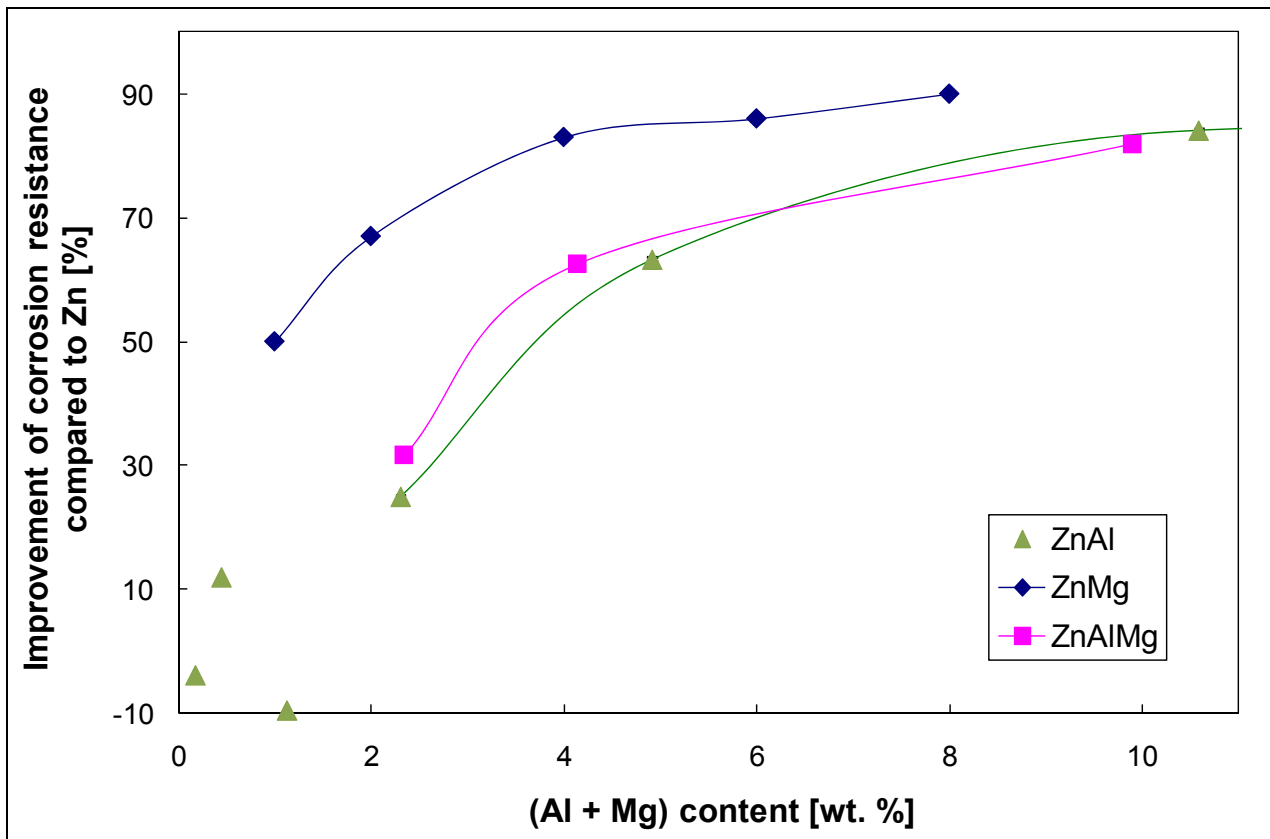


Figure 29 Corrosion resistance improvement compared to zinc as a function of total alloying from 0 to 11 %; ZnAl and ZnAlMg results are from the present study, results for ZnMg model alloys are from [12]

4.3 Corrosion testing of metallic coated panels in humid atmosphere

4.3.1 Corrosion properties at 20°C and 80 % of RH

Samples of GI, Galfan, ZAM, SD, AZ, and HD ZnAlMg 10 μ m with composition given in *Table 3* were exposed to humid air with sodium chloride deposits at 500, 1400, 2500, and 5000 mg/m² of chloride. Photographs of metallic coated panels exposed 4 weeks at 20°C and 80 % of RH are given in *Figure 30*. Hot dip galvanized steel (GI) was the most affected by corrosion (white rust). AZ was the only metallic coating which exhibited black rust. Visual aspect of all the other metallic coatings changed only little during exposure.

The wet mass gain versus time for the studied specimens is given in *Figure 31*. Wet mass gain is due to both water absorption in the layer of NaCl deposits on the metal surface and the formation of corrosion products. Stabilization of the mass gain occurred in the first days of exposure. For both 500 mg/m² and 1400 mg/m² levels of chloride contamination, a clear difference between GI and the other coatings is observed with higher wet mass gain for GI. The wet mass gain was the highest for GI also at other chloride concentrations, but the difference was low. Much higher variations between tested materials were seen in terms of dry mass gain shown in *Figure 32*. The dry mass gain was measured after keeping the samples for 48 hours in a desiccator with silica gel. The difference between the wet and dry mass gain can be explained by the fact that the mass gain of GI was mainly attributed to corrosion product formation whereas for the other coatings, the mass gain was strongly affected by water absorption in the layer of NaCl deposits. This is clearly seen in *Figure 33* which gives the wet and dry mass gain and calculated amount of free water on the surface of samples exposed with 1400 mg/m² chloride. The dry mass gain was clearly higher for GI than for any other metallic coating. Corrosion products on the alloyed coatings were more hygroscopic than those on GI.

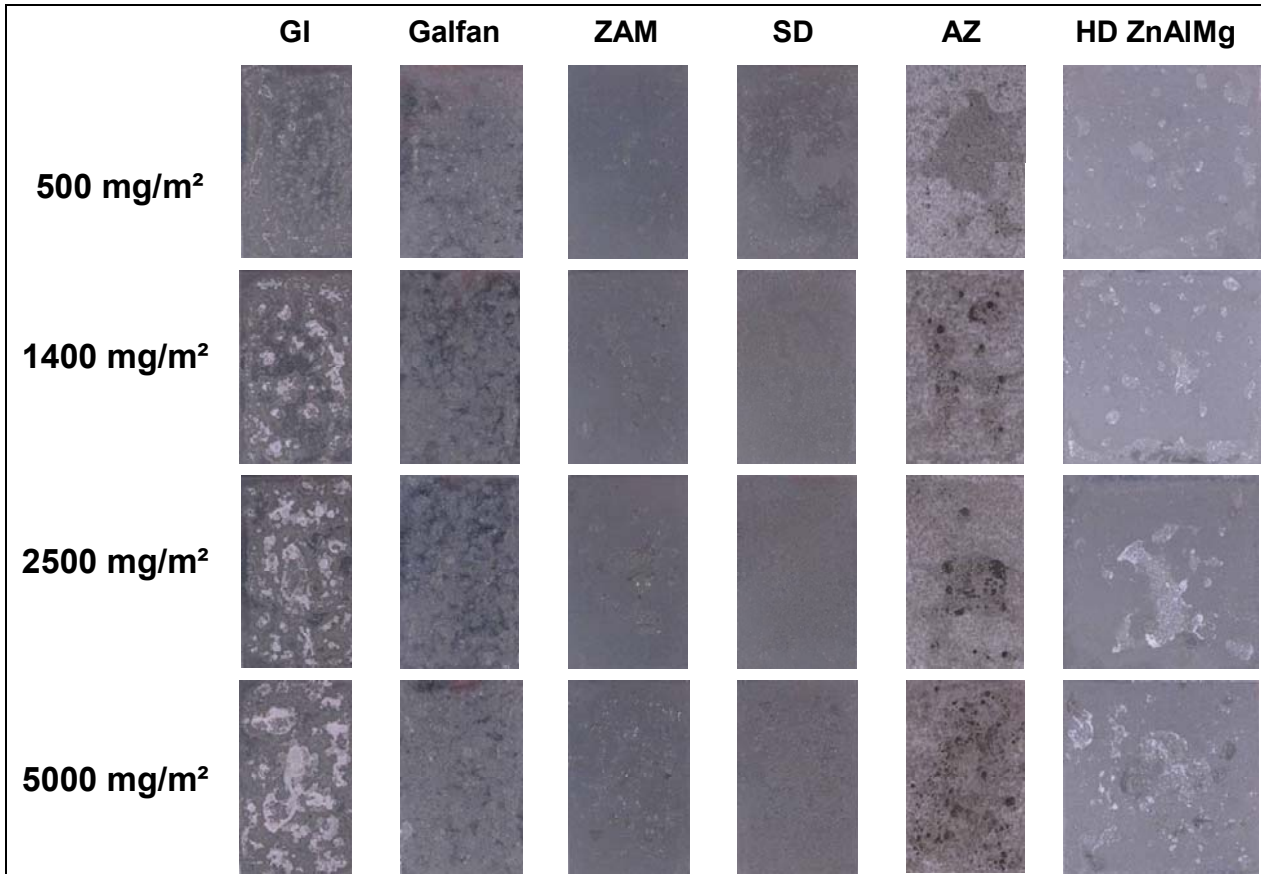


Figure 30 Visual aspect of coated steel sheets after 4 weeks of exposure at 20°C and 80 % RH

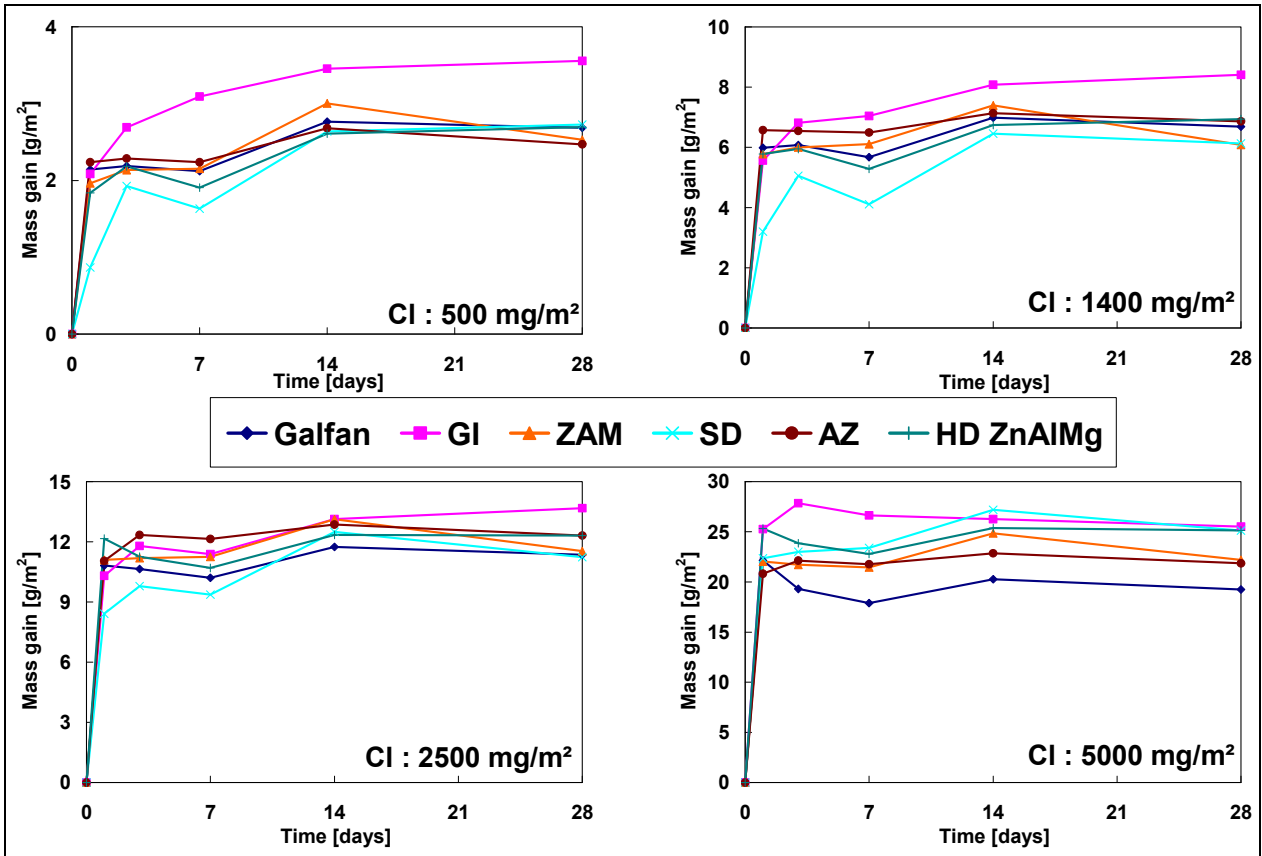


Figure 31 Wet mass gain of metallic coated steel during exposure at 20°C and 80 % RH

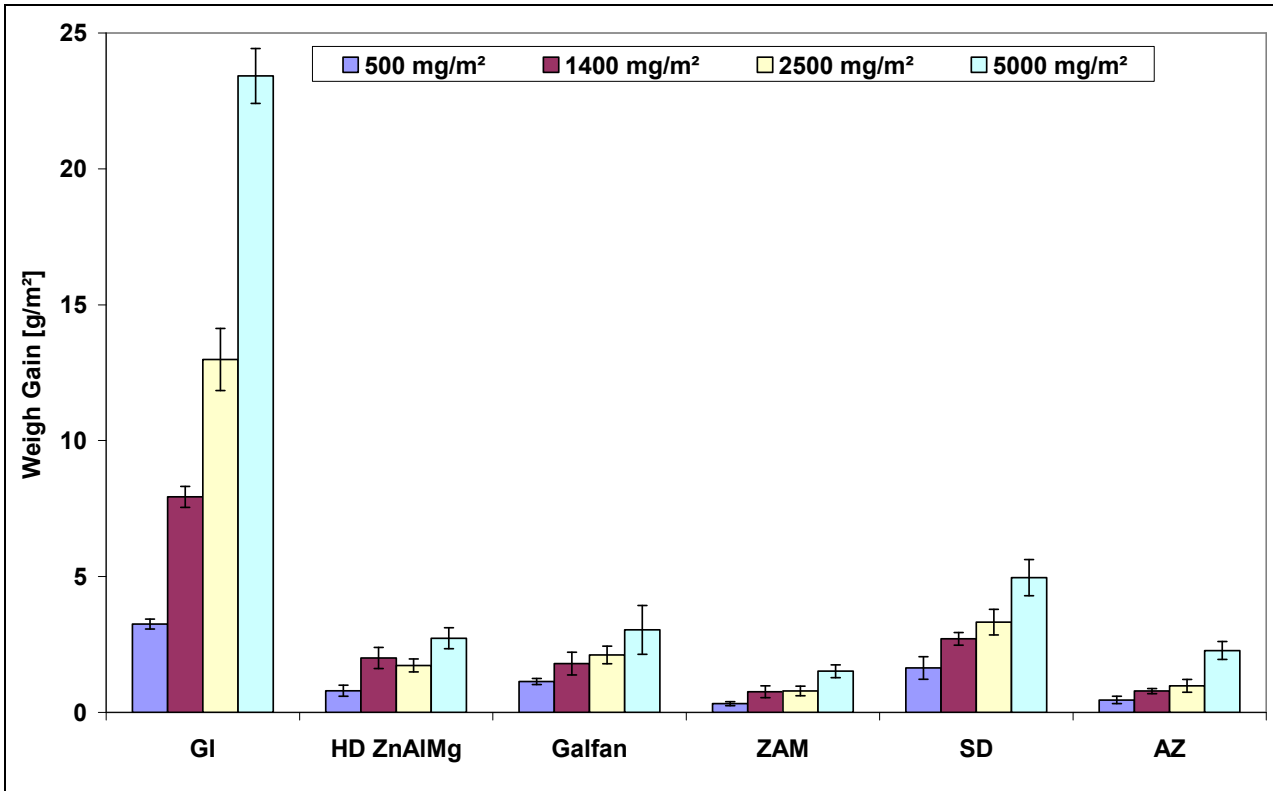


Figure 32 Dry weight gain of metallic coated steel after 4 weeks of exposure at 20°C and 80 % RH

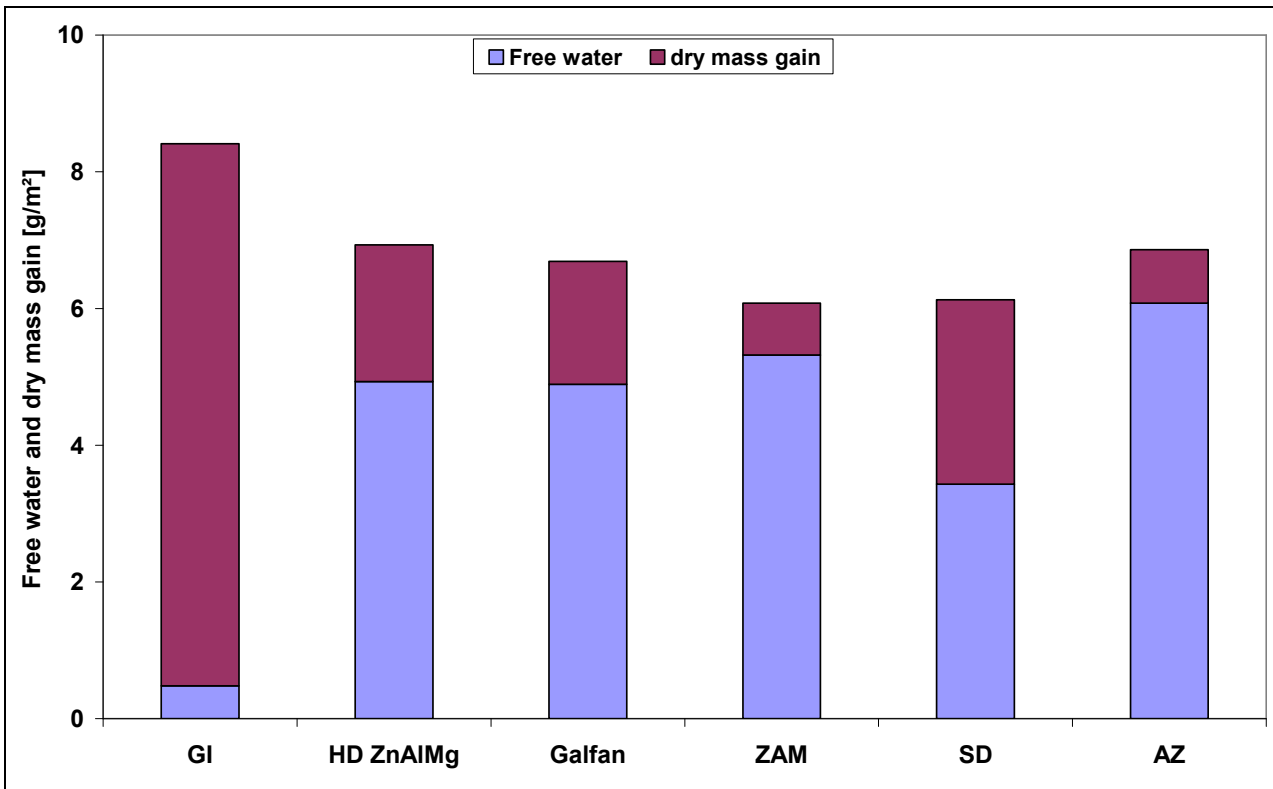


Figure 33 Dry mass gain and amount of free water on surfaces of coated samples contaminated with 1400 mg/m² of chloride after 4 weeks of exposure at 20°C and 80 % RH; the total height of the columns represent the wet mass gain after the test

The weight loss calculated from sample weight before exposure and contamination and after pickling is shown in Figure 34. The alloyed coatings were 66 to 96% less corroded than GI depending on their composition and chloride contamination.

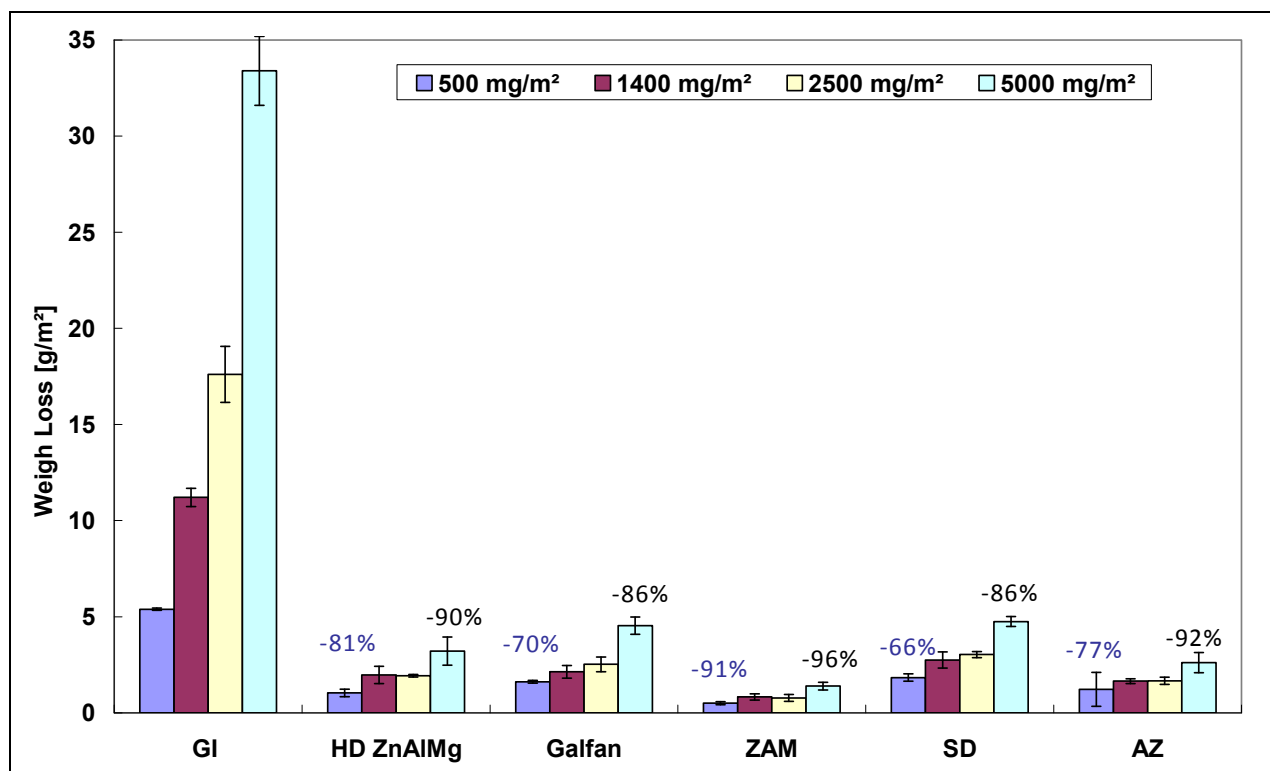


Figure 34 Weight loss of metallic coated steel after 4 weeks of exposure at 20°C and 80 % RH

It should be noted that a weight loss measurement is relevant only if corrosion is uniform. In case of alloy coatings with multiphase structure, it is probable that some phases are more corrosion resistant than others and corrosion is not fully uniform. Even pitting attack can develop on alloyed coatings as reported by other authors for AZ. Because a rapid microscopic evaluation of the samples did not reveal any strong non-uniformity, the weight loss data are considered representative in given experimental setup. However, this point should be address in more details in future work.

The effect of chloride contamination on the corrosion rate is shown in Figure 35 for all alloyed coatings. The dependence between chloride contamination and corrosion rate is more or less linear in this range of chloride concentration with the lowest slope for ZAM and AZ, higher slope for SD, Galfan, and HD ZnAlMg, and the highest slope for GI. Thus, the dependence of the weight loss on chloride concentration was generally lower for alloyed coatings than for GI. Consequently, variations between the tested materials were highest when contaminated with 5000 mg/m² chloride. The effect of zinc alloying was the strongest at this concentration and it relatively decreased at a lower surface contamination.

Except for GI, corrosion rates of the tested coatings were all rather low. However, from Figure 35, the following classification of corrosion performance can be given (from the least corrosion resistant material to the most stable one):

$$GI \ll SD < \text{Galfan} < \text{HD ZnAlMg} < \text{AZ} < \text{ZAM}.$$

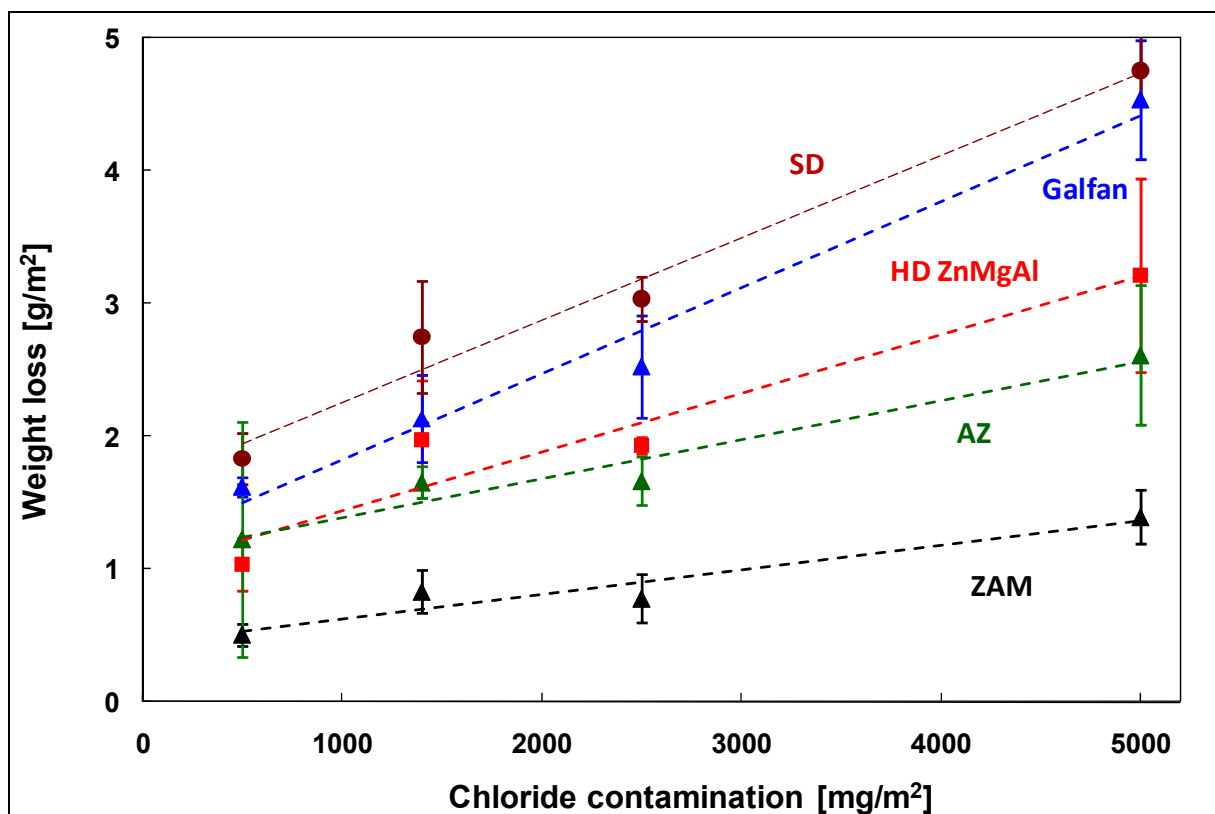


Figure 35 Weight loss vs. chloride contamination for coated steel panels after 4 weeks of exposure at 20°C and 80 % RH

4.3.2 Soluble species

Ion chromatography analysis of soluble species was performed after leaching of corrosion products in deionized water. The amount of soluble chloride and sodium analyzed in the extract was deduced from the initially applied amount to obtain the amount of insoluble species bonded in corrosion products. The results are given in Figure 36 and Figure 37. They show the amount of insoluble chloride and sodium related to the total quantity of chloride and sodium applied on the surface, i.e. chloride and sodium bonded in corrosion products after the test. As in case of the model alloys discussed in chapter 4.2, the amount of bonded chloride correlated well to weight loss, compare e.g. Figure 36 and Figure 34.

The amount of soluble zinc and magnesium species leached out of corrosion products are given in Figure 38 and in Figure 39, respectively. The same amounts related to the total corroded metal (weight loss) are plotted in Figure 40 and in Figure 41. For GI the total amount of soluble zinc decreases with the chloride contamination (Figure 38, Figure 40). It could be concluded that more Zn is bonded in corrosion products and then less Zn is soluble under more severe exposure conditions. Contrariwise, the lowest chloride contamination of 500 mg/m² led to the lowest quantity of soluble zinc for alloyed coatings, see Figure 38. Zinc solubility increased with the chloride contamination. However, when related to the amount of corroded metal, the chloride contamination level did not have any significant effect on the amount of soluble zinc, see Figure 40. This result suggests that alloying elements affected formation of stable zinc corrosion products. Since the solubility of zinc corrosion products was considerably higher on the surface of alloyed materials, it can be supposed that their improved corrosion stability was not connected to better protective ability of zinc corrosion products, but to formation of protective layers based on the alloying elements.

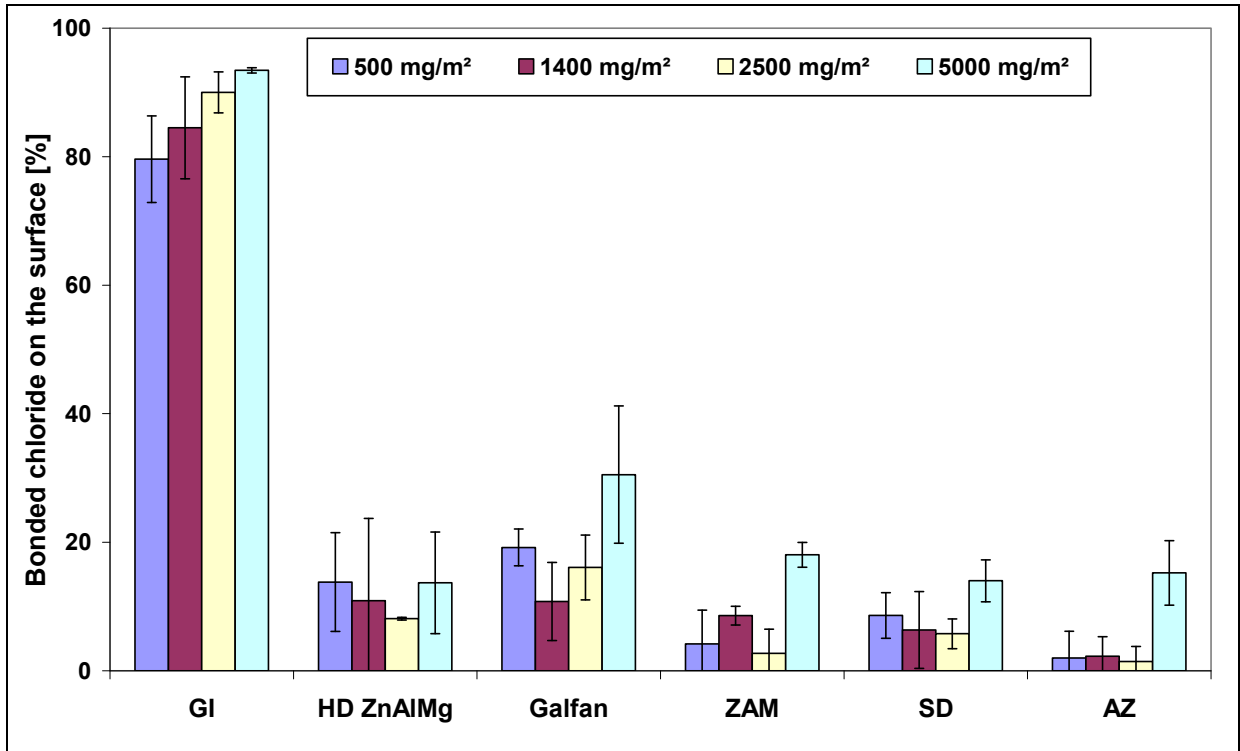


Figure 36 Bonded chloride on the surface from ion chromatography of water extract of corrosion products; results for coated panels exposed 4 weeks at 20°C and 80 % RH and contaminated with 500, 1400, 2500, and 5000 mg/m² of chloride

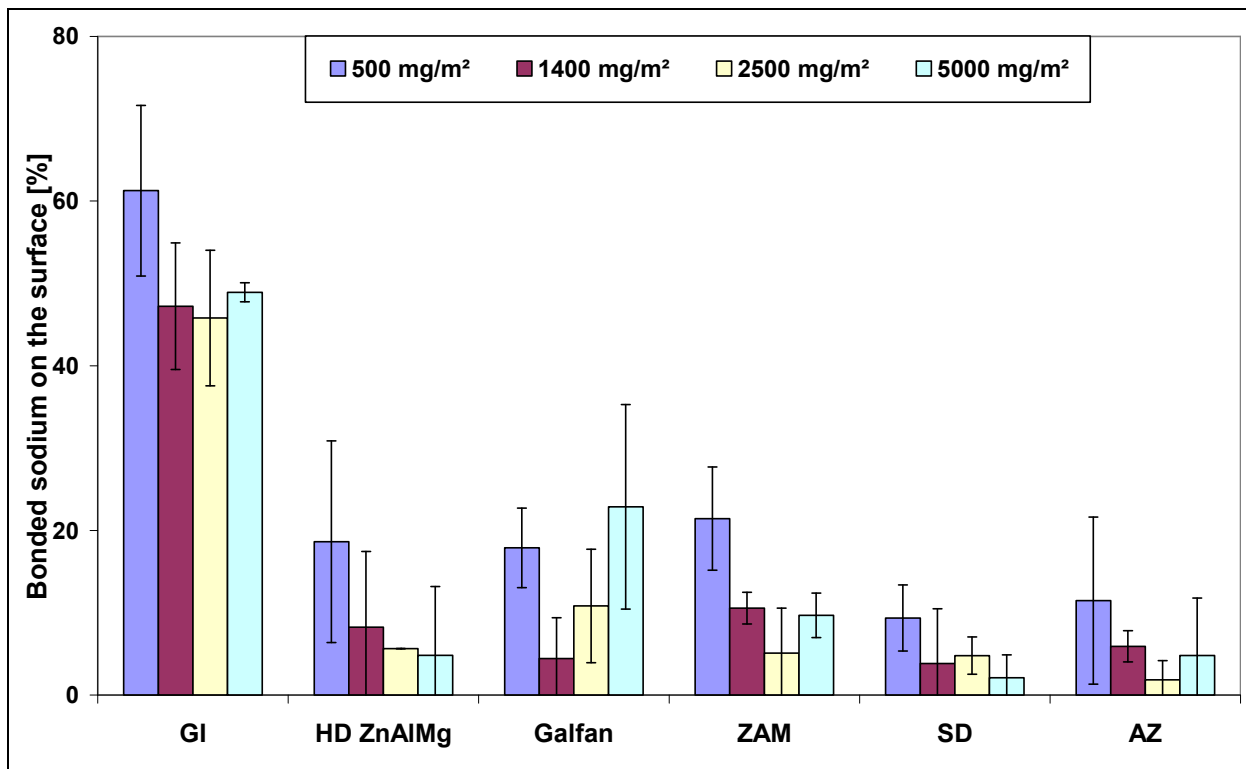


Figure 37 Bonded sodium on the surface from ion chromatography of water extract of corrosion products; results for coated panels exposed 4 weeks at 20°C and 80 % RH and contaminated with 500, 1400, 2500, and 5000 mg/m² of chloride and 324, 907, 1620, and 3240 mg/m² of sodium, respectively

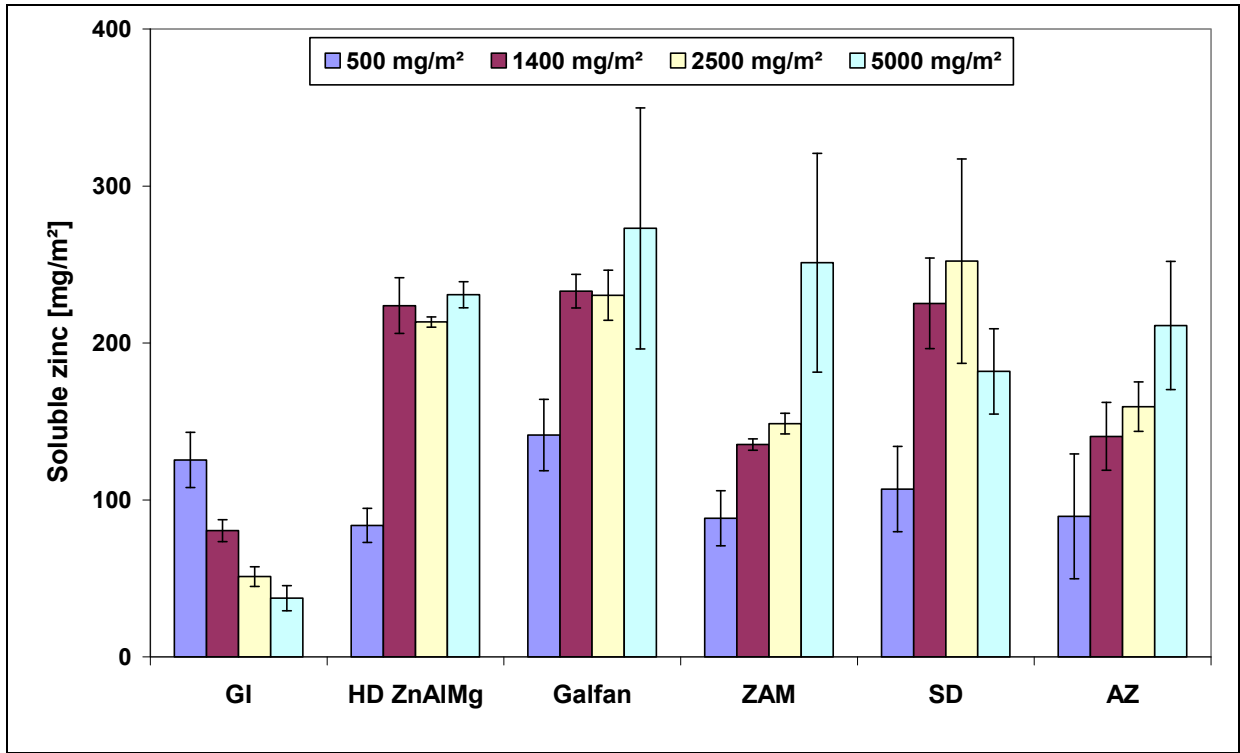


Figure 38 Soluble zinc on the surface from ion chromatography of water extract of corrosion products; results for coated panels exposed 4 weeks at 20°C and 80 % RH and contaminated with 500, 1400, 2500, and 5000 mg/m² of chloride

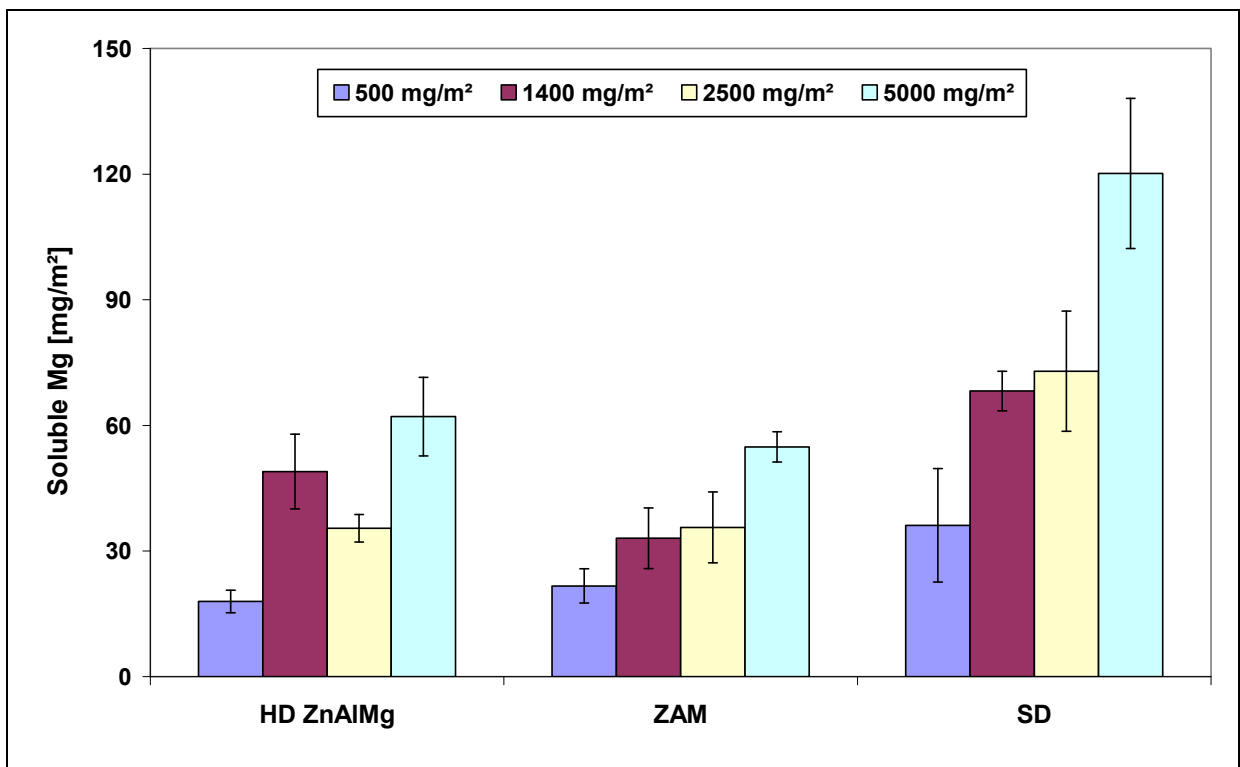


Figure 39 Soluble magnesium on the surface from ion chromatography of water extract of corrosion products; results for coated panels exposed 4 weeks at 20°C and 80 % RH and contaminated with 500, 1400, 2500, and 5000 mg/m² of chloride

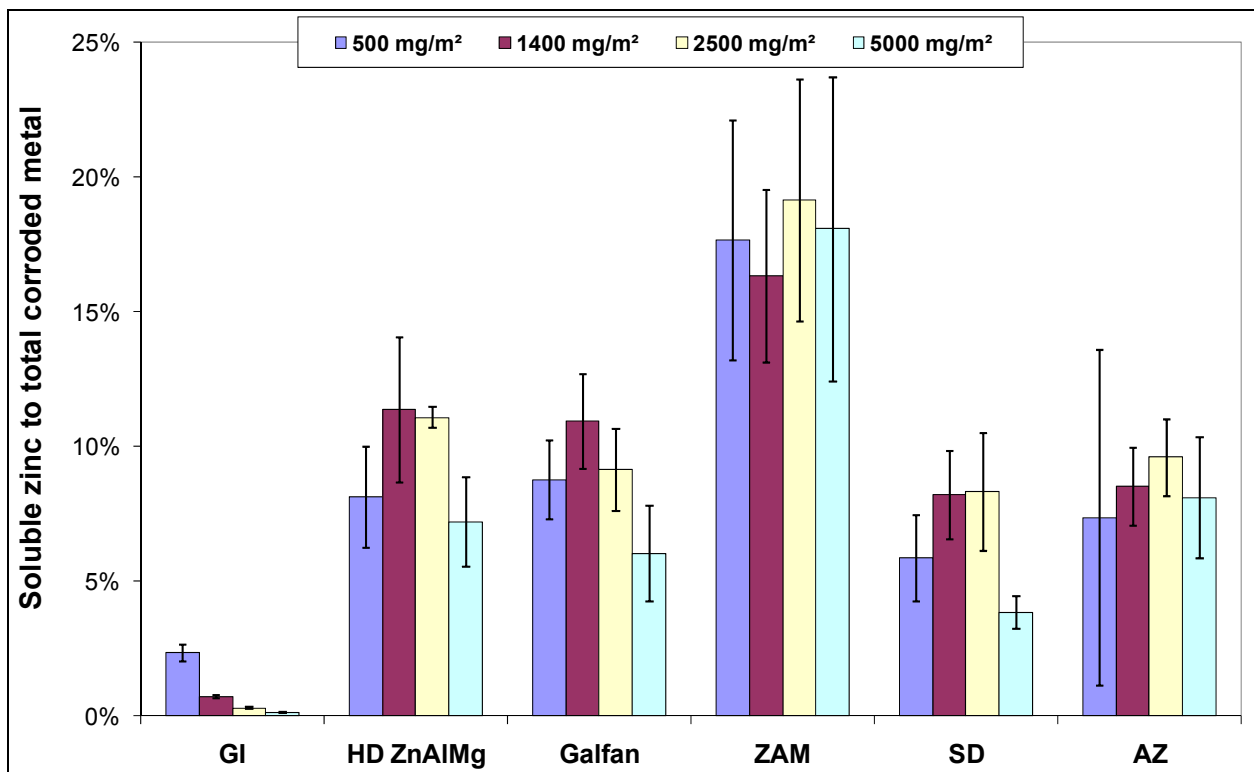


Figure 40 Ratio of soluble zinc to weight loss (total corroded metal); results for coated panels exposed 4 weeks at 20°C and 80 % RH and contaminated with 500, 1400, 2500, and 5000 mg/m² of chloride

The amount of soluble magnesium also increased with the chloride concentration, see Figure 39. It was higher for SD than for ZAM and HD ZnAlMg. When related to weight loss (total corroded metal), approximately constant ratios of soluble magnesium to corroded metal were obtained, see Figure 41. About 2.5 % of total corroded metal was found in form of soluble magnesium in extracts from corrosion products on SD. Since SD contains 3 wt. % Mg, this shows that either practically all corroded magnesium was soluble or magnesium corroded preferentially from the alloy. In case of ZAM and HD ZnAlMg, more than 4 and about 2 % of total corroded metal was found in form of soluble magnesium. Because the respective materials contain only 3 and 1.5 wt. % magnesium, it must be dissolved preferentially.

The pH of water extracts obtained by dissolving the corrosion products in demineralized water is given in Figure 42. A general trend is an increase in pH with increasing weight loss.

Results obtained for commercial metallic coated panels were compared to the ones obtained for model alloys. Weight loss after removal of corrosion products and bonded chloride are compared in Figure 43 and Figure 44, respectively. From these figures it seems that for similar alloying element content, commercial metallic coatings were less susceptible to corrosion than model alloys (e.g. ZnAl5 vs. Galfan, ZnAl2Mg2 vs. HD ZnAlMg). Only ZnAl55 model alloy was less corroded than the commercial AZ coating. This is even more visible in Figure 45 and Figure 46 where the weight loss is plotted as a function of alloying element in coatings and in model alloys. It is evident in Figure 46 that corrosion resistance of metallic coatings and model alloys with comparable content of alloying elements differed significantly particularly below 5 % of the total alloying. Although the tests for commercial metallic coatings and for model alloys were not performed in the same time, it is probable that the observed difference cannot be explained by experimental error. The generally better corrosion resistance of metallic coatings compared to model alloys might be explained by the passivation treatment of metallic coatings or by segregation of alloying elements to the outer surface of the coatings. The latter effect was observed by authors of this study on other Rhescacoated samples studied using XPS. It is possible that the effective content of alloying elements in the outer

part of hot-dip coatings was significantly higher than the bulk concentration. This would indeed improve corrosion performance in a test where only the top coating layer is corroded.

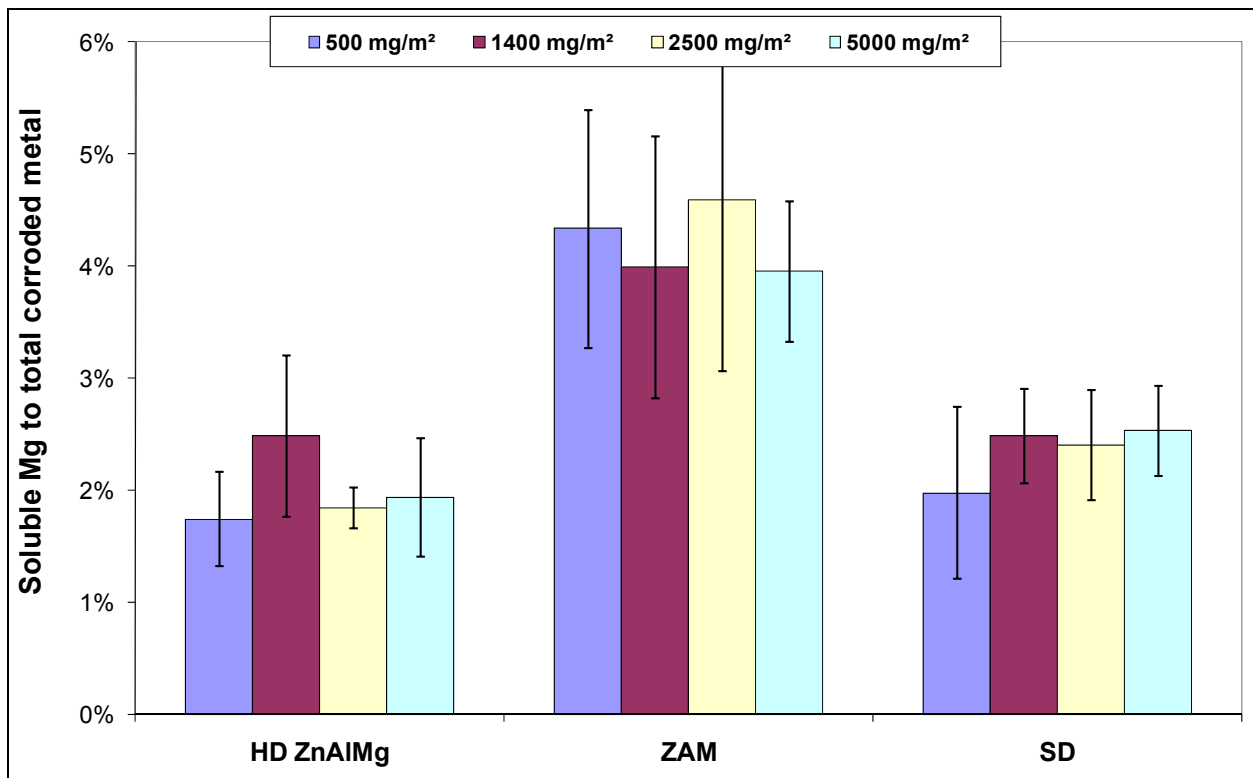


Figure 41 Ratio of soluble magnesium to weight loss (total corroded metal); results for coated panels exposed 4 weeks at 20°C and 80 % RH and contaminated with 500, 1400, 2500, and 5000 mg/m² of chloride

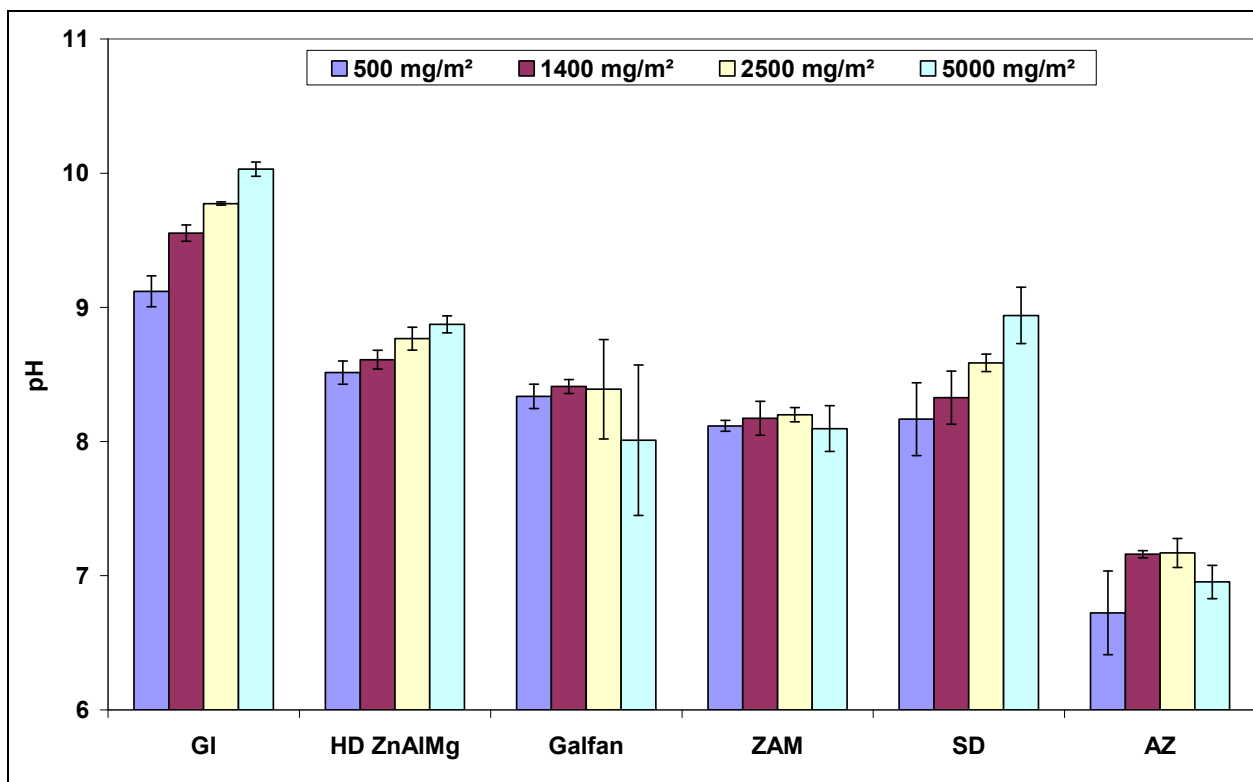


Figure 42 pH of water extracts obtained by dissolving corrosion products

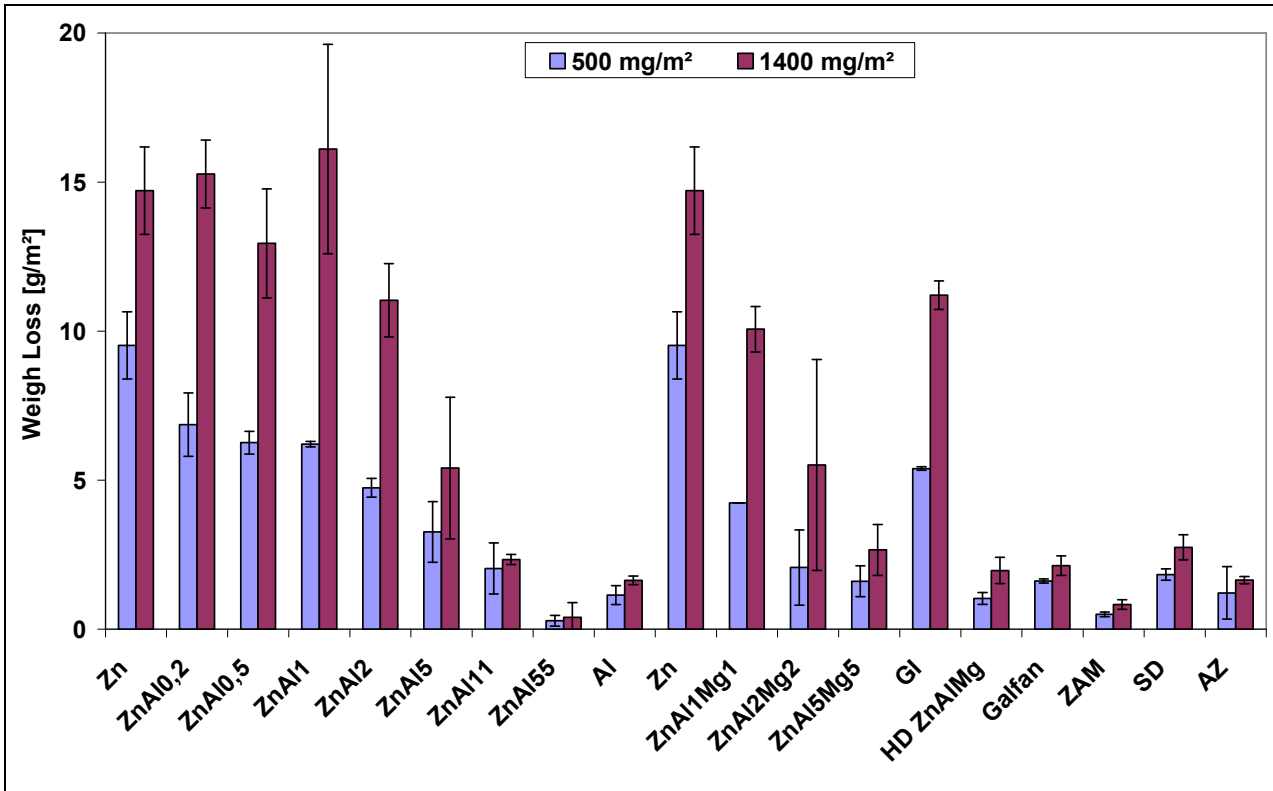


Figure 43 Weight loss comparison between commercial metallic coated steel and model alloys after 4 weeks of exposure at 20°C and 80 % RH

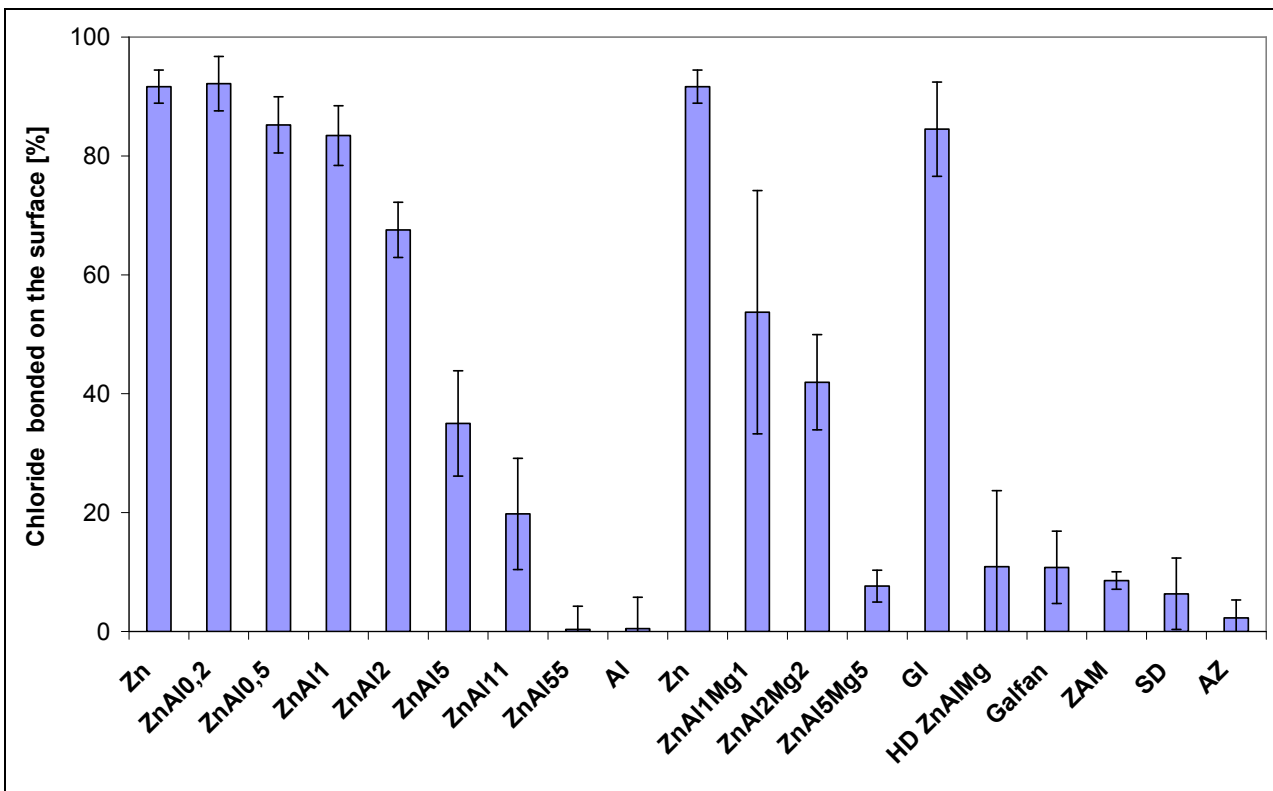


Figure 44 Bonded chloride comparison between commercial metallic coated steel and model alloys after 4 weeks of exposure at 20°C and 80 % RH

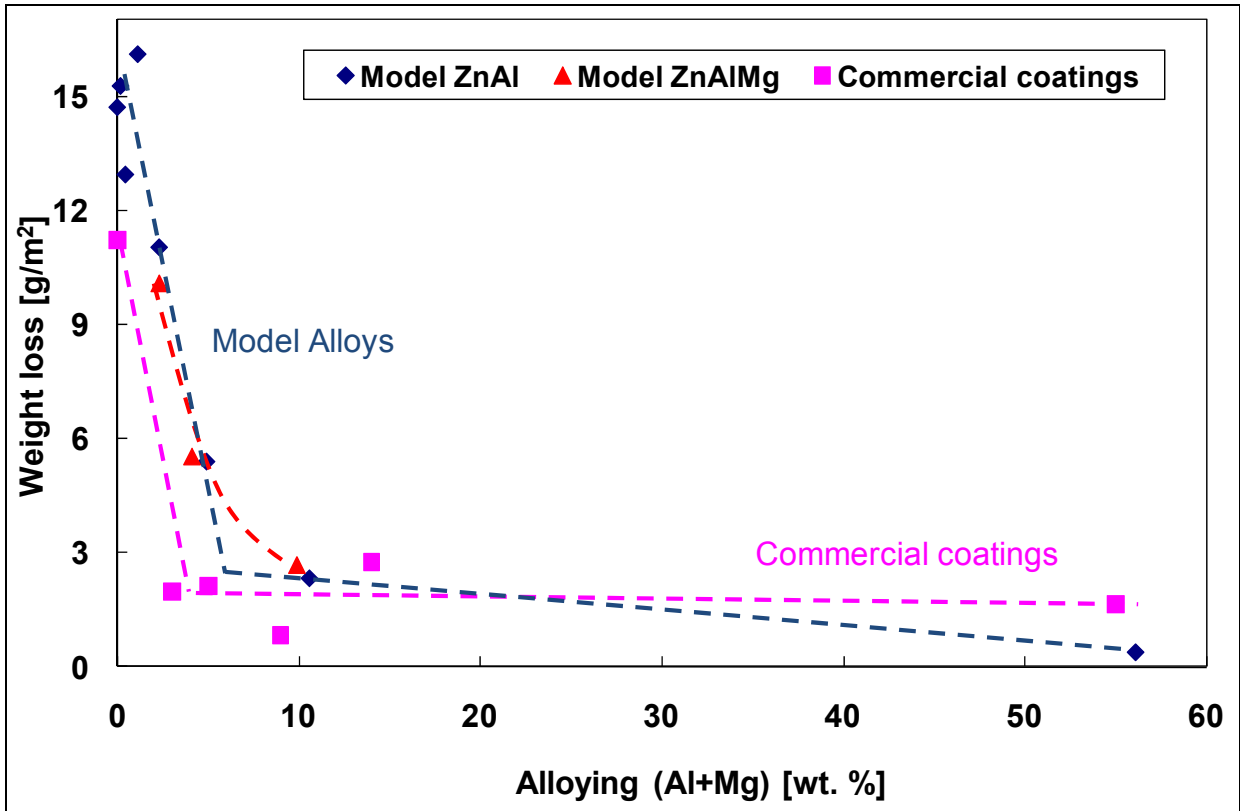


Figure 45 Weight loss versus alloying from 0 to 55%; comparison of metallic coatings and model alloys after 4 weeks of exposure at 20°C and 80 % RH at the chloride contamination of 1400 mg/m²

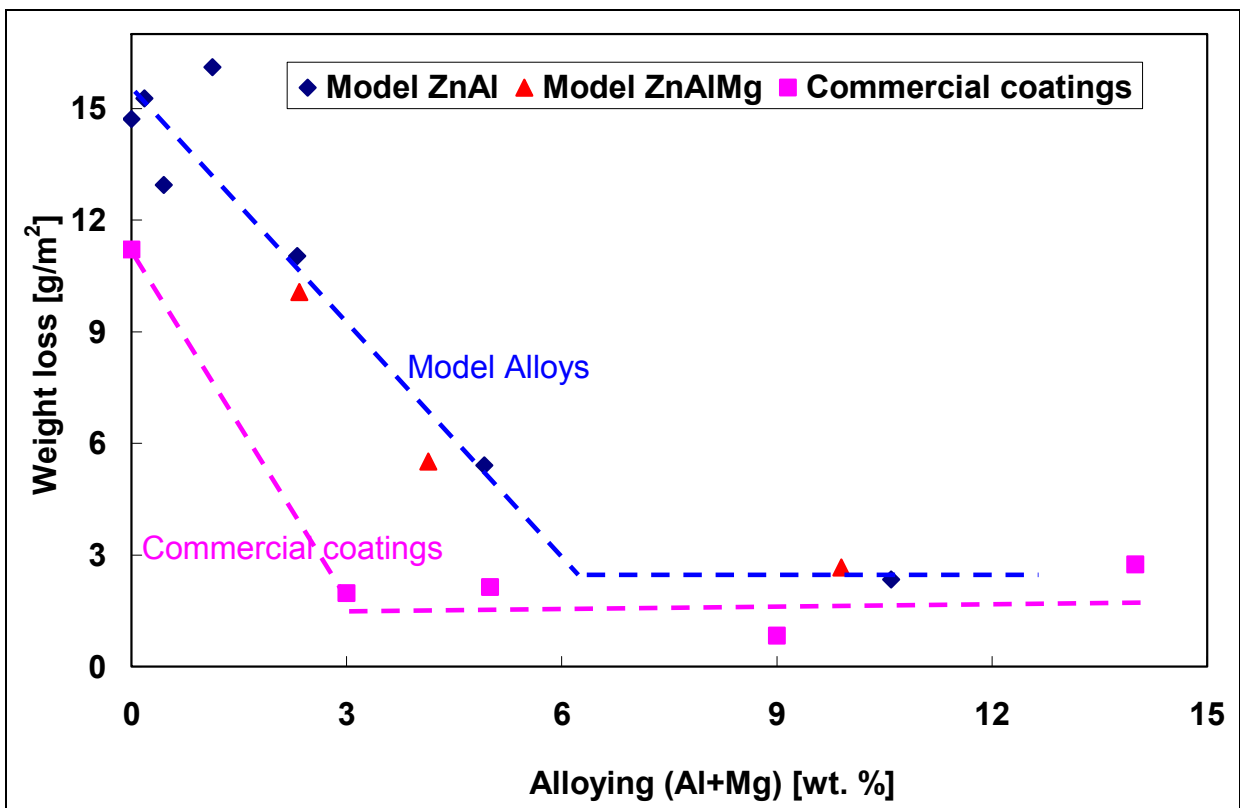


Figure 46 Weight loss versus alloying from 0 to 14%; comparison of metallic coatings and model alloys after 4 weeks of exposure at 20°C and 80 % RH at the chloride contamination of 1400 mg/m²

4.3.3 Phase composition of corrosion products

Corrosion products from commercial coated materials and HD ZnAlMg contaminated by sodium chloride at 1400 mg/m² chloride and exposed for 28 days at 20°C and at 80 % RH were analyzed by FTIR. The spectra are plotted in Figure 47 and results are summarized in Table 10. Results of analyses of products from GI and HD ZnAlMg contaminated with 5000 mg/m² chloride and exposed at the same conditions are in Figure 48 and Table 11. Reference spectra can be seen in Figure 22 and Figure 23.

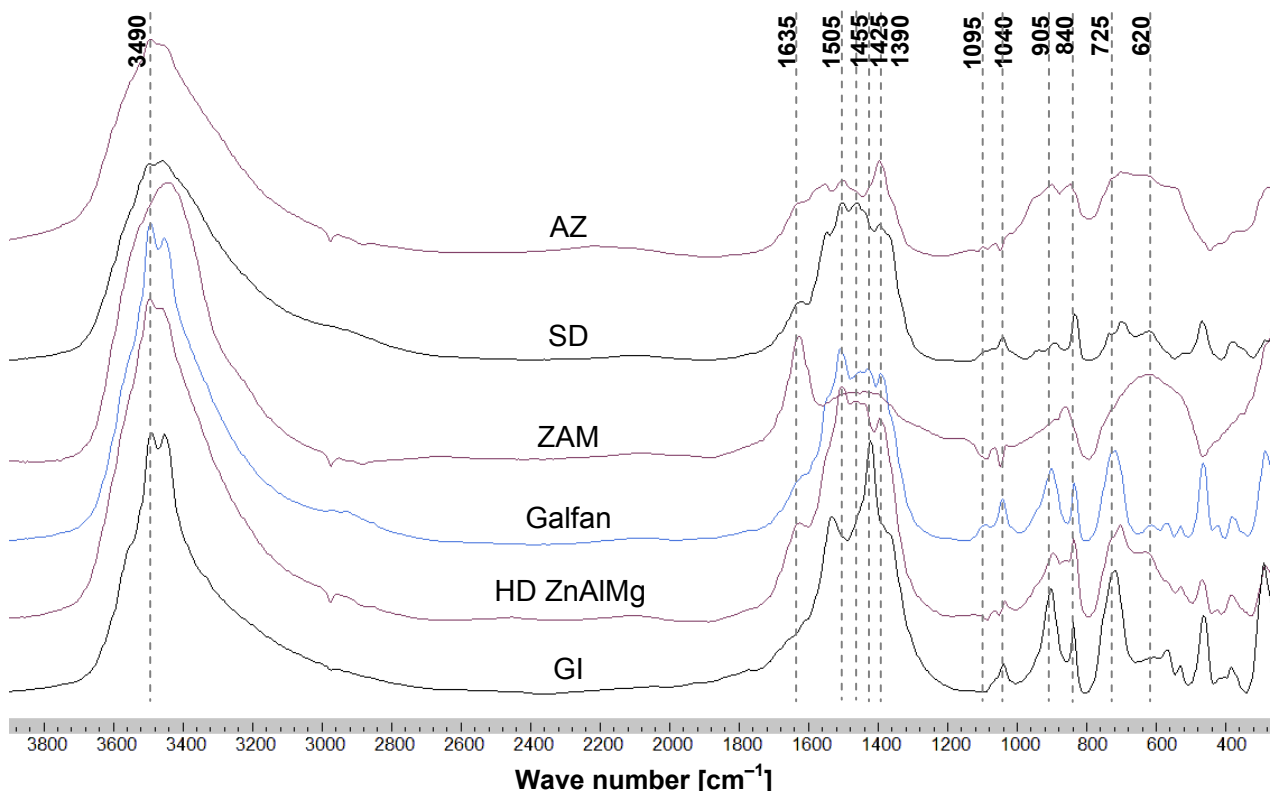


Figure 47 Infrared transmission spectra of corrosion products collected on coated materials with deposited sodium chloride at the chloride concentration of 1400 mg/m² exposed for 28 days at 20°C and at 80 % RH

Table 10 Phase composition of corrosion products collected from coated steel panels contaminated with 1400 mg/m² chloride after 28 days of exposure in humid air at 80 % RH and at 20°C

Alloy	Hydrozincite (1505 cm ⁻¹)	Simonkolleite (905 cm ⁻¹)	C/S ratio [×]	Sodium carbonate (1455 cm ⁻¹)	Unidentified carbonate (1425 cm ⁻¹)	Water (1630 cm ⁻¹)	AlOOH (1095, 620 cm ⁻¹)	Others
GI	Yes	Yes	2.5	Yes	Yes +	No	No	
HD ZnAlMg	Yes	Yes	3.8–12.9	Yes	No	Yes	Yes –	MgCO ₃
Galfan	Yes	Yes	3.3	Yes	Yes	Yes	Yes	
ZAM	Yes	No	–	–	–	Yes +	Yes +	
SD	Yes	Yes –	21.6	Yes	No	Yes	Yes	MgCO ₃
AZ	Yes	Yes	2.2–5.9	Yes	No	Yes	Yes	

[×] Carbonate to simonkolleite peak height ratio; – Weak peak, lower quantity; + Strong peak, higher quantity

As for model alloys, the presence of aluminum and magnesium in the structure caused an increase in the width of the OH peak at 3600–3200 cm⁻¹. A C/S ratio was higher for alloyed materials than for GI. Aluminum-based products were detected in corrosion products from all coatings containing aluminum. A weak peak at about 1440 cm⁻¹ was observed in spectra of HD ZnAlMg and SD. It might be associated with

magnesite, $MgCO_3$. In all cases, hydrozincite, simonkolleite, and sodium carbonate were found. Peaks in the spectrum of another material containing magnesium, ZAM, were broad and it was difficult to analyze it properly. The composition of corrosion products formed in presence of 1400 and 5000 mg/m^2 chloride on GI and HD ZnAlMg was similar. In case of GI, the strong peak at 1425 cm^{-1} dominated in the carbonate region. Carbonate-based corrosion products on HD ZnAlMg were composed mainly of hydrozincite.

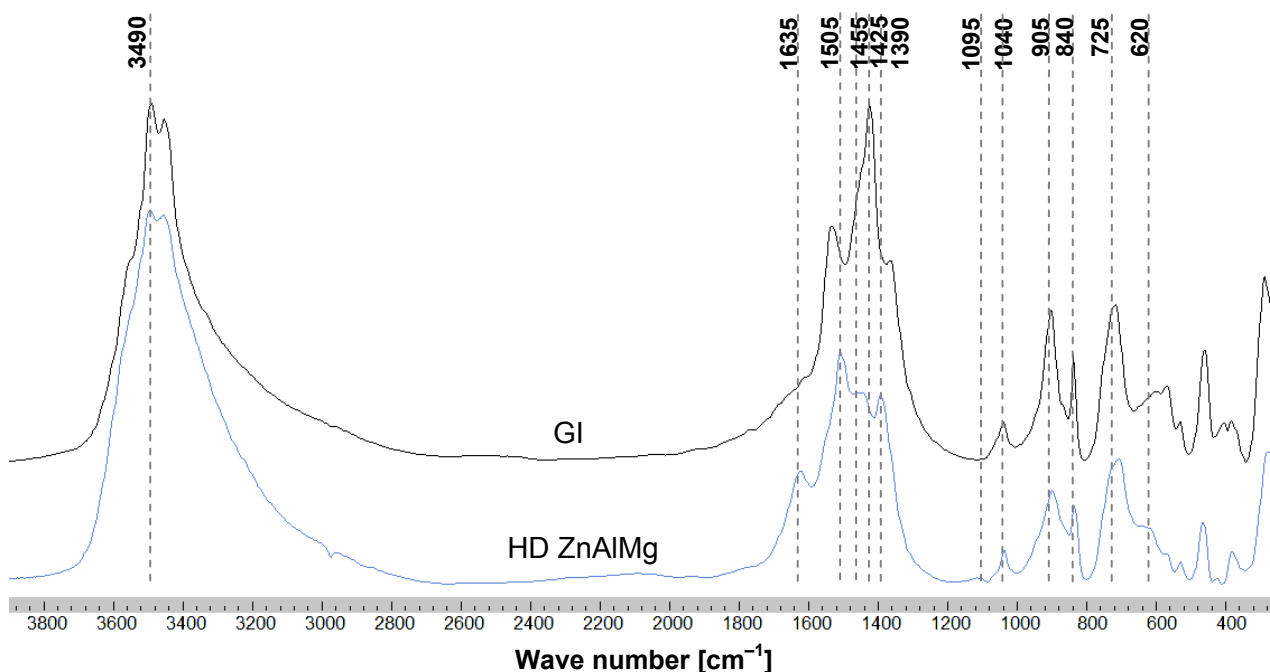


Figure 48 Infrared transmission spectra of corrosion products collected on coated materials with deposited sodium chloride at the chloride concentration of 5000 mg/m^2 exposed for 28 days at 20°C and at 80 % RH

Table 11 Phase composition of corrosion products collected from coated steel panels contaminated with 5000 mg/m^2 chloride after 28 days of exposure in humid air at 80 % RH and at 20°C

Alloy	Hydrozincite (1505 cm^{-1})	Simonkolleite (905 cm^{-1})	C/S ratio ^x	Sodium carbonate (1455 cm^{-1})	Unidentified carbonate (1425 cm^{-1})	Water (1630 cm^{-1})	AlOOH ($1095, 620\text{ cm}^{-1}$)	Others
GI	Yes	Yes	2.5	Yes –	Yes +	No	No	
HD ZnAlMg	Yes	Yes	2.6	Yes –	No	Yes	Yes –	$MgCO_3$

^x Carbonate to simonkolleite peak height ratio; – Weak peak, lower quantity; + Strong peak, higher quantity

The composition of corrosion products on HD ZnAlMg was similar to those collected from model alloys ZnAl1Mg1 and ZnAl2Mg2. However, there was relatively more sodium carbonate on the model alloys whereas hydrozincite dominated in the carbonate region in the spectrum of HD ZnAlMg. Peaks at 1445 and 620 cm^{-1} associated with magnesium and aluminum corrosion products were also more profound for HD ZnAlMg. This again shows on the concentration of alloying elements in the outer layer of the coating.

Corrosion products from commercial coated materials and HD ZnAlMg contaminated by sodium chloride at 1400 and 5000 mg/m^2 and exposed for 28 days at 20°C and at 80 % RH were also analyzed by XRD. Results are given in Table 12. It should be mentioned that except for GI, collected corrosion products were in a very limited quantity near the minimum required quantity to perform XRD. Results show that practically all NaCl on GI reacted to form corrosion products (simonkolleite and probably hydrozincite and sodium(hydroxy)carbonate). Only simonkolleite was clearly identified in other corrosion products. Thus,

XRD did not provide much information except that as expected, more non-reacted NaCl was present on the alloyed coatings and its quantity also increased with the chloride contamination.

Table 12 XRD semi-quantitative results

Coating	Chloride contamination mg/m ²	NaCl	Simonkolleite	Other(s)	Comments
GI	1400	0	92	8	Probably hydrozincite and sodium(hydroxy)carbonate
	5000	4	88	8	
HD ZnAlMg	1400	66	34	-	
	5000	95	5	-	
Galfan	1400	76	24	-	
	5000	84	16	-	
ZAM	1400	99	0	1	Unidentified compound
	5000	99	1	-	
SD	1400	82	18	?	Other reflection in spectra, not clear
	5000	93	7	?	
AZ	1400	97	3	-	
	5000	98	2	-	

4.3.4 Effect of temperature

The effect of temperature on corrosion of metallic coated panels was studied at 80 % of relative humidity. Results obtained at 10, 20 (see chapter 4.3.1) and 40°C are compared. The weight loss for samples exposed at 10°C after removal of corrosion product is given in Figure 49. For the chloride contamination from 500 to 5000 mg/m², GI showed an increase in the weight loss from 4 to 26 g/m². The amount of corroded metal did not exceed 3.2 g/m² for any other tested coating at any chloride concentration after 4 weeks of exposure at 10°C. The effect of the surface chloride concentration on the weight loss of all alloyed coatings was very limited at 10°C. The materials can be classified in following order from the most to the least corroded one:

$$GI \ll HD \text{ ZnAlMg} < SD < AZ < \text{Galfan} < ZAM$$

Wet mass gain evolution of specimens during test at 40°C is given in Figure 50. The variation in mass gain between tested coatings is clearly more profound than at 20°C. It can be noted that the mass gain was not stabilized even after 4 weeks of exposure at 40°C. Thus, it is possible that the results would be somewhat altered if the exposure time is longer. Weight loss data are shown in Figure 51. The following classification of the corrosion stability at 40°C can be obtained from the data:

$$GI < HD \text{ ZnAlMg} < \text{Galfan} < ZAM < SD < AZ$$

It should be noticed that higher temperature generated bigger differences between alloyed coatings. The effect of temperature on weight loss of GI was small. The fact that zinc shows a rather flat dependence on temperature in CO₂ containing air is known and has been published. Therefore, the gap between GI and alloyed materials was reduced at the elevated temperature.

Figure 52 shows dependence of the weight loss on total amount of magnesium and aluminum at 40°C. The total amount of alloying elements had a strong effect on the weight loss. It strongly decreased from 0 to 5 % of the alloying content at all levels of chloride contamination. From 5 %, the alloying content had still well

visible, but somewhat weaker effect, particularly at lower chloride concentrations. This observation is in good agreement with results obtained for ZnAl and ZnAlMg model alloys at 20°C, compare Figure 52 and Figure 15.

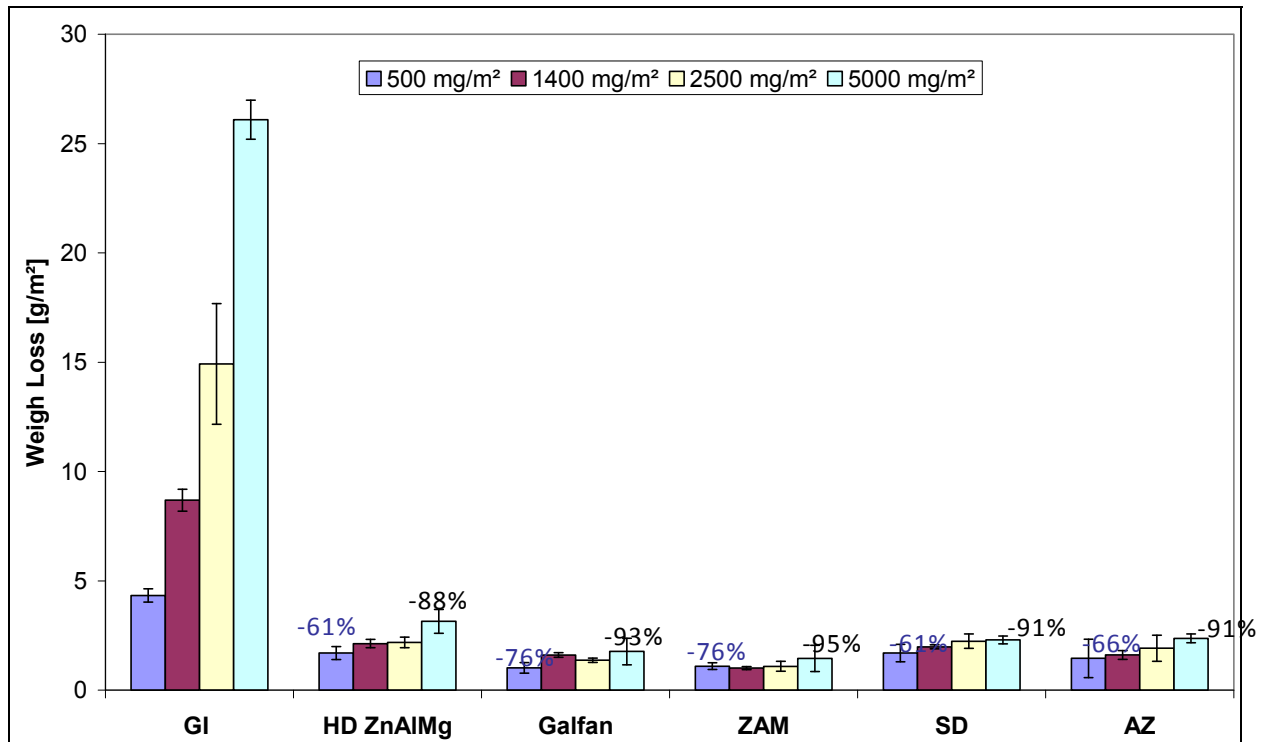


Figure 49 Weight loss of metallic coated steel panels after 4 weeks of exposure at 10°C and 80 % RH

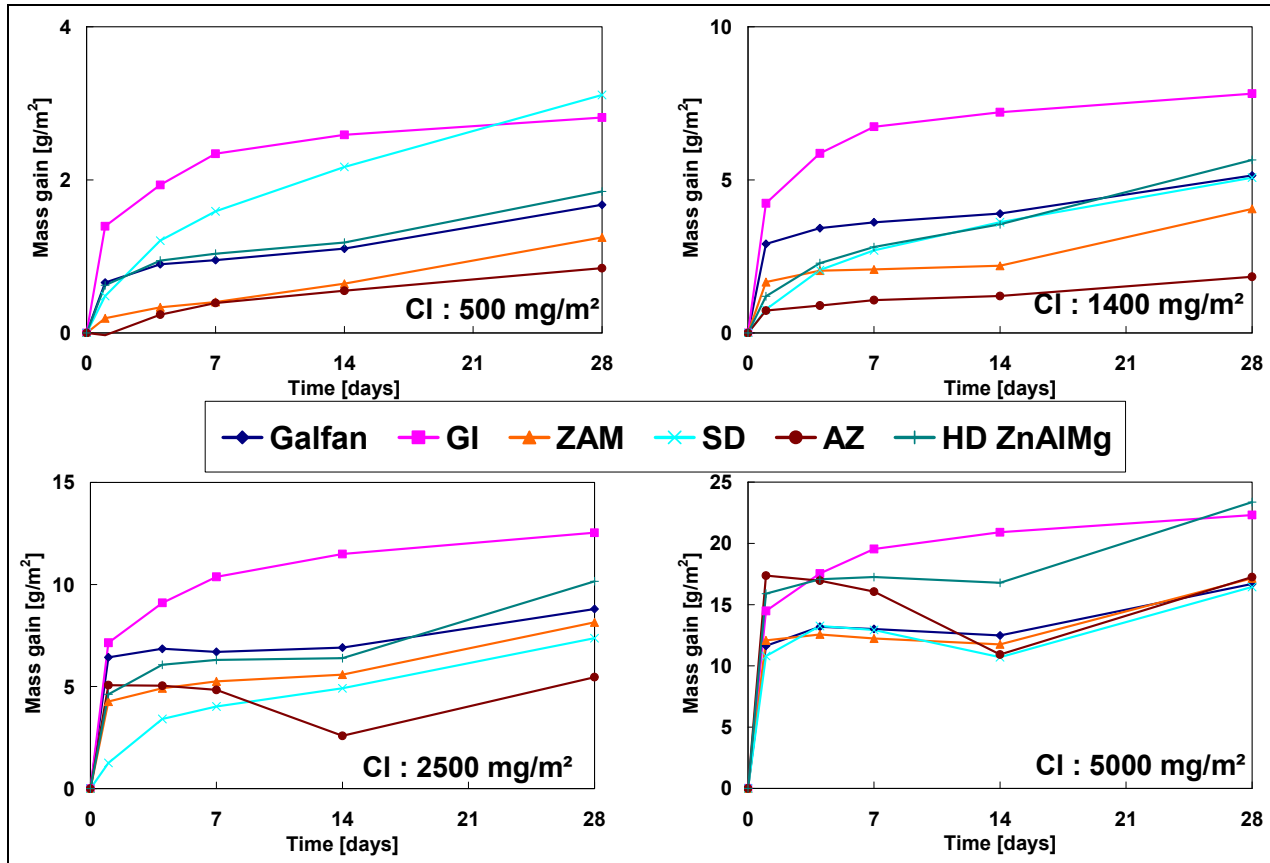


Figure 50 Wet mass gain of metallic coated steel during exposure at 40°C and 80 % RH

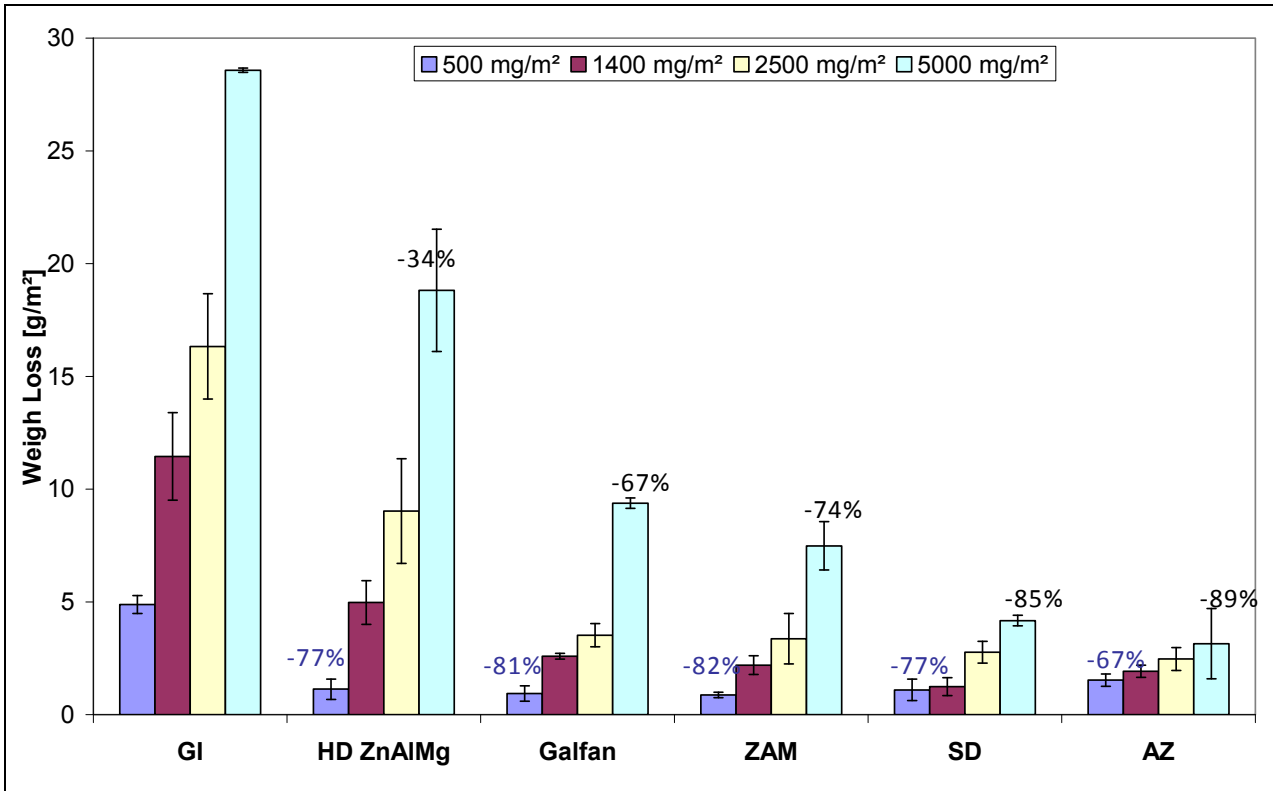


Figure 51 Weight loss of metallic coated steel after 4 weeks of exposure at 40°C and 80 % RH

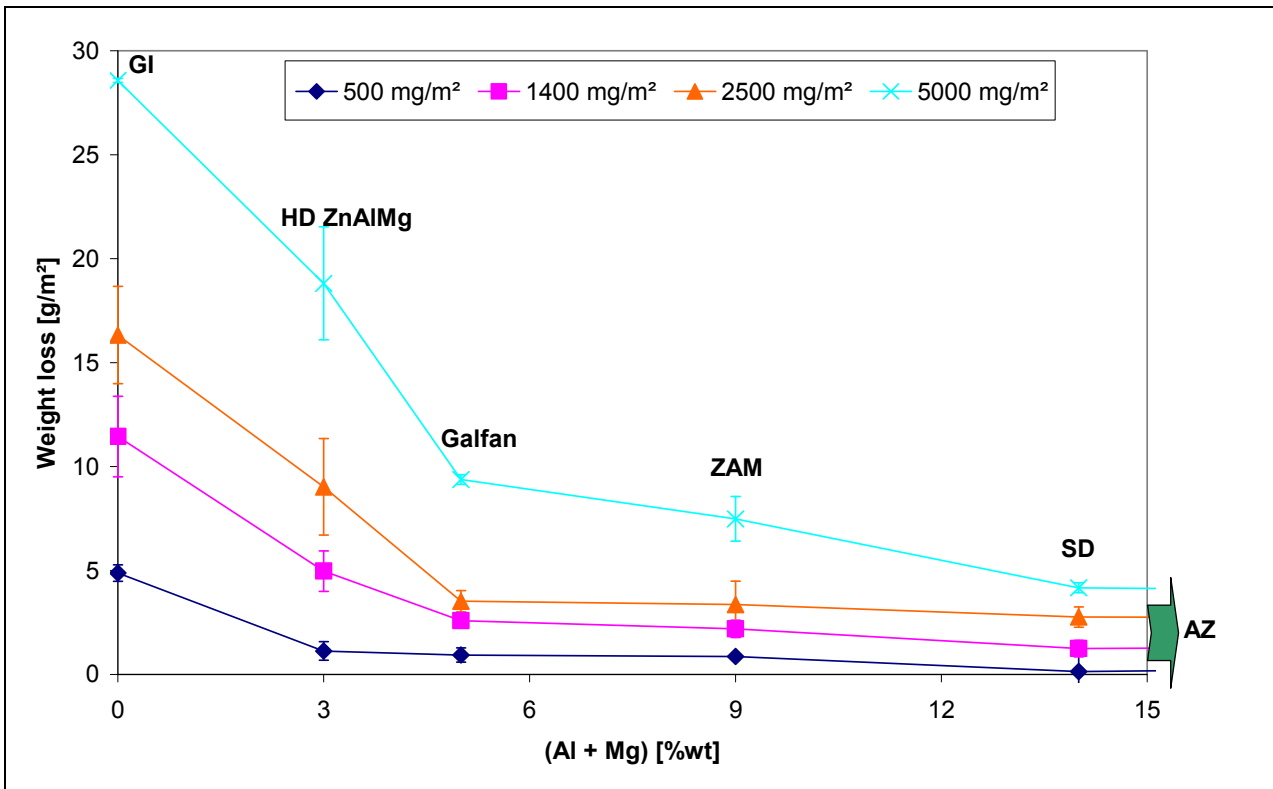


Figure 52 Weight loss vs. alloying for metallic coated steel after 4 weeks of exposure at 40°C and 80 % RH

The weight loss of coated steel panels exposed at 40°C and at 80 % RH depended on the total amount of the alloying elements as observed previously for model alloys exposed at 20°C and the same relative humidity.

Interestingly, the order of corrosion performance was somewhat different at 10 and 20°C for the coated materials. It is possible that the corrosion resistance of the commercial coated materials was partly affected by surface treatment or passivation. The samples were obtained from several suppliers and although they were stated as ‘non-treated’, this cannot be fully neglected. Before exposure, they were degreased in acetone, but any other surface preparation such as polishing was not applied. Since the weight loss at 10 and 20°C were usually lower than at 40°C, less metal was corroded and the state of the surface layer played more important role in the overall corrosion performance.

The weight loss data at 10, 20, and 40°C for samples contaminated with 500, 1400, 2500, and 5000 mg/m² chlorides are summarized in Figure 53. The dependence of the weight loss on temperature was rather flat for GI, SD, and AZ. Contrariwise, an increase in the weight loss with temperature was seen for HD ZnAlMg, Galfan, and ZAM. In general, the alloying was most efficient (the difference between GI and other coatings was the highest) at low temperature and high chloride concentration.

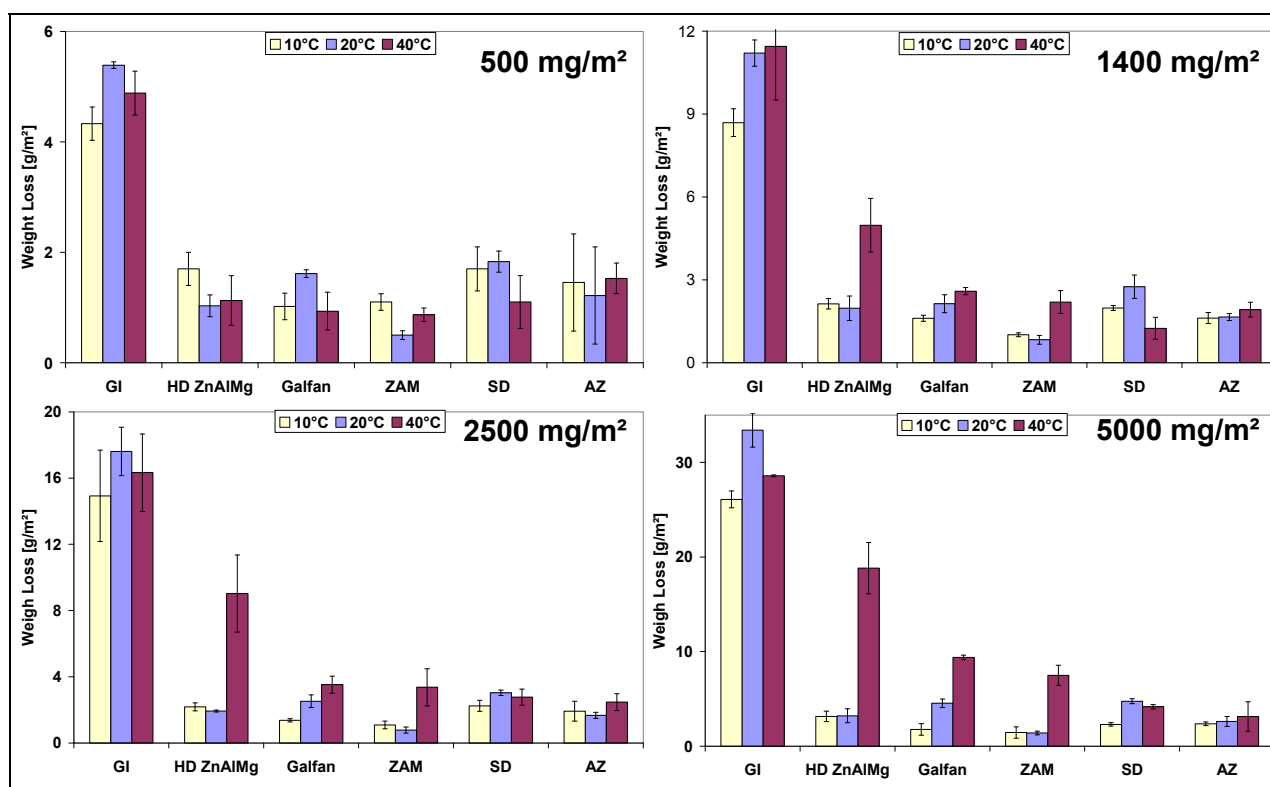


Figure 53 Weight loss comparison between 10°C, 20°C and 40°C at 80 % RH after 4 weeks of exposure at the chloride contamination from 500 to 5000 mg/m²

At 500 mg/m² of chloride contamination, the corrosion rate of all alloyed coatings was low and less than 2 mg/m² of metal corroded in 4 weeks of exposure. Since the experimental error was relatively high in this case, the analysis of results at this chloride concentration is more difficult.

The effect of temperature on the weight loss of GI, HD ZnAlMg and AZ is shown in Figure 54. The difference between the weight loss at 10 and 20°C is low for the alloyed coatings. An increase in the temperature to 40°C was more detrimental for coatings with 3 to 9 % of alloying elements. The weight loss of AZ was almost independent of temperature as it increased only by 19 % from 10 to 40°C, whereas it increased by 133 % for HD ZnAlMg. Consequently, the efficiency of HD ZnAlMg related to GI was reduced at the elevated temperature.

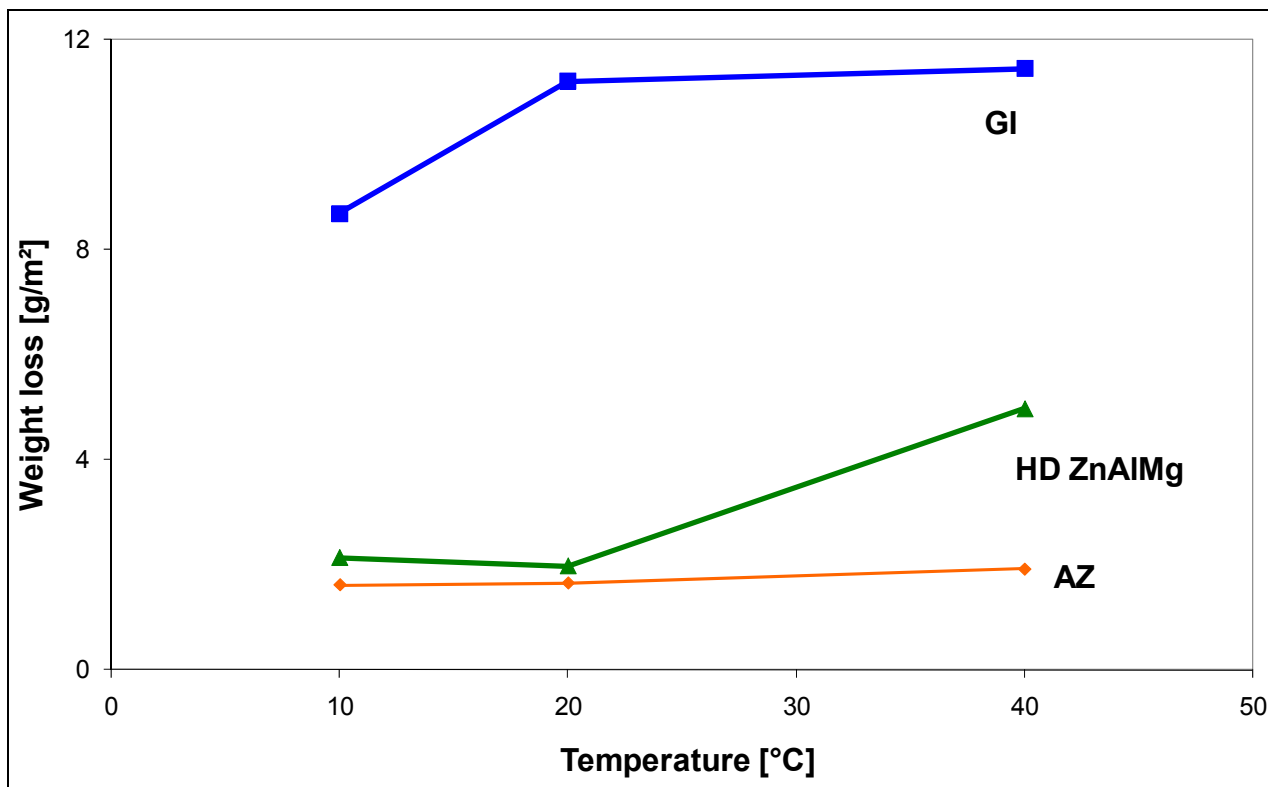


Figure 54 Weight loss dependence of GI, HD ZnAlMg and AZ on temperature at 80 % RH after 4 weeks of exposure of samples contaminated by 1400 mg/m² of chloride

4.3.5 Effect of relative humidity

The effect of relative humidity on corrosion of metallic coated panels was studied at 20°C at 65, 80 and 95 % RH. The lowest relative humidity level was selected to be below the deliquescence point of NaCl. Thus, considering only NaCl, no solution should be formed on the metal surface at 65 % RH.

The wet mass gain during tests at 65, 80 and 95 % RH in presence of 1400 mg/m² chloride is given in Figure 55, Figure 56 and Figure 57, respectively. At 65 % RH, the mass gain during test can be mainly attributed to corrosion product formation on the surface. The kinetics of the process was slow on SD, AZ, and ZAM. Very low mass gains were recorded within 4 weeks for these materials. The kinetics of less alloyed materials HD ZnAlMg and Galfan was also slow during first 14 days of exposure, but it increased considerably in second 2 weeks. The build-up of the surface electrolyte and corrosion products on GI was also slower than at higher RH, but the final mass gain was not significantly lower than at 80 % RH.

At 95 % of RH (Figure 57), the wet mass gain is mainly due to water adsorption in the NaCl layers on the surface of the specimens. It was almost the lowest for GI, revealing that surface deposits were less hygroscopic than on other materials. The difference between different coatings was rather small.

Figure 58 shows the weight loss after the removal of corrosion products for specimens tested at 95 % RH and at 20°C. The same general trend as at 80 % RH and 20°C was observed. Again, the effect of the chloride concentration was the most profound on GI. The following classification from the least resistant to the most stable material can be given:

$$GI \ll HD \text{ ZnAlMg} < \text{Galfan} < AZ < SD < ZAM.$$

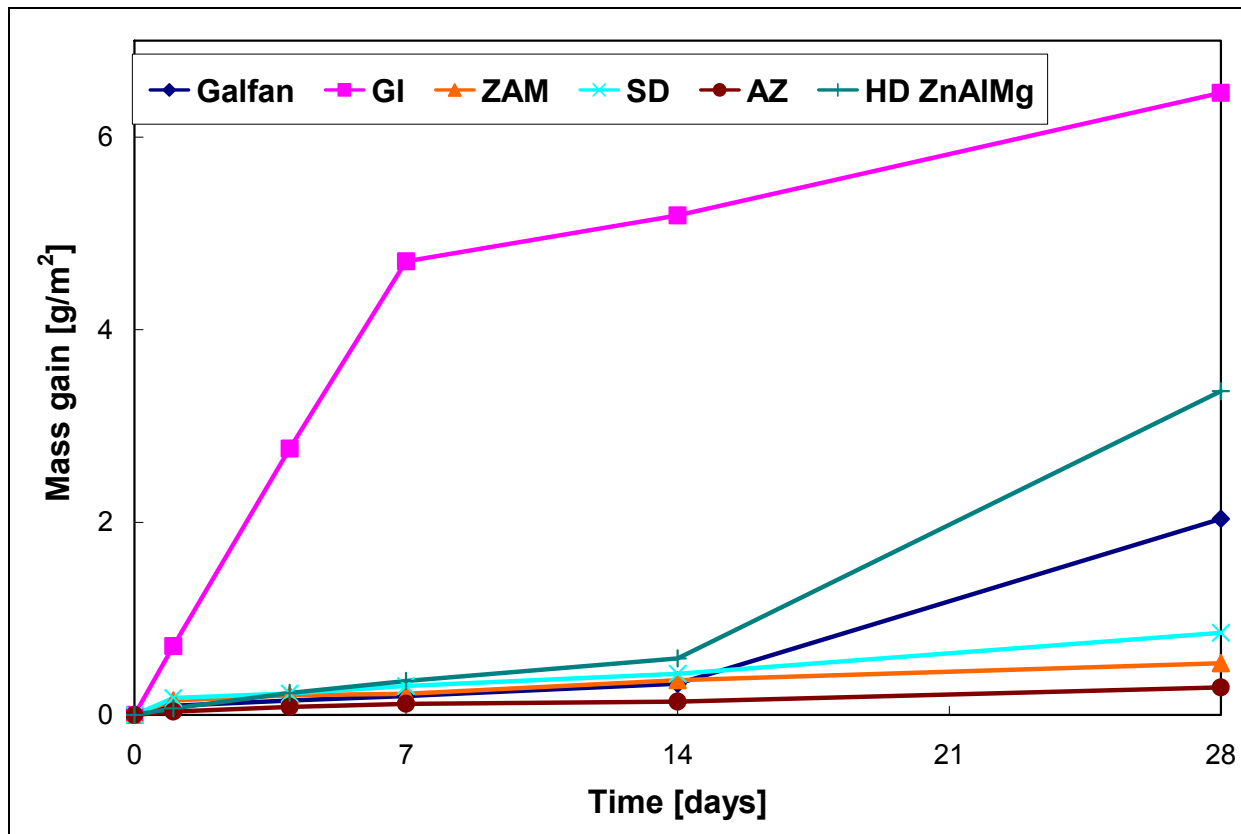


Figure 55 Wet mass gain of metallic coated steel sheets during exposure at 20°C and 65 % RH with 1400 mg/m² chloride

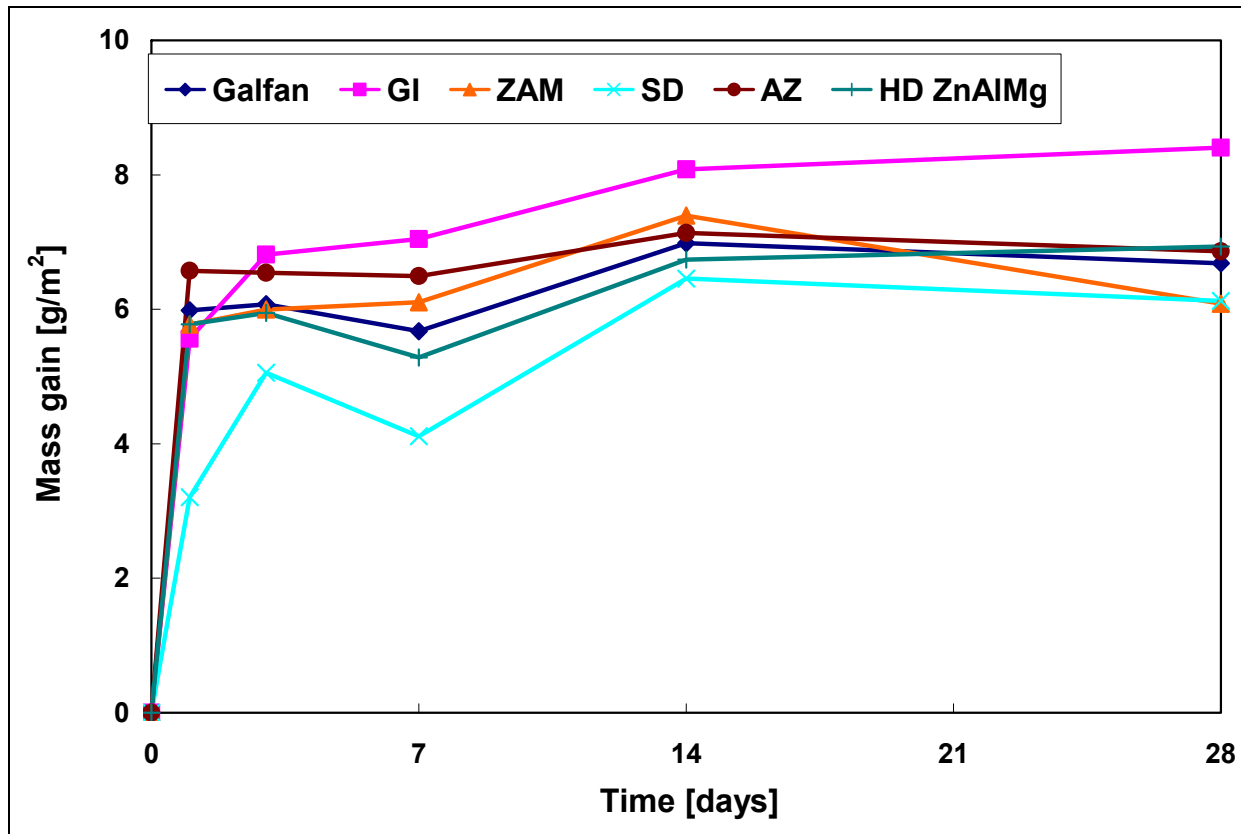


Figure 56 Wet mass gain of metallic coated steel sheets during exposure at 20°C and 80 % RH with 1400 mg/m² chloride

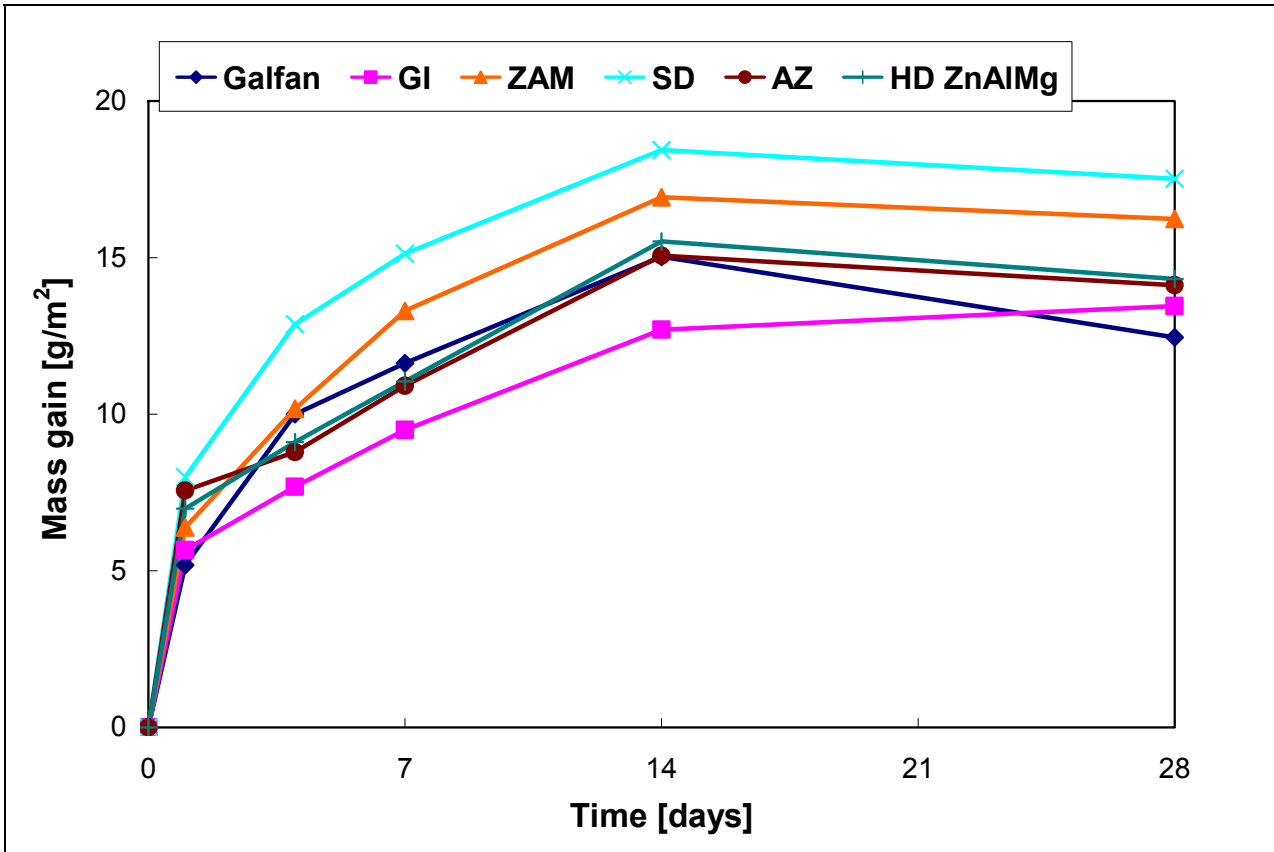


Figure 57 Wet mass gain of metallic coated steel sheets during exposure at 20°C and 95 % RH with 1400 mg/m² chloride

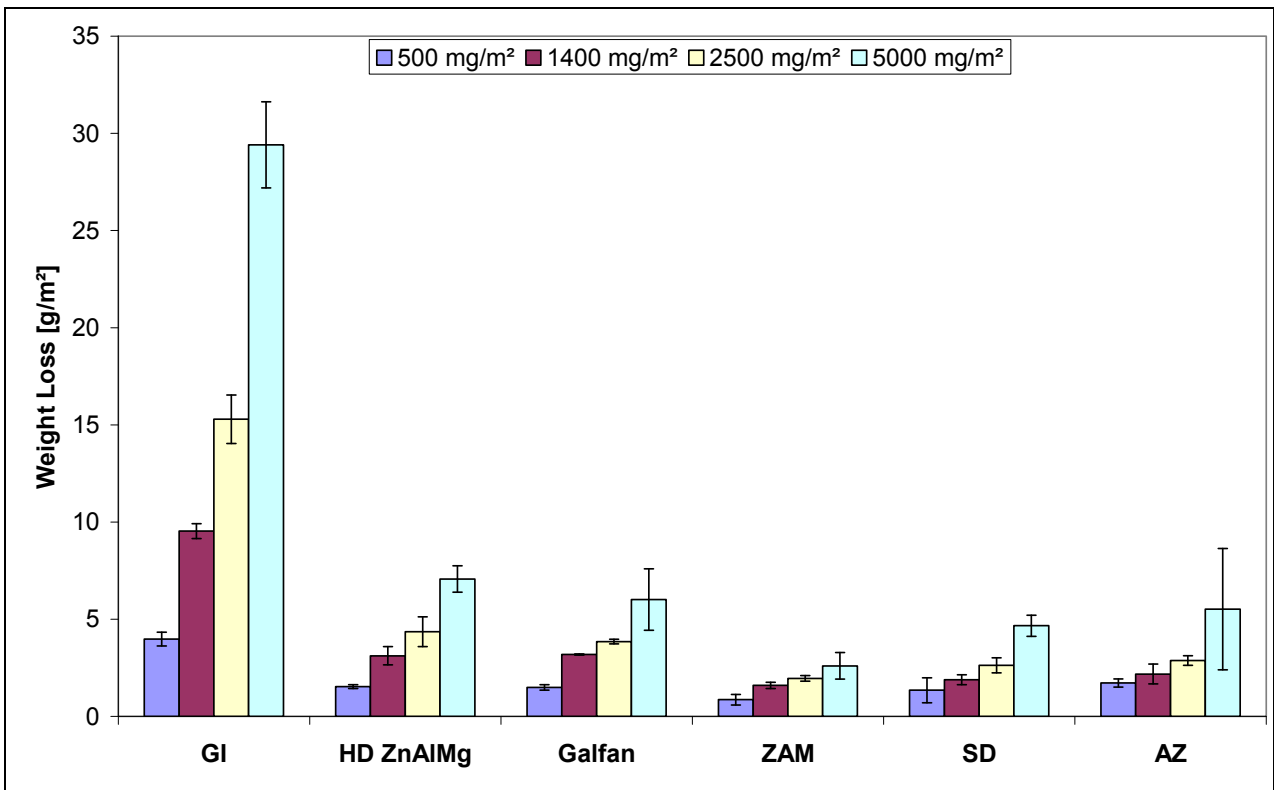


Figure 58 Weight loss of metallic coated steel after 4 weeks of exposure at 20°C and 95 % RH

At 65 % RH, only samples contaminated with 1400 mg/m² chloride were exposed. As seen in Figure 59, the weight loss was again the highest for GI and decreased in following order:

$$GI \ll HD \text{ ZnAlMg} < \text{Galfan} < SD < ZAM < AZ,$$

i.e. almost fully in order of increasing total content of alloying elements.

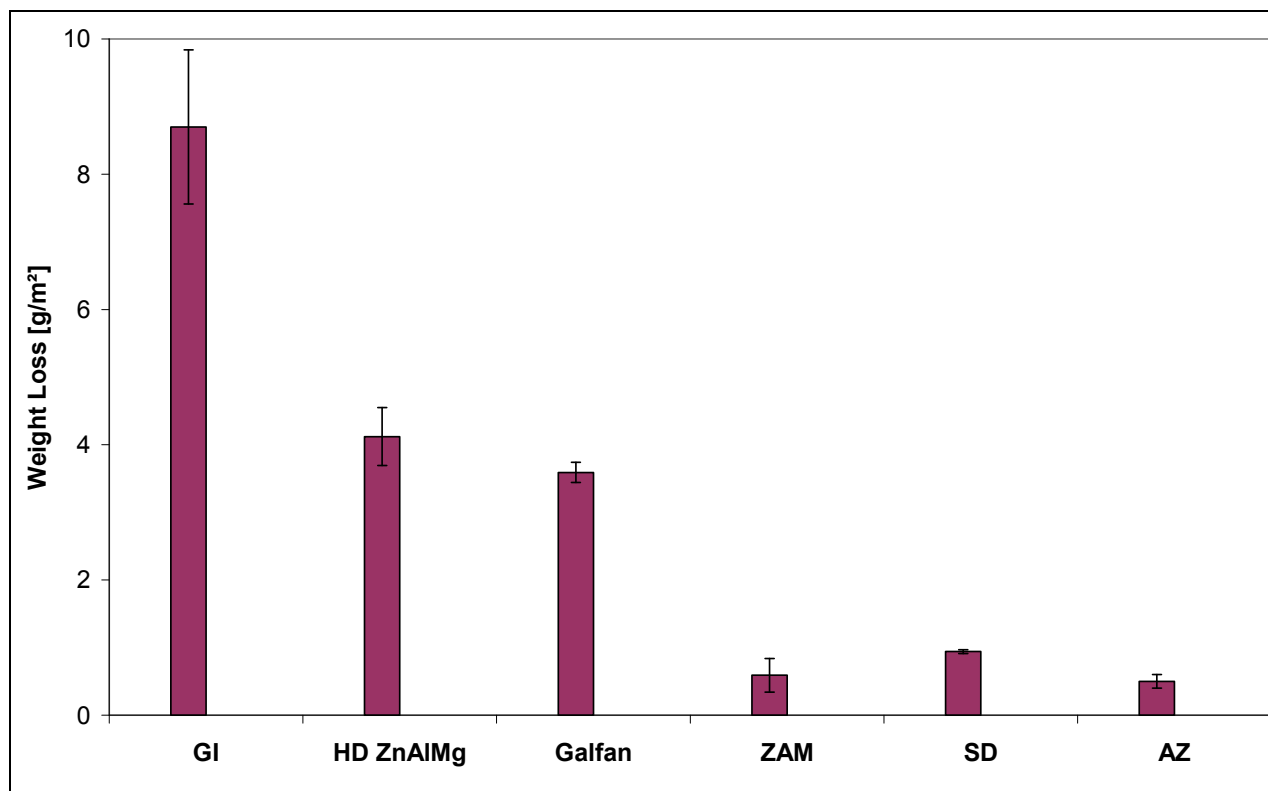


Figure 59 Weight loss of coated steel panels after 4 weeks of exposure at 20°C and 65 % RH at chloride contamination of 1400 mg/m²

Weight loss obtained at 80 and at 95 % RH are compared in Figure 60. For GI, the weight loss decreased from 12 to 26 % depending on the chloride contamination. This result is surprising as the weight loss of zinc coatings generally increase with the relative humidity. A decrease in the weight loss was seen also for SD. The other tested coatings showed higher corrosion at 95 % of RH than at 80 % of RH.

Figure 61 gives a comparison of results obtained at 65, 80, and 95 % RH for samples contaminated with 1400 mg/m² of chloride. The effect of relative humidity was low for GI, HD ZnAlMg, and Galfan. The strongest increase in the weight loss was observed for AZ. Also ZAM was rather sensitive to the relative humidity.

The fact that the weight loss at 65 % RH was not negligible in comparison to more humid exposure conditions is primarily surprising. The deliquescence point of NaCl is 75 % at 20°C. Thus, no solution should be formed under NaCl deposits. However, Shinohara et al [28] showed that ZnCl₂-NaOH mixed electrolytes can be formed even after very short contact of the metal surface to water environment. It was confirmed that in presence of ZnCl₂-NaOH mixed electrolytes the water film can be formed at RH below 20 %. So, zinc might corrode even at RH < 75 % if ZnCl₂-NaOH mixed electrolytes were formed after corrosion of zinc started, while it can corrode only at RH > 75 % if only deposits of NaCl are present on the surface. It can be supposed that during contamination of GI and zinc-based alloy coatings by methanol/water solutions, a small quantity of zinc was corroded. It was sufficient for attracting enough

water at 65 % RH to continue the corrosion process. Further dissolution of zinc would increase the rate of the process. This can also explain delays in the kinetics of mass gain changes seen in Figure 55.

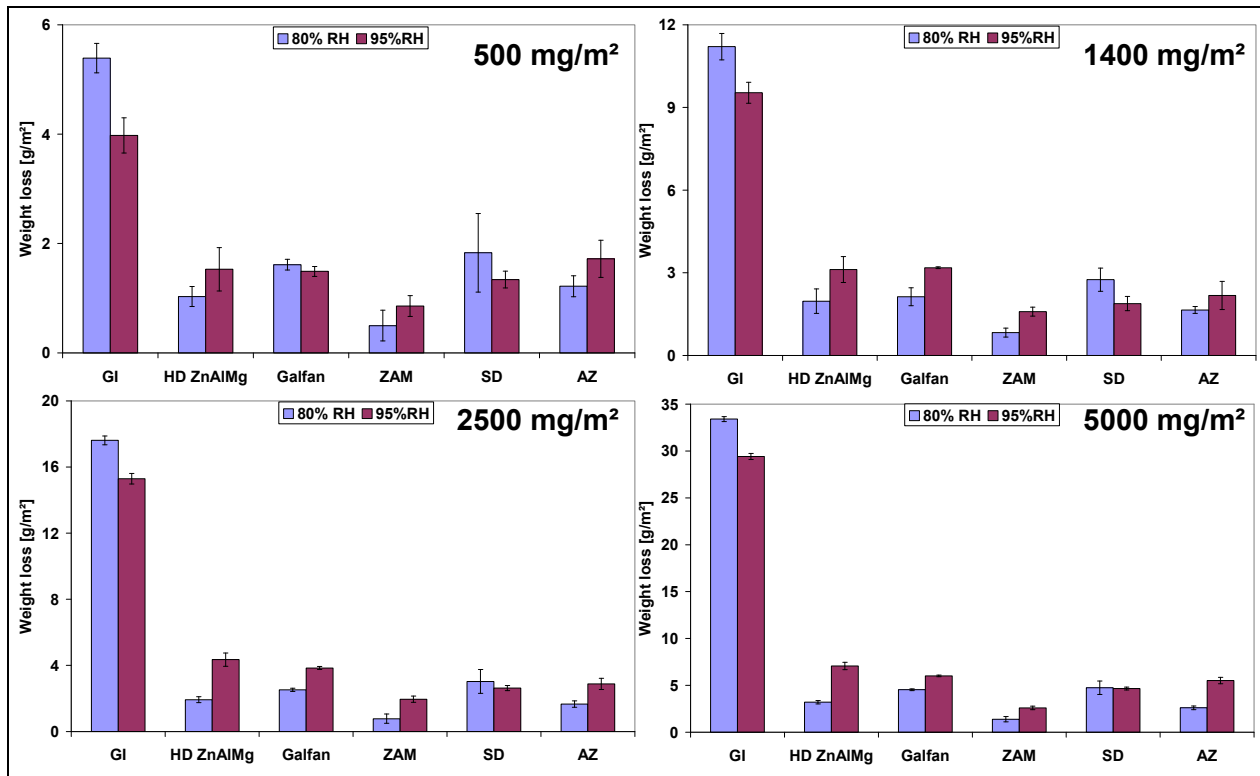


Figure 60 Weight loss comparison between 80 and 95 % RH at 20°C, after 4 weeks of exposure

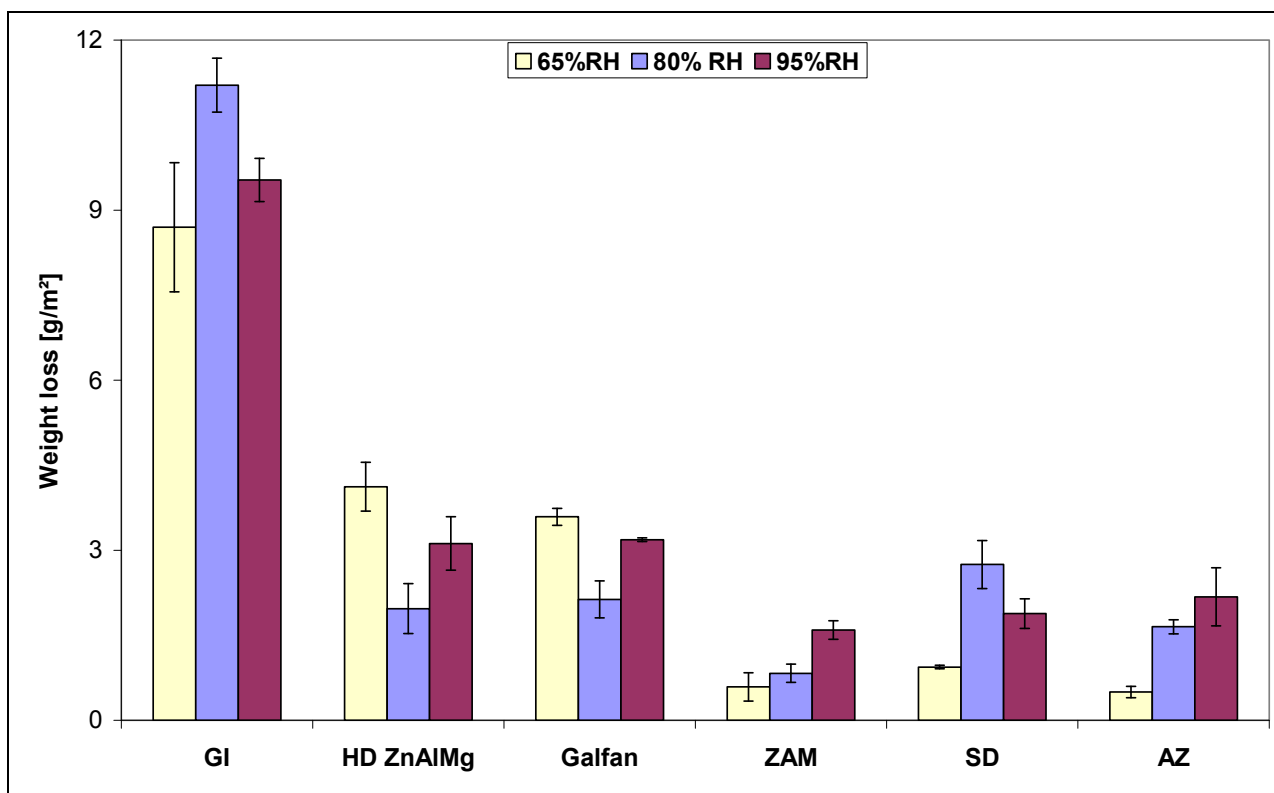


Figure 61 Weight loss comparison at 65, 80 and 95 % RH at 20°C after 4 weeks of exposure of metallic coatings contaminated with 1400 mg/m² chloride

HD ZnAlMg and Galfan were less stable at 65 % RH than at 80 % RH (Figure 61). This is seen e.g. in Figure 62 where the weight loss related to GI is plotted as a function of total alloying of the coatings tested at different relative humidity. It seems that the relative efficiency of less alloyed materials is more sensitive to the exposure conditions. It is more affected by both temperature (Figure 54) and relative humidity than the efficiency of more alloyed materials.

The lower corrosion stability of HD ZnAlMg and Galfan at the low RH might be connected to the composition of corrosion products. Ohtsuka and Matsuda [29] showed for zinc covered with NaCl precipitates that when the RH was below 80 % the main corrosion product was ZnO while simonkolleite was formed when the RH was above 80 %. Since simonkolleite can be considered as more protective than zinc oxide, this might indeed affect the corrosion performance. However, GI was less corroded at 65 % RH than at 80 % RH. Further investigation and careful analysis of corrosion products would be required to prove the effect of RH on composition of corrosion products.

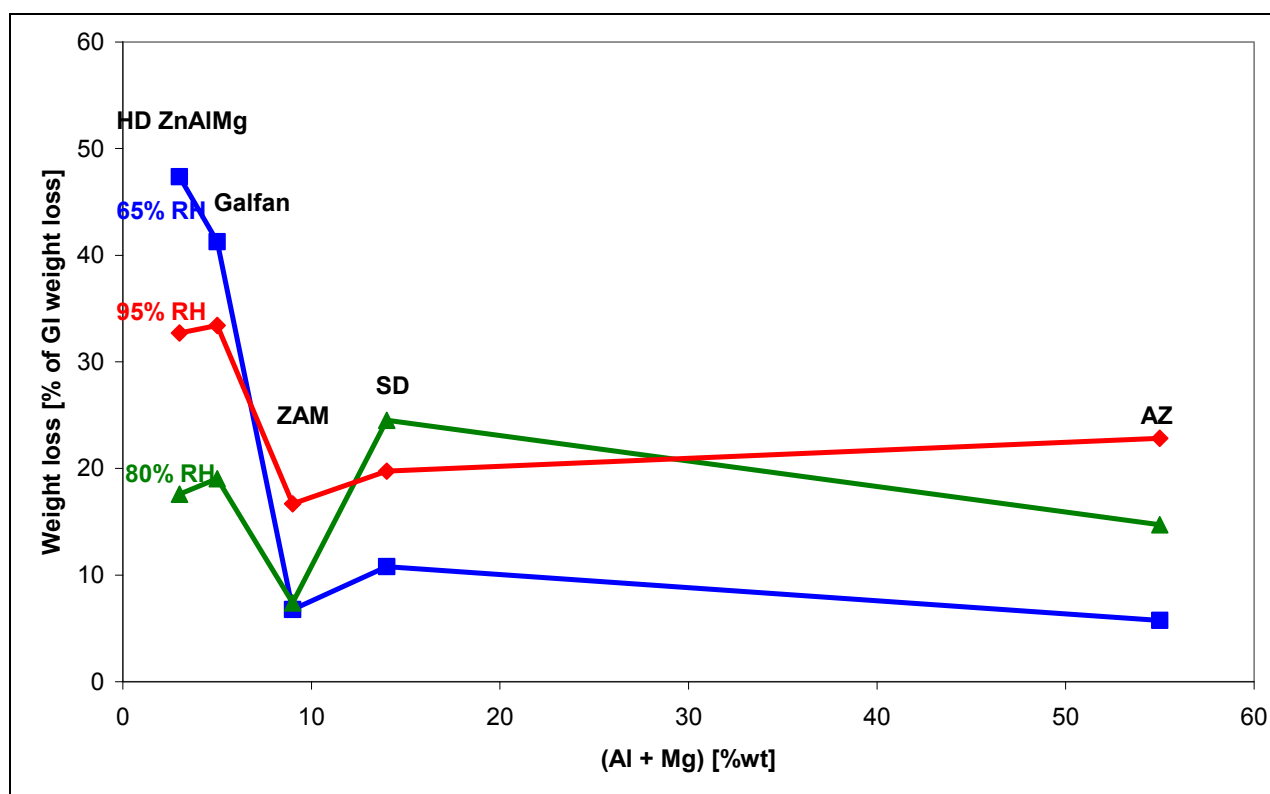


Figure 62 Relative weight loss to GI versus alloying, comparison between 65, 80 and 95 % RH at 20°C, after 4 weeks of exposure for a chloride contamination of 1400 mg/m²

4.4 Effect of dry time in a cyclic test at 35°C

Metallic coated panels tested in previously described experiments and panels coated in Rhesca simulator, see Table 3, were exposed at 35°C in three different wet/dry cycles. The cycles are described in Figure 63, Figure 64 and Figure 65. The humidity varied between 85 (wet) and 50 (dry) percent of RH. The wet time was 4 hours, drying and wetting period was 2 hours, and number of cycles was 56 in all tests. Thus, the total wet time of 224 hours was identical in all tests. The cycles differed only in the dry time at 50 % RH, which was 2, 4, and 8 hours for *short cycle*, *basic cycle*, *long cycle*, respectively. Samples were contaminated with sodium chloride at the chloride surface concentration of 1400 mg/m² before testing. The goal was to evaluate the effect of dry time to the weight loss and type of corrosion products formed.

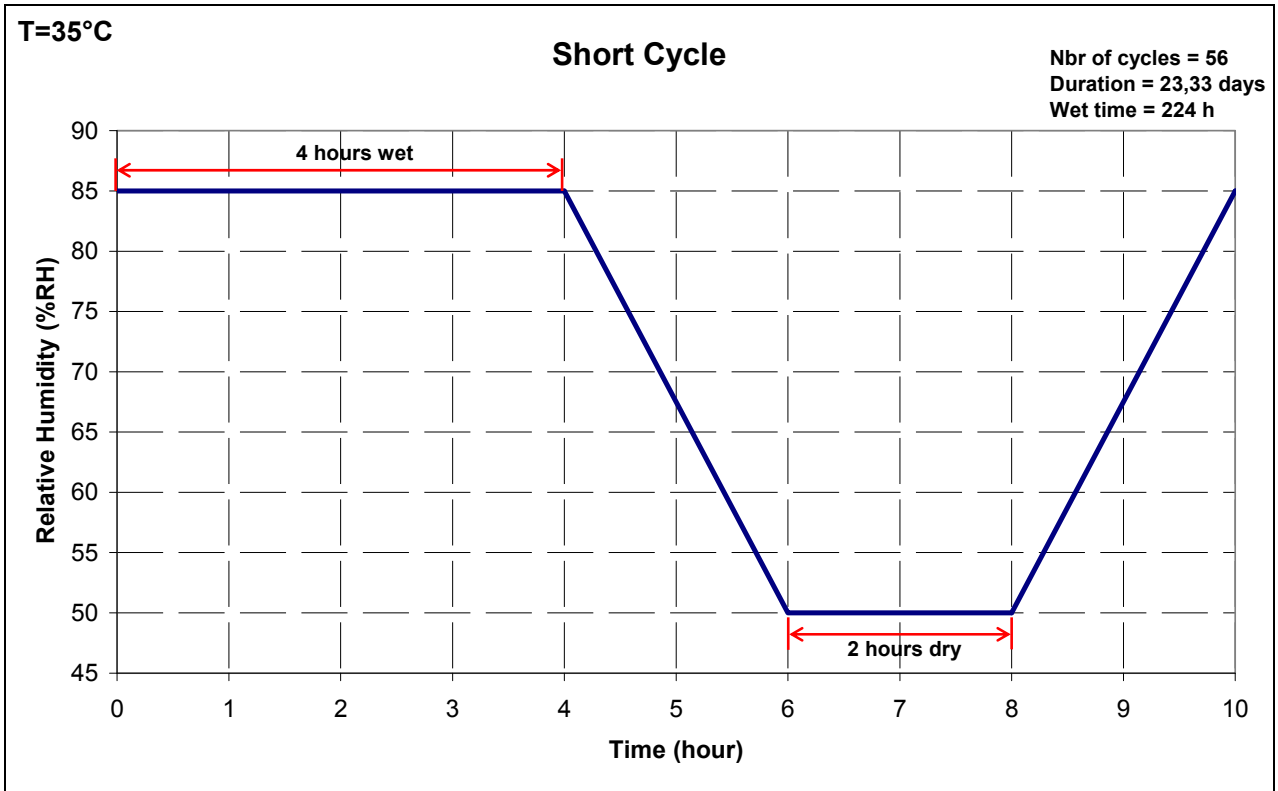


Figure 63 Wet (80 % RH) / dry (50 % RH) short cycle

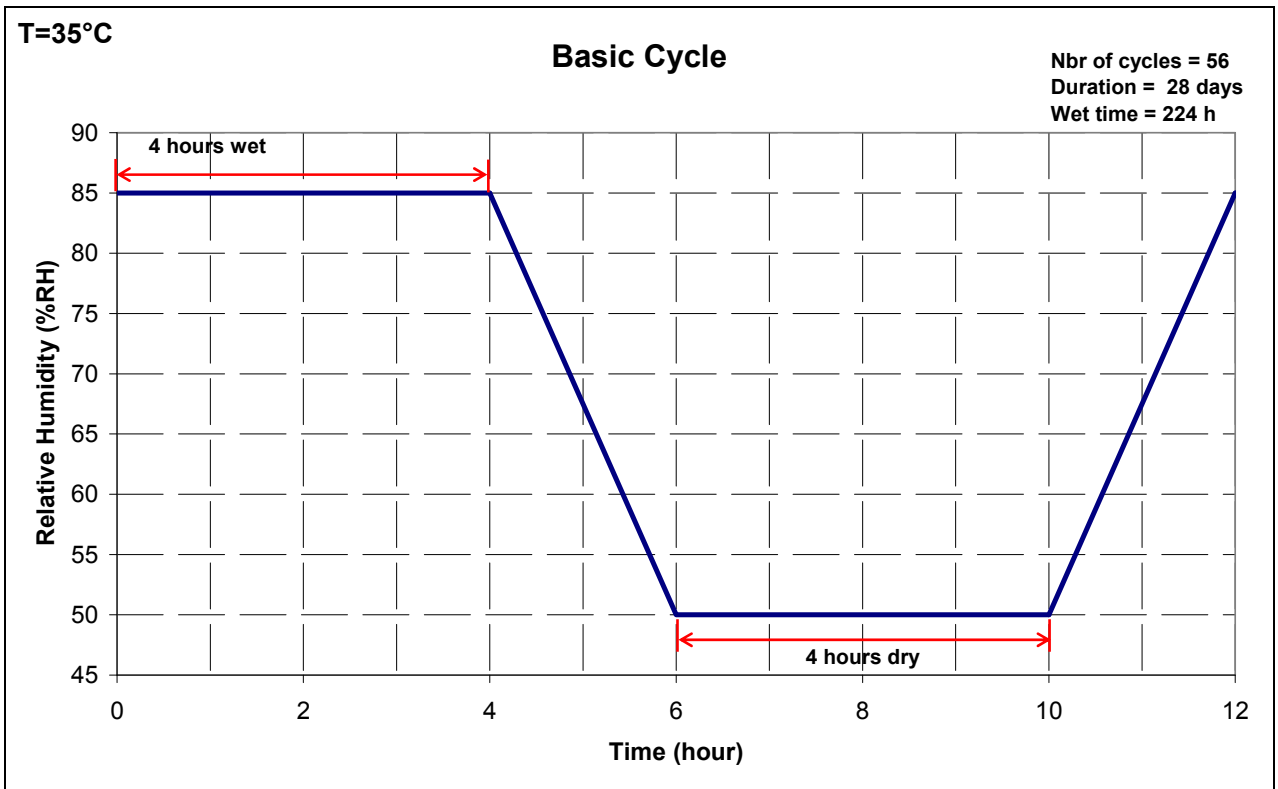


Figure 64 Wet (80 % RH) / dry (50 % RH) basic cycle

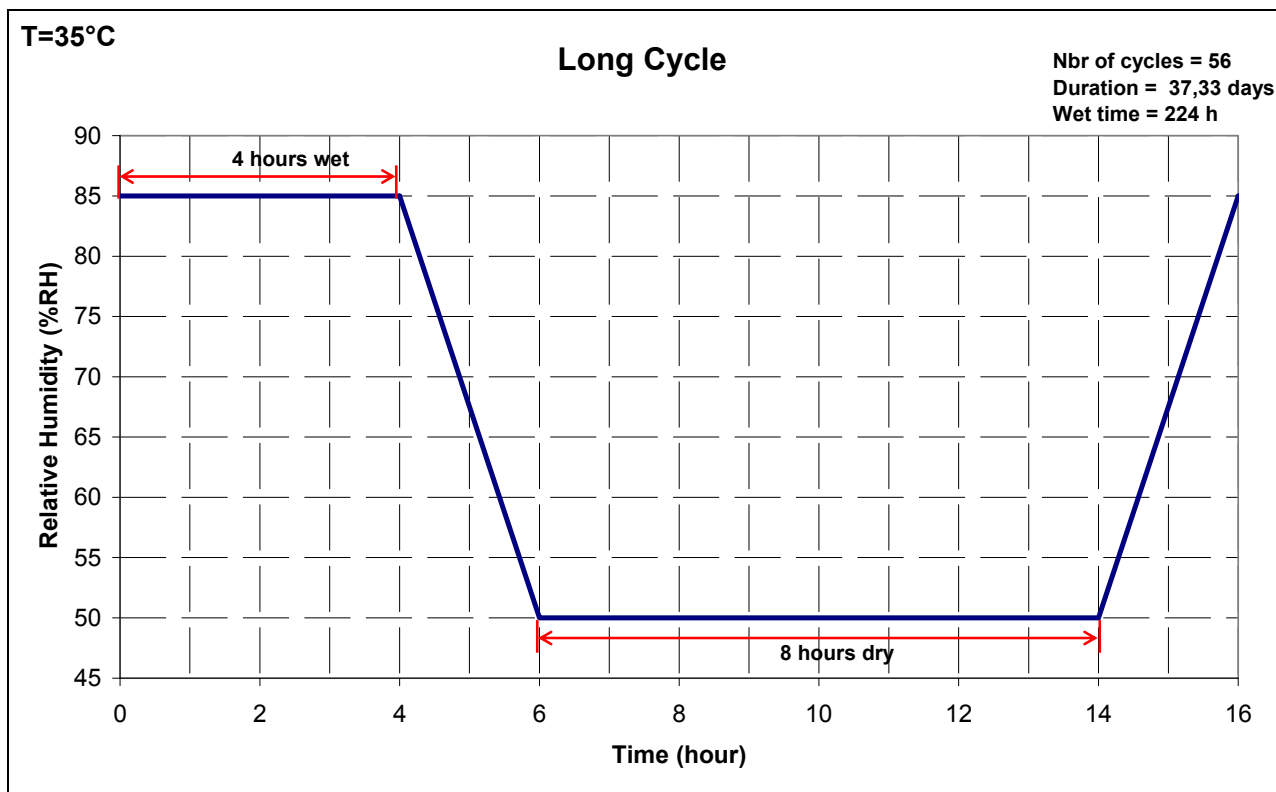


Figure 65 Wet (80 % RH) / dry (50 % RH) long cycle

The mass gain during the basic cycle is given in Figure 66 and in Figure 67 for commercial specimens and specimens coated with Rhesca simulator. In all cases, mass gain was measured during the drying period of the cycle. The mass gain during short, basic and long tests are compared for GI, HD ZnAlMg and Galfan in Figure 68, Figure 69 and Figure 70, respectively. It is clearly observed that the test with the shortest drying period caused the highest mass gain. As shown in Figure 71, the weight loss of the most part of tested materials decreased with the increasing length of dry period from 2 to 4 hours. Further increase of the dry period to 8 hours caused a small increase in the weight loss, but it was usually within the experimental error. The average weight loss for each cycle (calculated from the weight loss of all the tested materials) are 8.5 ± 1.0 , 5.7 ± 0.7 and 6.9 ± 1.1 g/m² for the short, basic and long cycle, respectively. GI and ZAM behaved differently as no effect of the dry time was observed.

The short cycle with only 2 hours of drying per cycle was clearly the most severe of the 3 cycles, especially for coatings with less than 5 % of total alloying element, i.e. HD ZnAlMg and Galfan. It is supposed that the decrease in weight loss with increasing dry time from 2 to 4 hours was caused by formation of more protective corrosion products.

It is not fully clear why the weight loss somewhat increased with further prolongation of dry time. It is supposed that particularly after longer time of exposure, the layer of corrosion products was not dried completely in the dry period. The amount of water on the surface was significantly reduced but the corrosion process was probably not stopped fully. Thus, although at limited rate, metals might corrode even in the dry phase.

Average weight loss from three test cycles is plotted versus the total alloying in Figure 72. A linear dependence between weight loss and alloying is observed from 0 to about 7 wt. % of alloying elements independently of the nature of the alloying.

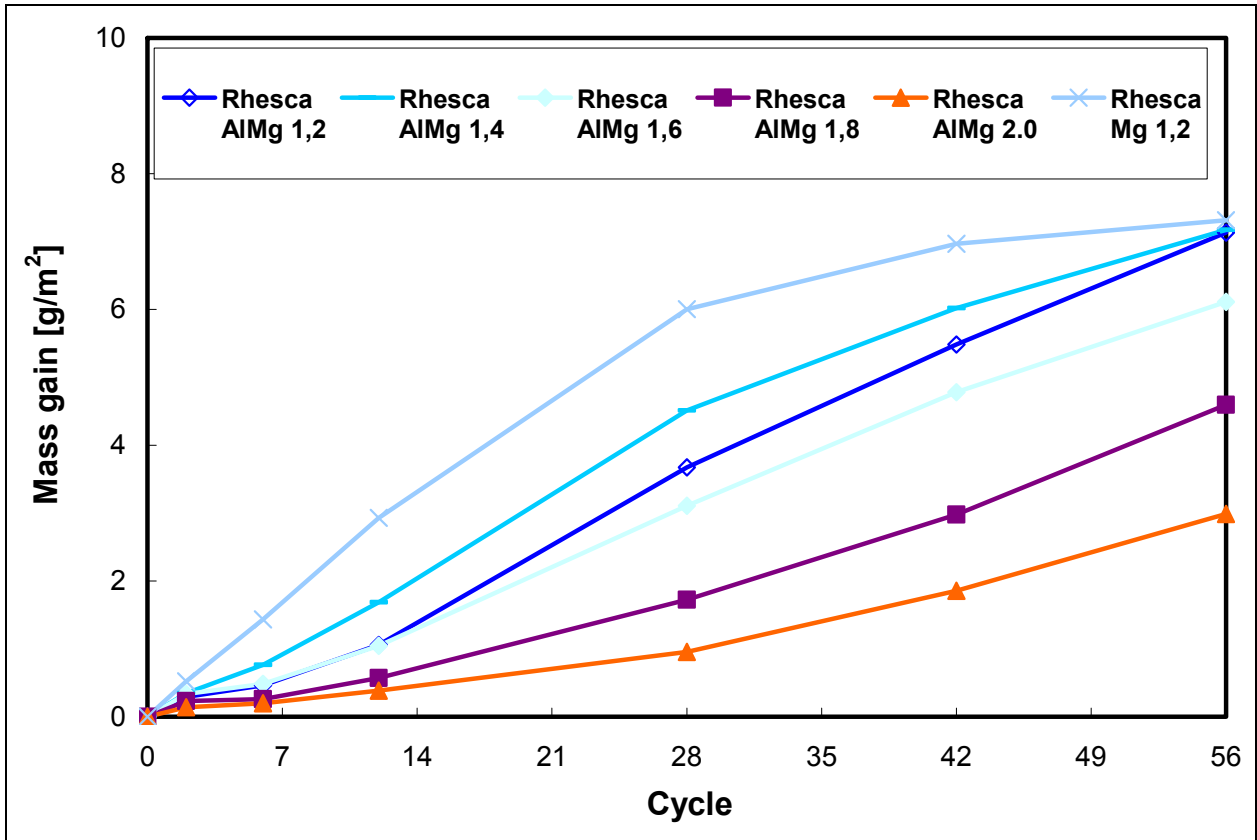


Figure 66 Wet mass gain of Rhesca coated steel panels during exposure in basic cycle

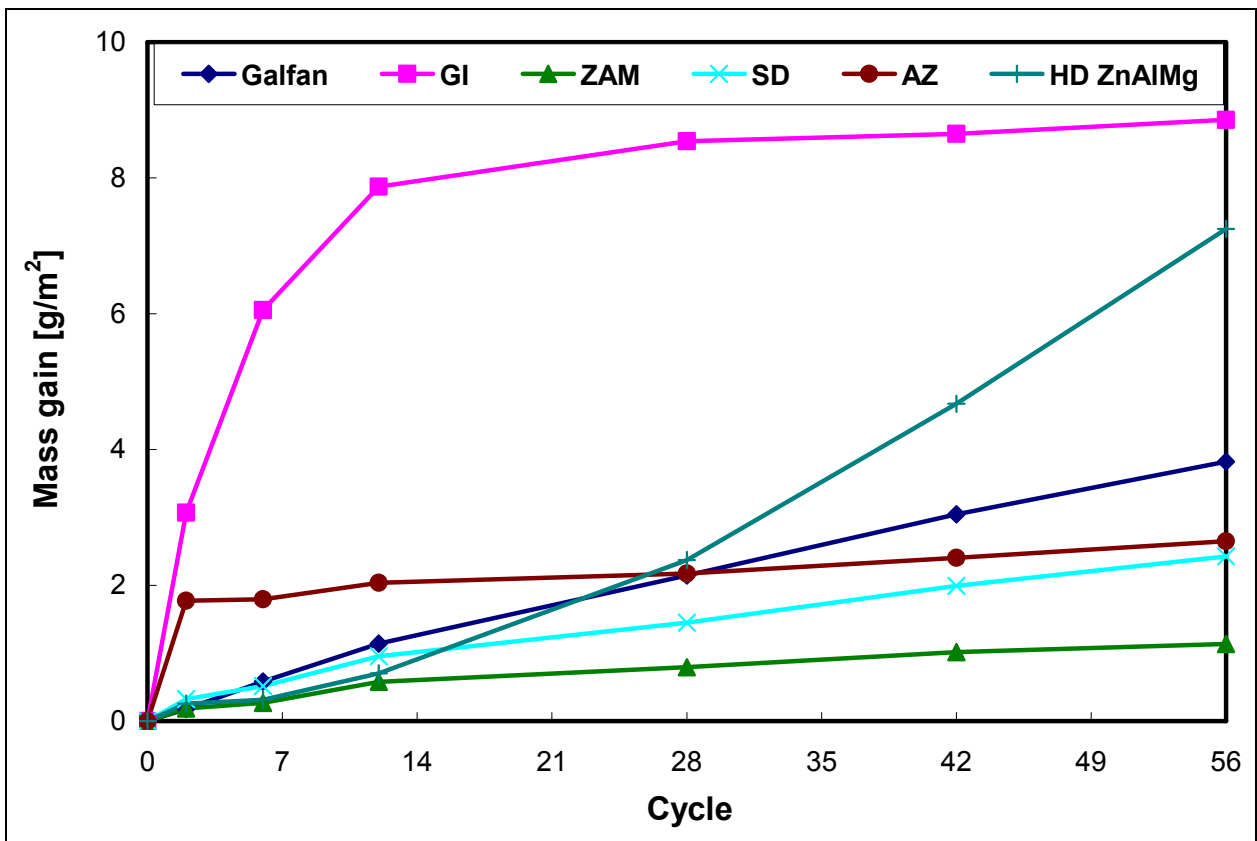


Figure 67 Wet mass gain of coated steel panels during exposure in basic cycle

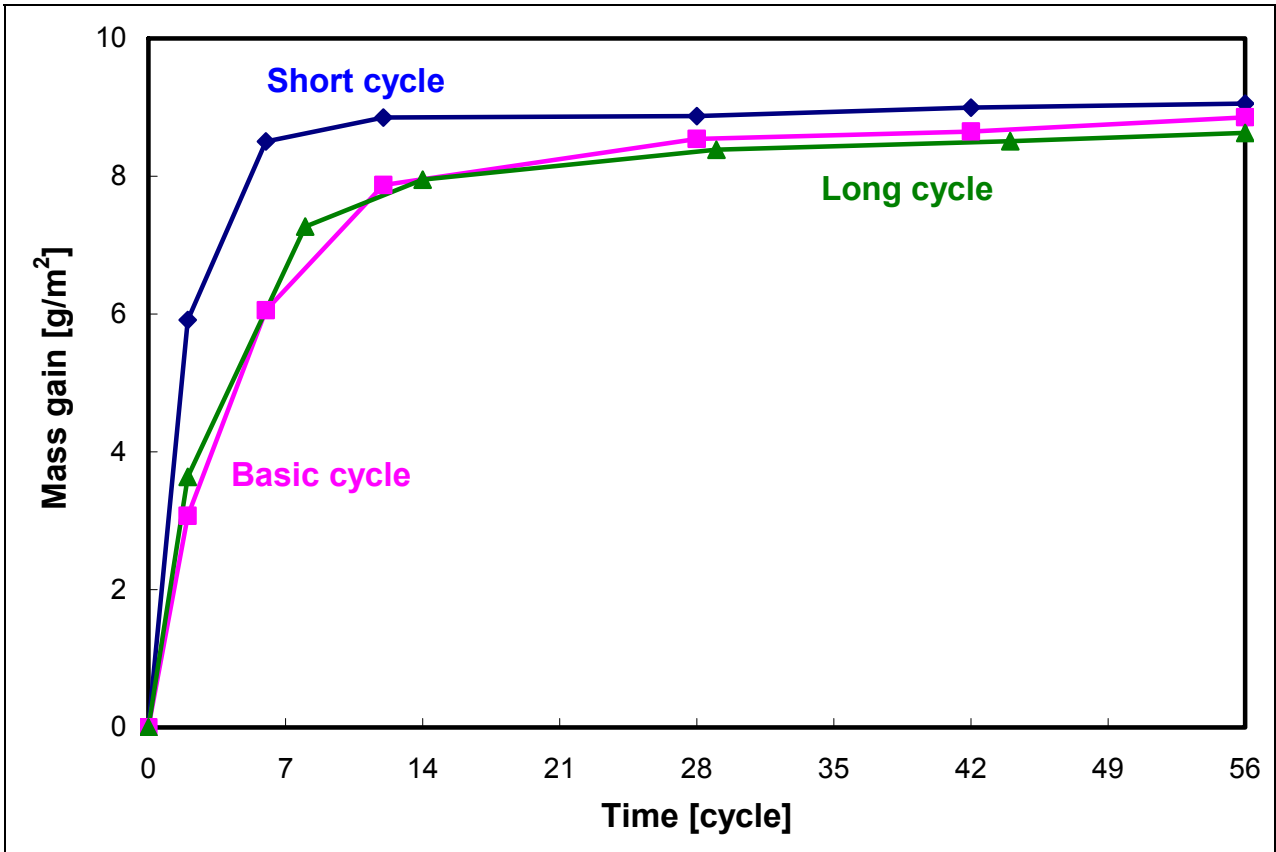


Figure 68 Wet mass gain of GI in three test cycles

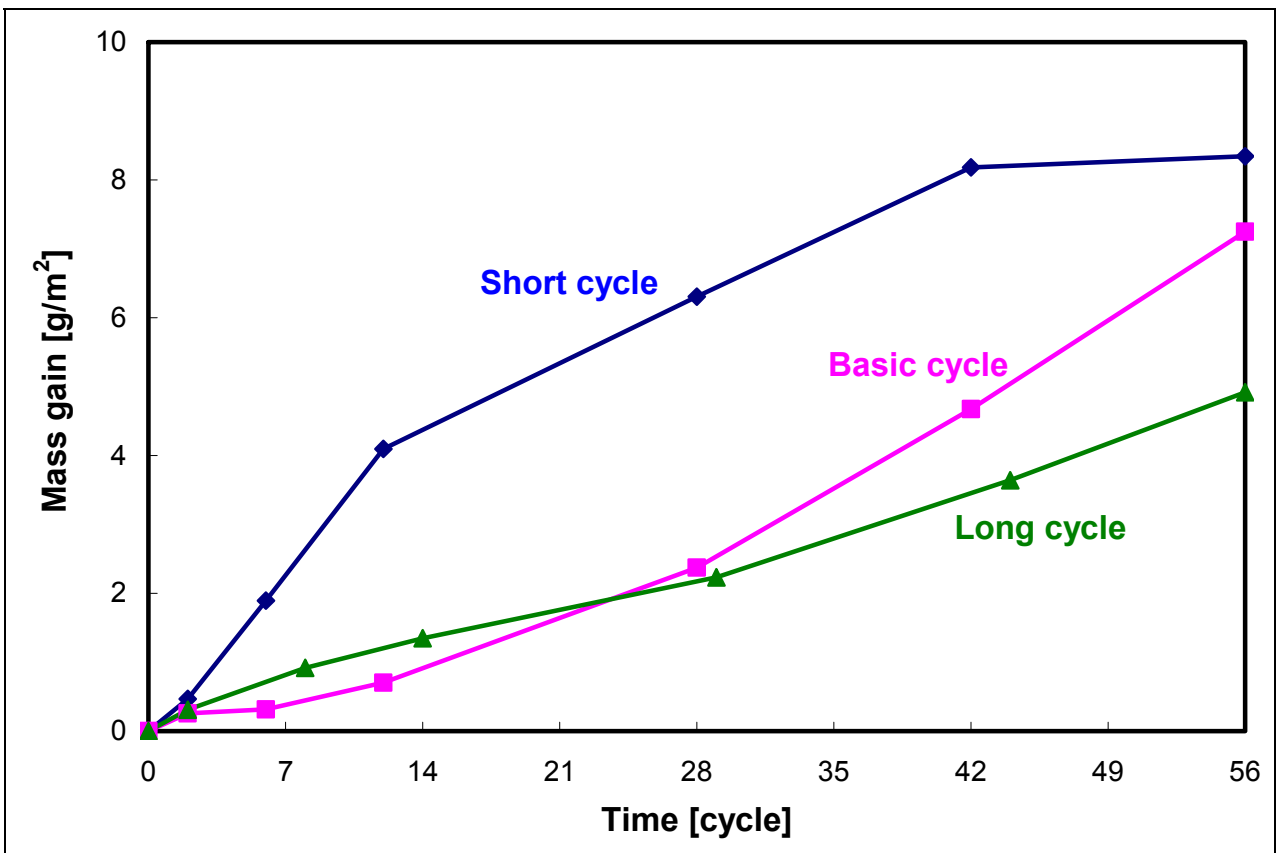


Figure 69 Wet mass gain of HD ZnAlMg in three test cycles

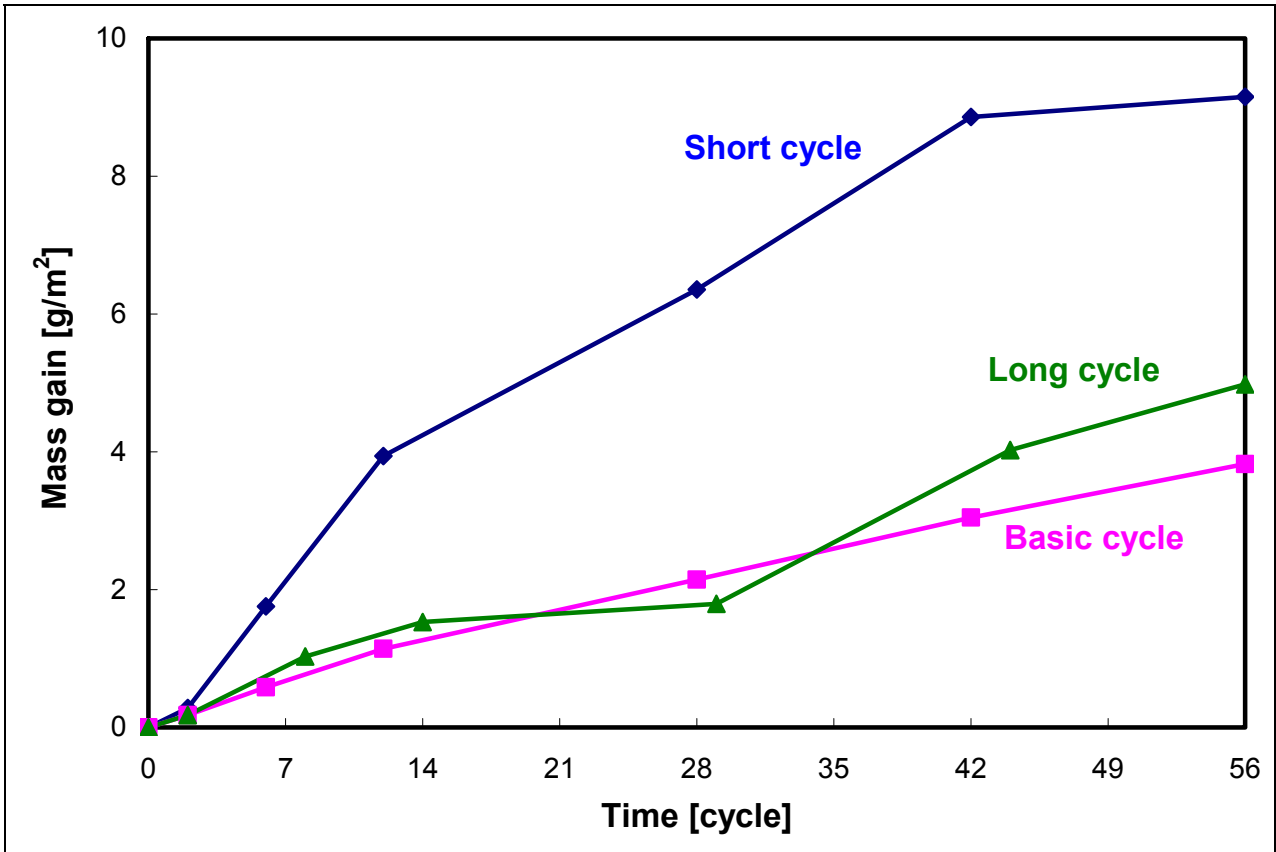


Figure 70 Wet mass gain of Galfan in three test cycles

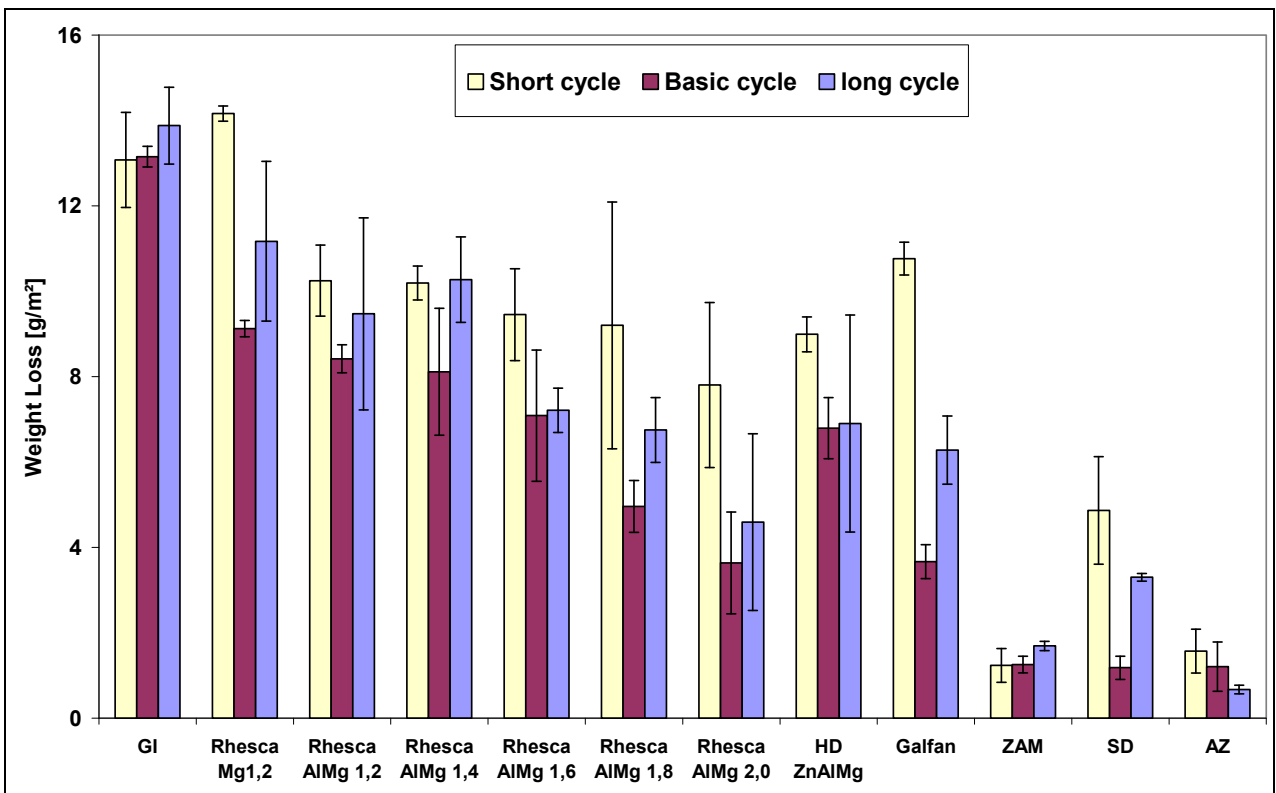


Figure 71 Weight loss of metallic coated panels after tests differing in the length of the dry period

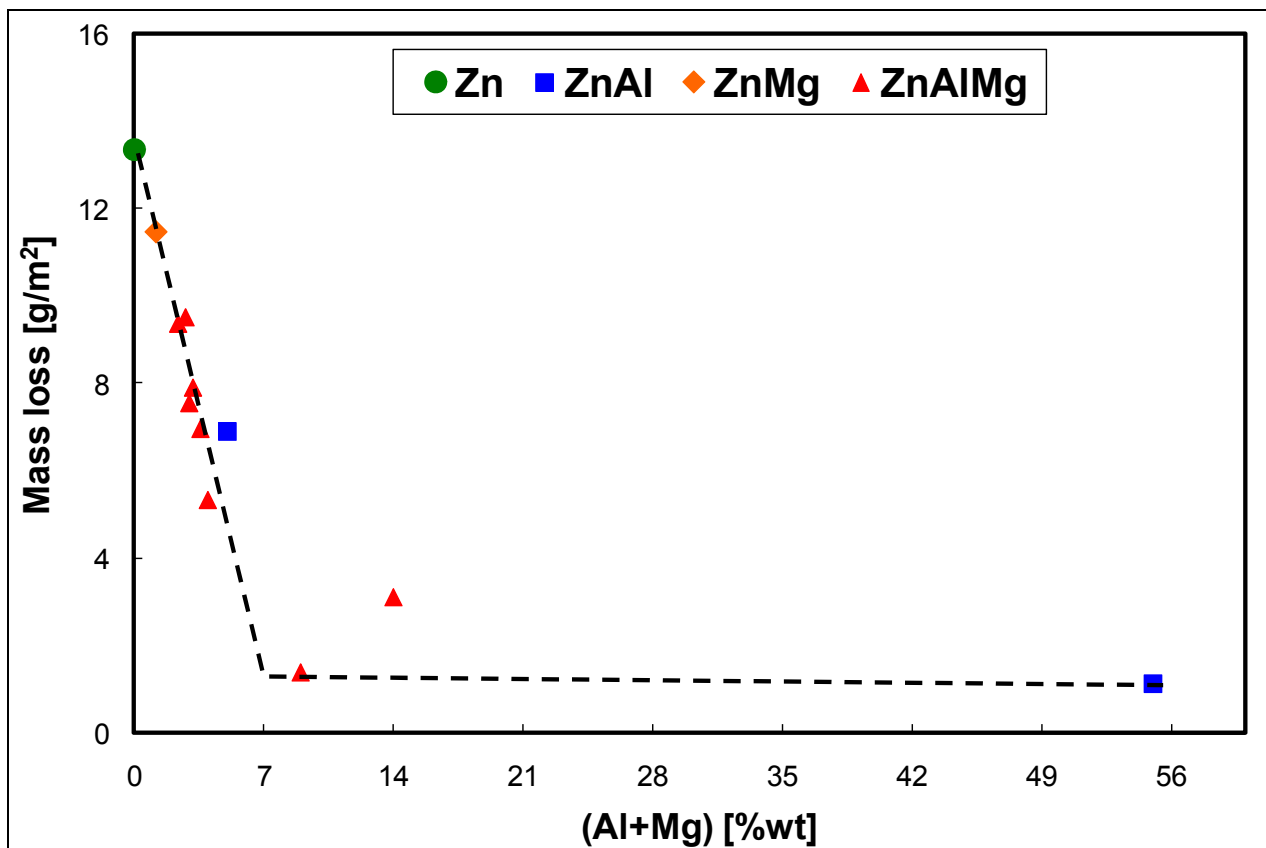


Figure 72 Average weight loss of metallic coated panels exposed in 3 test cycles at 35°C versus alloying; Zn: GI, ZnAl: Galfan, AZ; ZnMg: Rhesca Mg 1.2, ZnAlMg: Other coatings

In principle, a similar effect of both alloying elements on corrosion were observed in the cycles. For instance, similar results were obtained for HD ZnAlMg (1.5 % Mg, 1.5 % Al) and Rhesca AlMg 1.6 (1.6 % Mg, 1.6 % Al) in all tests. While a slightly better corrosion resistance is observed for Galfan compared to HD ZnAlMg in basic drying cycle and long drying cycle, a better corrosion resistance is obtained from HD ZnAlMg compared to Galfan in the most severe short drying cycle. Corrosion resistance of Rhesca Mg 1.2 coating was also lower in this test. This indicates that the presence of both aluminum and magnesium is required for superior corrosion stability in the short cycle. The formation of sufficiently protective corrosion products in the cycle with short dry time might be disturbed more strongly on materials alloyed only with magnesium or only with aluminum. This is illustrated in Figure 73 where the weight loss of coatings tested in the short test is plotted as a function of total alloying.

It seems that corrosion decreases with the total alloying content in environments where stable corrosion products are formed and an additive effect of Al and Mg with no significant synergy is observed. The effect of alloying elements on the weight loss in the basic cycle is shown in details in Figure 74 and Figure 75. Again, the weight loss depends more or less linearly on alloying from 0 to 5 wt. % and the effect of Al and Mg is additional. No synergy between Al and Mg is observed in this test. Figure 75 shows a break in the dependence of weight loss on the content of alloying elements at about 6 wt. % of the total alloying element content. From ZAM with 9 % of magnesium and aluminum, the corrosion is low and stable with about 1 mg/m² of weight loss in 4 weeks of exposure. The same trend was observed in the test at 40°C and 80 % of RH, i.e. linear dependence of weight loss on alloying from 0 to 5 % and stabilization of corrosion rate from 8 % of alloying.

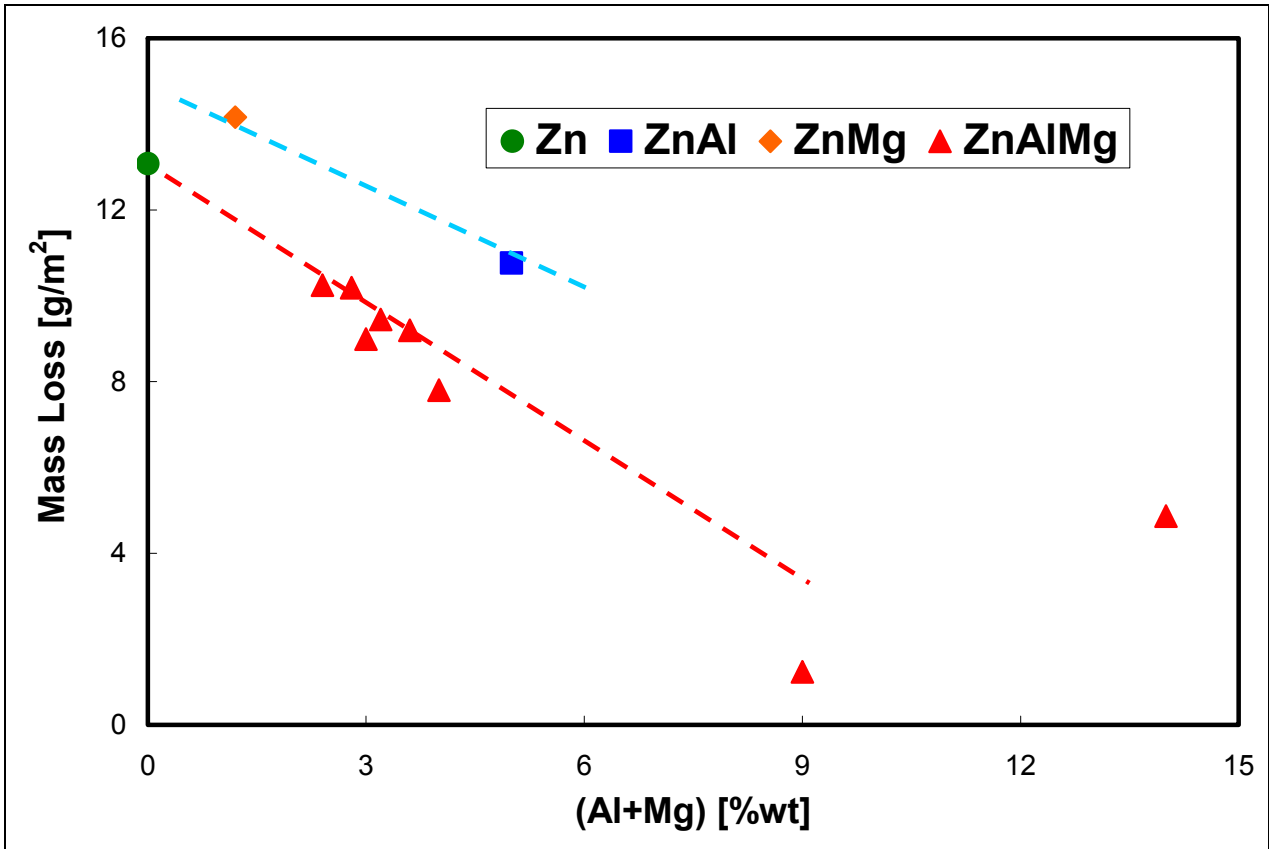


Figure 73 Weight loss of metallic coated panels versus alloying in the short cycle; Zn: GI, ZnAl: Galfan, AZ; ZnMg: Rhesca Mg 1.2, ZnAlMg: Other coatings

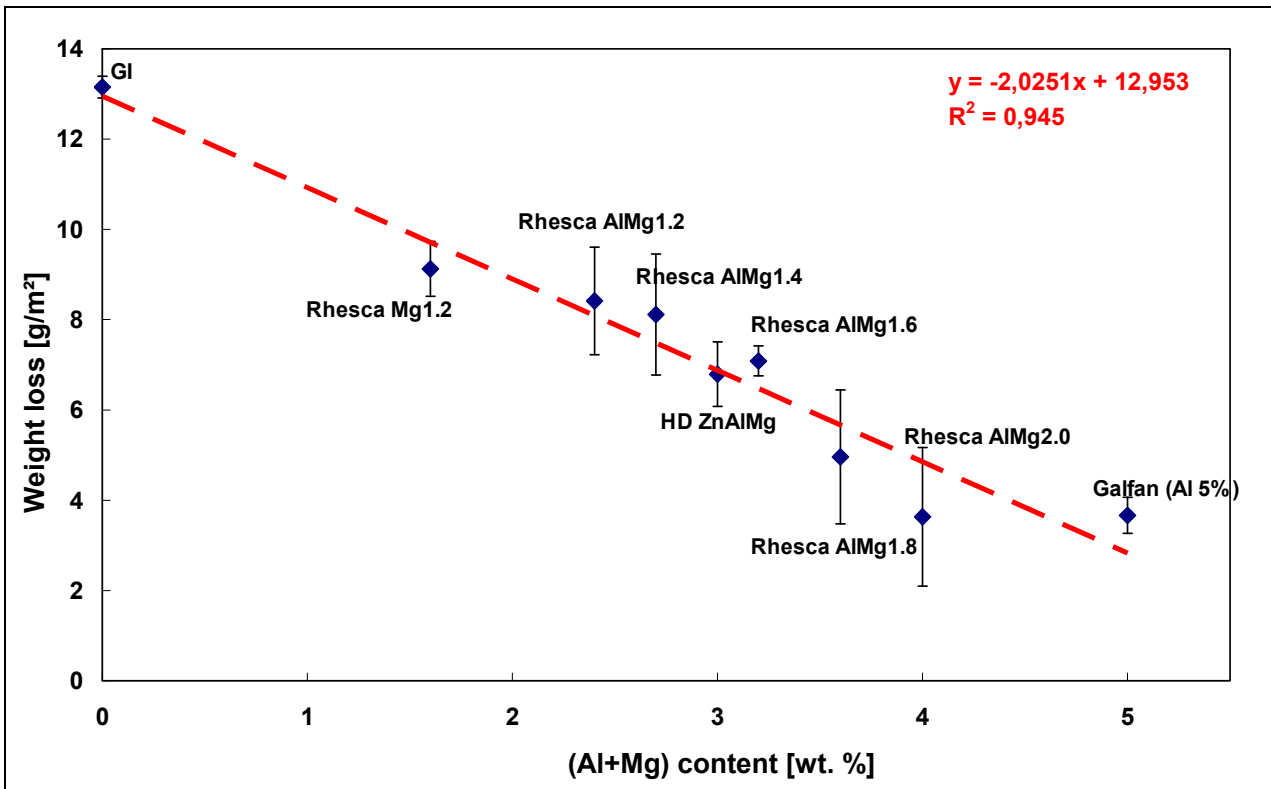


Figure 74 Weight loss vs. alloying from 0 to 5 wt. % for metallic coated panels exposed in the basic cycle

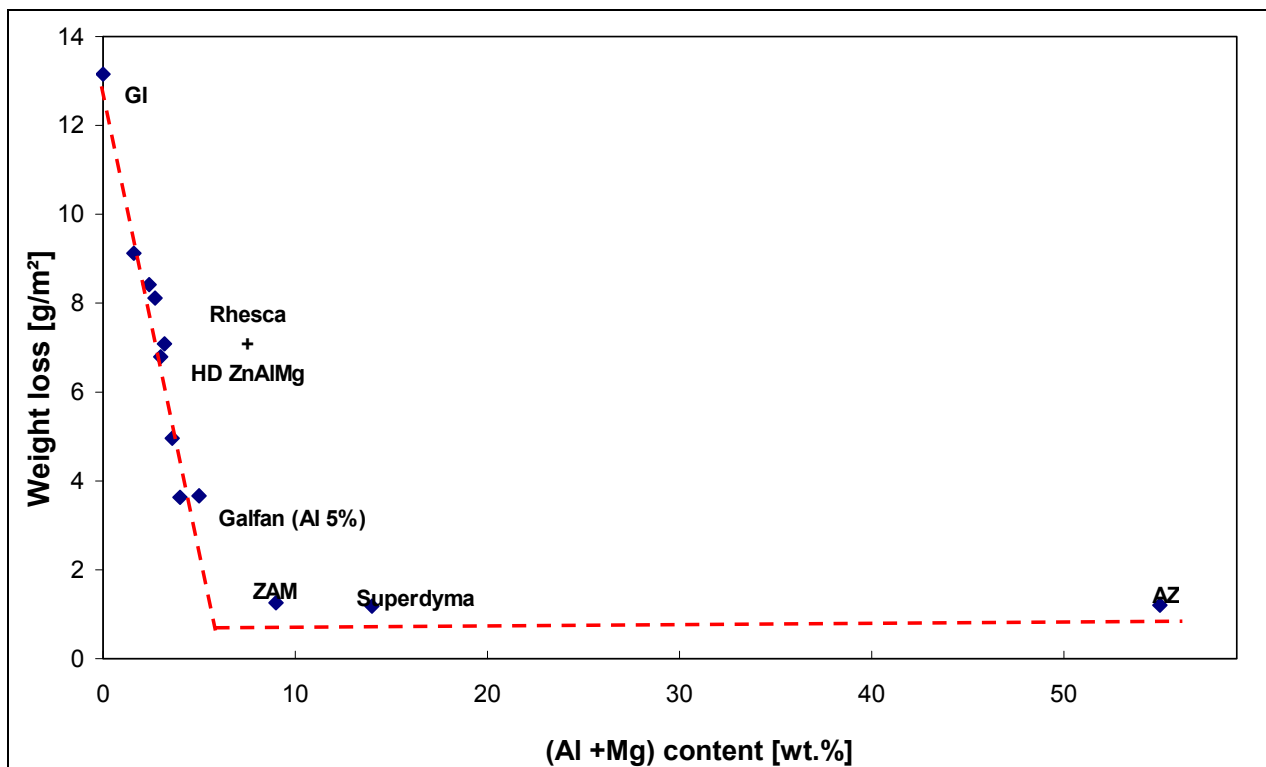


Figure 75 Weight loss vs. alloying from 0 to 55 wt. % for metallic coated panels exposed in the basic test

Ion chromatography analysis of soluble corrosion products was performed after dissolution of corrosion products in deionized water for selected samples exposed in the cyclic tests. Results are given in Figure 76 and in Figure 77 for bonded chloride and bonded sodium, respectively. Once again, when comparing results for coatings exposed in any particular cycle, the tendency is completely in accordance with weight loss results. However, when comparing the effect of dry time on the amount bonded chloride and sodium for a particular coating with Al and Mg from 1.4 %, it is observed that it is increasing with decreasing dry time. Because in other tests the amount of bonded chloride and sodium reflected well the weight loss data, it might suggest that the composition of corrosion products and eventually the corrosion mechanism was affected by the length of dry time.

Amounts of soluble zinc and magnesium are given in Figure 78 and in Figure 79, respectively. It seems that more soluble zinc was present on the surface of less alloyed materials with Mg content up to 1.4 wt. % in the test with short dry time, whereas zinc was more soluble from corrosion products formed on more alloyed materials in tests with longer dry time. Total soluble Mg decreased with increasing dry time. Contrary to model alloys tested at 20°C and 80 % RH, more soluble Mg was found for coatings with higher Mg content.

pH of water extracts after dissolution of corrosion products in deionized water is given in Figure 80. Besides GI, pH tendencies followed the weight loss tendencies with more alkaline pH for more corroded specimens.

The phase composition of corrosion products was evaluated by FTIR after three exposure cycles differing in the length of the dry period. FTIR spectra for HD ZnAlMg 10 µm are shown in Figure 81 and results are given in Table 13. It is evident that the spectra were similar to each other. In all cases, simonkolleite, hydrozincite, sodium carbonate, and aluminum corrosion products, probably mainly AlOOH (boehmite or diasporite) were identified. The peak at 1435 cm⁻¹ can be associated to magnesite, MgCO₃ or magnesium hydroxycarbonate. It is slightly offset from the position found in the reference spectrum in Figure 22, where

the maximum is seen at 1445 cm^{-1} . However, the presence of magnesite is supported by the peak at 890 cm^{-1} , which is well visible in spectra of corrosion products from samples exposed for 2 and 4 hours.

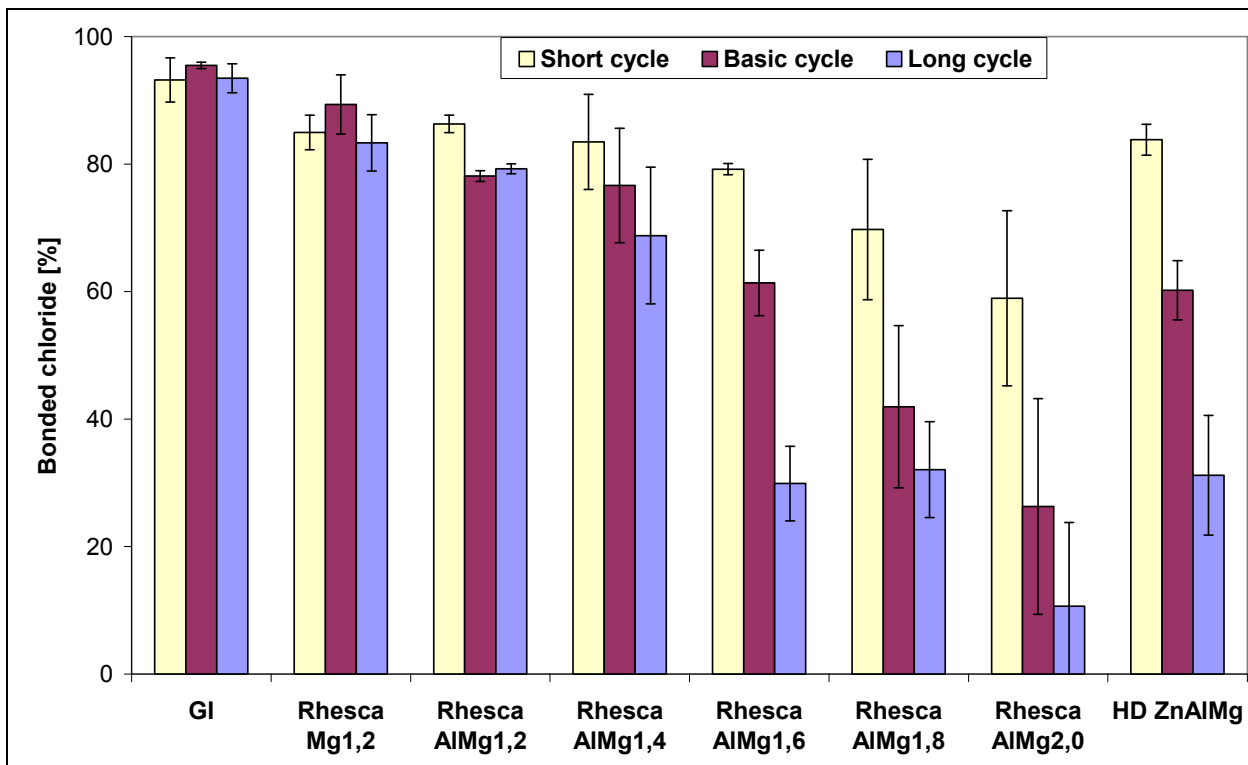


Figure 76 Bonded chloride on the surface from ion chromatography of water extract of corrosion products; results for coated panels exposed in three cyclic tests contaminated with 1400 mg/m^2 of chloride

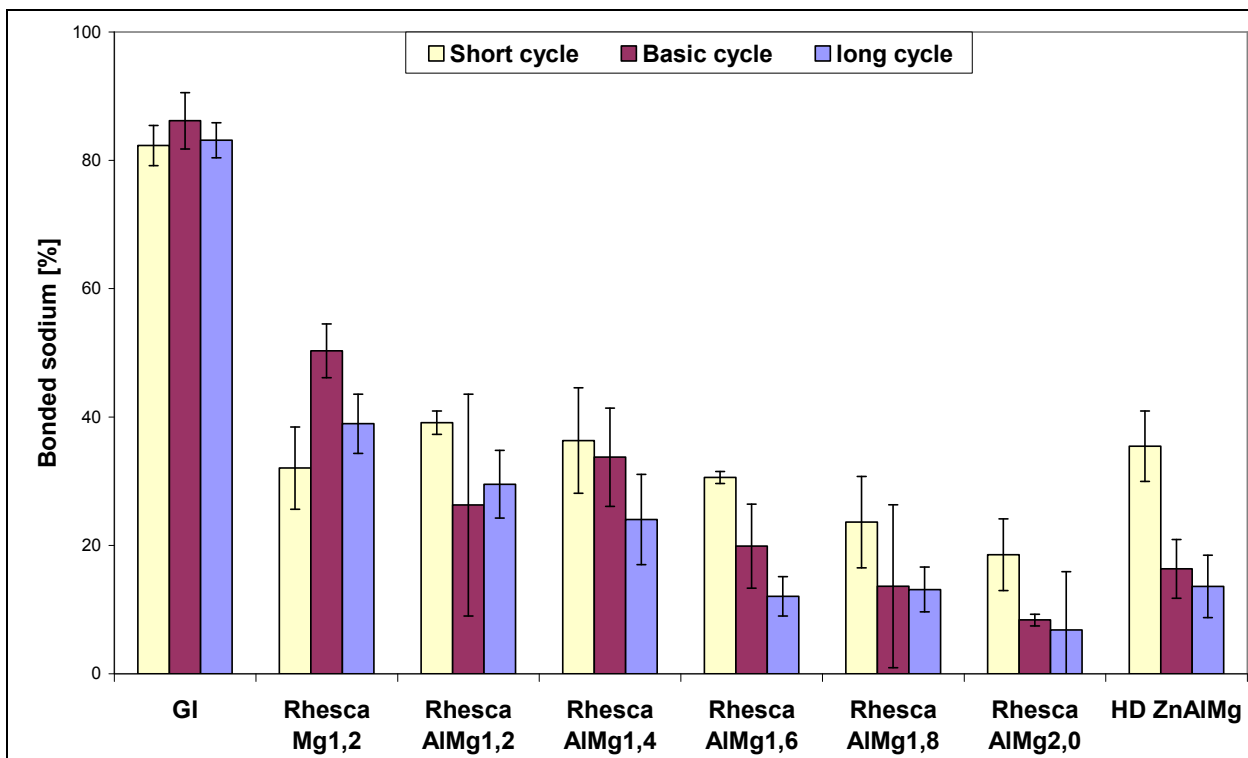


Figure 77 Bonded sodium on the surface from ion chromatography of water extract of corrosion products; results for coated panels exposed in three cyclic tests and contaminated with 1400 mg/m^2 of chloride and 907 mg/m^2 of sodium

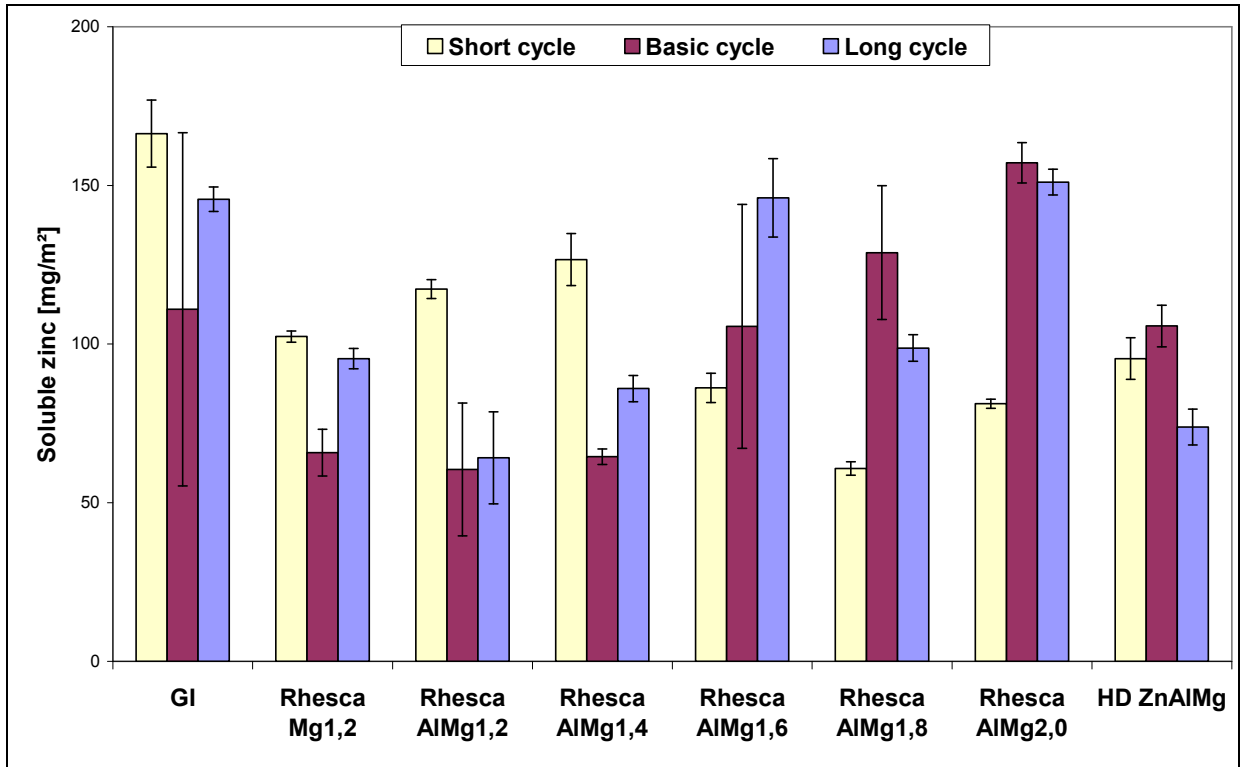


Figure 78 Soluble zinc on the surfaces, from ion chromatography of water extract of corrosion products; results for coated panels exposed in three cyclic tests and contaminated with 1400 mg/m² of chloride and 907 mg/m² of sodium

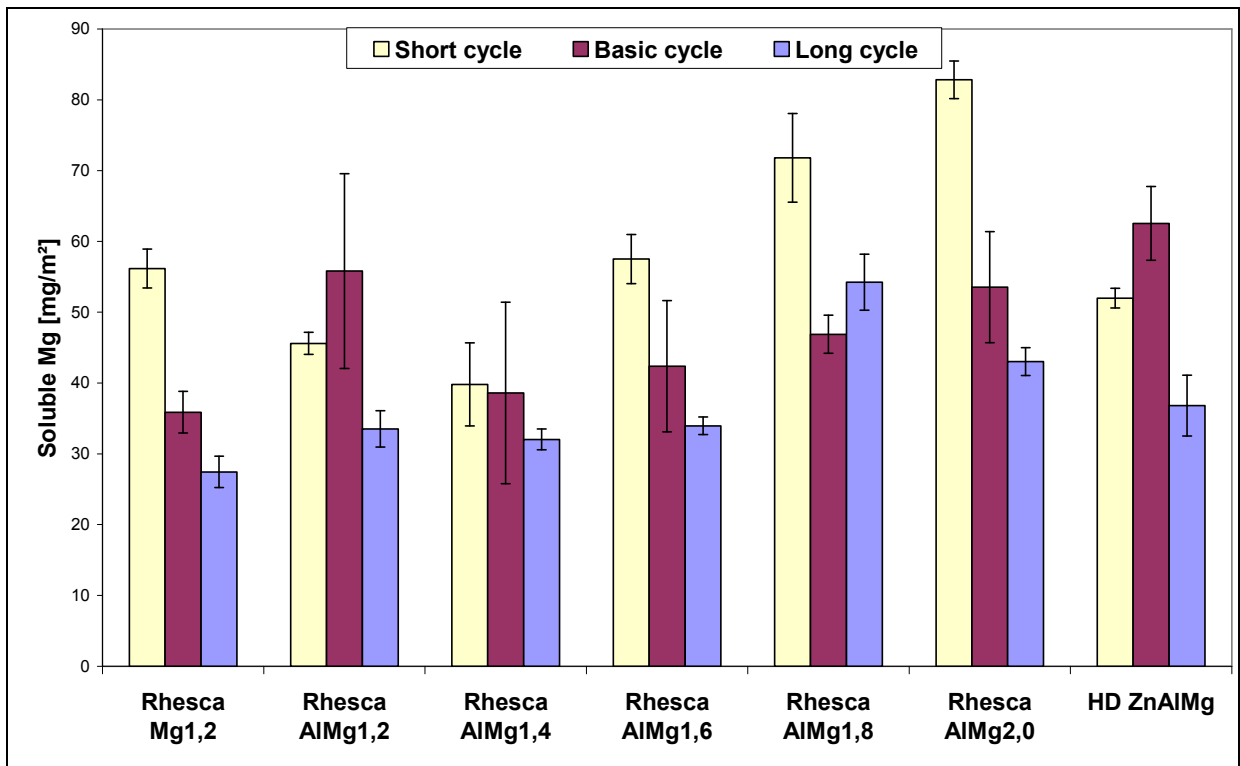


Figure 79 Soluble magnesium on the surfaces, from ion chromatography of water extract of corrosion products; results for coated panels exposed in three cyclic tests and contaminated with 1400 mg/m² of chloride and 907 mg/m² of sodium

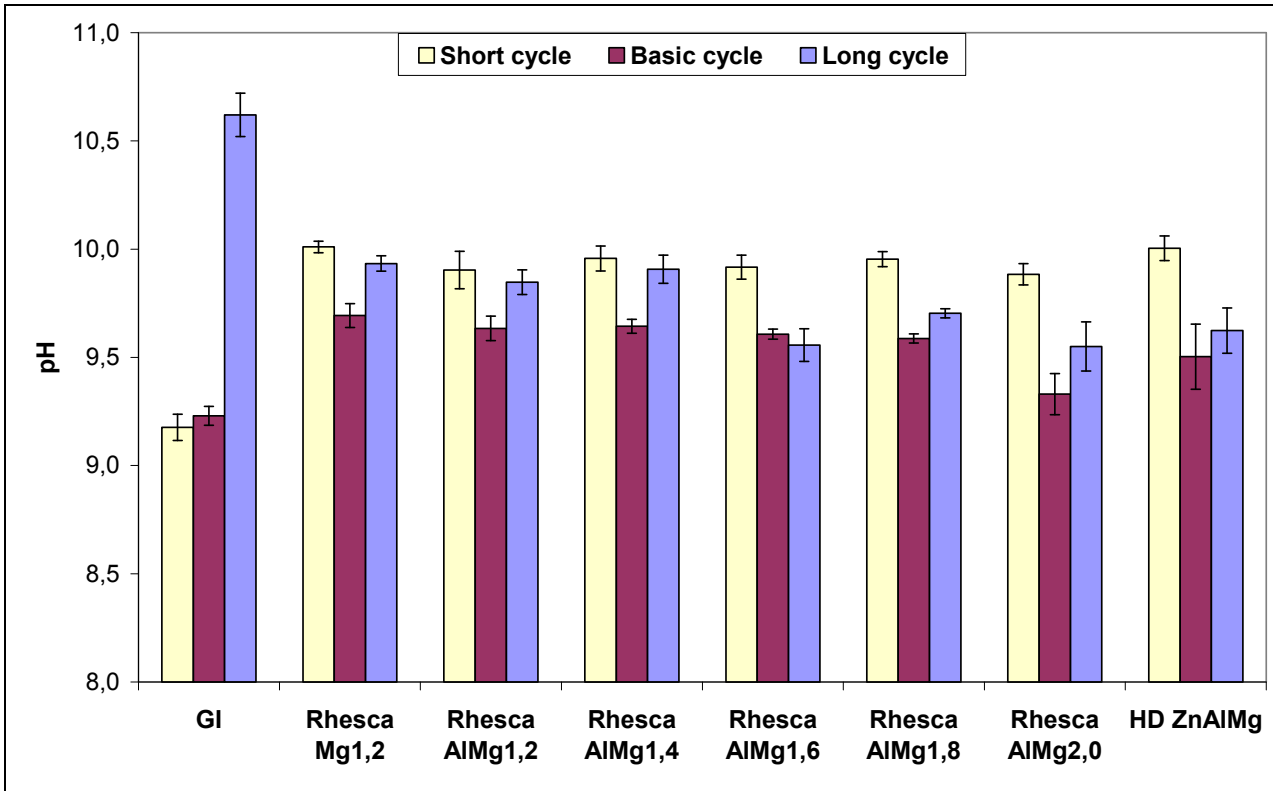


Figure 80 pH of water extracts obtained by dissolving corrosion products after cyclic tests

The relative total quantity of sodium and zinc carbonates decreased with increasing drying time. It is observed in the spectra and can be quantified using the C/S ratio. It dropped from 3.2 for 2 hours of drying to 2.4 for 8 hours of drying.

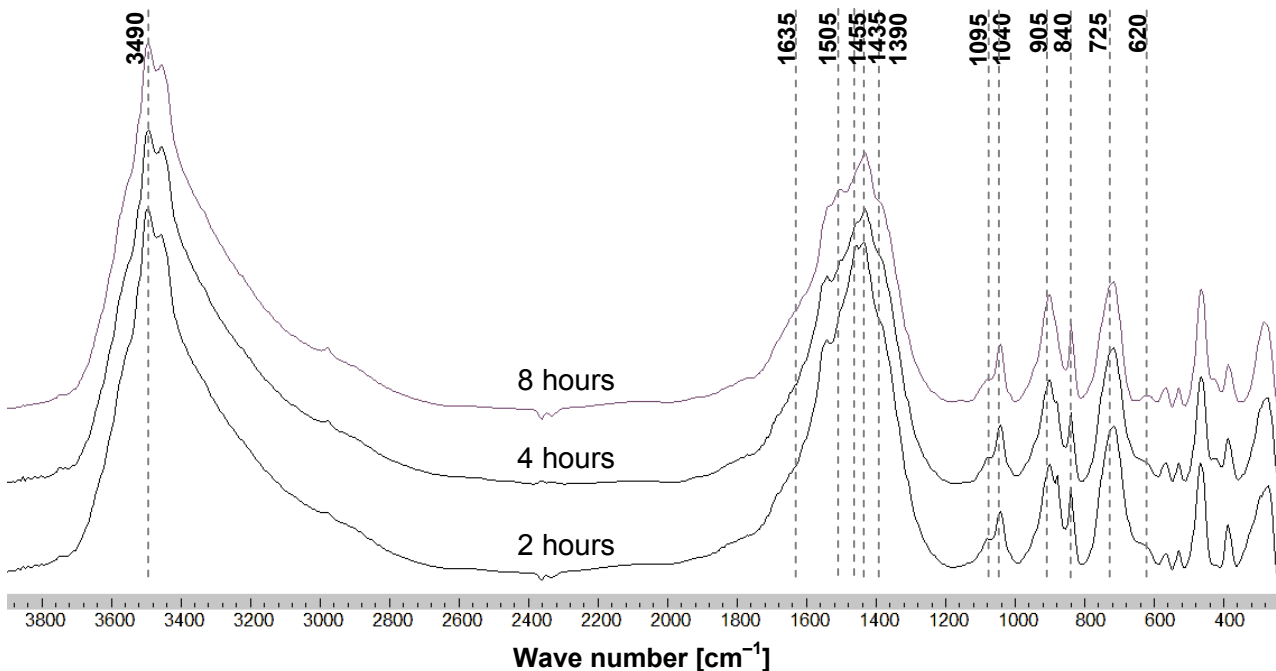


Figure 81 Infrared transmission spectra of corrosion products collected on HD ZnAlMg with deposited sodium chloride at the chloride concentration of 1400 mg/m² exposed in wet/dry cycles with different drying time

Table 13 Phase composition of corrosion products collected from HD ZnAlMg contaminated with 1400 mg/m² chloride after exposure in wet/dry cycles with different drying time

Drying time	Hydrozincite (1505 cm ⁻¹)	Simonkolleite (905 cm ⁻¹)	C/S ratio [×]	Sodium carbonate (1455 cm ⁻¹)	Unidentified carbonate (1425 cm ⁻¹)	Water (1630 cm ⁻¹)	AlOOH (1095, 620 cm ⁻¹)	Others
2 hours	Yes	Yes	3.2	Yes	No	No	Yes	MgCO ₃
4 hours	Yes	Yes	2.8	Yes –	No	No	Yes	MgCO ₃
8 hours	Yes	Yes	2.4	Yes	No	No	Yes	MgCO ₃

[×] Carbonate to simonkolleite peak height ratio; – Weak peak, lower quantity; + Strong peak, higher quantity

FTIR spectra of corrosion products collected on GI samples exposed to the same cycles are in Figure 82. Again, there was no big difference between obtained spectra. Surprisingly, peaks in the carbonate region at 1600–1300 cm⁻¹ did not match those of hydrozincite. They were either offset or more probably, it was not hydrozincite which dominate in the corrosion products. It was probably other zinc and/or sodium carbonate. Simonkolleite was found in all cases. A C/S ratio did not change systematically with the drying time, see Table 14.

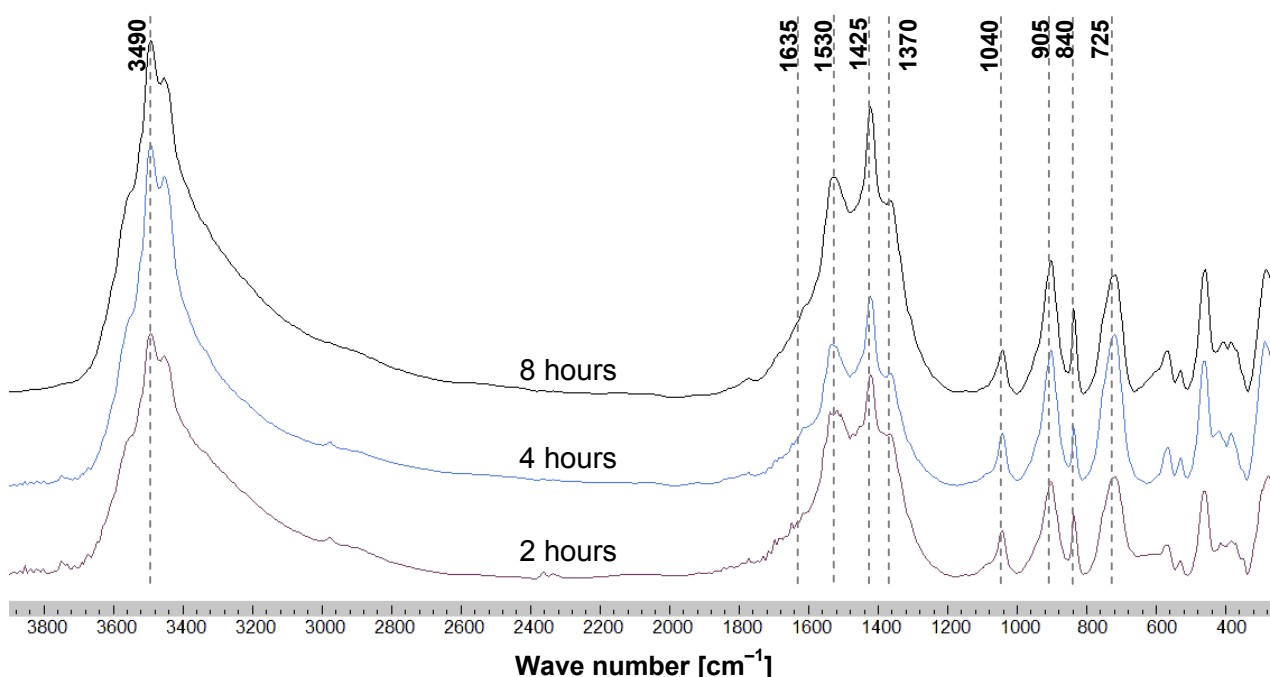


Figure 82 Infrared transmission spectra of corrosion products collected on GI with deposited sodium chloride at the chloride concentration of 1400 mg/m² exposed in wet/dry cycles with different drying time

Table 14 Phase composition of corrosion products collected from GI contaminated with 1400 mg/m² chloride after exposure in wet/dry cycles with different drying time

Drying time	Hydrozincite (1505 cm ⁻¹)	Simonkolleite (905 cm ⁻¹)	C/S ratio [×]	Sodium carbonate (1455 cm ⁻¹)	Unidentified carbonate (1425 cm ⁻¹)	Water (1630 cm ⁻¹)	AlOOH (1095, 620 cm ⁻¹)	Others
2 hours	–	Yes	2.2	No	Yes	No	No	
4 hours	–	Yes	1.5	No	Yes	No	No	
8 hours	–	Yes	2.1	No	Yes	No	No	

[×] Carbonate to simonkolleite peak height ratio

As in case of corrosion products analyzed previously, there was relatively less carbonate on the surface of GI than on HD ZnAlMg exposed under identical conditions.

4.5 Effect of CO₂ on metallic coated panels at 20°C and in air saturated with water

Metallic coated panels were exposed for 4 weeks in ambient air and in CO₂-free air at high relative humidity close to 100 %. The relative humidity was not controlled during the test. CO₂ was removed from ambient air with a CO₂-adsorber VCD3-21 from Twin Tower Engineering. According to technical specifications, air with CO₂ content below 1 ppb should be provided by the apparatus. The CO₂ content was measured by FTIR to be equal or below 10 ppb. The CO₂ in ambient air is about 380 ppm. Exposed samples were contaminated with sodium chloride at the chloride concentration of 1400 mg/m². The goal of this test was to evaluate the role of carbon dioxide in mechanism of zinc and ZnAlMg corrosion.

Dry weight gain after test and weight loss after corrosion product removal are given in Figure 83 and in Figure 84, respectively. Important differences were observed for the tested metallic coatings. For instance, the dry mass gain was almost zero with CO₂-free air for ZAM. The other coatings gave higher dry mass gain in CO₂-free air. The biggest differences were observed for HD ZnAlMg and for Galfan with an increase of the dry mass gain after test of about 3 and 4-times in CO₂-free air, respectively. The weight loss measurements confirmed that CO₂-free air was considerably more corrosive than ambient air for HD ZnAlMg and for Galfan, see Figure 84. Thus, these two materials are very sensitive to the presence of carbon dioxide in air. This might indicate that either carbonate-based corrosion products are essential for high corrosion stability of HD ZnAlMg and Galfan or carbon dioxide affects e.g. the pH of the surface electrolyte. For the other materials, i.e. ZAM, SD and AZ, differences in weight loss between the two tests were inside the experimental error. Clearly more black corrosion products formed on AZ in the CO₂-free air test, see Figure 85, photographs of specimens after test.

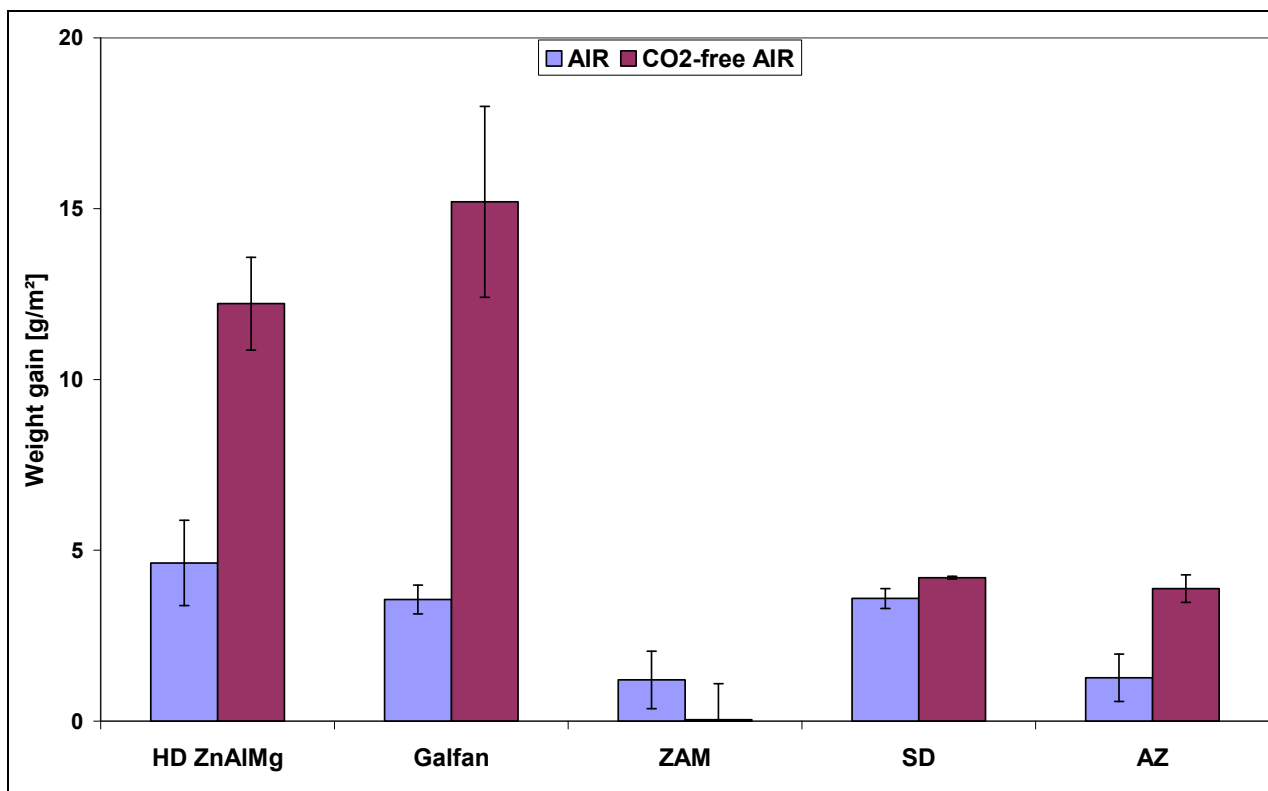


Figure 83 Weight gain after drying of metallic coated panels after 4 weeks of exposure in humid ambient and CO₂-free air at 20°C

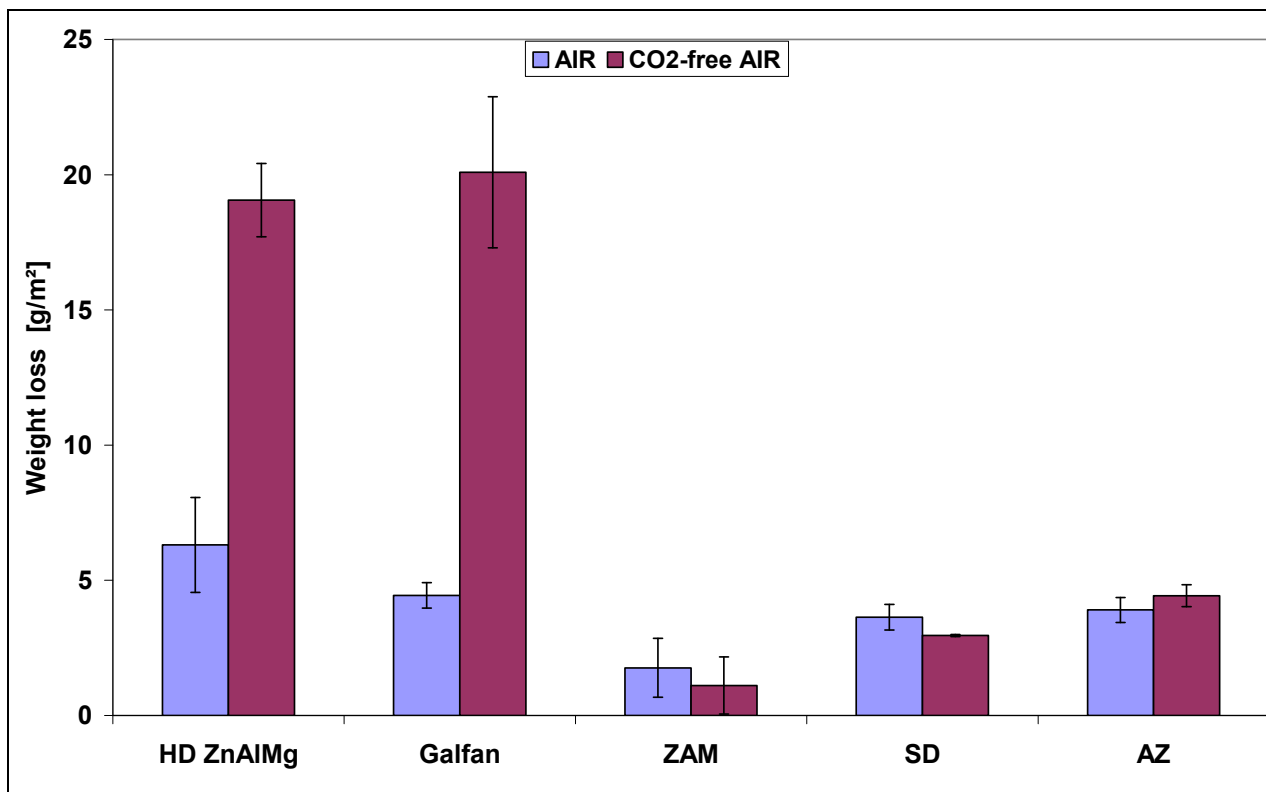


Figure 84 Weight loss of metallic coated panels after 4 weeks of exposure in humid ambient and CO₂-free air at 20°C

Ion chromatography analysis of soluble corrosion products was performed after dissolution of corrosion products in deionized water. Results are given in Figure 86 and in Figure 87 for bonded chloride and bonded sodium, respectively. Significantly more bonded chloride was found on the surface of HD ZnAlMg and Galfan in the CO₂-free air test compared to ambient air test. It correlates well to the weight loss data showed above. The effect of CO₂ presence on the amount of bonded chloride was lower and often within the experimental error for the other materials. No general tendency can be drawn from results for bonded sodium in Figure 87. Although much more corrosion products were formed on HD ZnAlMg in CO₂-free air, the amount of bonded sodium seems to be even somewhat lower. It can be supposed that less sodium carbonate was formed on the surface of HD ZnAlMg in CO₂-free air. Similar effect can be seen for Galfan.

The amount of soluble zinc and magnesium are given in Figure 88 and in Figure 89, respectively. For HD ZnAlMg and Galfan, clearly less soluble Zn was found in the CO₂-free air test compared to ambient air test. Since higher weight loss and therefore total amount of oxidized zinc was obtained under these conditions, it indicates that the tendency of zinc to form stable corrosion products was higher in CO₂-free air. Similar but weaker effect was observed also for the other materials.

For all the Mg-containing coatings, less soluble Mg was found in the CO₂-free air test compared to ambient test. It is expectable for ZAM and SD, but somewhat surprising for HD ZnAlMg, which was 3-times more corroded in CO₂-free air. Either less magnesium was released to the surface electrolyte or it was bonded in more stable corrosion products.

pH of extract water after dissolution of corrosion products in deionized water are given in Figure 90. HD ZnAlMg and Galfan exposed in CO₂-free air have more alkaline pH compared to specimens exposed in ambient air.

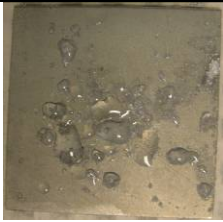

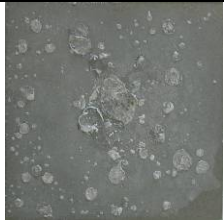
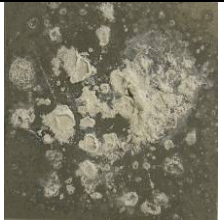












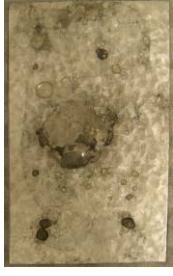



Coating	After test, before drying		After test, after drying	
	Ambient air	CO ₂ -free air	Ambient air	CO ₂ -free air
HD ZnAlMg				
Galfan				
ZAM				
SD				
AZ				

Figure 85 Photographs of specimens after exposure in humid ambient and CO₂-free air

FTIR analysis was performed for the corrosion products from HD ZnAlMg. Results are given in Figure 91 and Table 15. Simonkollite and hydrozincite were formed both in air and in CO₂-free environment. There was even slightly more hydrozincite on the sample exposed in air with lowered CO₂ content than on the sample exposed in air in relative quantity, see C/S ratios in Table 15. The wide peak at 360–580 cm⁻¹ indicates presence of zincite, ZnO in corrosion products formed without presence of carbon dioxide. The presence of aluminum and magnesium corrosion products was not proved clearly. More water was found in products on the sample exposed in air.

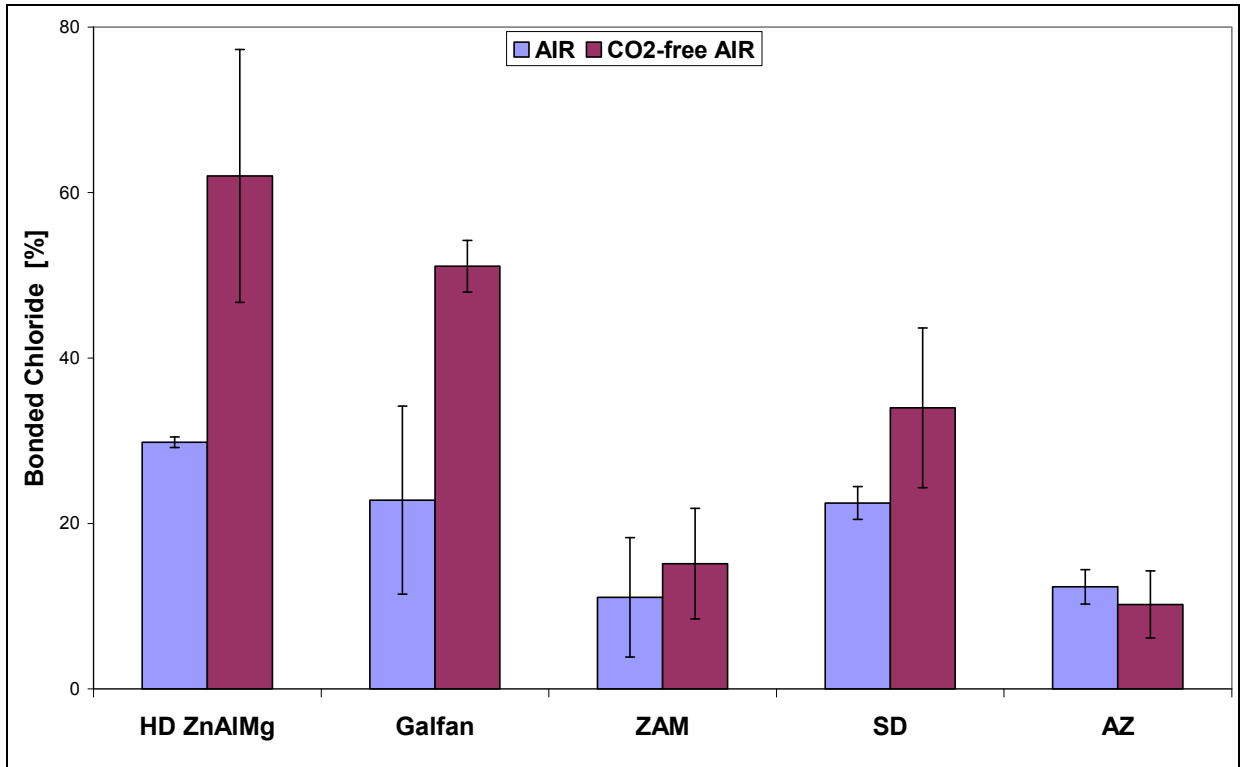


Figure 86 Bonded chloride from ion chromatography of water extract of corrosion products; results for metallic coated panels contaminated with 1400 mg/m² of chloride and exposed 4 weeks in air and in CO₂-free air at 20°C and high RH

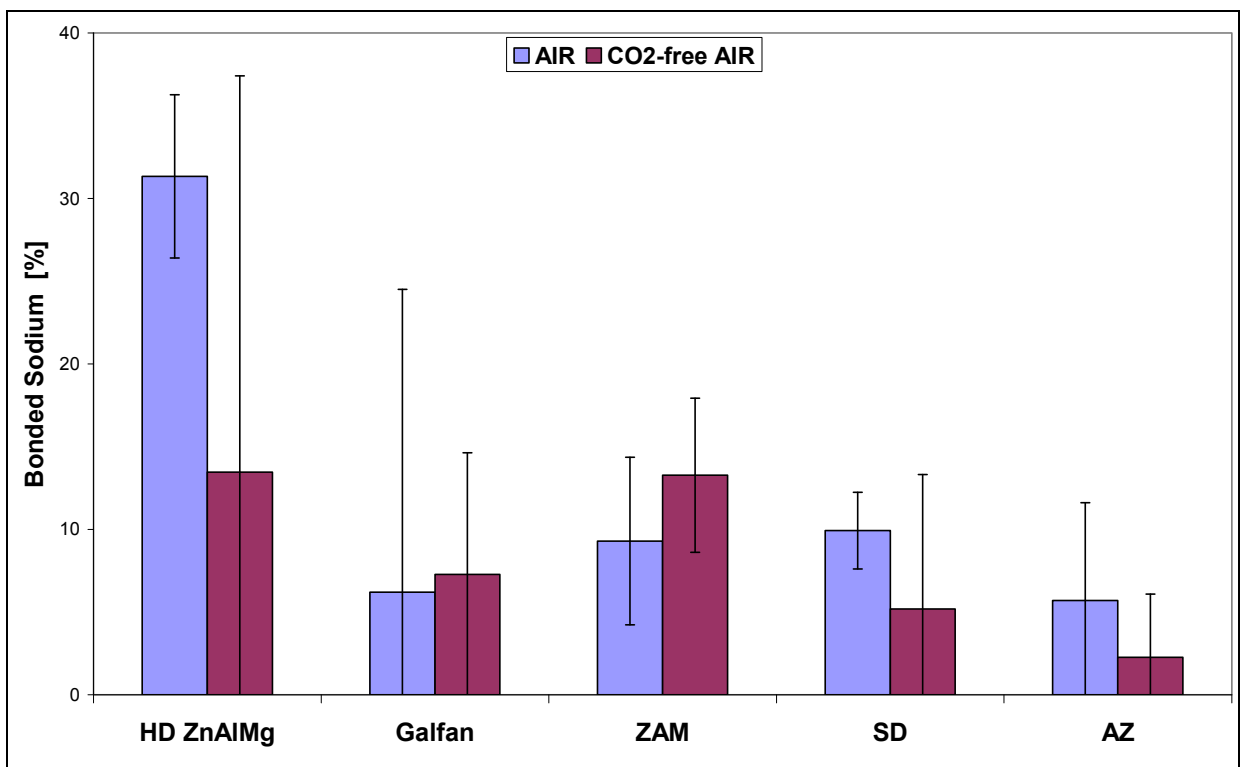


Figure 87 Bonded sodium from ion chromatography of water extract of corrosion products; results for metallic coated panels contaminated with 1400 mg/m² of chloride and 907 mg/m² of sodium and exposed for 4 weeks in air and in CO₂-free air at 20°C and high RH

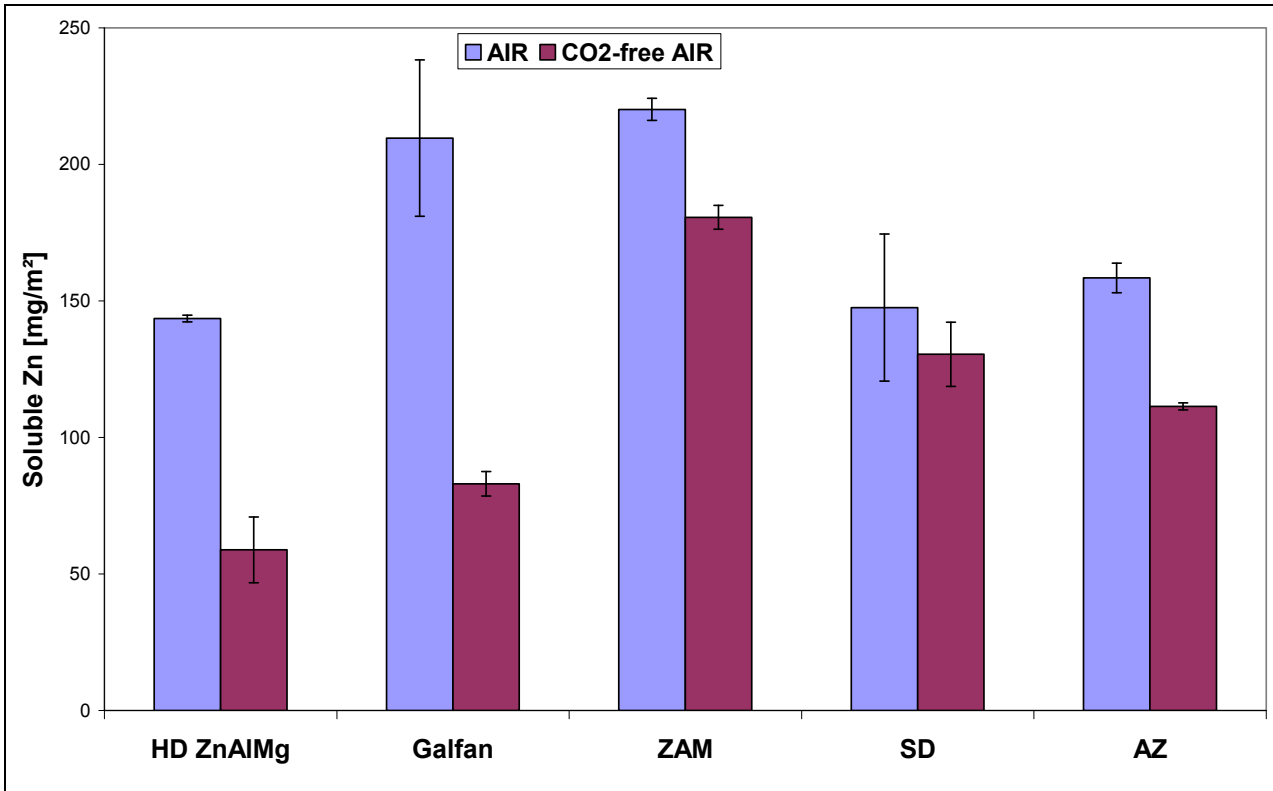


Figure 88 Soluble zinc on the surface from ion chromatography of water extract of corrosion products; results for metallic coated panels exposed in air and in CO₂-free air at 20°C and high RH

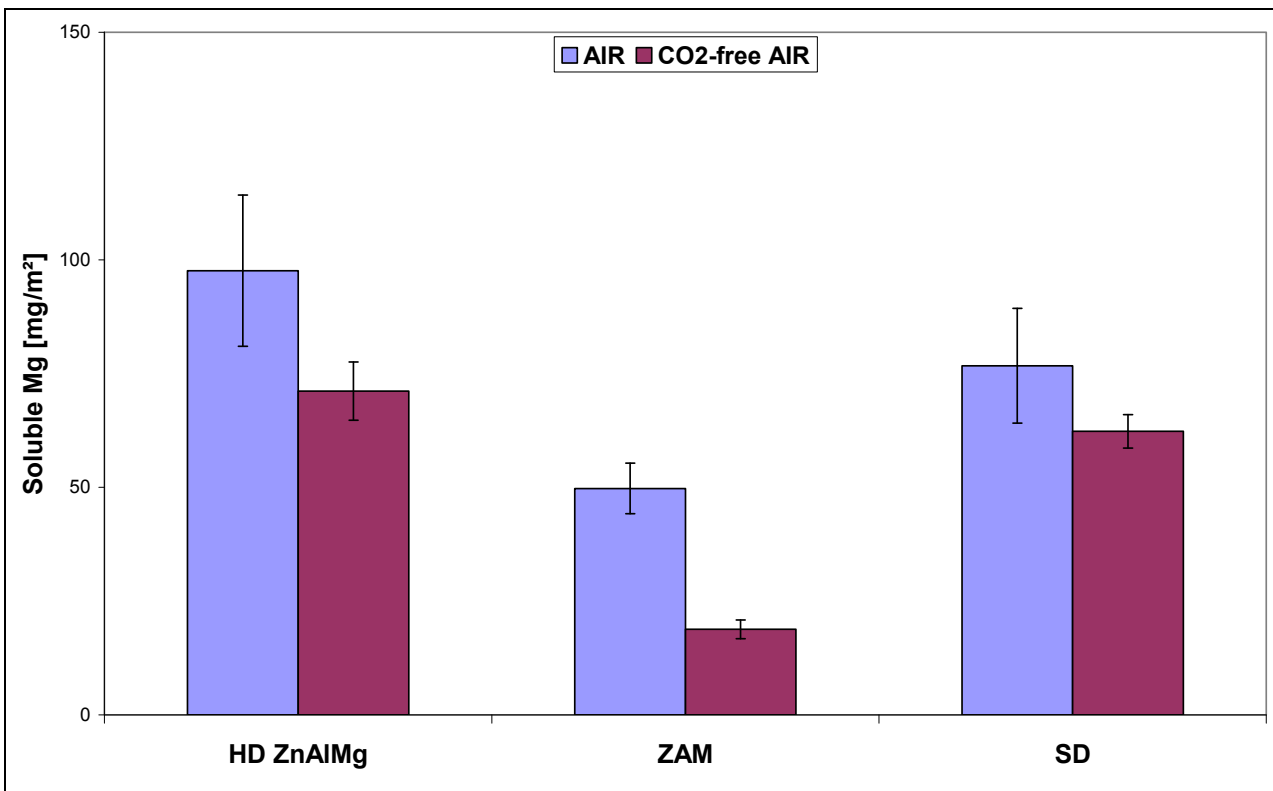


Figure 89 Soluble magnesium on the surface from ion chromatography of water extract of corrosion products; results for metallic coated panels exposed in air and in CO₂-free air at 20°C and high RH

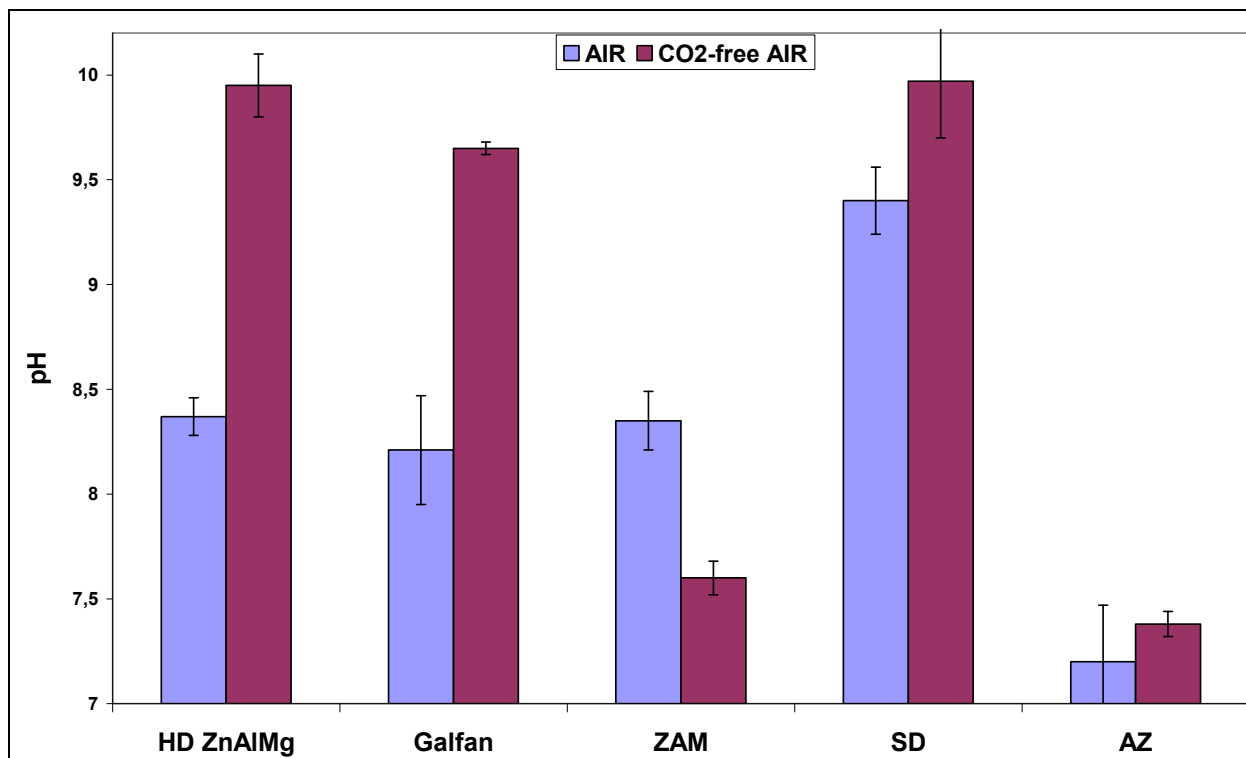


Figure 90 pH of water extracts obtained by dissolving the corrosion products after tests in air and in CO₂-free air at 20°C and high RH

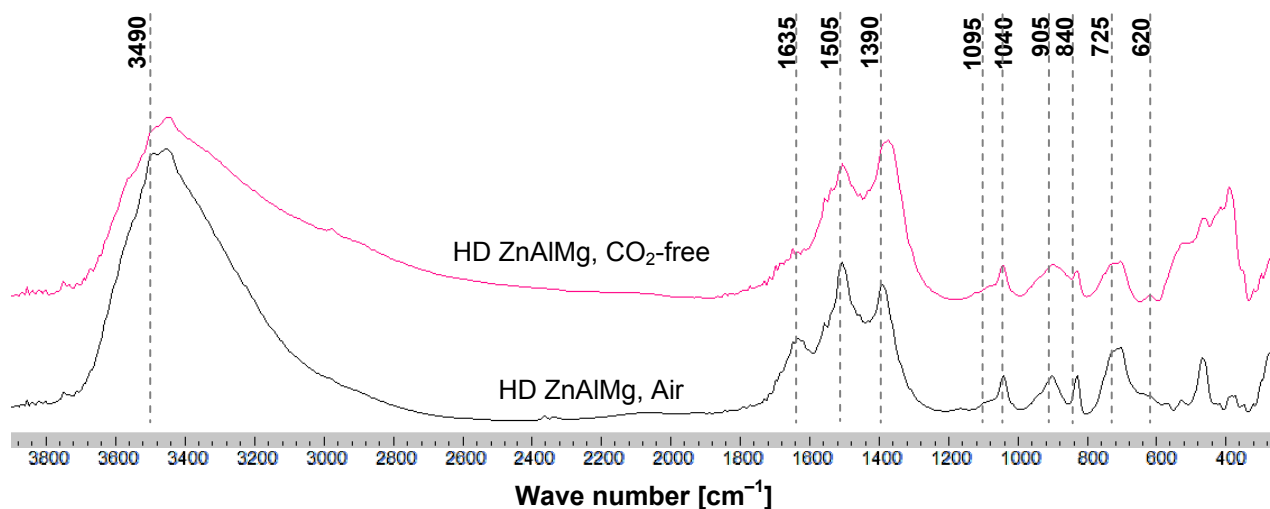


Figure 91 Infrared transmission spectra of corrosion products collected on GI and HD ZnAlMg with deposited sodium chloride at the chloride concentration of 1400 mg/m² exposed for 28 days at 20°C and at high RH in air and in air with removed carbon dioxide

Table 15 Phase composition of corrosion products collected from HD ZnAlMg contaminated with 1400 mg/m² chloride after 28 days of exposure at 20°C and at high RH in air and in air with removed CO₂

Alloy, conditions	Hydrozincite (1505 cm ⁻¹)	Simonkolleite (905 cm ⁻¹)	C/S ratio [×]	Zincite (about 490 cm ⁻¹)	Water (1630 cm ⁻¹)
HD ZnAlMg, Air	Yes	Yes	4.2	Low	Yes
HD ZnAlMg, CO ₂ -free	Yes	Yes	5.1	Yes	Yes –

[×] Carbonate to simonkolleite peak height ratio; – Weak peak, lower quantity; + Strong peak, higher quantity

Thus, the removal of CO₂ promoted formation of zincite, ZnO on the surface of HD ZnAlMg. In work of Lindström et al. [30], similar experiment was done with zinc. A strong increase in weight loss in CO₂-free air was observed at 20°C. As in this work for HD ZnAlMg, formation of a high amount of zincite on the metal surface was detected. It is much less protective than hydrozincite or simonkolleite and its presence explains reduced corrosion stability of this material in CO₂-free air. The presence of carbonates on the sample exposed in CO₂-free air is surprising. It is possible that it was formed after the exposure when the sample was dried in a desiccator in ambient air.

The data on the pH of extracts of corrosion products in Figure 90 shows that except ZAM, the pH after the CO₂-free test was higher even for materials that were less corroded. In previous experiments, a correlation between the weight loss and pH was seen. Thus, it is possible that the removal of CO₂ from air led to formation of surface electrolytes with higher pH. It can cause both inhibition or increase of the rate of the corrosion process depending on the material. Average pH of extracts of corrosion products after the CO₂-free air test was above 9.0 while it was about 8.5 in ambient air.

Although the results presented in this chapter must be understood as preliminary, they indicate a strong effect of carbon dioxide on corrosion of coatings alloyed with Mg and Al at lower amounts. The exact mechanism of the detrimental effect of CO₂ removal on corrosion of these materials is not fully clear yet. Carbon dioxide can influence the pH of the surface electrolyte or be directly involved in formation of protective carbonate-based corrosion products. Further work under more controlled conditions at lower RH more relevant to atmospheric conditions is planned.

4.6 Corrosion in confined areas

4.6.1 Renault crevice configuration

Renault crevice panels were exposed in ACT test for 6 weeks. Photographs of specimens after the test are given in Figure 92 to Figure 98 (both the “cover” and the “back” parts are shown). As expected, red rust in important quantity was rapidly formed on CRS panels, see Figure 92. Red rust was also observed on GI 10µm but not on GI 20µm after 6 weeks of exposure, see Figure 93 and Figure 94. Galfan at 20 µm did not show any red rust after exposure (Figure 95) whereas HD ZnAlMg coatings at the thickness from 7 to 14 µm exhibited red rust only around the hole for screws, see Figure 96, Figure 97 and Figure 98.



Figure 92 CRS Renault crevice panels after 6 weeks in ACT test

The metal loss on CRS crevice panels was evaluated after removing the corrosion products by pickling in Clark solution. It was done by comparing the thickness of the corroded area to the thickness of intact metal sheet using a micrometer gauge equipped with a sharp tip. It should be mentioned that no significant

differences were noticed in the corrosion attack as a function of the gap in the range 0–250 μm . Therefore, an average value is plotted in Figure 99 for CRS panels. The extent of red rust inside the crevice is also given. Considering the coated materials, the only material which exhibited considerable amount of red rust was GI at 10 μm . The steel metal loss for GI at 10 μm is also given in Figure 99. For GI 20 μm , Galfan 20 μm and HD ZnAlMg 7, 10, and 14 μm , the metallic coating loss and red rust appearance was calculated and it is presented in Table 16. Red rust with the extent inferior to 4 % was observed for HD ZnAlMg at all thicknesses, but it should be mentioned that it was located only under the screw. GI 10 μm exhibited a metallic coating loss of 11.0 ± 3.7 μm while Galfan lost 1.5 ± 2.6 μm of the coating in 6 weeks of exposure. HD ZnAlMg at all thicknesses exhibited a metallic coating loss from 2.9 to 3.7 μm . The metallic coating loss is plotted against the content of alloying elements in Figure 105 and a rather linear dependence is shown.



Figure 93 GI Renault crevice panels with the coating thickness of 10 μm after 6 weeks in ACT test



Figure 94 GI Renault crevice panels with the coating thickness of 20 μm after 6 weeks in ACT test



Figure 95 Galfan Renault crevice panels after 6 weeks in ACT test

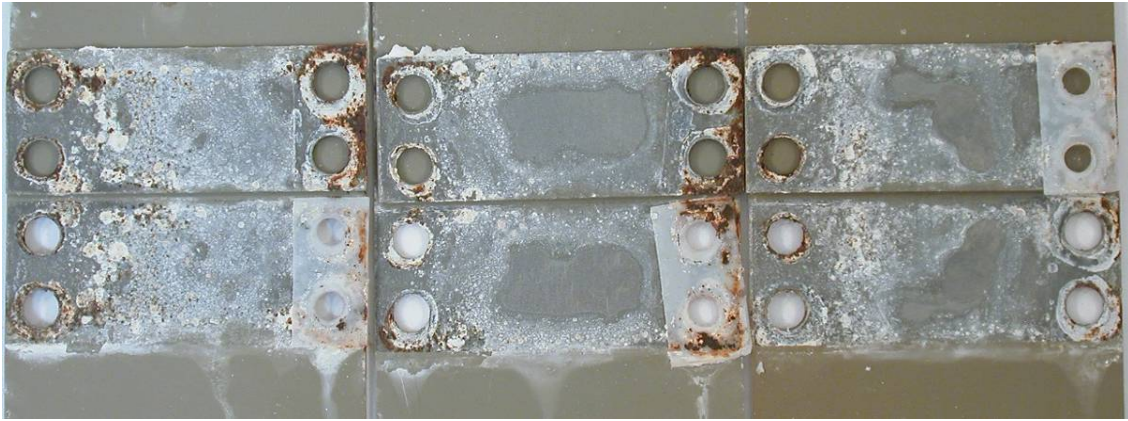


Figure 96 HD ZnAlMg 7 μm Renault crevice panels after 6 weeks in ACT test

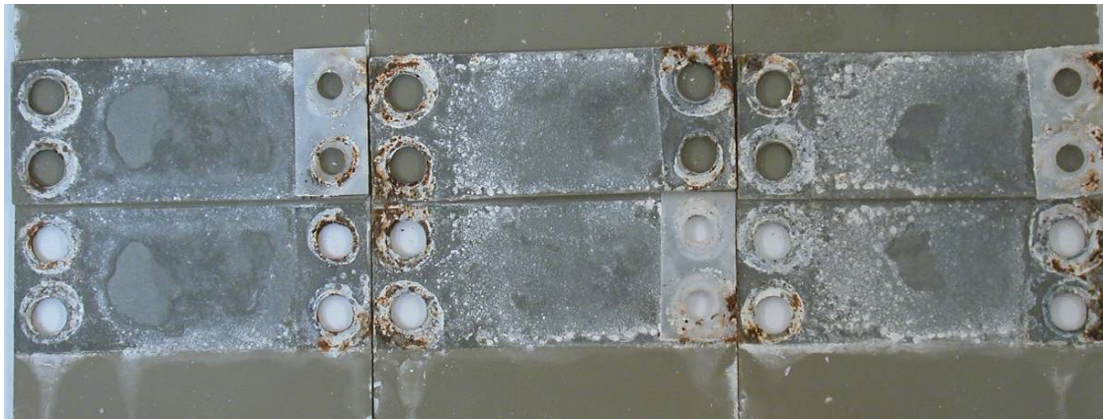


Figure 97 HD ZnAlMg 10 μm Renault crevice panels after 6 weeks in ACT test

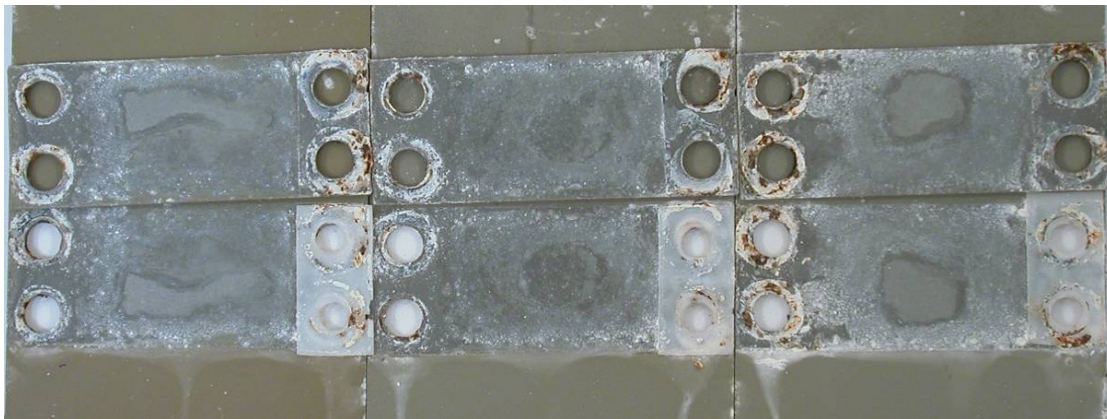


Figure 98 HD ZnAlMg 14 μm Renault crevice panels after 6 weeks in ACT test

Table 16 Metallic coating loss for Renault crevice panels exposed 6 weeks in ACT test

Coating	% of red rust	Metallic coating loss [μm]	Observation
GI 10 μm	30.0 ± 6.1	NA	Red rust
GI 20 μm	0	11.0 ± 3.7	No red rust
Galfan 20 μm	0	1.5 ± 2.6	No red rust in crevice
HD ZnAlMg 7 μm	2.8 ± 1.3	2.9 ± 0.8	Red rust mainly in screw location
HD ZnAlMg 10 μm	3.3 ± 1.2	3.7 ± 0.9	Red rust only in screw location
HD ZnAlMg 14 μm	2.0 ± 0.9	3.6 ± 1.7	Red rust only in screw location

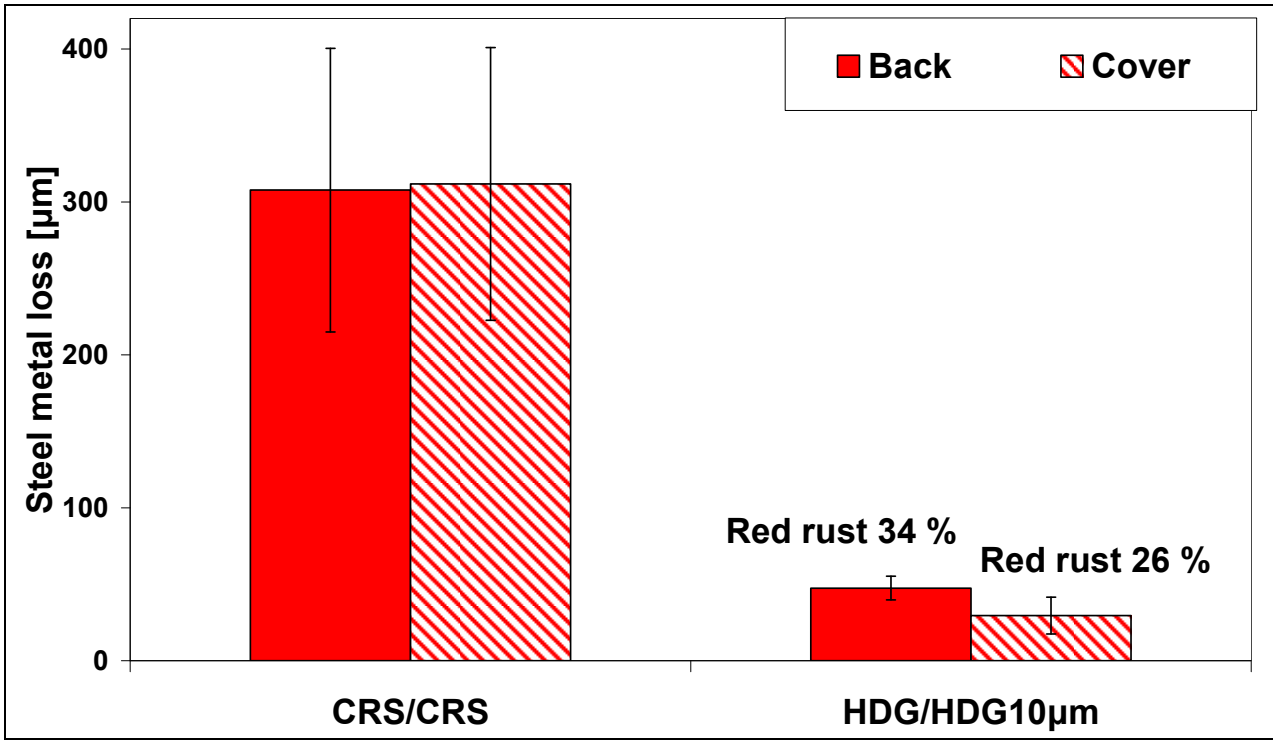


Figure 99 Corrosion of steel of Renault crevice panels made of CRS and GI at 10 µm with the extent of red rust in percentage (results for both the "cover" and the "back" parts of the Renault crevice configuration are showed)

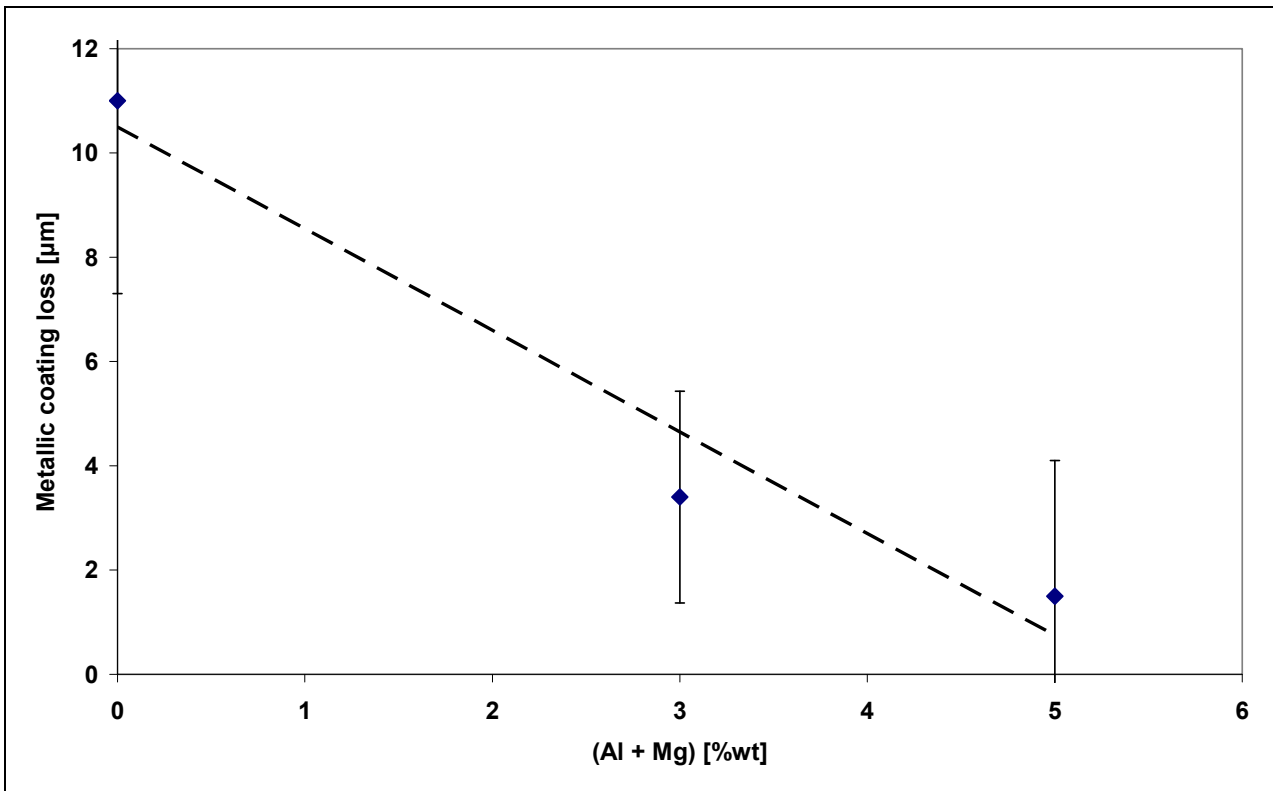


Figure 100 Metallic coating loss versus total alloying elements

4.6.2 Volvo crevice panels

CRS, GI 10 μm , GI 20 μm , Galfan 20 μm , and HD ZnAlMg 7, 10 and 14 μm were tested in ACT for 18 weeks in Volvo crevice configuration and Volvo open configuration. Volvo open configuration have the same design as crevice configuration panels but without a glass cover forming the confined zone. Crevice and open panels in the Volvo design were used to monitor the corrosion propagation by mass gain measurement. Once a week, samples exposed in ACT were removed from a test chamber before the salt spray phase and after the drying phase and weighed. As it is described in the experimental section, the opening of the confined area ranged from 0 to 250 μm as for the Renault crevice coupon.

The accumulated mass gain on panels in open and crevice configurations is plotted as a function of exposure time in Figure 101 and Figure 102 together with data recorded on CRS panels for comparison. Photographs of the panels after 18 weeks of testing are presented in Figure 103 to Figure 108 for crevice configuration and in Figure 109 to Figure 114 for the open configuration. After 18 weeks of exposure, important amount of red rust in confined areas was observed for CRS, GI 10 μm , GI 20 μm and HD ZnAlMg 7 μm , see Figure 103, Figure 104, and Figure 106. Clearly less red rust was observed for Galfan 20 μm and HD ZnAlMg 10 μm , see Figure 105 and Figure 107. However, the coating exhibiting the lowest amount of red rust after this test was HD ZnAlMg 14 μm , see Figure 108. The same coating classification can be done for the open configuration. Again, Galfan 20 μm and HD ZnAlMg 10 μm are comparable in terms of red rust propagation, see Figure 111 and Figure 113. HD ZnAlMg 14 μm was the only coating, which remained fully resistant to red rust appearance in the open configuration after 18 weeks in ACT, see Figure 114.

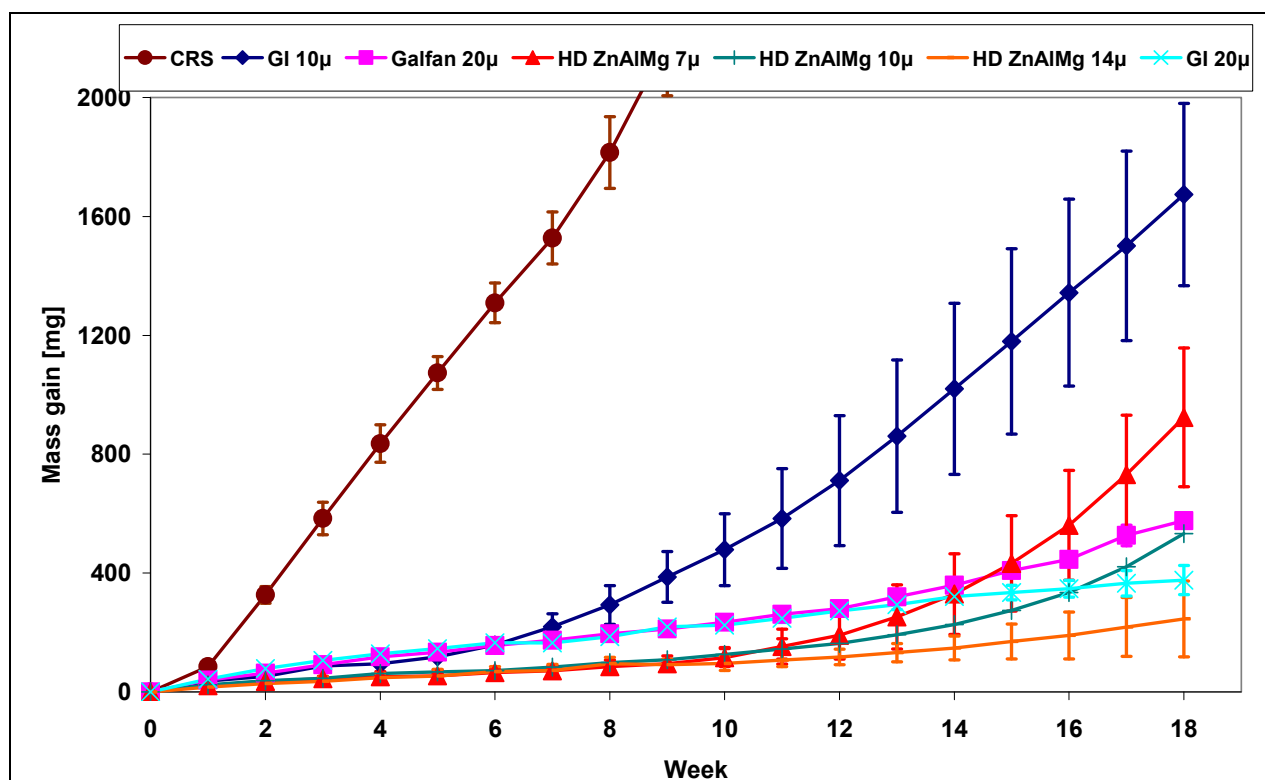


Figure 101 Weight gain of Volvo crevice panels exposed in ACT

Fujita et al. [31] showed that corrosion of Zn-based coatings in confined areas (corrosion perforation) could be described in 4 stages. In stage 1, the Zn-based coating is covering the entire surface of the steel substrate and the corrosion only affect the coating. In stage 2, Zn-based coating is partially lost and the remaining Zn film is sacrificially protecting the steel substrate. In stage 3, the steel substrate is corroding but corrosion is restrained by zinc corrosion products. In stage 4, the steel substrate is corroding at the same rate as

uncoated steel. Such a corrosion process is schematically described in Figure 115 for GI. The corrosion-resistance period of the coating is considered between stage 1 and stage 3.

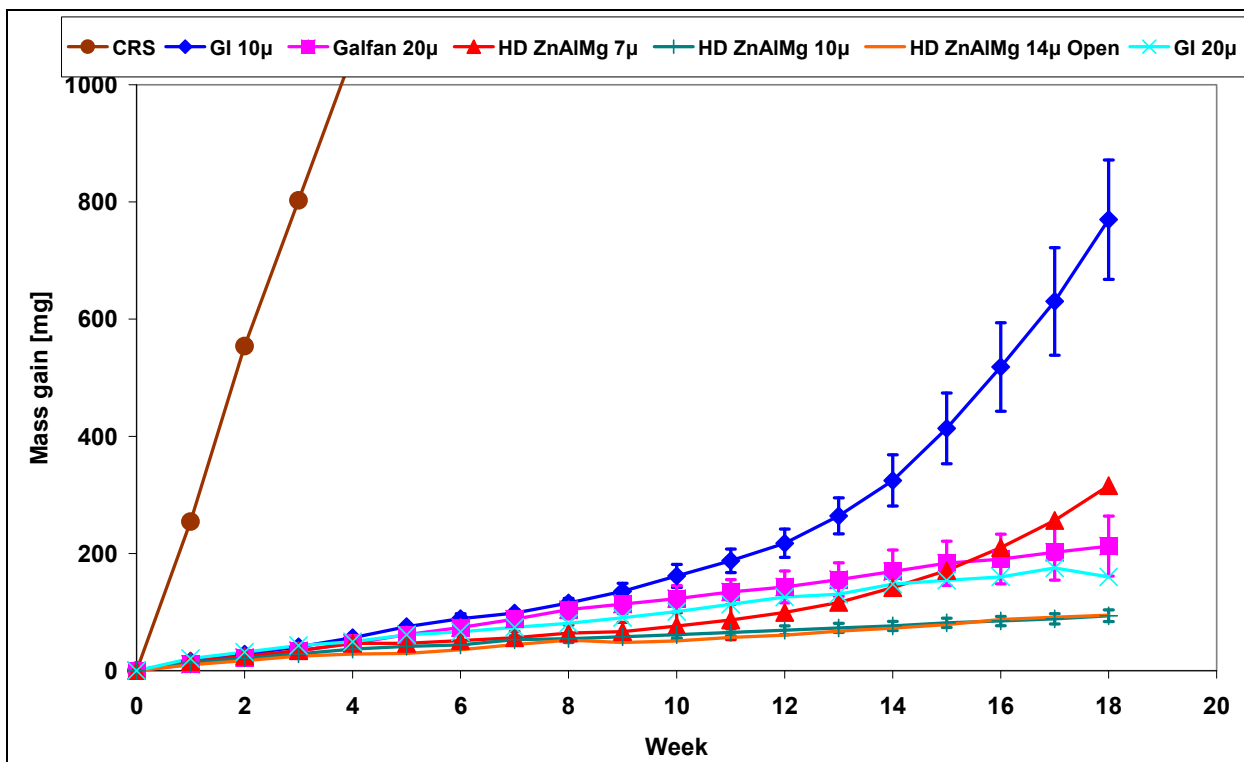


Figure 102 Weight gain of panels in open configuration exposed in ACT



Figure 103 CRS in Volvo crevice configuration after ACT



Figure 104 GI 10 µm in Volvo crevice configuration after ACT



Figure 105 Galfan 20 µm in Volvo crevice configuration after ACT



Figure 106 HD ZnAlMg 7 μm in Volvo crevice configuration after ACT



Figure 107 HD ZnAlMg 10 μm in Volvo crevice configuration after ACT

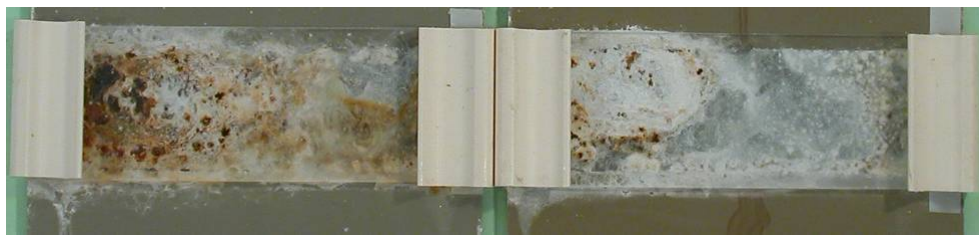


Figure 108 HD ZnAlMg 14 μm in Volvo crevice configuration after ACT



Figure 109 GI 10 μm in open configuration after ACT



Figure 110 GI 20 μm in open configuration after ACT



Figure 111 Galfan 20 μm in open configuration after ACT

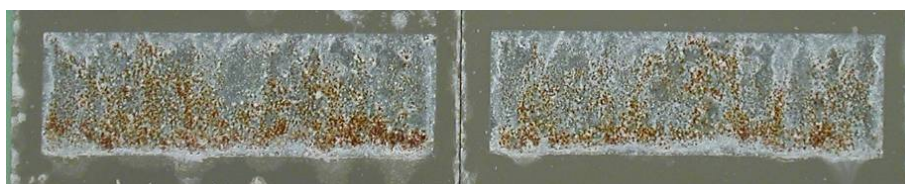


Figure 112 HD ZnAlMg 7 μm in open configuration after ACT

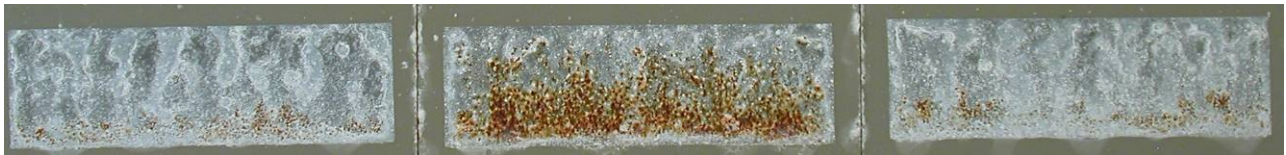


Figure 113 HD ZnAlMg 10 μm in open configuration after ACT



Figure 114 HD ZnAlMg 14 μm in open configuration after ACT

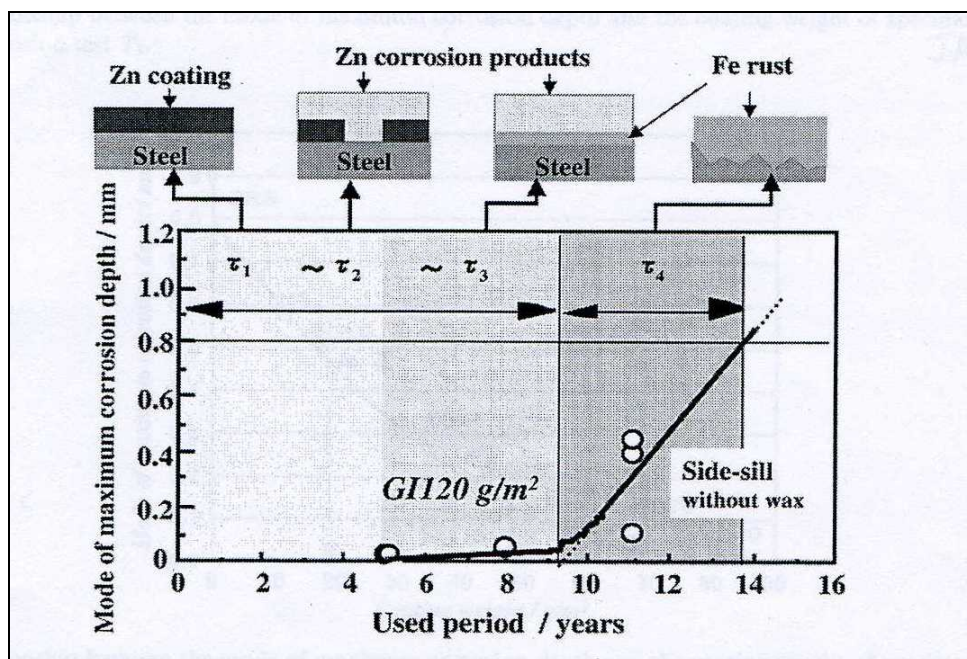


Figure 115 Schematic corrosion process of zinc coated steel in the crevice of lapped panels in cars [31]

As expected, a higher mass gain was measured for samples in the crevice configuration in comparison to the openly exposed surfaces, see Figure 101 and Figure 102. Changes in the corrosion mode of confined GI 10 μm are observable after 6 and 11 weeks. Before week 6, the metal surface is protected by zinc, it is covered by zinc corrosion products and no red rust is formed (Stage 1+2). Between week 6 and 11, red rust is present on the surface but zinc corrosion products still provide protection to the steel substrate (Stage 3). After week 11, the slope of the mass gain is almost reaching the mass gain slope of CRS panel without any coating (Stage 4). The same behavior with a delay of about 5 weeks was observed for HD ZnAlMg 7 μm. The crevice areas for both coatings were indeed completely rusted at the end of the test. Looking at GI 10 μm in the open configuration, similar changes of the slope were observed after week 8 and 13, indicating also changes in the corrosion mode (zinc corrosion products from weeks 0 to 8, zinc products and red rust from weeks 8 to 13 and red rust from week 13). The same trend with a delay of 4 weeks was observed for HD ZnAlMg 7 μm. For GI 20 μm and HD ZnAlMg 10 μm in the crevice configuration, zinc corrosion products were still visible after 18 weeks ensuring a protection of steel. However, the slope changed in week 12 for both coatings, indicating a change in the corrosion mode from Stage 1+2 to Stage 3. Red rust is

indeed visible in Figure 101. In both crevice and open configurations, mass gain of Galfan 20 µm was similar to that of GI 20 µm and was clearly higher than that of HD ZnAlMg 14 µm.

The corrosion attack in steel substrate and the percentage of observed red rust were measured after test for specimens in the crevice and open configuration. Results are given in Table 17 and in Table 18, respectively. These tables also indicate eventual changes in corrosion modes evaluated from wet mass gain measurements. The week of red rust appearance is also given in these tables. In both confined and open configuration, HD ZnAlMg 10 µm was comparable to Galfan 20 µm in terms of red rust initiation and red rust spreading after test. Both coatings delayed the appearance of the first pit of red rust by 25% compared to GI 20 µm and by 50% compared to GI 10 µm and the spreading of red rust after test was 19 to 36% lower for HD ZnAlMg 10 µm and Galfan 20 µm than for GI 20 µm in the crevice configuration. In open configuration, red rust spreading on HD ZnAlMg 10 µm and Galfan 20 µm was 49 to 54% lower than for GI 20 µm at the end of the test. In both confined and open configuration the best corrosion resistance was clearly observed for HD ZnAlMg 14 µm. 19 % less red rust than on Galfan in the crevice configuration and no red rust at all in the open configuration was observed. These results are summarized graphically in Figure 116 where red rust spreading after 18 weeks of the test is shown with the delay of red rust appearance related to GI 10 µm.

Table 17 Evaluation of Volvo crevice panels after 18 weeks of ACT in terms of red rust appearance and percentage of red rust after test

Material	Red rust appearance [week]	Change from stage 1+2 to 3 [week]	Change from stage 3 to 4 [week]	Area covered by red rust [%]	Max. depth of corrosion in the steel [µm]
CRS	1	–	–	100 ± 0	649 ± 98
GI 10 µm	2	6	11	100 ± 0	359 ± 98
GI 20 µm	3	–	–	87 ± 10	150 ± 64
Galfan 20 µm	4	12	–	51 ± 21	312 ± 19
HD ZnAlMg 7 µm	4	11	16	100 ± 0	277 ± 32
HD ZnAlMg 10 µm	4	12	–	68 ± 17	207 ± 25
HD ZnAlMg 14 µm	7	14	–	32 ± 18	112 ± 80

Table 18 Evaluation of specimens in the open configuration after 18 weeks of ACT in terms of red rust appearance and percentage of red rust after test

Coating	Red rust appearance [week]	Change from stage 1+2 to 3 [week]	Change from stage 3 to 4 [week]	Area covered by red rust [%]	Max. depth of corrosion in the steel [µm]
CRS	1	–	–	100 ± 0	501 ± 63
GI 10 µm	4	8	13	73 ± 5	105 ± 29
GI 20 µm	12	–	–	62 ± 8	21 ± 17
Galfan 20 µm	14	–	–	8 ± 2	23 ± 9
HD ZnAlMg 7 µm	6	12	16	24 ± 2	26 ± 8
HD ZnAlMg 10 µm	8 (14)*	–	–	13 ± 12	36 ± 26
HD ZnAlMg 14 µm	No red rust	–	–	0	0

*Only one of the three specimens showed red rust in week 8

4.7 Accelerated corrosion testing of formed and flat panels

Formed and flat panels were tested in ACT for 18 weeks. Weekly mass gain of formed and flat panels are given in Figure 117 and Figure 118, respectively. Table 19 gives the time of initiation of red rust at the top edge of formed panel and its extent after 18 weeks in ACT. The definition of the top edge is given in Figure 119. Red rust initiated after week 4 on both GI 10 μm and GE 10 μm . However, it was noticed that corrosion developed more uniformly on GE than on GI. Pits of red rust appeared on Galfan after week 11 while no red rust at the top edge was observed for HD ZnAlMg 14 μm after 18 weeks of exposure in ACT. Pits of red rust appeared at top edges after week 14 and 15 for HD ZnAlMg 7 μm and HD ZnAlMg 10 μm , respectively. Red rust spreading at top edges and delay of red rust appearance related to GI 10 μm are schematically summarized in Figure 125.

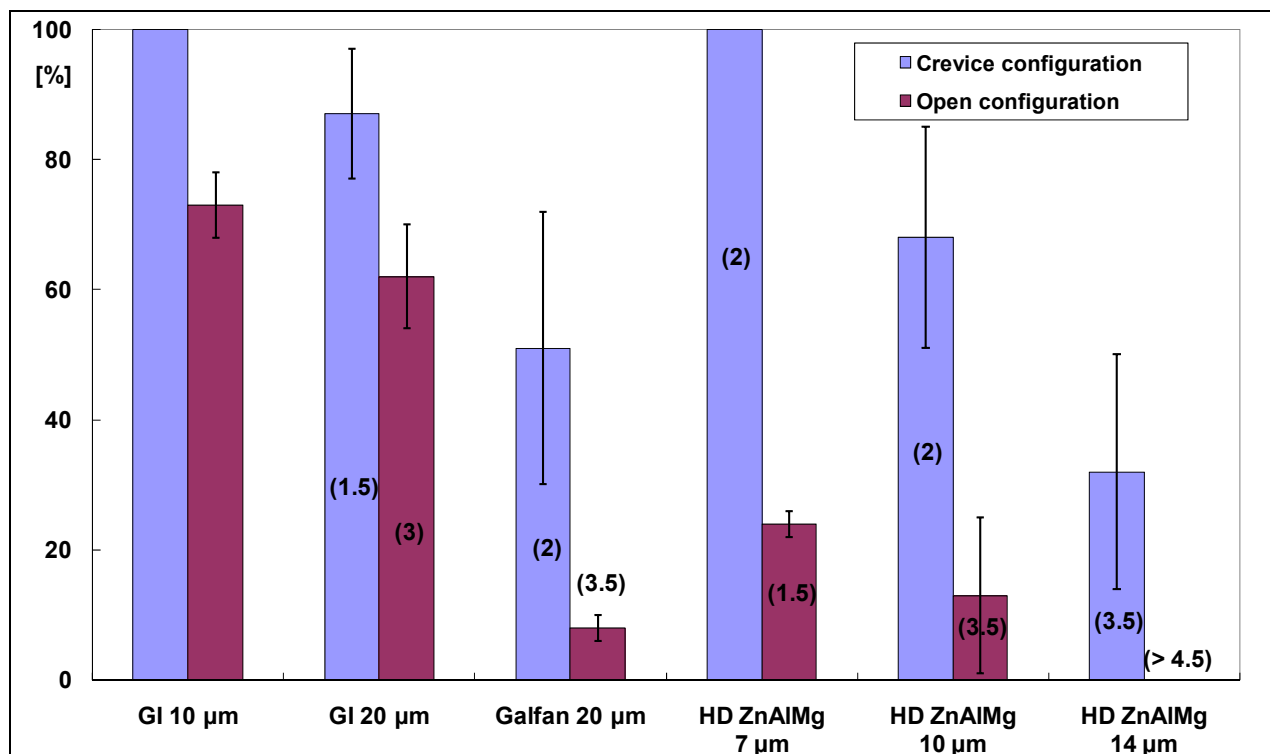


Figure 116 Summary of red rust spreading after 18 weeks of ACT for specimens in crevice and open configurations; delay of red rust appearance related to GI 10 μm is indicated in brackets

Rust with heterogeneous morphology in form of rather high “islands” was seen on Galfan while the growth of white rust was more uniform on HD ZnAlMg, see Figure 121 to Figure 124. This observation can explain higher mass gain of Galfan in comparison to that of HD ZnAlMg coatings, see Figure 117.

Galfan and HD ZnAlMg at 10 μm and 14 μm were cross cut and steel degradation at top edges was observed by optical microscopy. Micro photographs of cross sections at different locations are reported in Figure 126 to Figure 128. It is shown that the layers of corrosion products on Galfan are clearly more heterogeneous than those on HD ZnAlMg. The presence of less protective and voluminous oxides on the surface of Galfan can explain its lower corrosion resistance compared to HD ZnAlMg which apparently developed a more homogeneous and stable oxide layer on the surface of formed panels.

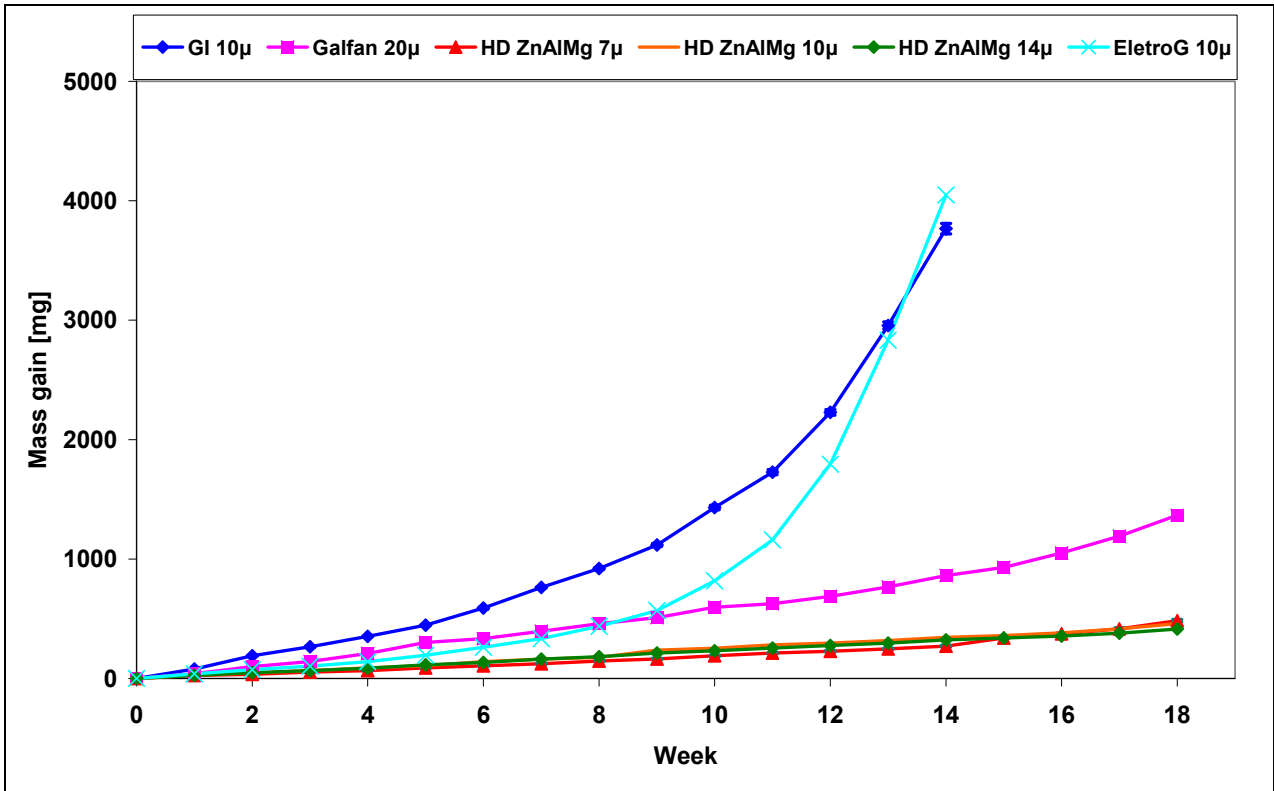


Figure 117 Weight gain of formed panels during accelerated ACT test

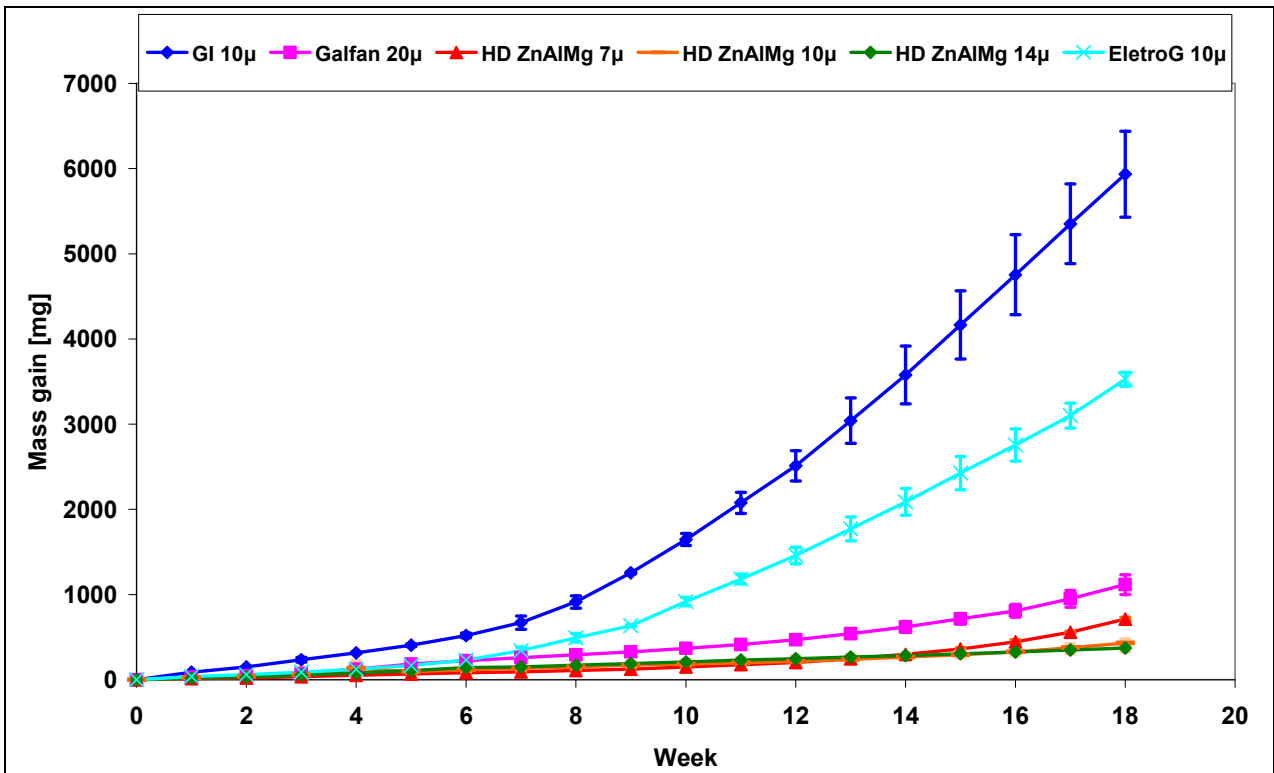


Figure 118 Weight gain of flat panels during accelerated ACT test

Table 19 Red rust appearance and percentage of red rust at the top edge after 18 weeks in ACT

	GI 10µm	GE 10µm	Galfan 20µm	HD ZnAlMg 7µm	HD ZnAlMg 10µm	HD ZnAlMg 14µm
Week of red rust appearance at the top edge*	4	4	11	14	15	No red rust
% of red rust at the top edge after 18 weeks	100	100	90	75	55	No red rust

* The top edge of the cup is shown in Figure 119

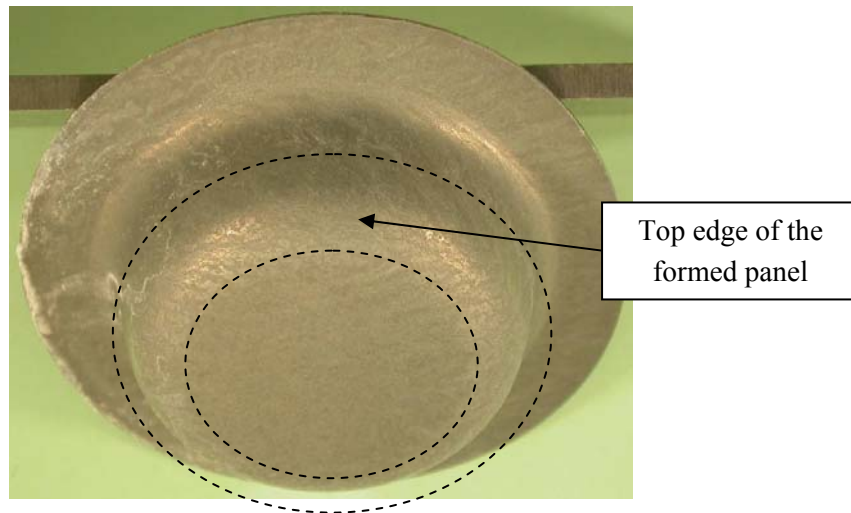


Figure 119 Illustration of the top edge of the button

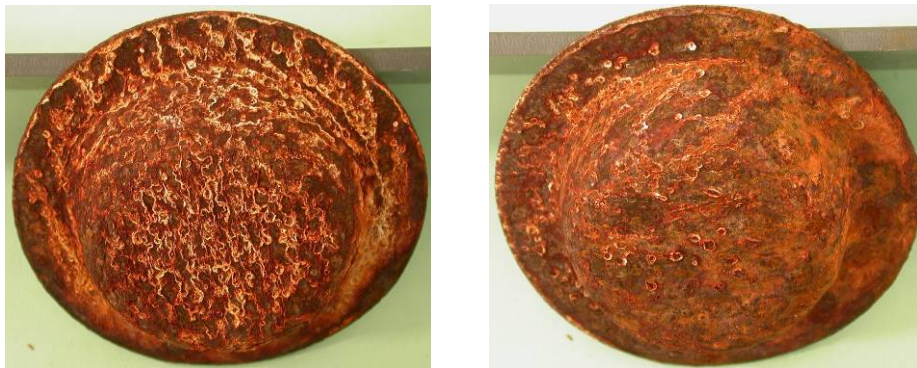


Figure 120 Formed GI 10 µm (left) and GE 10 µm (right) after 14 weeks in ACT



Figure 121 Formed Galfan 20 µm after 18 weeks in ACT



Figure 122 Formed HD ZnAlMg 7 μm after 18 weeks in ACT



Figure 123 Formed HD ZnAlMg 10 μm after 18 weeks in ACT



Figure 124 Formed HD ZnAlMg 14 μm after 18 weeks in ACT

Photographs of flat panels after test are given from Figure 129 to Figure 134. The inclination of 45° of the specimens exposed to the ACT test caused an increasing gradient of concentration of NaCl salt on the surface from the top to the bottom of the specimen as the salt solution run from the top to the bottom of specimens. This is why all specimens exhibited red rust at the bottom. The position of the red rust front can be used as an indication of the material corrosion resistance. The following classification can be done:

GI 10 μm < GE 10 μm << Galfan 20 μm ~ HD ZnAlMg 7μm < HD ZnAlMg 10μm < HD ZnAlMg 14 μm.

The oxides formed on Galfan were again more voluminous and heterogeneous than the ones formed on HD ZnAlMg.

It is interesting to notice that in non-confined areas, HD ZnAlMg 7 μm has even better corrosion resistance than Galfan 20 μm for both flat and formed panels. HD ZnAlMg coating with thickness of 14 μm showed excellent corrosion resistance for both flat and formed panels.

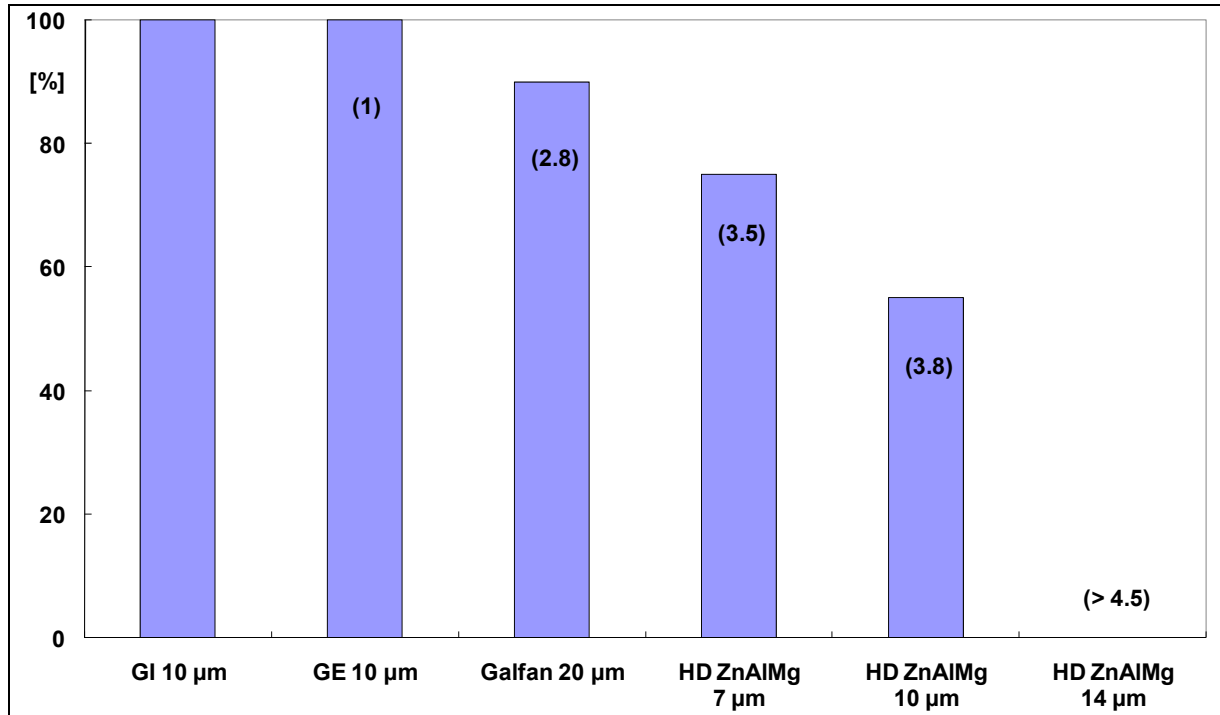


Figure 125 Summary of red rust spreading on the top edge of formed panels after ACT; delay of red rust appearance related to GI 10 µm is indicated in brackets

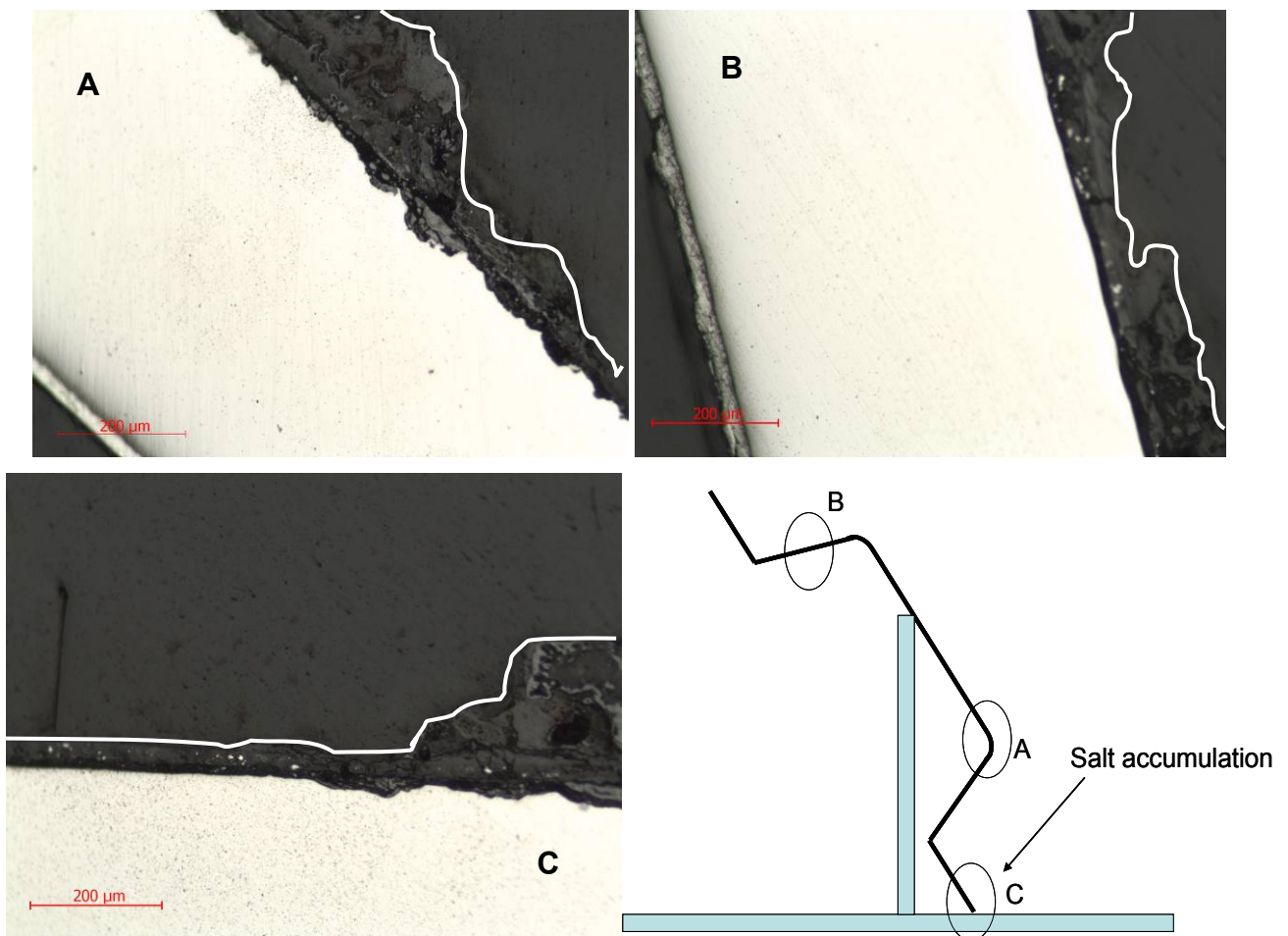


Figure 126 Microscopic observation of cross section of formed specimen of Galfan 20 µm after ACT; the boundary of the layer of corrosion products is shown with white line

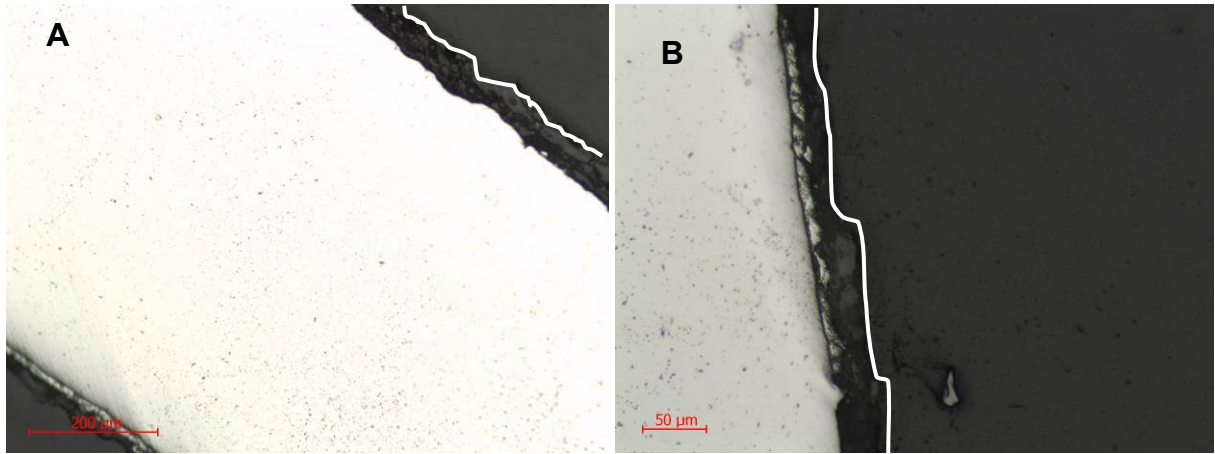


Figure 127 Microscopic observation of cross section of HD ZnAlMg 10µm formed specimen after ACT; the boundary of the layer of corrosion products is shown with white line

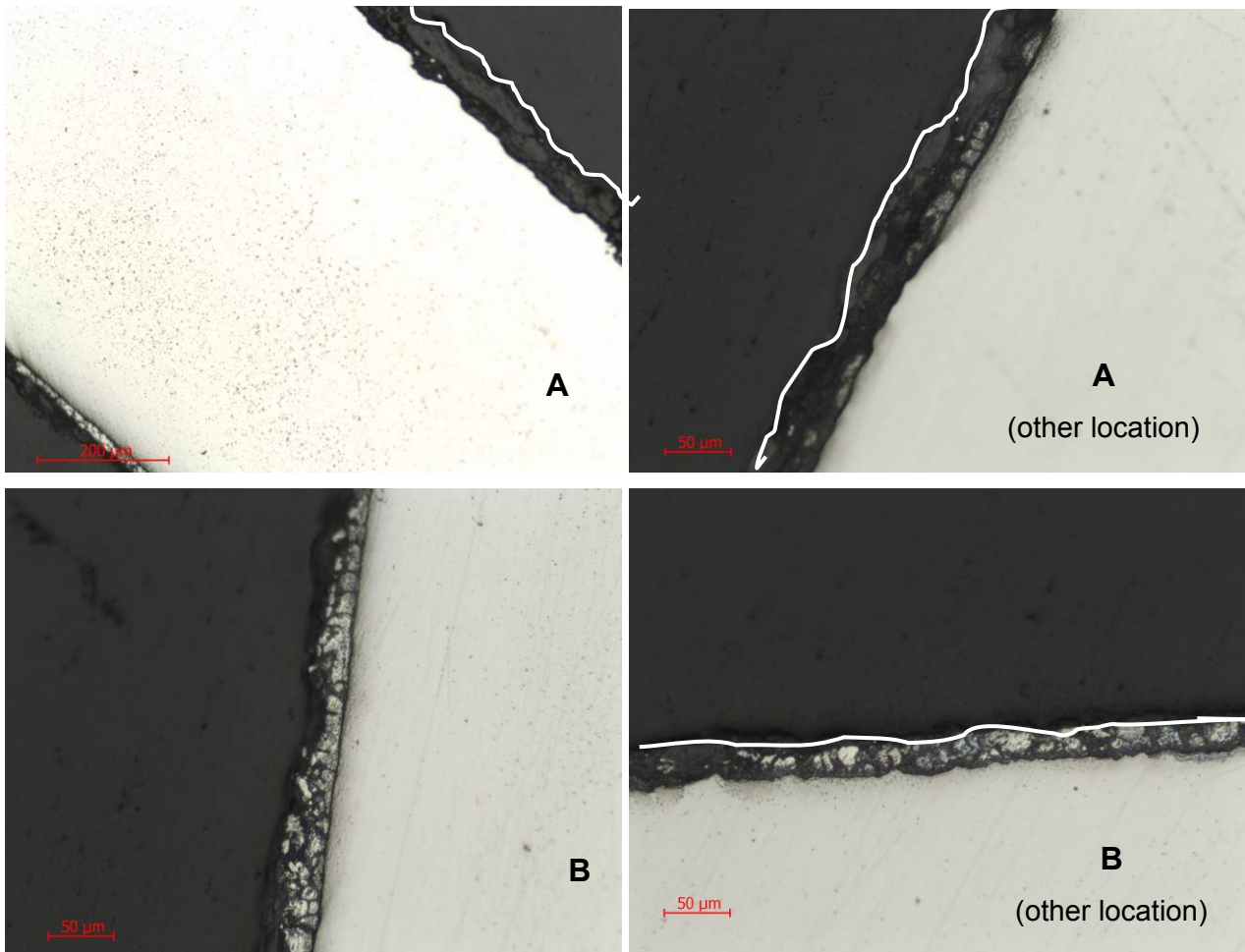


Figure 128 Microscopic observation of cross section of HD ZnAlMg 14µm formed specimen after ACT; the boundary of the layer of corrosion products is shown with white line



Figure 129 Flat GI 10 μm after 18 weeks in ACT



Figure 130 Flat GE 10 μm after 18 weeks in ACT



Figure 131 Flat Galfan 20 μm after 18 weeks in ACT

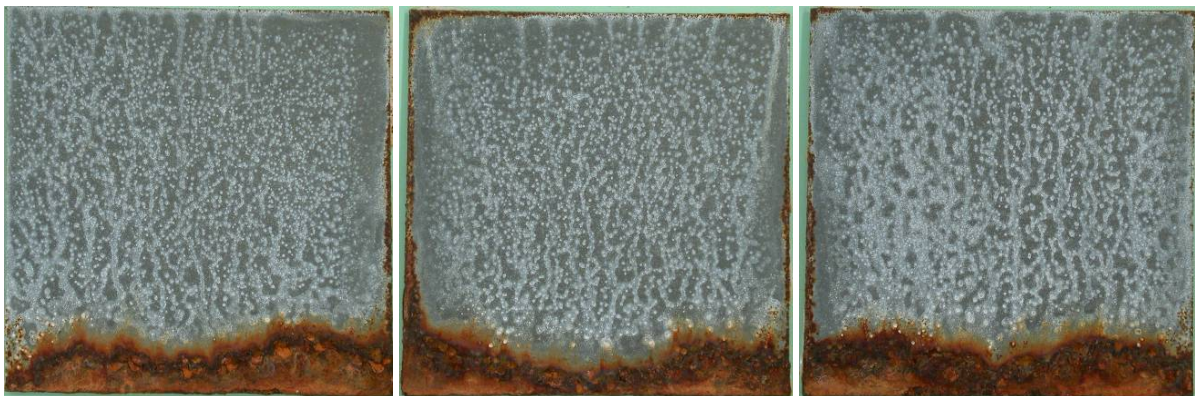


Figure 132 Flat HD ZnAlMg 7 μm after 18 weeks in ACT



Figure 133 Flat HD ZnAlMg 10 μm after 18 weeks in ACT



Figure 134 Flat HD ZnAlMg 14 μm after 18 weeks in ACT

4.8 Evaluation of painted panels with Scanning Kelvin Probe

4.8.1 Delamination from scratches

A scribe 1 mm wide was applied to GI 10 μm and HD ZnAlMg 10 μm painted with the same process as for tests in confined areas. The scribe was done down to metallic coatings. Specimens were exposed for 24 hours in a salt spray test at 5 % NaCl to initiate the corrosion delamination. Then, they were cleaned with demineralized water and introduced into an SKP chamber with controlled humidity at 95 % RH. Measurements were done also in humid nitrogen at 95 % RH and in dry air at 50 % RH.

White rust formation was visually observed on the GI sample. HD ZnAlMg coating did not show any visible corrosion in the scratch. No visible coating delamination was observed.

Figure 135 shows an area around the scratch on GI. The formation of the corrosion products usually increased the Volta potential. This can be the reason of more positive potentials in humid air in the scratch area. The width of the area of increased potential is about 1.5–2 mm. This can indicate that the delamination process started and the corrosion was slightly spreading under the coating. Exchange of air to nitrogen at the same humidity decreased the potential in the scratch. Hence, it is probable that both anodic reaction (formation of the white rust) and cathodic reaction took place in the defect.

Measurements for HD ZnAlMg coating are in Figure 136. Only small areas with increased potential less than 1 mm wide can be seen in the scratch. Cathodic locations are more positive and the potential dropped there during exchange of air to nitrogen. Both corrosion reactions were concentrated in the defect and no significant corrosion spreading took place.

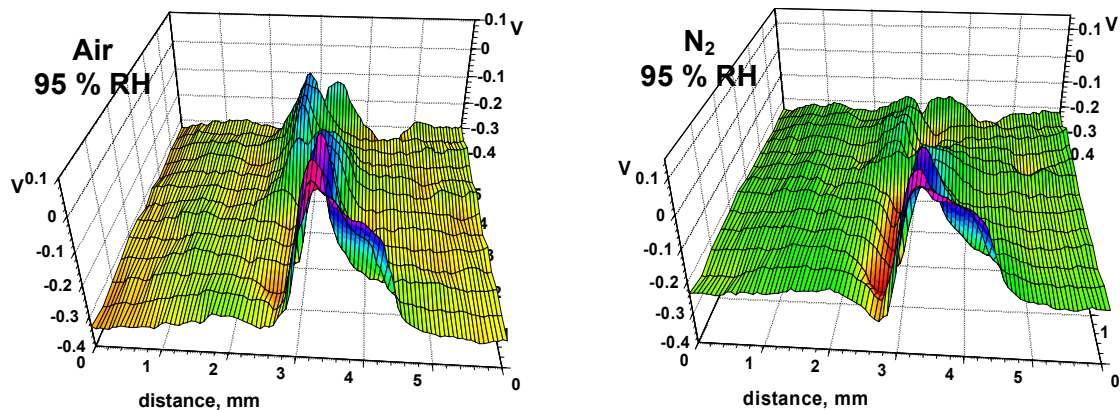


Figure 135 Volta potential profiles of GI in humid air and humid nitrogen at 20°C after pre-exposure in salt spray test for 24 hours; scratch is located in the middle part of the profile

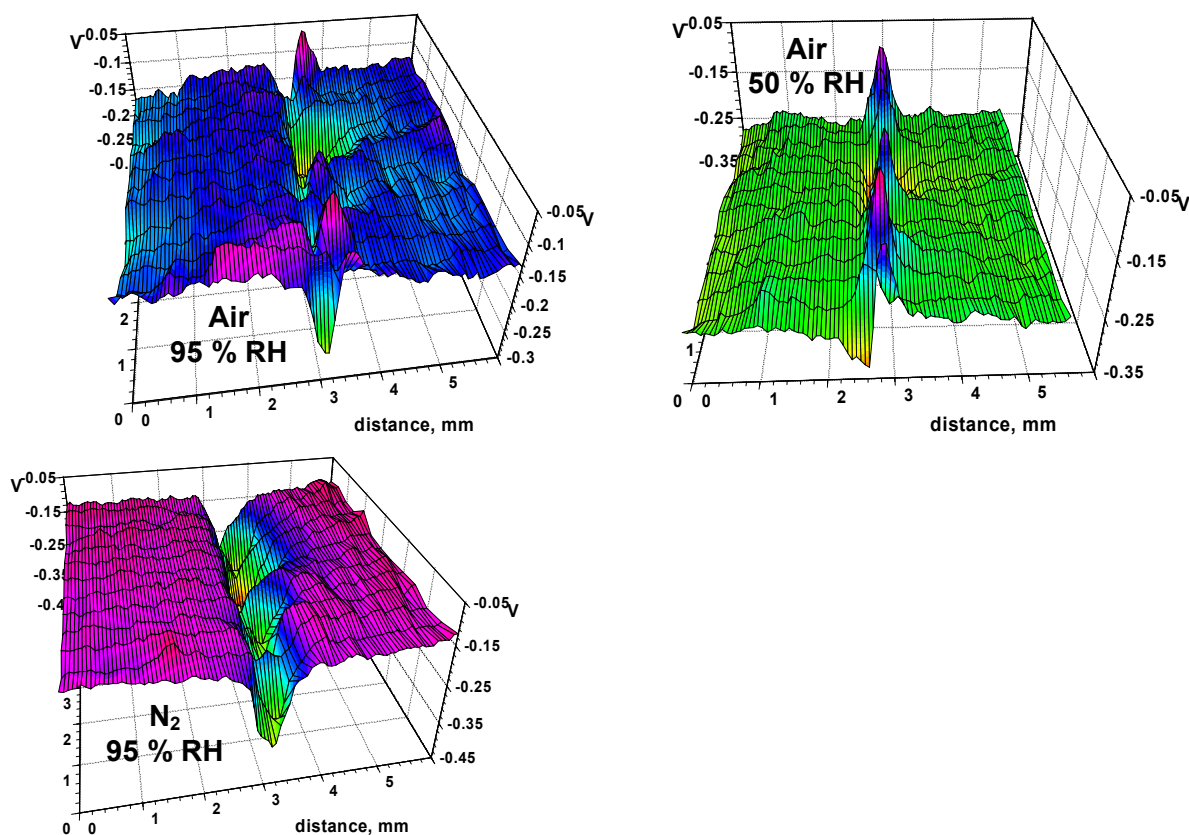


Figure 136 Volta potential profile of HD ZnAlMg in humid air, dry air, and humid nitrogen at 20°C after pre-exposure in salt spray test for 24 hours; scratch is located in the middle part of the profile

Thus, no delamination was observed on HD ZnAlMg and the process only started for GI after 24 hours of exposure in salt spray. These results are different from results concerning galvanized steel described in literature [17,23]. It was shown that polymeric coatings very quickly delaminated from defects filled with 0.5M NaCl electrolyte. After 6 hours of exposure, the cathodic front moved by 7 mm from the defect. In our case, 24 hours exposure in salt fog chamber mainly led to corrosion inside of the defect without significant spreading. It is possible to suppose that the reason is mainly due to much more protective nature of the automotive cathaphoretic coating. Much longer exposure time would be needed to induce the delamination process.

4.8.2 Delamination from cut edges

Specimens of painted GI 10 μm , Galfan 20 μm , and HD ZnAlMg 10 μm that were exposed to ACT test for 18 weeks in the open configuration were analyzed at bottom cut edges with SKP. Figure 137 contains geometrical and Volta potential profiles for GI in humid air and humid nitrogen. The bottom edge of the studied panel is located at the left hand side. Blisters spread from the edge. Low potentials were observed below blisters and more positive potentials were observed close to the edge. An intact paint area at the right hand side showed more positive potentials. Most negative (active) potentials are in the front of the delamination with small blisters at the boundary between the intact and delaminated paint. Exchange of the air to nitrogen increased the potential in the front for 70–100 mV showing anodic activation of the zinc coating at the front in humid air. The galvanic couple consists of cathode (more noble potentials at the edge and corroded part of the panel close to the edge) and anode (active metal below blisters and at the delamination front). It is possible to suppose from this geometry that the delamination mechanism was anodic undermining from the edge. This kind of undercutting is normally observed for cut edge corrosion of galvanized steel.

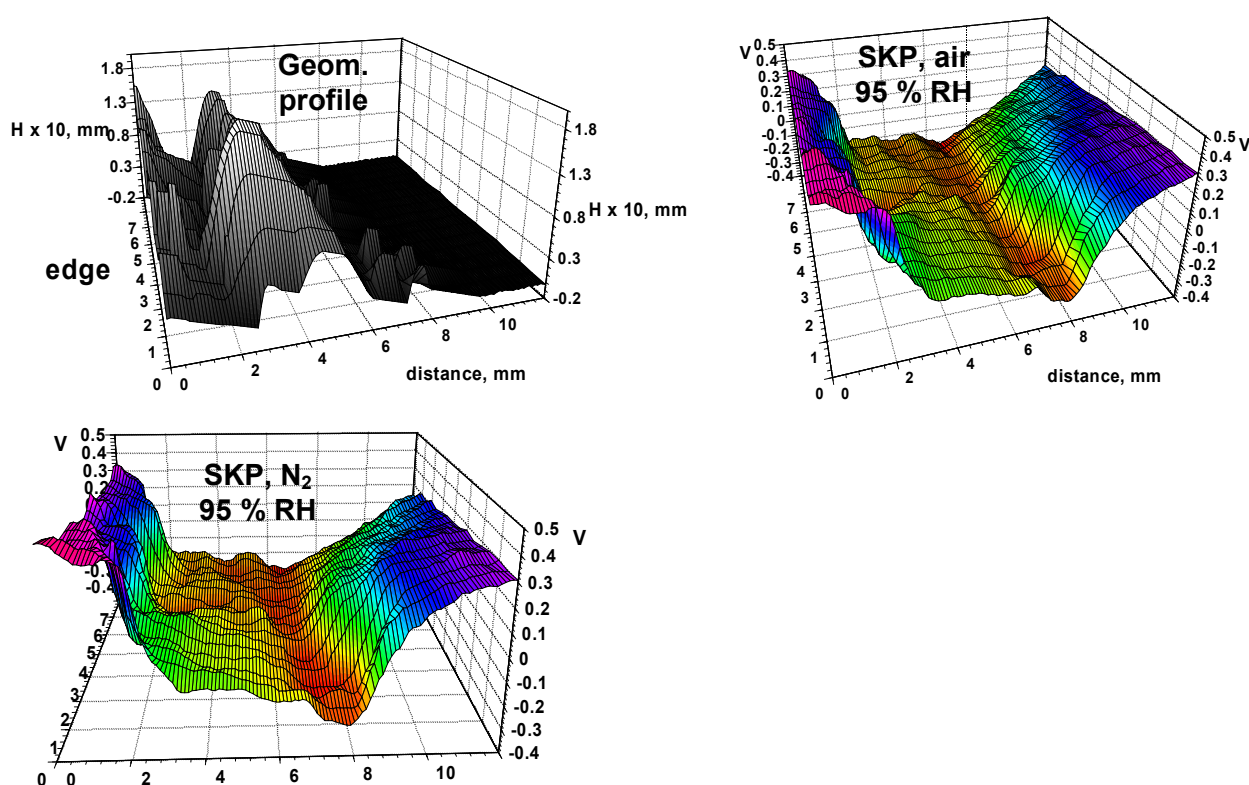


Figure 137 Geometrical and Volta potential profiles for GI 10 μm in Volvo open configuration exposed in ACT for 18 weeks; measurement was done at the bottom edge (left hand side of profiles)

Figure 138 shows similar measurements for the HD ZnAlMg sample. The geometry of galvanic couple and Volta potential profiles are similar to those for GI. However, the delamination distance from the edge is 2-fold lower. The low potential area (the front) is narrower and it is related to presence of small blisters. The potential at the front is near identical for GI and HD ZnAlMg. Humid air to humid nitrogen transition increased the potential at the front. The anodic undermining mechanism can be supposed for the coating delamination from the HD ZnAlMg coating close to the edge.

Figure 139 contains geometrical and Volta potential profiles for Galfan exposed under the same conditions. The delamination creep is large and close to that of GI. Comparison of the geometrical and potential profiles reveals that the real delamination area (area of low potentials) is larger than the area of blistering. The front is 2–3 mm further from the edge than visible blisters. High potentials at the edge (left hand side)

correspond to the corroded surface, which can work as a cathode polarizing the nearest anodic interface. The mechanism of the coating delamination is anodic undermining.

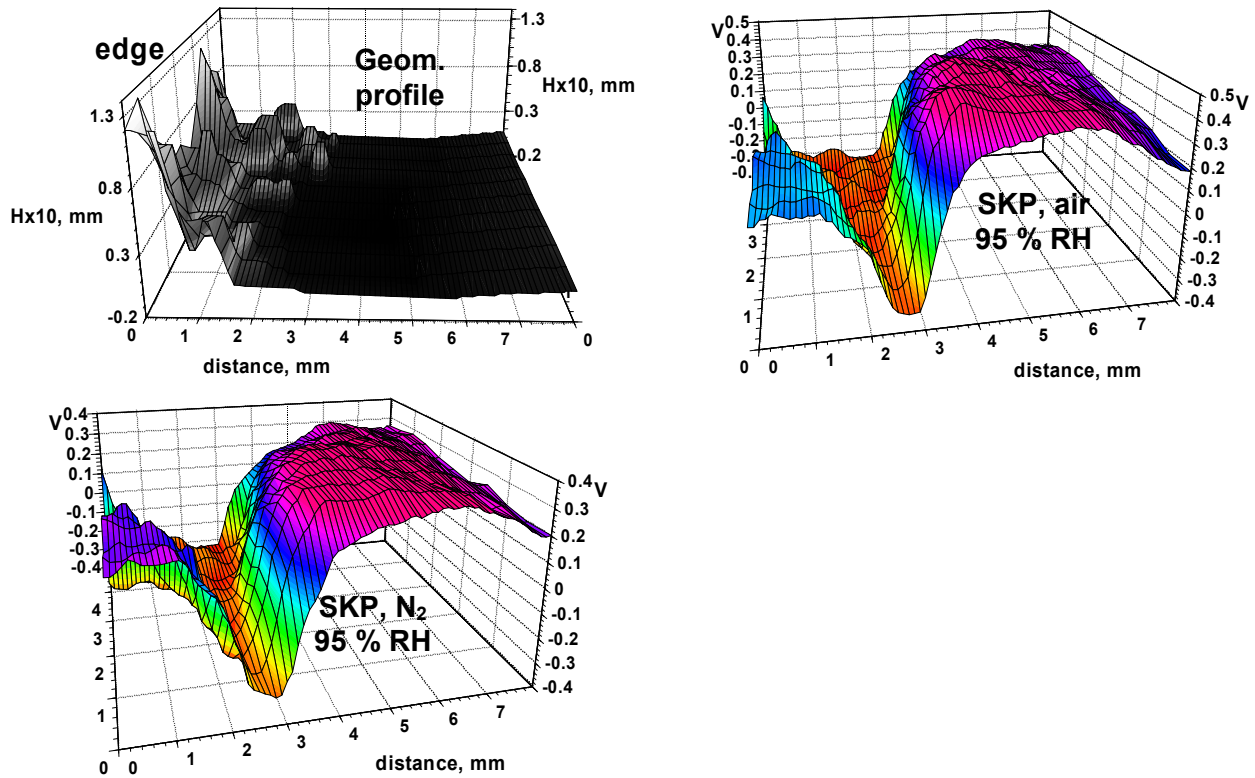


Figure 138 Geometrical and Volta potential profiles for HD ZnAlMg 10 μm in Volvo open configuration exposed in ACT for 18 weeks; measurement was done at the bottom edge (left hand side of profiles)

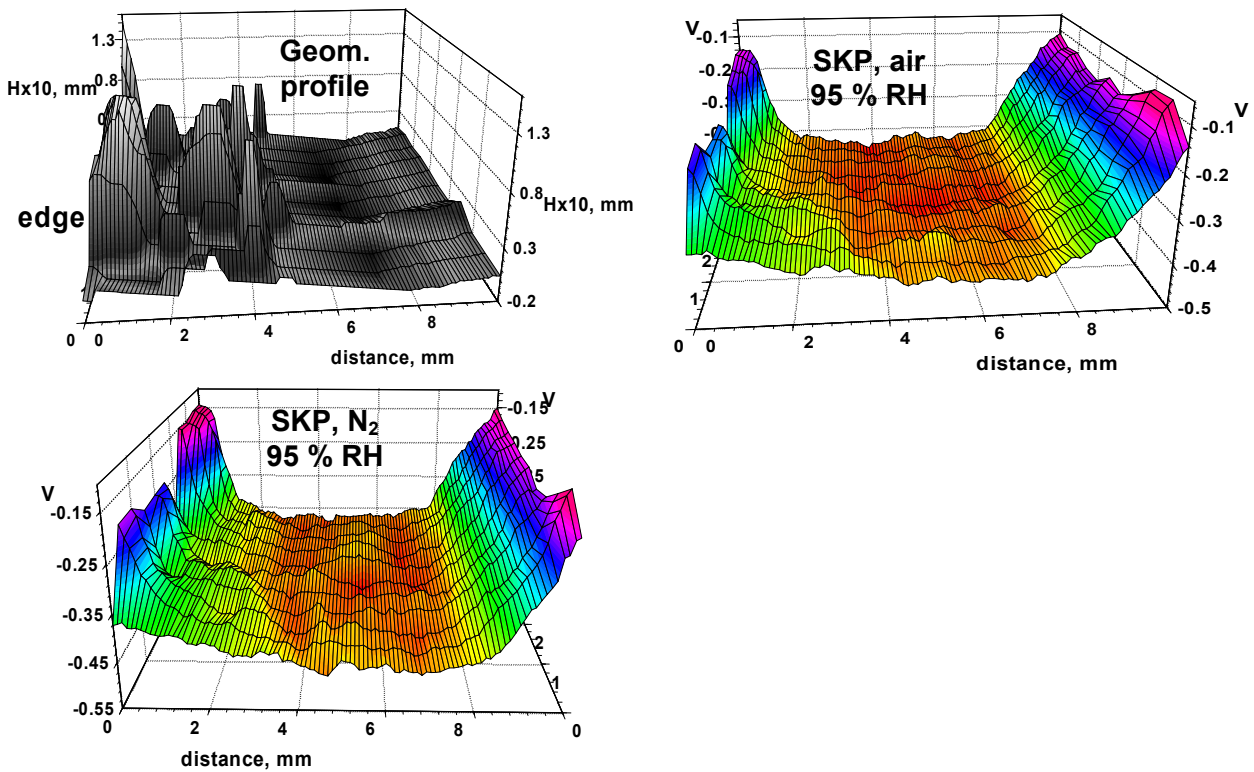


Figure 139 Geometrical and Volta potential profiles for Galfan 20 μm in Volvo open configuration exposed in ACT for 18 weeks; measurement was done at the bottom edge (left hand side of profiles)

It is possible to conclude that galvanic cells formed close to the edge had the same structure for all tested materials and the undercutting follows the anodic undermining mechanism. Formation of a galvanic cell with a cathode at the edge and an anode below the polymeric coating close to the edge is the main moving force for polymer delamination and edge corrosion. The potential below blisters adjacent to the edge is more positive in case of HD ZnAlMg, i.e. the interface is more passive. It can be due to a lower efficiency of the galvanic couple. It can be due to a lower rate of oxygen reduction close to the edge or a lower efficiency of anodic dissolution of the alloy. In case of HD ZnAlMg, deposition of magnesium oxide/hydroxide close to the edge can decrease the oxygen reduction rate. However, the inhibition of anodic dissolution by alloying with magnesium is also possible.

4.8.3 Delamination from large defects in the polymeric coating

Specimens of painted GI 10 μm , Galfan 20 μm , and HD ZnAlMg 10 μm that were exposed to ACT test for 18 weeks in the open configuration were analyzed in the area between the non-painted and painted part with SKP. Thus, paint delamination from a large defect was inspected.

The unpainted area was very strongly corroded in case of GI covered by red and white rust. Blisters spreading from the defect were observed. SKP measurements in Figure 140 showed that a low potential anodic area with the potential of -400 mV was associated to the blisters and high potentials of $400\text{--}500\text{ mV}$ were detected in the defect. High potential in the defect is due to the presence of red rust adherent to the steel surface. The large difference in potentials of 800 mV between the unpainted area and front beneath the polymer is the reason of the fast paint delamination. The most negative potentials were detected at the front between blistered and intact paint. The potential at the front increased by 70 mV after exchange of humid air to humid nitrogen. The mechanism of the delamination in given time was anodic undermining.

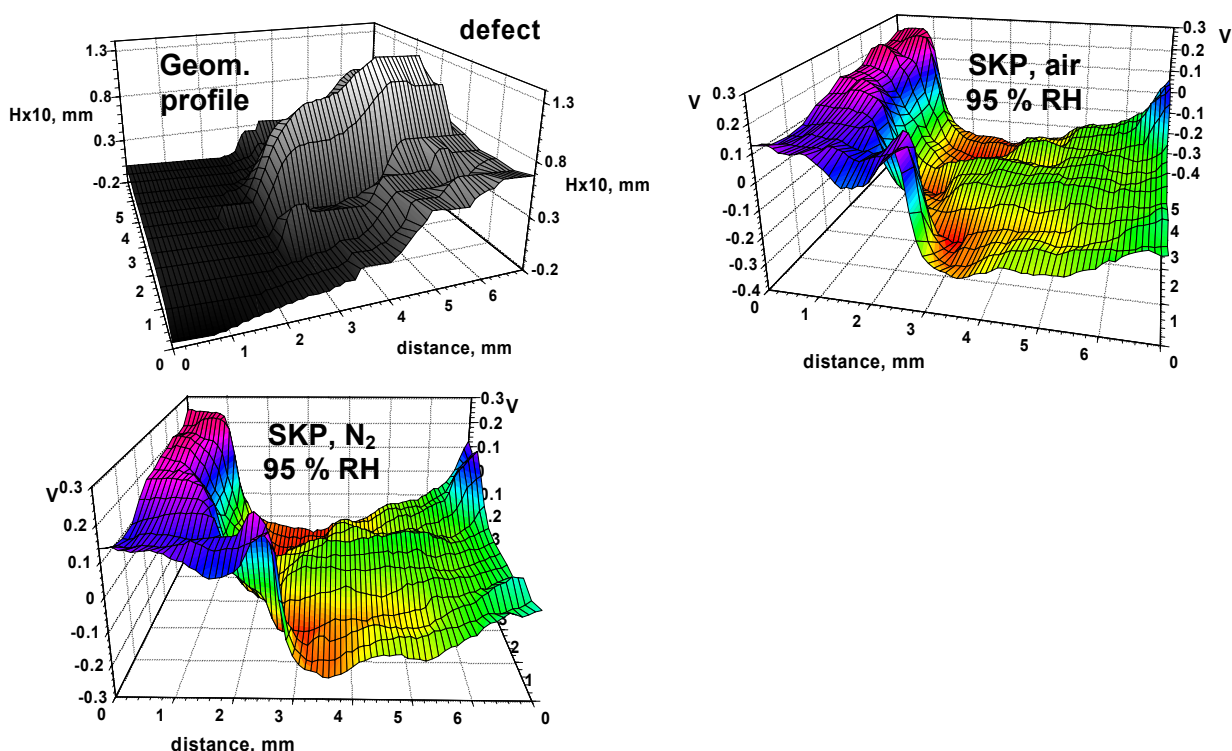


Figure 140 Geometrical and Volta potential profiles for GI 10 μm in Volvo open configuration exposed in ACT for 18 weeks; measurement was done at the boundary of unpainted (right hand side) and painted area

Figure 141 contains profiles for HD ZnAlMg coating with the unpainted area at the right hand side. No significant delamination from the defect was observed in the Volta potential profile. No blistering is visible from the geometrical profile. No formation of red rust in the defect was observed. The potential in the defect was negative at -200 to -300 mV. The potential of intact coating was -100 mV. The gradient of 100 – 200 mV in the potential is reversed and smaller then in case of the GI sample with red rust.

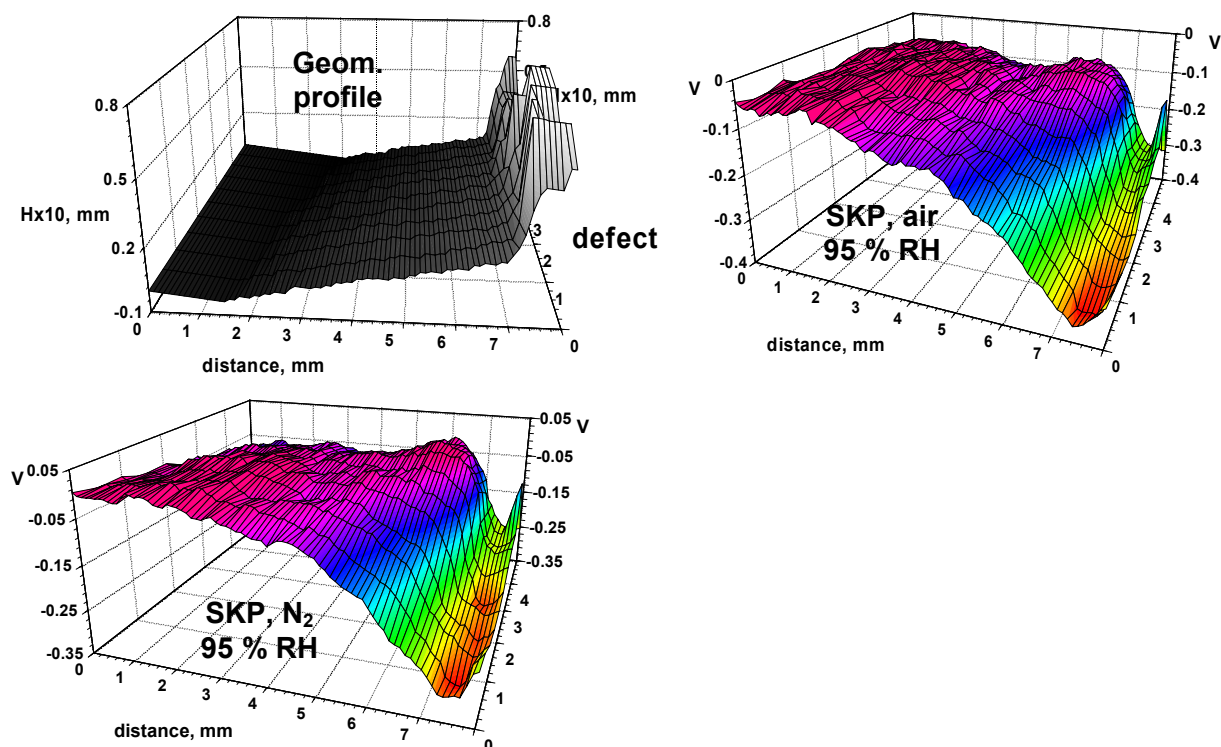


Figure 141 Geometrical and Volta potential profiles for HD ZnAlMg 10 μ m in Volvo open configuration exposed in ACT for 18 weeks; measurement was done at the boundary of unpainted (right side) and painted area

Data for Galfan are given in Figure 142. The unpainted area is at the left hand side. Galfan behaved similarly to HD ZnAlMg. No delamination and no blistering from the defect took place. No significant red rust formation was observed in the defect and the potential in the defect was -400 to -300 mV, i.e. more negative than for the intact coating (-100 to 0 mV). The potential gradient is reversed compare to rusted GI protecting the paint system from anodic undermining.

It is possible to suppose that a low efficiency of the oxygen reduction in the defect and negative gradient in the potential across the intact paint/defect are main factors protecting coatings on HD ZnAlMg and Galfan coatings from anodic undermining. Formation of red rust can lead to a fast anodic undermining process. Red rust can be a strong cathodic reactant due to participation of different iron species (Fe^{2+} , Fe^{3+}) in the reaction with oxygen in air.

A summary of potential distribution in the defect and under the intact coating is presented in Figure 143. The difference between the potentials represents the moving force of the paint delamination. The Volta potential in the defect was monitored during increasing of the air humidity from 50 to 95 % RH. It is possible to see that GI covered with red rust had very positive potential and a high positive potential gradient developed between the defect and intact polymer. This gradient governs the anodic undermining process, which rate depends on the efficiency of oxygen reduction on the surface of the corroding defect. GI pre-corroded in salt fog chamber for 24 hours without red rust on the surface showed a slightly more positive potential than that of the intact coating and the anodic undermining would be much slower in this case. The potential of Galfan and HD ZnAlMg coatings were more negative then the potential of the coated

material. In this case cathodic delamination of the coatings can be expected. However, since the cathodic reaction below the polymer coating is strongly inhibited by oxide films at the interface of Galfan and HD ZnAlMg and the polymer coating, the delamination rate is very slow.

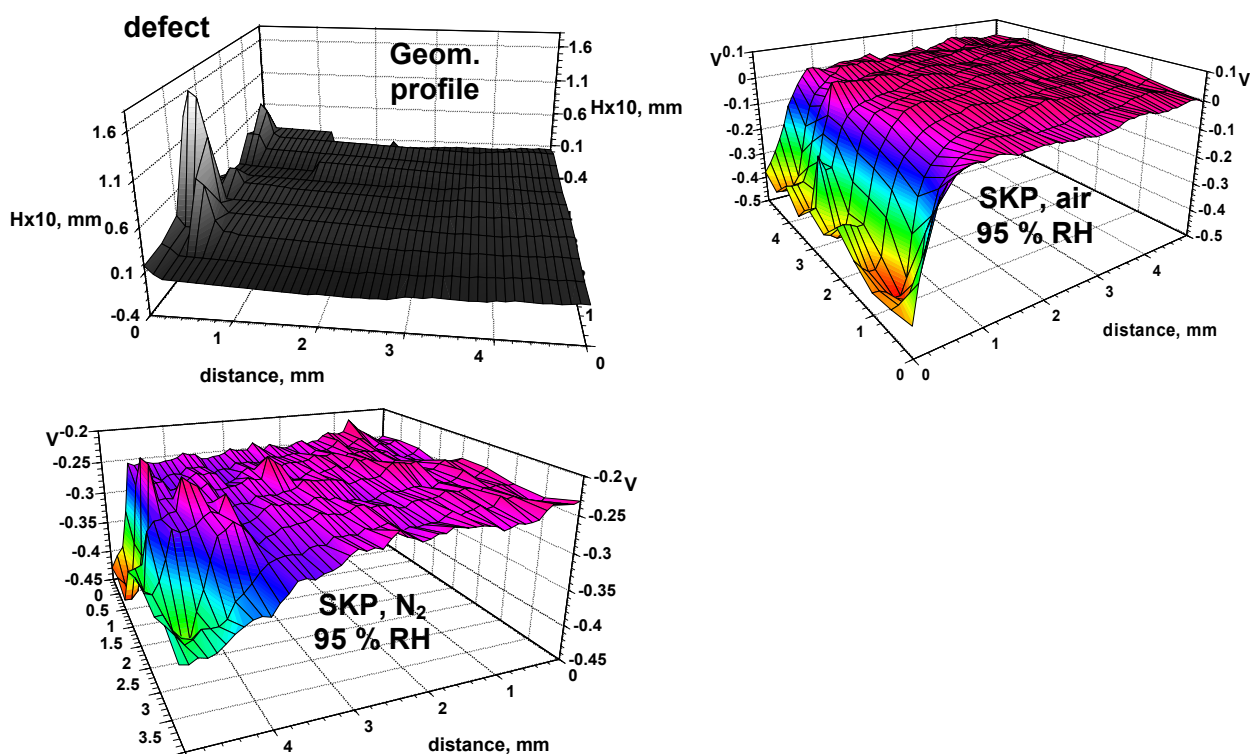


Figure 142 Geometrical and Volta potential profiles for Galfan 20 μm in Volvo open configuration exposed in ACT for 18 weeks; measurement was done at the boundary of unpainted (left side) and painted area

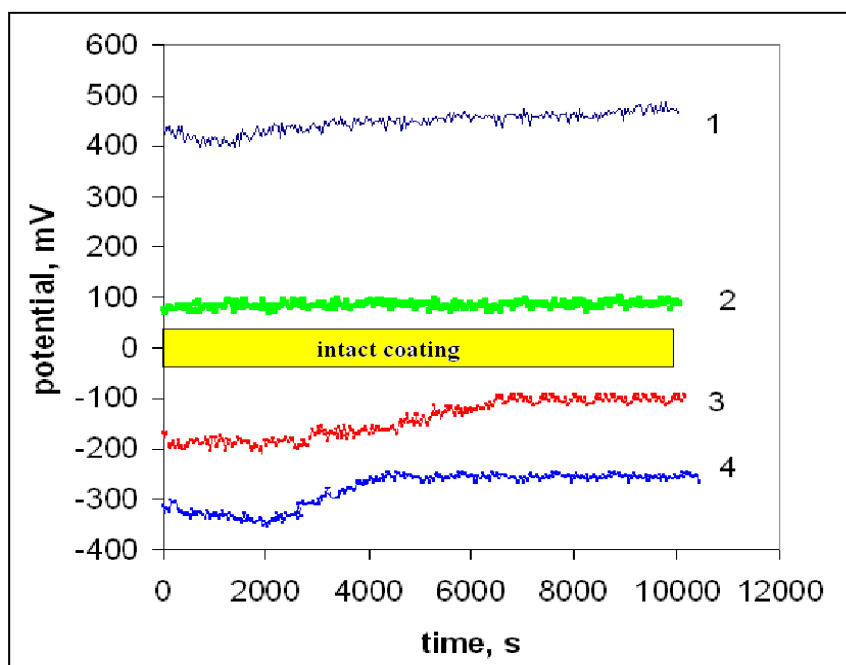


Figure 143 Change in the Volta potential during an increase in relative humidity from 50 to 95 % RH at 20°C; the yellow bar is the potential of the coated surface, 1... defect in GI containing red and white rust, 2... corroded surface of GI without red rust, 3 ... corroded surface of Galfan, 4 ... Corroded surface of HD ZnAlMg

As seen in Figure 140, Figure 141, and Figure 142, the potential of metal covered with an intact paint was almost identical for GI, HD ZnAlMg, and Galfan. Based on previous works, it was supposed that there would be larger differences since the ZnMg surface covered with Mg-based oxide has more negative potential than that of zinc. However, it is possible that the phosphatation process removed the oxide layer or the phosphate layer largely influence the measured potential. Thus, for basic understanding of the paint delamination mechanism of ZnAl(Mg) materials, model systems need to be used. This will be done in future.

5 Summary

ZnAl and ZnAlMg model alloys were contaminated with sodium chloride and exposed in a climatic chamber at 20°C and 80 % of RH for 28 days. The addition of 0.2, 0.5, and 1 wt. % of Al did not have any significant effect on corrosion properties of studied alloys. A strong improvement in corrosion resistance was observed for alloys containing from 2 wt. % of alloying elements. The weight loss decreased with the increasing content of Al and Mg. It was the lowest for ZnAl55. Under these experimental conditions, the effect of Al and of Mg was comparably strong and additive.

Results obtained for ZnAl and ZnAlMg model alloys were compared to those for ZnMg model alloys studied in a previous work. Curves of the weight loss of ZnAl and ZnAlMg alloys related to zinc reference have a shape similar to that for ZnMg alloys. However, a shift of 20 to 40 % was observed. It is supposed to be due to slight differences in the experimental setup.

The analysis of corrosion products with FTIR showed that the amount of carbonates on the surface increased relatively to the amount of simonkolleite with the aluminum and magnesium content in ZnAl and ZnAlMg model alloys. This was in agreement to data on soluble chloride species obtained from ion chromatography. The fraction of chloride bonded in corrosion products clearly decreased with the aluminum and magnesium content. Thus, an important part of applied sodium chloride stayed non-reacted and soluble on the surface of model alloys even after 28 days of exposure in humid air. This is in agreement to results of the previous study on corrosion properties of model ZnMg alloys. It indicates that the surface of ZnAl(Mg) alloys was protected by a stable passive layer reducing substantially the rate of corrosion.

AlOOH (boehmite or diasporite) was detected in corrosion products formed on ZnAl and ZnAlMg alloys. Al(OH)₃ was found on samples of ZnAl5Mg5, ZnAl55, and Al. A small amount of magnesite, MgCO₃ and/or magnesium hydroxycarbonate was probably present on the surface of ZnAl1Mg1 and ZnAl2Mg2. The analysis of soluble corrosion products revealed that much less corroded zinc was bonded in stable corrosion products on the surface of model alloys containing aluminum and magnesium. Only 0.5 % of corroded metal was soluble on the surface of pure zinc, whereas it was 47 % on ZnAl55. Because lower amounts of stable zinc corrosion products and simonkolleite that is considered to be more protective than hydrozincite [32] were found on alloys with improved corrosion stability, it is supposed that formation of bulk corrosion products with better protective ability was not the reason of the positive effect of alloying elements. So far acquired data suggest that the mechanism of aluminum and magnesium protection might be similar. The superior corrosion stability of ZnAl, ZnMg, and ZnAlMg alloys is probably connected to presence of oxide layers with better protective properties than those of zinc-based oxide layers. They may either limit the rate of oxygen reduction or anodic dissolution. This will be addressed in further research.

Metallic coated panels were also contaminated with sodium chloride and tested at 20°C and 80 % of RH for 28 days. Samples of GI, Galfan, ZAM, SD, AZ, and HD ZnAlMg were exposed to humid air with sodium chloride deposits at 500, 1400, 2500, and 5000 mg/m². Besides GI, weight losses of tested coatings were low. Depending on the coating and chloride concentration, the weight loss dropped by 66 to 92% in comparison to reference GI. The improved corrosion stability was again connected to a significant decrease

in the amount of bonded chloride in corrosion products and preferential formation of carbonate-based corrosion products instead of simonkolleite. Magnesite and/or magnesium hydroxycarbonate was identified in corrosion products formed on HD ZnAlMg and SD and AlOOH on all coatings containing aluminum.

The weight loss of all coatings increased approximately linearly with chloride contamination. The weight loss of GI strongly depended on the chloride concentration. It was less affected in case of the alloyed materials. The weight loss of the alloyed materials related to that of GI decreased with the increasing chloride concentration, i.e. the alloyed materials were the most efficient at the highest chloride concentration of 5000 mg/m².

Results obtained for the coated panels were compared to results obtained for model alloys. It was shown that the metallic coatings were less susceptible to corrosion than model alloys at similar alloying element content, especially up to 5 wt. % of alloying elements. Only the ZnAl55 model alloy was less corroded than the commercial AZ coating. The generally better corrosion resistance of the metallic coatings compared to model alloys might be caused by alloying element segregation in the top layer of the coatings. It was observed for other hot-dip coated materials that magnesium tended to segregate in the outer part of the coating increasing thus its effective amount available for inhibition of the corrosion process. Also an effect of any surface treatment of the metallic coatings in production cannot be fully disregarded.

The effect of temperature from 10°C to 40°C was investigated at 80 % of RH for metallic coated panels contaminated with chloride deposits and exposed for 28 days. The difference between the performance of the coatings at 10 and 20°C was limited. Higher aggressiveness of the exposure conditions at 40°C generated larger differences between the alloyed coatings. This temperature was clearly more detrimental for coatings with 3 to 9 % of alloying elements. Dependence of the weight loss on temperature was rather flat for GI, SD, and AZ. An increase in the weight loss with temperature was seen for HD ZnAlMg, Galfan, and ZAM, particularly at higher chloride contaminations.

The effect of the relative humidity on corrosion of contaminated metallic coatings was investigated from 65 to 95 % RH at 20°C. A clear difference was observed between coatings with the total alloying equal or below 5 %, i.e. Galfan and HD ZnAlMg, and coatings with total alloying equal or above 9 %, i.e. ZAM, SD and AZ. The first group showed rather high weight loss at low RH of 65 %, even higher than at 80 and 95 % RH. Coatings containing from 9 % of alloying elements showed an expected trend, i.e. the weight loss increased with the relative humidity.

Both commercial coated panels and panels coated in a Rhesca simulator contaminated with 1400 mg/m² of chloride were exposed at 35°C in three different wet/dry cycles with the humidity cycling between 85 and 50 % RH. The wet time was 4 hours, drying and wetting period were 2 hours, and number of cycles was 56 in all tests. The total time of wetness was identical in all tests. The cycles differed only in the dry time at 50 % RH, which was 2, 4, and 8 hours for the short, basic, and long cycle, respectively. The goal was to evaluate the effect of dry time to the weight loss and type of corrosion products formed.

The test with the shortest drying period was the most aggressive. The average weight loss was 49 % higher than in the basic cycle. Indeed, different materials responded differently. The shortening of dry time was particularly detrimental for coatings with the total alloying equal or below 5 %. A linear dependence between weight loss and alloying was obtained in the basic test with 4 hours of dry time independently of the nature of the alloying, i.e. the effect of Al and Mg was comparable and additive. However, ZnAlMg coatings were more corrosion resistant than ZnAl or ZnMg coatings in the short cycle with dry time of 2 hours. In this case, a synergetic effect of Al and Mg was observed.

The composition of corrosion products on GI and HD ZnAlMg did not change much with the length of the dry period. Somewhat higher amount of carbonates was found on the surface of HD ZnAlMg after the short and most aggressive test than after the other tests.

In another experiment, some coated materials were exposed in humid air with and without presence of CO₂. The content of CO₂ in air in the CO₂-free and normal conditions was below 1 ppm and about 380 ppm, respectively. A strong increase in the weight loss was obtained for lower alloyed coatings HD ZnAlMg and Galfan in CO₂-free air. ZAM, SD, and AZ were not very sensitive to the presence of carbon dioxide. The analysis of corrosion products on HD ZnAlMg revealed presence of a high amount of zincite, ZnO after the CO₂-free test.

The relative efficiency of the alloyed materials to reference GI at different exposure conditions at constant chloride concentration of 1400 mg/m² is compared in Table 20. It was generally more stable for more alloyed materials. Their performance in comparison to GI did not vary much with temperature, relative humidity, chloride concentration, and dry time. It is also seen that the performance of ZAM, SD, and AZ was comparable in many tests, i.e. the amount of alloying elements from 9 to 55 wt. % usually affected the weight loss only slightly. Relatively stable performance was observed also for GI. Lower alloyed coatings HD ZnAlMg and Galfan were more sensitive to exposure conditions. For HD ZnAlMg, the most detrimental was the elevated temperature, low RH, short dry time in the cyclic test, and atmosphere with reduced content of carbon dioxide.

Table 20 Improvement of protective ability of ZnAl(Mg) coatings in comparison to GI in different tests for samples contaminated with 1400 mg/m² of chloride

Exposure conditions			Weight loss of GI [g/m ²]	Relative improvement to GI [%]				
T [°C]	RH [%]	Note		HD ZnAlMg	Galfan	ZAM	SD	AZ
10	80		8.7	76	82	88	77	81
20	80		11.2	82	81	93	76	85
40	80		11.4	57	77	81	89	83
20	65		8.7	53	59	93	89	94
20	95		9.5	67	67	83	80	77
35	50/80	Dry time 2 h	13.1	31	18	91	63	88
35	50/80	Dry time 4 h	13.2	48	72	91	91	91
35	50/80	Dry time 8 h	13.9	50	55	88	76	95

In the second part of this study, the perforation corrosion in confined areas was addressed. Coated panels were phosphated and painted in an industrial line by cathaphoresis. Two designs of crevice panels were used. Renault crevice panels were exposed in Atmospheric Corrosion Test (ACT) according to a Volvo standard for 6 weeks. This configuration is probably closer to real geometry of hem flanges as the phosphate layer can be partly formed in the confined zone but paint cannot penetrate there. Red rust was observed on CRS and GI 10 µm but not on GI 20 µm and Galfan 20 µm after 6 weeks of exposure. HD ZnAlMg coatings at all thicknesses exhibited some red rust around screw holes. The red rusted area was 10 times smaller on the surface of HD ZnAlMg 10 µm than GI 10 µm. The metallic coating loss was calculated for the materials. It depended on the total amount of alloying elements in the coatings approximately linearly. It was the highest for GI and lowest for Galfan.

CRS, GI 10 µm, GI 20 µm, Galfan 20 µm, and HD ZnAlMg 7, 10 and 14 µm were tested in ACT in the Volvo crevice configuration and open configuration for 18 weeks. A strong point of the Volvo configuration is the possibility to follow corrosion in time. Red rust appearance can be visually observed and weight gain is followed in time. Less red rust was observed on Galfan 20 µm and HD ZnAlMg 10 and 14 µm than on CRS, GI 10 µm, GI 20 µm, and HD ZnAlMg 7 µm in confined areas. The best corrosion

resistance showed ZnAlMg 14 μm . Red rust appeared after the longest delay and its extent was the lowest at the end of exposure. In comparison to GI 10 μm , HD ZnAlMg at the same thickness delayed red rust appearance by a factor of 2 (week 4 instead of 2) and the maximal depth of corrosion in steel was 42% lower (207 instead of 359 μm). Even higher efficiency provided HD ZnAlMg in the open configuration. In comparison to GI, red rust appeared 4 to 10 weeks later (week 8 or 14 instead of 4), the maximal depth of corrosion in steel was 66% lower, and the red rusted area after the end of the test was 13 instead of 73 %. The corrosion performance of HD ZnAlMg 10 μm was similar to that of Galfan with 2-fold higher coating thickness of 20 μm .

Formed panels were tested in ACT for 18 weeks. Red rust initiation at the top edges of formed panels was clearly delayed for HD ZnAlMg 7 and 10 μm compared to Galfan 20 μm . No red rust at top edges was observed for HD ZnAlMg 14 μm . White rust with heterogeneous morphology in form of rather high 'islands' was seen on Galfan while on HD ZnAlMg the growth of white rust was more uniform.

Flat coated panels were exposed in the same test as formed panels. The inclination of 45° of the specimens exposed to the ACT test induced an important gradient of concentration of NaCl salt on the surface from the top to the bottom of the specimen. Therefore, the red rust front advanced from bottom to top. In this test, GE and GI were the most corroded, Galfan 20 μm less and the front advanced only little on HD ZnAlMg coatings. It should be noted that in both latter tests, even HD ZnAlMg 7 μm was performing better than much thicker Galfan 20 μm .

It can be summarized that although the corrosion performance of zinc-based alloys and coatings alloyed with aluminum and magnesium was governed by the total amount of alloying elements in most of the tests, under certain exposure conditions lower alloyed HD ZnAlMg outperformed more alloyed Galfan. It is supposed that it was due to a synergistic effect of Al and Mg. However, it is so far not clear which conditions must be fulfilled to observe this synergistic effect.

Corrosion degradation of coated steel panels in vicinity of defects was studied for GI, Galfan and HD ZnAlMg. After 24 hours of exposure in salt spray test, practically no spreading of corrosion from scratches took place. The corrosion process was concentrated in the area of the defect. After prolonged exposure in ACT for 18 weeks, no coating delamination and corrosion spreading from unpainted areas was observed for Galfan and HD ZnAlMg coatings. It can be due to strong inhibition of oxygen reduction at the alloy/polymer interface and reversed potential gradient between the defect and intact interface. Formation of red rust on the surface of GI led to the anodic undermining of the surrounding paint.

Corrosion degradation from the cut edge was also studied. In all cases the delamination and blistering was observed. The degradation followed the anodic undermining mechanism. The rate of delamination was near 2-fold lower for HD ZnAlMg than for Galfan and GI. It can be explained by limited rate of oxygen reduction at the edge and/or corroded area close to the edge.

6 Conclusions

Corrosion properties of ZnAl, ZnMg, and ZnAlMg materials were studied in a number of laboratory and accelerated tests. The effects of relative humidity, temperature, chloride contamination, cyclic exposure conditions, presence of carbon dioxide, confined areas, and forming were studied. Although further experiments are necessary to fully understand the acquired data, these conclusions can be drawn:

- Addition of aluminum and magnesium decreased the weight loss of zinc-based materials substantially. The effect was usually low up to 1 wt. % of alloying elements. The weight loss dropped strongly with increasing content of Al and Mg from 2 to 5 wt. % and it was low and relatively constant at higher alloying. The drop was observed up to 9 wt. % at more detrimental exposure conditions.

- In most exposure conditions, the effect of aluminum and magnesium was comparably strong and additional. However, lower alloyed ZnAlMg materials outperformed more alloyed ZnAl under certain exposure conditions. It is supposed that it was due to a synergistic effect of Al and Mg. This behavior was observed mainly in cyclic tests.
- Corrosion stability of less alloyed materials was more affected by exposure conditions. They provided somewhat worse protection at low relative humidity of 65 % RH, elevated temperature of 40°C, and reduced content of carbon dioxide. They were also less protective when exposed to cyclic exposure conditions with a short dry phase. More alloyed materials with the content of Al and Mg from 9 wt. % provided stable protection little affected by the exposure conditions.
- The sensitivity of the alloyed materials to chloride contamination was lower than in case of GI. The protection efficiency of the alloyed materials generally increased with the increasing surface chloride concentration.
- In an accelerated automotive test, ZnAlMg coating with 1.5 wt. % of Mg and the same amount of Al with the thickness of 10 µm provided similar protection as Galfan coating at 20 µm in both confined and open configurations. In comparison to hot-dip galvanized steel (GI) with the same thickness of 10 µm, the ZnAlMg coating delayed red rust appearance by a factor of 2 and the maximal depth of corrosion in steel substrate was 42% lower. Even higher efficiency provided ZnAlMg in the open configuration. In comparison to GI, red rust appeared 4 to 10 weeks later, the maximal depth of corrosion in steel was 66% lower, and the red rusted area after the end of the test was 13 instead of 73 %. The best corrosion resistance was clearly obtained for the same coating with higher thickness of 14 µm.
- Red rust appearance on formed panels of Galfan 20 µm and ZnAlMg 7, 10, and 14 µm was delayed in comparison to GI 10 µm by a factor of 2.8, 3.5, 3.8, and >4.5, respectively. It shows that ZnAl(Mg) panels are well formable as well.
- It is supposed that formation of bulk corrosion products with better protective ability was not the reason of the positive effect of alloying elements on corrosion stability of zinc alloys in performed tests. So far acquired data suggest that the mechanism of aluminum and magnesium protection might be similar. The superior corrosion stability of ZnAl, ZnMg, and ZnAlMg alloys is probably connected to presence of oxide layers with better protective properties than those of zinc-based oxide layers. They may either limit the rate of oxygen reduction or anodic dissolution. This will be addressed in further research.

Based on results obtained within this project and described in this report, several research activities should be further undertaken to fully understand the mechanism and application limits of ZnMg and ZnAlMg coated materials. Detail analysis of corrosion products by several complementary techniques, particularly surface sensitive ones and a study of the initial phases of the corrosion process should be done. This is necessary in order to reveal the nature of the protective surface layers providing superior corrosion stability of the alloyed materials. The electrochemistry of these materials in air and water environments should be also studied. Climatic conditions limiting the efficiency of low alloyed ZnAlMg alloys should be addressed, e.g. elevated temperature, low relative humidity, full immersion conditions, and exposure in air with reduced content of carbon dioxide. Corrosion performance in real environments need to be studied as well. On-vehicle exposures and static outdoor exposures in industrial, marine, tropical, and urban conditions are needed for acceptance of these materials by end-users.

7 Agreement with aims of proposal

The objective of the project was to evaluate the corrosion stability of non-painted ZnMg coated panels in laboratory and accelerated tests. The effect of temperature, relative humidity, detrimental ions contamination, length of dry phase, and presence of carbon dioxide was studied. A greater understanding of the influence of climatic parameters on the degradation of ZnMg coated steel was obtained. Another objective was to study perforation corrosion of coated steel sheets. Two designs of crevice panels were used and corrosion performance in confined zones was compared to behavior on free surfaces. Finally, the project should help in understanding the mechanisms of the protective action of magnesium (and aluminum) in the coatings. Model alloys of ZnAl and ZnAlMg were prepared and studied. Although this work is considered as one of the first steps in research of ZnMg(Al) alloy coatings and further research activities are necessary to complete the work, it fulfilled all objectives and the work plan.

8 Acknowledgements

We gratefully acknowledge the help of Frank Goodwin of ILZRO and Sven-Erik Hörnström of SSAB in formulating the work program. Margot Vlot and Jon Elvins of CORUS are thanked for providing samples and reference materials. The authors wish to thank Jan Šerák of Institute of Chemical Technology, Prague for preparation of model alloys.

9 References

1. Vlot M., et al., *MagiZinc™: a new generation of hop-dip galvanised products*, Proc. of Galvanized Steel Sheet Forum 2006, Dusseldorf, Germany, Organized by ILZRO and IZA, May 30-31, (2006).
2. Zhang X. G., *Corrosion and Electrochemistry of Zinc*, Plenum Press, NY, p. 180, (1996).
3. Bruno R. and Memmi M., *The development of new galvanised coatings for use in aggressive environments*, Proc. of Intergalva'76, 11th international galvanizing, Madrid, Spain 4-9 October, p.213-222, (1978).
4. Koll T., et al., *Properties and potential applications of ZnAlMgloy-coatings on steel sheet by PVD*, Proc. of Galvatech'04, 6th International Conference on Zinc and Zinc Alloy Coated Steel Sheet, Chicago, USA, April 4-7, p. 803-812, (2004).
5. Schwerdt C., et al., *A study of the application related properties of novel Zn-Mg coated steel sheet produced in a continuous pilot line*, Proc. of Galvatech'04, 6th International Conference on Zinc and Zinc Alloy Coated Steel Sheet, Chicago, USA, April 4-7, p. 783-793, (2004).
6. Hosking N. C., et al., *Corrosion resistance of zinc-magnesium coated steel*, Corrosion Science 49, p. 3669-3695, (2007).
7. Hosking N. C., et al., *Next generation galvanized steel for the automotive industry*, Proc. of Eurocorr, Freiburg im Breisgau, Germany, Sept. 9-13, (2007).
8. Prosek T., Thierry D., and Taxen C., *Effect of magnesium salts on the corrosion of coil-coated materials*, Institut de la Corrosion, Brest, France, Report 79016, (2005).
9. Prosek T., Thierry D., and Taxen C., *Effect of cations on the atmospheric corrosion of steel and zinc covered with chloride deposit*, Proc. of Galvanized Steel Sheet Forum 2006, Dusseldorf, Germany, Organized by ILZRO and IZA, May 30-31, (2006).
10. Prosek T., et al., *Effect of cations on corrosion of zinc and carbon steel covered with chloride deposits under atmospheric conditions*, Corrosion Science, 49 (6), p. 2676-2693, (2007).
11. Mg-Zn phase diagram, Journal of Phase Equilibria 15, N.1, (1994).
12. Prosek T., et al., *Corrosion properties of model zinc-magnesium alloys*, Proc. of Galvatech'07, 7th International Conference on Zinc and Zinc Alloy Coated Steel Sheet, Osaka, Japan, (2007).
13. Ström M., Ström G., and Strannhage G., *Making the best of corrosion testing?*, Proc. of Eurocorr, Maastricht, The Netherlands, September 24-28, (2006).

14. Barton K., Cuc T. D., and Bartonova S., *Einfluss der Kationenzusammensetzung von Chloridlösungen beim Modellieren von Korrosionseinflüssen der kustenatmosphären*, Werkstoffe und Korrosion (Materials and Corrosion) 28, p. 17-19, (1977).
15. Cole I. S., et al., *Response of 55% aluminium-zinc coated steel and zinc to well-defined salt doses under controlled environments*, Electrochemical Society Proceedings, Vol. 2000-23, (2000).
16. Stratmann M., Feser R., and Leng A., *Electrochimica Acta*, 39, p. 1207-1214, (1994).
17. Stratmann M., *Corrosion*, Vol. 61, N. 12, p 1115-1126, (2005).
18. Leng A., Streckel H., and Stratmann M., *Corrosion*, Vol. 41, p. 547-578, (1999).
19. Grundmeier G., Schmidt W., and Stratmann M., *Electrochimica Acta*, 45, p. 2515-2533, (2000).
20. Doherty M. and Sykes J. M., *Corrosion Science*, Vol. 46, p. 1265-1289, (2004).
21. Nazarov A. and Thierry D., *A Scanning Kelvin Probe Study of the delamination processes at the carbon steel/polymer interface*, EFC series book, Vol. 28, p. 73, (1999).
22. Nazarov A. and Thierry D., *Protection of metals*, Vol. 47, N. 2, p. 126-138, (2001).
23. Furberrth W. and Stratmann M., *Corrosion Science*, Vol. 43, N. 2, p. 207, (2001).
24. Zou F., et al., *Material Science Forum*, p. 298-292, (1998).
25. Falk T., Svensson J. E., and Johansson L. G., *The influence of CO₂ and NaCl on the atmospheric corrosion of zinc; a laboratory study*, Journal of the Electrochemical Society, Vol. 145 n°2, pp2993-2999, (1998).
26. Prosek T., et al., *Corrosion mechanism of model zinc-magnesium alloys in atmospheric conditions*, *Corrosion Science*, sent for publication, (2008).
27. Prosek T., Nazarov A., and Thierry D., *Corrosion protection of steel by zinc coatings alloyed with magnesium*, *Institut de la Corrosion, Brest France*, IC Report 2008:1, (2008).
28. Shinohara T., et al., *Calculation of relative humidity in equilibrium with water films containing strong electrolyte by thermodynamic data*, Galvatech'07, (2007).
29. Ohtsuka T. and Matsuda M., *In situ raman spectroscopy for corrosion products of zinc in humidified atmosphere in the presence of sodium chloride precipitate*, NACE, *Corrosion*, Vol. 59, N. 5, (2003).
30. Lindström R., Svensson J.-E., Johansson L.-G., *The Atmospheric Corrosion of Zinc in the Presence of NaCl; The Influence of Carbon Dioxide and Temperature*, Journal of The Electrochemical Society 147 (5), p. 1751-1757 (2000).
31. Fujita S. and Mizuno D., *Corrosion and corrosion test methods of zinc coated steel sheets on automobiles*, *Corrosion Science* 49, p. 211-219, (2007).
32. Ishikawa T., Matsumoto K., Yasukawa A., Kandori K., Nakayama T., Tsubota T., *Influence of metal ions on the formation of artificial zinc rusts*, *Corrosion Science* 46, p. 329–342, (2003).